An Assessment of Groundwater Contaminant Source and Evolution from Underground Coal Gasification at the Majuba Pilot Plant

Lehlohonolo Mokhahlane

Thesis submitted in fulfilment of the requirements for the degree of

Philosophiae Doctor

in the

Faculty of Natural and Agricultural Sciences

(Institute for Groundwater Studies)

at the

University of the Free State

Promoter: Prof. D. Vermeulen

Co promoter: Dr. M. Gomo

September 2019

Declaration

To my best knowledge and understanding, the thesis contains no material which has been previously published or written by another person except where due references has been given.

I, Lehlohonolo Mokhahlae declare that; this thesis hereby submitted by me for the Philosophiae Doctor degree in the Faculty of Natural and Agricultural Sciences, Institute for Groundwater Studies at the University of the Free State is my own independent work. The work has not been previously submitted by me or anyone at any university. Furthermore, I cede the copyright of the thesis in favour of the University of the Free State.

Signed **Date**

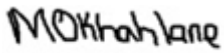

17 Dec. 19

Lehlohonolo Mokhahahlane

Table of contents

Table of figures

List of tables

List of acronyms

CV : Calorific Value

FC: Fixed Carbon

ICP-MS: Inductively Coupled Plasma Mass Spectrometer

IM: Inherent Moisture

M or m: Meters

Mm: Millimetres

Mamsl: Meters Above Mean Sea Level

Mbgl: Meters Below Ground Level

QEMSCAN: Quantitative Evaluation of Minerals by Scanning Electron Microscopy

TS: Total Sulphur

UCG: Underground coal gasification

VM: Volatile Matter

XRD: X-Ray Diffraction

XRF: X-ray Fluorescence

List of quantities

Area (A)	m^2
Concentration	mg\l or Kg\t
Electrical conductivity (EC)	µS\cm or mS\m
Hydraulic conductivity (K)	m\d

Acknowledgments

- This study was undertaken as part of the of Eskom's Majuba UCG pilot plant investigation into the gasification zone after the successful shutdown of gasifier 1. I am therefore very grateful to Eskom for affording me the opportunity to be part of this research.
- I am very grateful to have had Prof. D. Vermeulen as my supervisor. The confidence and freedom he gave me in the organisation of the work created a comfortable and productive atmosphere throughout the term of this research. I would like to express my sincere and special thanks to my academic co-promoter Dr. M. Gomo for all his academic and technical guidance.
- Special acknowledgment also goes to Prof. N. Wagner at the CIMERA, Department of Geology, University of Johannesburg, for all the assistance with petrological analysis of char samples.
- I would like to thank the Eskom Research and Testing and Development (RT&D) team that assisted in various tests and analysis including QEMSCAN analysis, proximate and ultimate analysis. The following deserve special mention: Dr Chris Van Alphen, Ms Shinelka Singh, Mr Shaun Pershad, Mr Mike Beeslaar, Mrs Chantelle Moll, Mr Verdine Samuels and Mr Xolani Ngubeni.
- I would like to thank Mr Gundo Mathoho for his assistance with groundwater sampling, GIS and data processing during this study.
- I would like to thank my family for all the support during this study especially my mother Mrs Mabatho Mokhahlane for all your encouragement.

Abstract

This study undertook to investigate the geochemistry of the potential sources of inorganic groundwater contamination from a spent UCG chamber. The Eskom Majuba UCG pilot plant in South Africa was the main study area for this research. Two core drills that intercepted the spent geo-reactor retrieved residue products (ash, char and heat affected host rocks). Geochemical and mineralogical characterization of UCG residue products was done to establish the inorganic groundwater contamination risk. QEMSCAN and XRD results indicated that most of the primary mineral phases were transformed into high temperature phases. Above average levels of high temperature minerals: mullite, cordierite, tridymite and cristobalite were detected in the roof of the spent UCG chamber. Pyrite transformed into pyrrhotite as recorded by the inverse relationship in the profiles of these sulphide minerals. In general, the results established that char and rocks in the vicinity of the gasification chamber contained relatively lower pyrite levels when compared with the original lithology. Total sulphur analysis of the char recorded comparatively lower sulphur levels as compared to natural coal and this rendered the spent geo-reactor more environmentally sustainable, as lower total sulphur equates to less risk of acid rock drainage. Most of the sulphur is converted to H_2S during the gasification process and transported with the syngas to the surface, where it can be removed and captured as elemental sulphur.

The second objective of the study dealt with the water-rock interaction in the spent geo-reactor. The assessment of the water-rock geochemistry was conducted through leaching tests under different geochemical environments. This task was achieved by subjecting different sections of the geo-reactor to leaching by the following mediums: deionized water, hydrogen peroxide and sulphuric acid. Elements showed a pH-dependent solubility as seen by the general negative correlation factor for each element. The water elution tests (no pH buffer), released the lowest concentrations of ionic species into solution and had an alkaline final pH in most cases. The water elution results were in the main, one or several orders of magnitude lower than the other elution tests results. The peroxide leaching results recorded lower pH levels as compared to the water elution results and consequently the solubility of elements increased. Peroxide elution induces full solution oxidation and this is the basis for acid rock drainage associated with coal mining. The decrease in pH is attributed to oxidation of sulphide minerals which acidify the solution thereby increasing the solubility of elements. Acid leaching was used to assess the leaching dynamics in the spent UCG geo-reactor if acidic conditions developed. Chemical dissociation of carbonates and silicates phases failed to buffer or counter the acidity by consuming the hydronium that is responsible for the low pH. It is therefore recommended that a drop in pH below 4 in mine water around a spent UCG geo-reactor must be countered by acid neutralization strategies such as lime injection to avoid development of acid mine drainage.

The mine water elution was utilized to assess the leaching dynamics under field conditions as water-rock interactions were subjected to experimental temperature of 25 and 70 °C, respectively. The following elements showed general decrease in concentration with increase in temperature Mn, Fe, Ni, Sr, Ca, M and V. The following elements however showed general increase in concentration with increase in temperature: B, K, Cu, and SO_4. The distribution coefficient was used to assess dissociation of elements between the mine water and the solid surfaces of the UCG residue products. Contaminant migration was confirmed with the heat affected roof releasing the most metals into solution at 25 °C while the highest concentrations of metals mobilized into solution at 70 °C emanated from both the

roof and char samples. Aluminium and Fe were the main non-mobile elements across all sections of the geo-reactor and their relative mobility was not affected by change in experimental temperature. The semi mobile metals were Ba, Ni, Cu, Mn, V while metals with great affinity to leach into water phase were Sr, V, Co, Mn, Cu, B and Pb. The higher elution ability of Pb from char samples at higher temperatures is an environmental concern as generally this element was not mobilized from other sections of the geo-reactor from both deionized water and mine water eluates, which indicates that temperature plays a role in dissolving this element from the organic surfaces.

Acid base accounting was used as a predictive tool to assess the acid producing capacity of the spent geo-reactor. The NNP (net neutralising potential) was calculated in terms of the difference between acid producing (AP) and neutralising potential (NP). The analysis utilized both the acid base accounting (ABA) and net acid generation (NAG) methods of acid generation prediction. Utilizing both NNP and NAG test for potential acid generation of samples provides a more reliable evaluation technique than either test used alone. NNP characterized around 13% of samples as acid generating with only 7.5% as non-acid generating. NAG classified 26 samples (49%) as high acid generating while only 13 (24.5%) was characterized as non-acid generating. In general, acid generation is a possibility in a spent geo-reactors however, UCG operations are usually at very deep locations (>200 mbgl) and there might not be sources of oxygen at this depths, for the oxidation of sulphide minerals. However, oxygenated water can be introduced into the chamber during quenching or through drainage of shallow aquifers via hydraulic connections with the spent geo-reactor.

The risk to groundwater contamination from UCG activities was assessed in terms of the source-pathway-receptor model. The spent geo-reactor was identified as the source, as it houses the residue material that contain toxic species as determined by the mineralogical assessment and leaching tests. The pathway was divided into two; (1) a borehole intercepting the spent geo-reactor which provided a vertical pathway from the coal seam aquifer to the overlying aquifers. (2) the in-seam groundwater pathway (lateral extent) that was assessed by monthly groundwater data from the coal seam aquifer taken from monitoring boreholes and compared with background. Stable isotope and hydrochemistry results show that the shallow aquifer and the deep aquifer are not hydraulically connected and therefore it is unlikely that groundwater from the gasification zone would contaminate the shallow aquifer. The deep aquifer had a distinctive isotopic signature for stable isotopes from the shallower aquifers which confirms that there was no groundwater mixing in these aquifers. There was stratification in all the boreholes (monitoring and verification) assessed in terms of EC and temperature. The stratification in EC showed that the quality of water that is sitting on top of the well is better than that in the bottom. This trend suggest that in the event of fractures forming due to roof collapse or any other event that could possibly create a flow path between the cavity water and the shallower strata, the water quality will not be uniform throughout the hydraulic connection. Better water quality will preferentially be at the shallow levels with low quality water concentrated at the bottom. Time series data displayed the chemical evolution of the coal seam aquifer. The results showed no evidence of inorganic contamination from UCG activities. In most cases, the water from the verification boreholes was of lower salinity than background and monitoring boreholes. This is due to surface water that was injected into the UCG cavity during quenching. The groundwater chemistry in the geo-reactor showed a general trend of degenerating to background levels.

Keywords

Underground coal gasification

Geo-reactor

Pyrometamorphism

Sanidinite facies

Acid base accounting

Mine water leaching

Stratification

1 Introduction

1.1 Background information

Underground coal gasification (UCG) is an unconventional mining method that converts in situ coal into fuel gas using high temperature conversion reactions. This process uses a panel of injection and production wells drilled into the coal seam to achieve gasification and transportation of the gas to the surface (Figure 1-1). Oxidants in the form of a mixture of air/oxygen and steam are transported into the gasification zone via injection wells and take part in UCG reactions. The gasification process converts solid coal into a combustible gas composed mainly of methane, hydrogen and carbon monoxide, collectively referred to as synthetic gas. The gas escapes through production wells to the surface where a number of gas scrubbing plants are installed to achieve the desired gas that can be used for electricity production. The mass transfer of solid coal to gaseous phases leaves a cavity in the coal seam that gets partially filled with residue products (ash and char) and eventually groundwater once the gasifier is shutdown.

Underground coal gasification has less surface environmental impact than conventional coal mining as most of the waste handling and coal processing is eliminated (Imran et al., 2014). In traditional coal mining techniques, coal is mined and transported to the point of use where it is stockpiled before processing. All these processes have unfavourable environment effects such as groundwater contamination, surface disturbance and atmospheric pollution. At the tail end of the coal value chain is the waste handling of ash which also adds to the environmental risk and cost. UCG technology has advantages that include improved health and safety of mining, reduction in coal processing and waste handling and less surface damage from mining activity (Pershad et al., 2018b). Carbon capture and sequestration technology can be incorporated into UCG by utilizing the cavity as a Carbon dioxide storage chamber hence further reducing the environmental effects from UCG activities (Bhutto et al., 2013).

Underground coal gasification offers a number of environmental solutions to coal exploitation, however groundwater contamination remains the main environmental risk (Kapusta and Stańczyk, 2011, Strugała-Wilczek and Stańczyk, 2015). Reports of groundwater pollution have been documented from the UCG test site in Hoe Creek, where product gas comprising of phenols and condensed vapours penetrated the overlying hydraulic units due to high pressures in the UCG reactor (Imran et al., 2014). Contaminants can migrate and penetrate the surrounding rocks as a result of an outward pressure from the gasification zone. It is widely accepted that operating the gasification zone at a pressure lower than the hydrostatic pressure in the immediate aquifers will cause all groundwater movement towards the gasification zone (Imran et al., 2014). This ensures that no outward pressure is exerted in the aquifers and hence containing the organic products within the gasification zone where there is constant decomposition and removal via the production wells. However, most of the inorganic contaminants remain in the cavity as ash and char (Liu et al., 2007). These residue products interact with groundwater after the gasifier shutdown when the natural groundwater head rebounds and water starts to fill the cavity. Natural flow of groundwater will leach residue products leading to groundwater pollution (Bhutto et al., 2013).

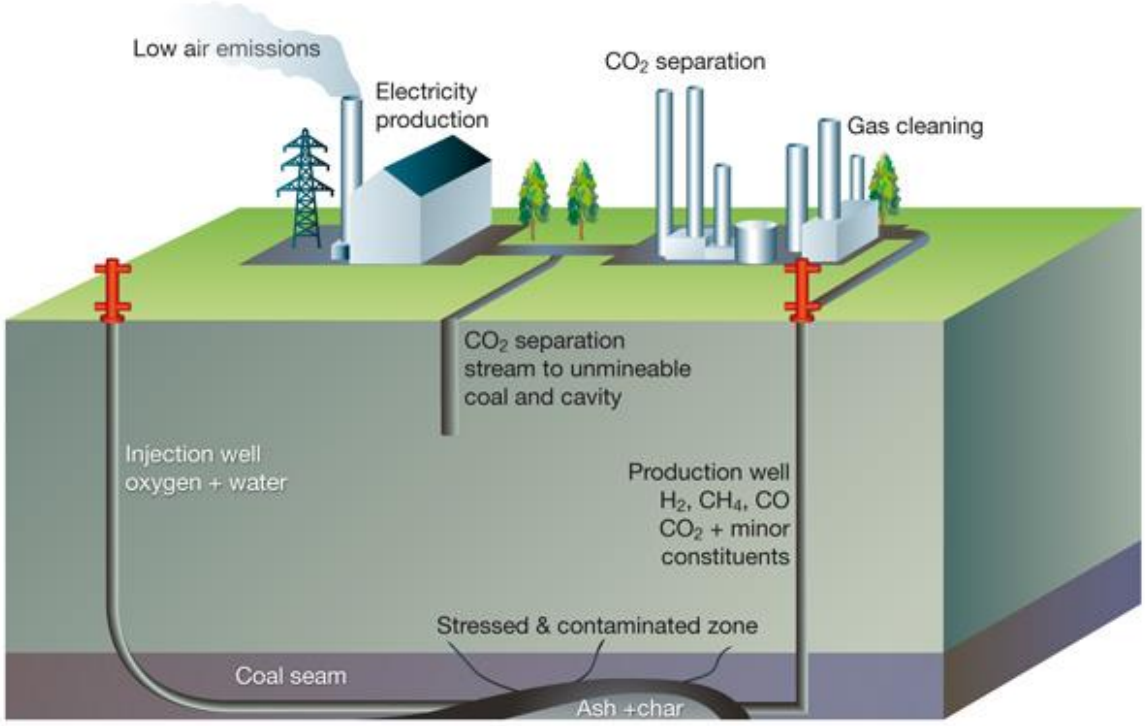

Figure 1-1 Outline of UCG process with CCS adapted from (Roddy and Younger, 2010)

Although considerable literature exists on the potential of groundwater contamination from UCG activities (Liu et al., 2007, Bhutto et al., 2013, Imran et al., 2014, Blinderman and Klimenko, 2018) however, these studies contain limited information on the geochemistry of residue products and leaching behaviour. The majority of existing literature only highlights the challenges associated with groundwater contamination without research that characterizes the impact that residue products have on groundwater. The impact on groundwater will be assessed in this study by determining the leaching dynamics of UCG residue products under site conditions and also under different chemical environments and hence making the results to have a world wide application.

1.2 Synthesis of literature

In 2012 the South African government released a roadmap for the country's vision leading to the year 2030 with the aim of improving the economy and living conditions of its citizens. The resultant document was called the National Development Plan (NDP), which charts the way forward for the country's development including on issues of energy security. Another key document that looks into South Africa's energy demands is the Integrated Energy Plan (IEP) which was published in the government gazette in 2019. The IEP is a forward-looking energy strategy that aims to deliver policy development and secure energy infrastructure.

Under the section looking into innovative and cleaner coal technologies the NDP states:

"There is potential to increase the efficiency of coal conversion, and any new coal power investments should incorporate the latest technology. As the existing fleet of old coal-fired power stations is replaced, significant reductions in carbon emissions could be achieved. Cleaner coal technologies will be supported through research and development and technology transfer agreements in ultra-

supercritical coal power plants, fluidised-bed combustion, ***underground coal gasification****, integrated gasification combined cycle plants, and carbon capture and storage, among others."*

There is clear support for UCG technology from the South African government as the integrated energy plan (IEP) 2019 also states:

"More funding should be targeted at long-term research focus areas in clean coal technologies such as CCS and ***UCG*** *as these will be essential in ensuring that South Africa continues to exploit its indigenous minerals responsibly and sustainably. Exploration to determine the extent of recoverable shale gas should be pursued and this needs to be supported by an enabling legal and regulatory framework."*

The legal and regulatory framework was spearheaded by the Minister of Water and Sanitation in October 2015, published in the government gazette, a notice in terms of section 38(1) and (4) of the National Water Act, 1998 (Act No. 36 of 1998). UCG was declared a controlled activity and that paved the way for the technology to be employed in South Africa. Even with government support, one of the challenges for UCG technology going commercial is the number of unknowns regarding potential groundwater contamination. While there is general acceptance on sources of organic groundwater contaminants emanating from incorrect operational mechanisms during the gasification stage, there is a knowledge gap in literature on inorganic contamination from residue products (Strugała-Wilczek and Stańczyk, 2016). This knowledge is key for governing authorities to regulate UCG projects going forward.

The main published research on ash and char from UCG is contained in studies from Poland (Kapusta and Stańczyk, 2011, Mocek et al., 2016, Strugała-Wilczek and Stańczyk, 2016) but the bulk of the studies are based on ex-situ gasification products. It is important to characterize in situ residue products since ex situ gasification of coal can produce different residue products as the operating conditions differ. This study will assess in situ UCG residue products from the Eskom UCG pilot plant in Majuba, South Africa. The research will further investigate the potential of acid generation from the gasification zone which is one of the major environmental concerns associated with coal mining. Acid rock drainage (ARD) involves oxidation of sulphide minerals that cause acidification of leachate and also increases the solubility of some environmentally toxic metals (As, Cd, Hg, Pb, Zn, etc)(Bouzahzah et al., 2015).

The outcomes of this study will provide key insights into the composition and evolution of UCG residue products and this information will be able to assist regulatory authorities in drafting regulations for environmental monitoring of UCG site in the future. With clear regulatory framework, regulators will be able to approve UCG projects. Rehabilitation of UCG sites can be planned efficiently with effective treatment as the leaching behaviour of residue products will be known. Furthermore, with appropriate characterization of residue products and leaching behaviour, UCG plants can modify their production processes to produce more environmentally friendly products.

1.3 Problem statement

The interaction of UCG residue products with groundwater has the potential for groundwater pollution in the surrounding aquifers. This is due the leaching of contaminants from the gasification zone into the local groundwater systems. Since groundwater is a valuable fresh water resource any

contamination becomes an environmental concern especially for regulatory authorities that are tasked with licencing activities such as UCG.

1.4 Aim of study

This research was part of the investigation into the gasification zone, using Eskom's Majuba UCG pilot plant as the main site of the study. The aim of the study is to investigate the geochemistry of the potential sources of groundwater contamination from the spent UCG chamber and their prospective chemical evolution. The objectives of the study can therefore be divided into two complementary sections:

1. Characterization of the geochemistry of the potential sources of groundwater contamination from the spent UCG chamber.
    - This aim will be achieved by undertaking geochemical and mineralogical characterization of residue products of UCG (ash, char, heat affected host rock). These products represents source-terms of groundwater contamination from the gasification zone.
2. Assessment of the chemical evolution of potential groundwater contaminants from the UCG chamber.
    - This will be determined through leaching tests under post gasification field conditions and expanded to different chemical environments for the results to have worldwide application.
    - Assessment of potential acid rock drainage from gasification products.
    - Field assessments relating to groundwater chemistry and evolution cycles.

1.5 Study Limitations

This research forms part of Eskom's Majuba UCG pilot plant investigation into the gasification zone after the successful shutdown of gasifier 1. The Eskom UCG team commissioned two Ph D studies where one researched the **organic** portion of the spent UCG chamber and the other the **inorganic**. This study represents the latter and is therefore limited to the **inorganic** pollutants **post-gasification**, however the associated organic components of the UCG process on the geochemistry of the post-gasification system will be assessed. The targeted coal seam was located at around 280 meter below surface and hence the study does not have surface geophysics data. This is due to the thick dolerite intrusions in the study area that eliminated most of the surface geophysical techniques, but borehole geophysical results and analysis will be presented. Some background information was unavailable as some of the tests done is this study were not done before the gasification stage (for example reflectance analysis of the pristine coal). This hence puts a limit in terms of comparison with pristine conditions.

1.6 Thesis outline

- Chapter 1 – Introduction;
- Chapter 2 – Study location;
- Chapter 3 – Literature review;
- Chapter 4 - Pyrometamorphism and mineralogical assessment of the spent gasifier;
- Chapter 5 – Petrographic and chemical analysis of coal relics from the spent geo-reactor;

- Chapter 6 – Acid base accounting and Leaching dynamics of post gasification products;
- Chapter 7 – Qualitative hydrogeological assessment of aquifers surrounding an underground coal gasification site;
- Chapter 8 – Conclusions and recommendations;

Appendices are included on a separate document included as a supplementary electronic disk. An online link to the appendices is also included below:

https://drive.google.com/drive/folders/1Yl6IGwB1yyEKN7p_MaCcrS-njSPJjsgR?usp=sharing

1.7 Summary

Chapter 1 provides background information on the research.. The main aim of the study is to assess the potential sources of groundwater contamination from the UCG gasification zone and their potential chemical evolution. A detailed study of the geochemistry of the gasification zone and interaction with groundwater provides a good basis for an environmental risk assessment of UCG sites. The assessment of the chemical reaction of UCG relics in varying conditions provides for extensive application of knowledge that can be applied in other UCG facilities worldwide. Overall, this research aim to provide insights into the geochemical characterization of in situ UCG residue products which is an area that is lacking in literature.

The next chapter is a detailed literature of the study area with special focus on the geological and hydrogeological aspects. This is important as UCG for an in situ based technology and therefore the hydrogeological conditions are paramount. The study site is located in Mpumalanga, South Africa, in the Majuba coalfield.

2 Site description

2.1 Regional Geology

The study site is found in the Majuba coalfield which forms part of the Vryheid formation of the Karoo Supergroup. Karoo Supergroup is the most extensive stratigraphic entity in south-central Africa and hosts all of the coal deposits found in this region (Figure 2-1). In South Africa it was formed in the Main Karoo Basin (MKB) which was part of the indigenous Gondwanan basins that originated through subduction, collision, compression and land deposition that occurred in the southern border of the supercontinent (Hancox and Götz, 2014). The MKB has an areal extend of around 550 000 Km^2 and is characterized as a foreland basin with the Cape Fold Belt forming the southern boundary while overlapping onto the Archean Kaapvaal Craton in the north (Cadle et al., 1993).

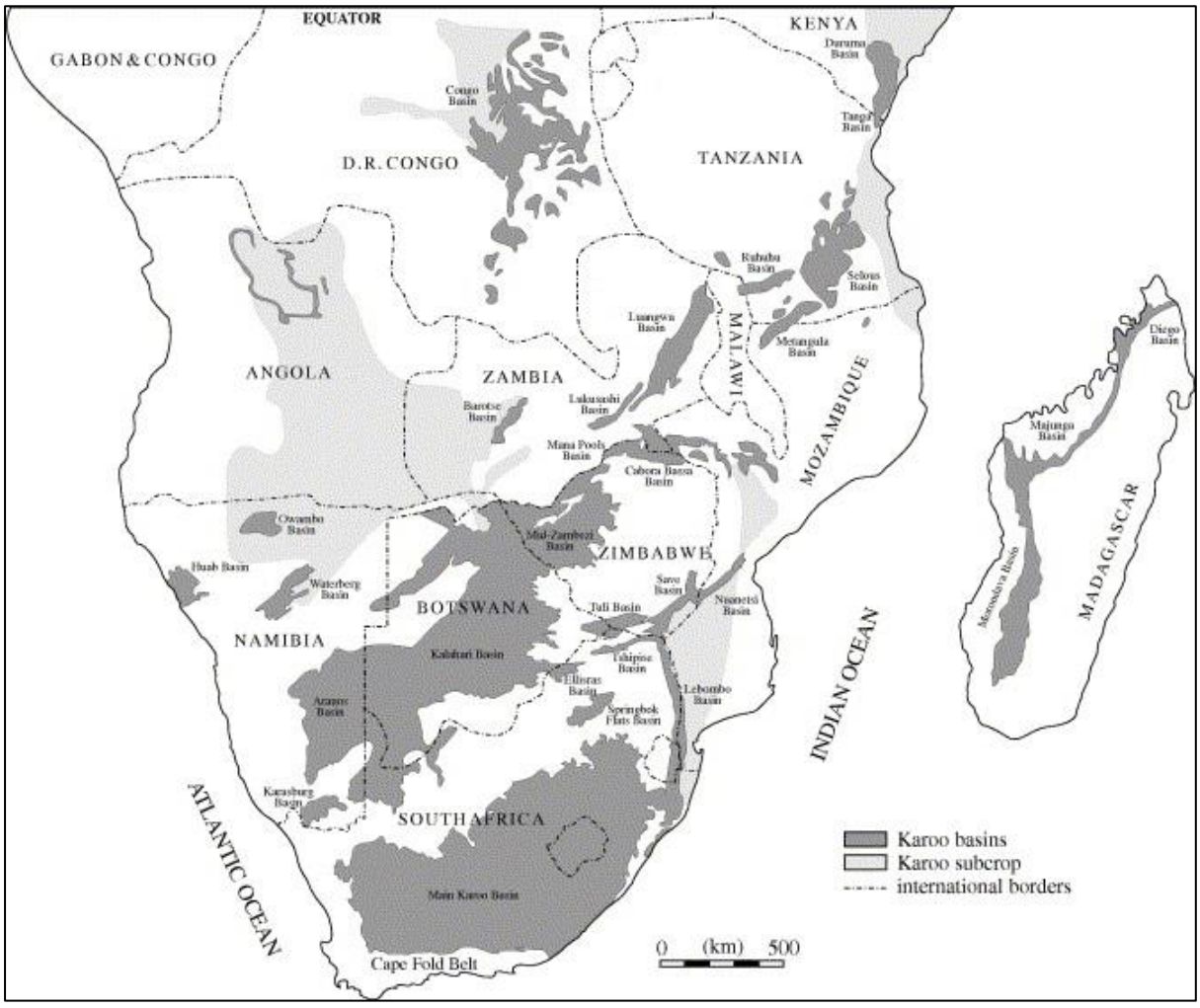

Figure 2-1 The dissemination of the Karoo basins in south-central Africa (Catuneanu et al., 2005)

Sediments filled the basin for about 120 million years during the period of Late Carboniferous to middle Jurassic until immense igneous activity replaced sediment accretion. During this time the climate changed from glacial to cool-warm temperate and ultimately to dry desert with shifting rain, and this combined with changing tectonic settings affected the sedimentary filling of the basin (Catuneanu et al., 2005). This resulted in a sequential sedimentary arrangement of the Karoo

Supergroup with the Carboniferous Dwyka as the bottommost formation followed by Ecca, Beaufort and Stormberg Group (Table 2-1). This sedimentary deposition was capped by the 1.4 km thick basaltic lavas of the Drankensberg Group which correlate with the Early Jurassic disintegration of Gondwana and the opening of the South Atlantic ocean (Flint et al., 2011, Hancox and Götz, 2014).

The Late Carboniferous to Early Permian Dwyka Group lies on a firm base of Precambrian glaciated bedrock in the Northern boundary of the MKB and in the east rests unconformably on the Namaqua-Natal Metamorphic Belt while overlain unconformably on the Cape Supergroup in the south (Figure 2-2) (Johnson et al., 1997). The Dwyka Group is thickest in the south and thins out towards the north and consists of tillite and other glacial associated rock forms (Lurie, 2008). Retreating and advancing ice sheets at the border of the basin deposited the sediments (Cadle et al., 1993). The glacial depositional environment have curved striated pavements in the rocks that illustrate the ice flow movement. The deposition of the Dwyka took place under varying tectonic conditions from the retroarc foreland arrangement of the MKB to the extensional basins towards the north (Catuneanu et al., 2005). This deposition was the precursor to the coal bearing formations of the Ecca group.

Table 2-1 Simplified stratigraphy of the Karoo Basin of southern Africa (north-eastern), coal bearing strata highlighted in grey (Lurie, 2008).

	PERIOD		GROUP	FORMATION / FACIES
MESOZOIC	JURASSIC		DRAKENSBURG	DRAKENSBURG
			STORMBERG	CLARENS
	TRIASSIC			ELLIOT FORMATION
				MOLTENO FORMATION
			UPPER BEAUFORT	TARKASTAD SUBGROUP
PALAEOZOIC	PERMIAN	UPPER	LOWER BEAUFORT	ADELAIDE SUBGROUP
		MIDDLE	ECCA GROUP	VOLKRUST/ GROOTEGELUK FORMATION
				VRYHEID FORMATION
		LOWER		PIETERMARITZBURG FORMATION
	CARBONIFEROUS		DWYKA GROUP	Tillite (Diamictite)

The Permian Ecca Group is made up of 16 formations which depict the lateral facies changes that define this geological unit (Johnson et al., 2006). The Group exhibits mostly continental deposition with plant fossils *Glossopteris* and *Gangamopteris* present amongst Ecca rocks, however short-lived marine intrusions are also evident (Lurie, 2008). Coal is predominantly found in the north-eastern Vryheid formation which is underlain by the Pietermaritzburg formation, Table 2-1. The Pietermaritzburg formation with a maximum thickness of 400 m represents shelf shales and overlies the Dwyka with a sharp contact in the northeast (Cadle et al., 1993, Johnson et al., 1997). It consists of upward coarsening dark grey laminated siltstones, mudrocks and subordinate sandstones (Hancox and Götz, 2014). The Pietermaritzburg formation thins out towards the north and outcrops mostly in the eastern boundary of the basin whilst underlying most of the Vryheid formation in the north-eastern parts (Johnson et al., 2006).

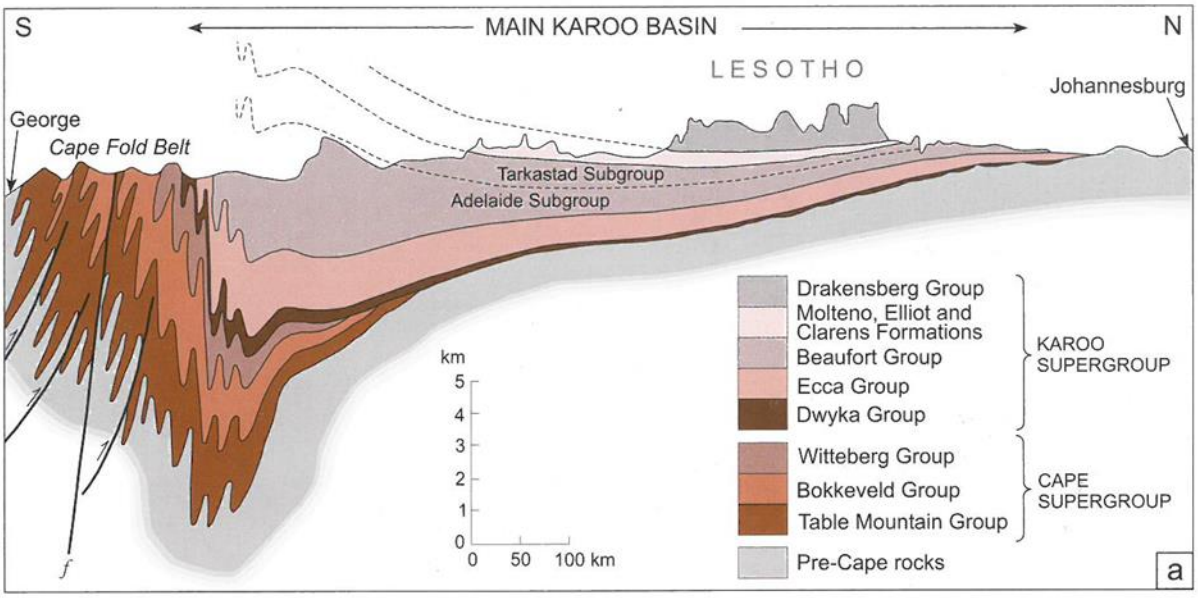

Figure 2-2 North South Cross section of the Karoo basin adapter from (Johnson et al., 1997)

The Vryheid formation has a maximum thickness of around 500 m and thins out in a siliciclastic wedge towards the south, west and northern parts (Johnson et al., 2006). In the north it lies directly on the pre-Karoo rocks or Dywka Group. The formation thins and pinches out in the south and south-west and has a gradational upper and lower contact with the shales of the Pietermaritzburg and Volkrust formations which consequently merge towards the south (Figure 2-3). The Vryheid formation denote deltaic, fluvial and shallow marine sediments that assembled in upper and lower delta plains and fluvial settings (de Oliveira and Cawthorn, 1999). Clastic sediment was initially deposited by deltaic systems upon which peat swamps developed, however this sediments were later modified by partial and total erosion by superimposed fluvial systems which sliced through already deposited deltaic sediment (Cairncross, 2001). The lithofacies contained within this formation form a vertical pattern of alternating sandstones, conglomerates, shales and the economic coal seams (Cadle et al., 1993).

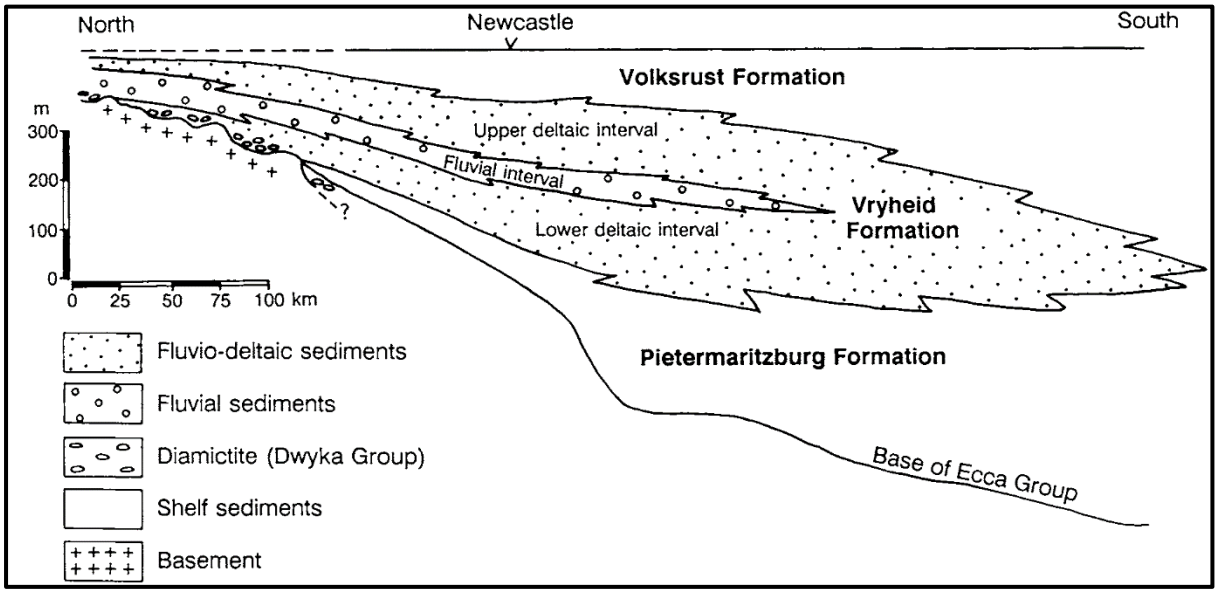

Figure 2-3 Schematic north-south section through the north-eastern part of the Ecca Group adapted from (Johnson et al., 1997)

The lithofacies are primarily organized in coarsening-upward cycles that have a deltaic character, however thin fining-upward fluvial cycles intervenes towards the middle of the formation (Johnson et al., 1997, Cairncross, 2001). A complete succession of each of the five coarsening-upward sequences begins with fine-grained marine sediments and grades upwards into coarser delta front and delta plain-fluvial facies (Hancox and Götz, 2014). The fluvial cycles transition upwards from coarse grained subordinate sandstones to fine grained sediments and coal seams (Figure 2-4). The sequence is laterally repetitive and its formation is attributed to braided streams or meandering rivers while the coal seams evolved as peat swamps developed on wide abandoned alluvial plains in cool temperate climate (Cadle et al., 1993, Johnson et al., 1997). The coal of the Vryheid formation on average comprises of higher inertinite content than the northern hemisphere coals and this suggest that the peat swamps were exposed to microbial attack and high level of oxidation, however marine transgressions eventually ended peat creation periods (Cadle et al., 1993, Cairncross, 2001).

The Vryheid formation is overlain by the mudrocks of the Volkrust formation which represent transgressive shelf sediments consisting mostly of mud deposited from suspension (Johnson et al., 2006). The sedimentology of the Volkrust formation shows a coarsening-upward trend with coal occurring interbedded with mudstones (Hancox and Götz, 2014). The Beaufort Group superseded the Ecca and consists of mudstones with interbedded sandstones. It is the formation that outcrops over the most surface area of South Africa (Lurie, 2008). The formation can be lithostratigraphically divided into the lower Adelaide and upper Tarkastad Subgroups. The Late Triassic Molteno formation lies lithostratigraphically above the Beaufort Group and also hosts coal seams. These Molteno coals are thin, laterally impersistent vitrinite rich coal seams which formed within aerially restricted swamps under warm temperate climate (Cadle et al., 1993). The Drakensburg group capped the sedimentation of the MKB with some 1.4 Km basaltic lava intrusions. This was accompanied by dolerite sills and dykes that are considered feeders to the Drakensburg lavas (Lurie, 2008). The intrusive sills affected the mineability of the coal as they displaced some of the coal seams causing structural problems and in some cases devolatilised the coal (Hancox and Götz, 2014). The coal rank encountered is generally medium to high-volatile bituminous coal but anthracite have been encountered in the eastern sections of the MKB (Cairncross, 2001).

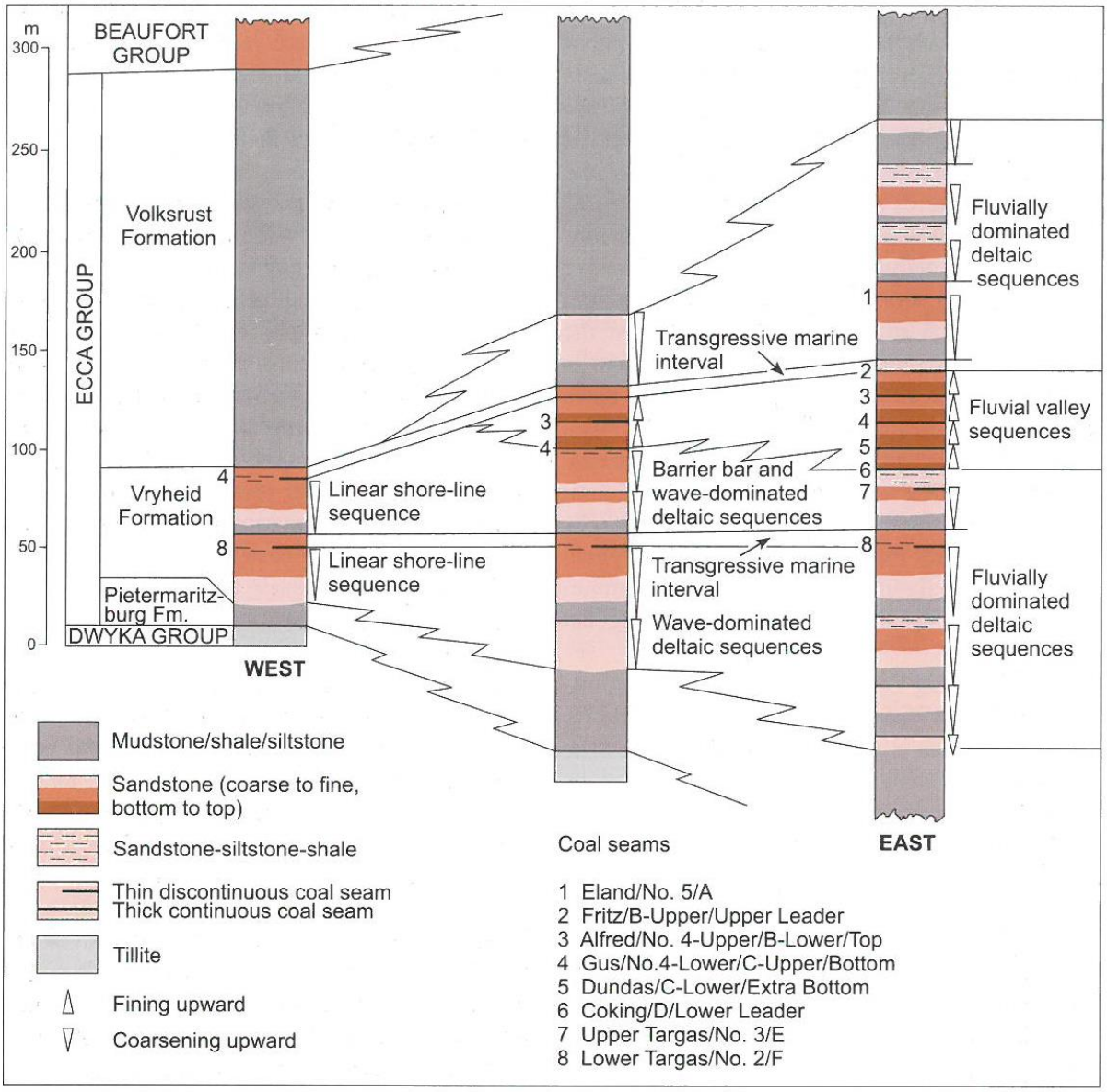

Figure 2-4 West-east section through Ecca Group in the northeastern part on MKB adapted from (Johnson et al., 1997)

2.2 Ermelo coalfield

The Ermelo coalfield is part of several coalfields that are part of the economic Vryheid formation. It lies east of the Highveld coalfield and towards the south of the Witbank coalfield (Figure 2-5). The coalfield has several collieries and hosts three coal fired power stations; Hendrina (2000 MW), Camden (1600 MW) and Majuba Power Station (4100 MW). The coalfield generally has thin coal seams which hosts Medium Rank C bituminous coal (Wagner et al., 2018). The placement of the coal seams is shown in (Figure 2-4) with the Eland on top and Targas as the bottom seam.

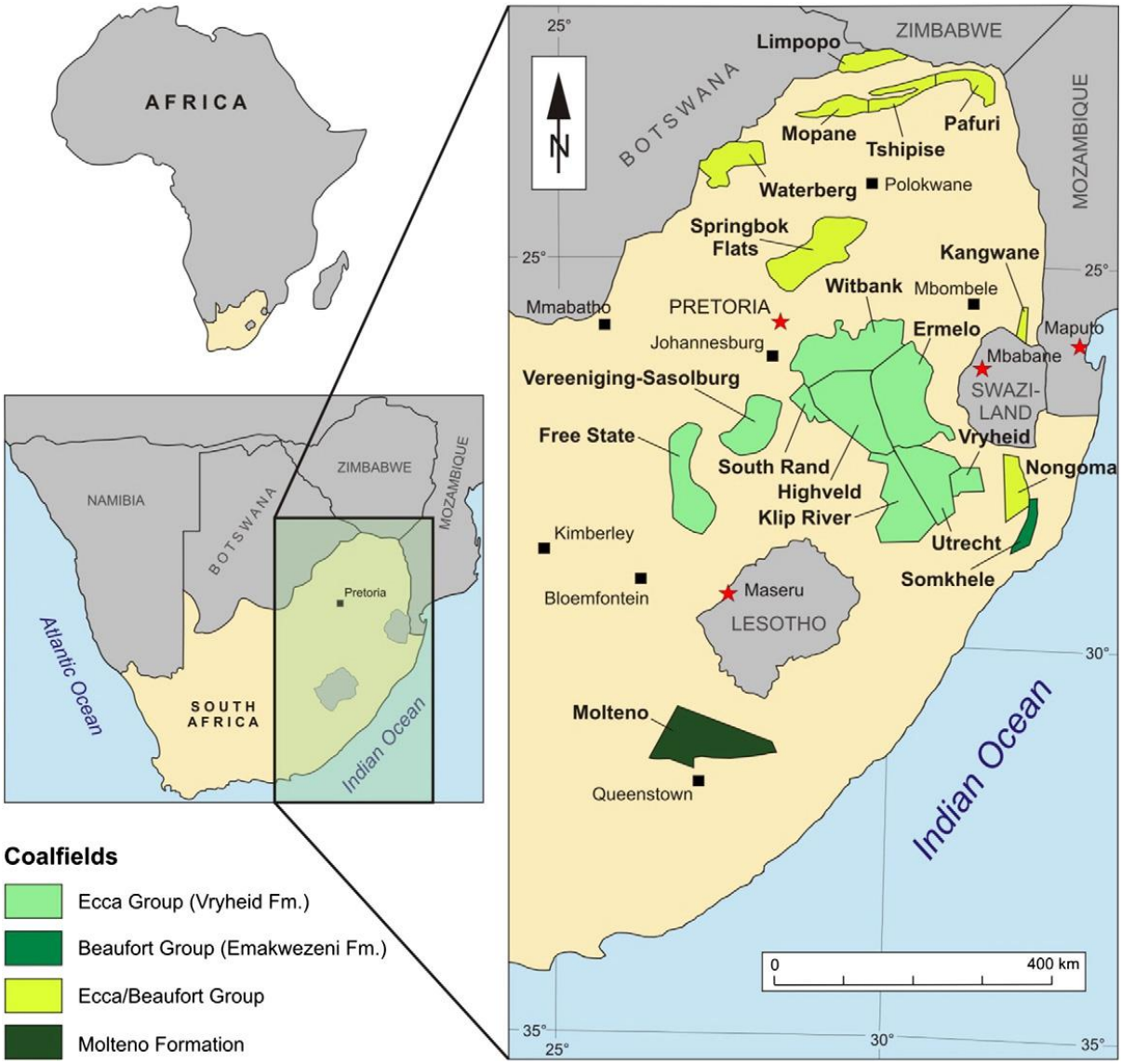

Figure 2-5 Coalfields of South Africa (Hancox and Götz, 2014)

The Ermelo coalfield consists of a number of isolated blocks which are found in an area bounded by Carolina, Morgenzon, Charlestown, Dirkiesdorp and Hendrina (Figure 2-6). Surface outcrops in the coalfield is dominated by Permian Vryheid rocks and the intrusive Jurassic aged dolerites (Hancox and Götz, 2014). Eight dolerite sills have been identified in the coalfield and have preserved coal from denudation but in some cases have altered it by displacement or devolatilization (Lurie, 2008). A number of collieries have developed in the area over the last few decades. In 1975, 3 Mt of coal was produced form three collieries and by 1985 ten collieries produced some 8 Mt, most of which came from the Usutu and Ermelo collieries (Snyman, 1998). In 2001 Ermelo coalfield contributed 7.2 Mt of the 222.551 Mt saleable production of coal from South Africa (Jeffrey, 2005). More recently, the Penumbra underground mine came into operation in 2011 with an average RoM production of 55,000 tpm and has a gross coal reserve of about 68.3 Mt (Hancox and Götz, 2014). The Majuba colliery which is located northwest of the town of Volkrust was commissioned in early 1980s to supply 12 Mt annually to the adjacent Majuba Power Station but due to adverse geological conditions (uplift of coal seam by dolerite dyke) the mine was closed in 1993 (Snyman, 1998). Eskom is currently exploring underground coal gasification technology to exploit the coal reserves in the now defunct Majuba colliery.

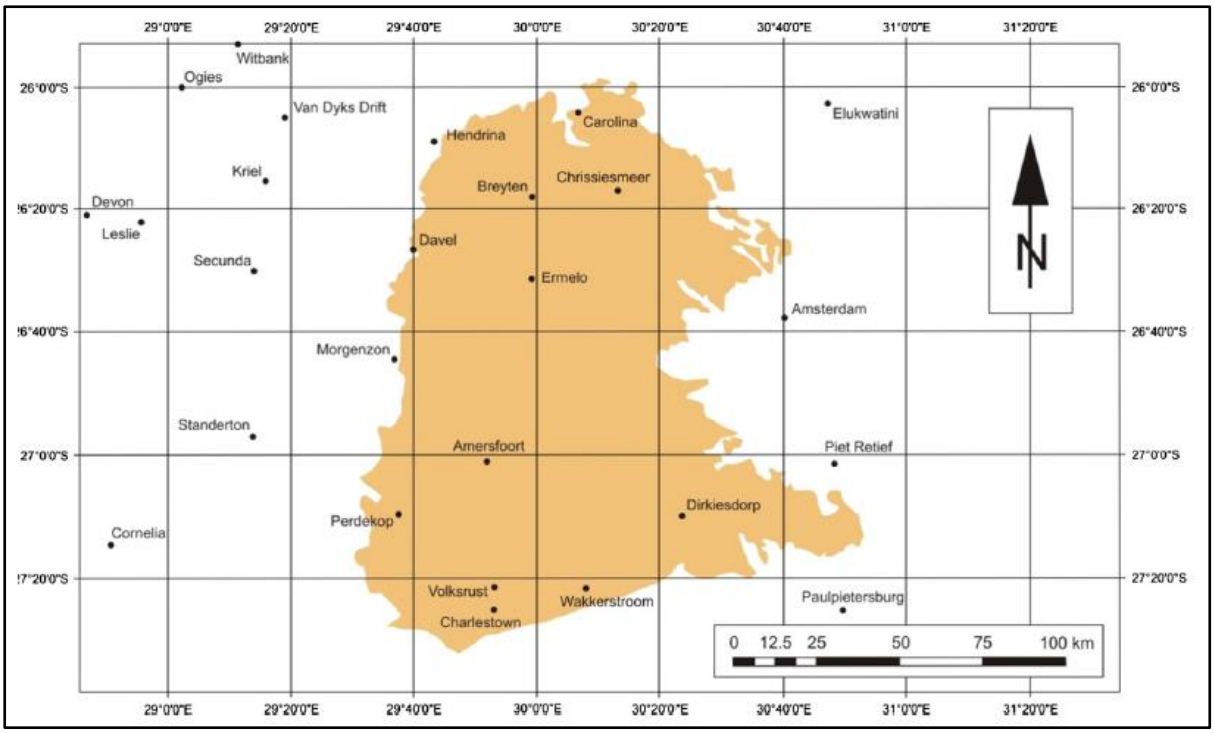

Figure 2-6 Geographical extent of the Ermelo coalfield (Hancox and Götz, 2014). Study site located north east of the town Volksrust

The coal seams encountered in the Ermelo coalfield are numbered either alphabetically or with names depending on the location (Table 2-2). They are correlated easier with seams of the Natal coalfields than the Witbank coalfields and fluctuate in various localities in quality, number and extent (Lurie, 2008). Seam A is therefore correlated with Eland, B with Alfred, C with Gus, and eventually E with Targas.

Table 2-2 coal seam correlations after (Snyman, 1998, Lurie, 2008)

Highveld coalfield	**Ermelo coalfield**		**Utrecht Coalfield**
	North	South	
No. 5	A	Eland	Eland
No. 4A	B	Alfred	Alfred
No. 4 Upper	C	Gus	Gus
No. 4 Lower	C-Lower	Dundas	Dundas
No. 3	D	Coking	Coking
No. 2	E	Targas	Targas

The coal seams of the Ermelo coalfield are generally horizontal to marginally undulating and are separated by upward fining sedimentary sequence of coarse-grained sandstones, siltstones and mudstones (Hancox and Götz, 2014). The general stratigraphic columns of Ermelo are shown in Figure 2-7 with various localities displayed from the coalfield. The overall coal quality is better than that of the Highveld and Witbank coalfield even though dolerite dykes and sills have devolatilized some of the coal seams (Wagner et al., 2018). The Gus seam is the most important economic deposit in the coalfield whilst Eland, Coking (D) and Targas are too thin for any economic importance (Hancox and Götz, 2014). The coalfield currently produces steam and beneficiated export coal with average coal

qualities of: CV = 22.57 MJ/Kg, ash = 26.74%, IM = 3.11%, VM = 23.64%, FC = 46.72% and TS = 1.65% (Wagner et al., 2018). Table 2-3 provides the summary of each seam from the Ermelo coalfield.

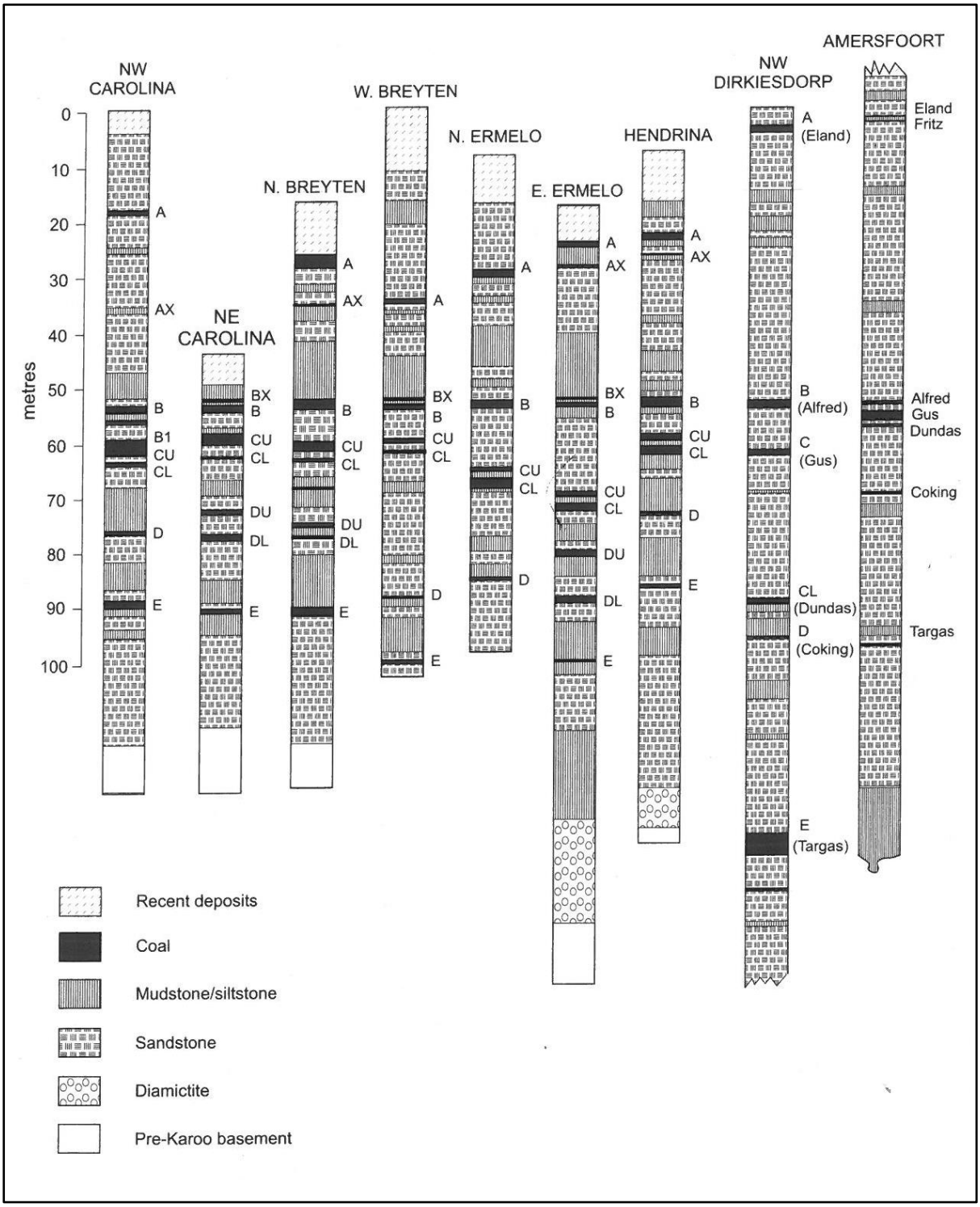

Figure 2-7 Simplified stratigraphic columns in the Ermelo coalfield (former Eastern Transvaal coalfield), adapted from (Snyman, 1998). The Amersfoort statigraphic column is the one that is relevant to the study area.

The Amersfoort stratigraphic column in Figure 2-7 shows the A seam divided into Alfred and Fritz coal seams respectively. The two seams can occur within 1 – 5 cm of each other separated by sediments. The economically important Gus seam is also found in close proximity (centimetres) of the Alfred and

Dundas seams. The position of the coal seams vary throughout the coal seam and in the Majuba area the coal seams can be displaced by over 70 m due to the dolerite sills (de Oliveira and Cawthorn, 1999).

Table 2-3 Description of Ermelo coal seam (raw coal analysis), summarised from (Snyman, 1998, Jeffrey, 2005, Lurie, 2008, Hancox and Götz, 2014, Wagner et al., 2018)

Seam	Description
Eland	Between 0 – 1.5 m in thickness, not economic. Eroded in most part of the coalfield and becomes shaly in the south. Raw coal qualities in Sheepmoor area: CV = 27.27 MJ/Kg, Ash = 11.93%, IM = 0.39%, VM = 3.85%, and TS = 0.39%.
Alfred	2 – 4 m thick, low quality dull coal with alternating bands of poor and fair coal. In places Alfred seam (B seam) may be split into three separate plies; B1, B and BX. CV = 23.31 MJ/Kg, Ash = 24.86%, FC = 48.98%, IM = 0.39%, VM = 23.42%, and TS = 2.5%.
Gus	This is the most important economic seam throughout the Ermelo coalfield. It is has sandstone, siltstone or mudstone that split the seam into partings of varying thickness. Seam is well developed over the whole coalfield and attains thickness of 0.7 – 4 m. CV = 22.28 MJ/Kg, Ash = 24.96%, FC = 46.59%, IM = 3.36%, VM = 23.34%, and TS = 1.3%.
Dundas	Thin seam (0.5 – 2 m) and not developed over the whole coalfield. It is of little economic significance when considered alone but has opencast potential when explored with other seams. CV = 24 MJ/Kg, Ash = 24.79%, FC = 45.75%, IM = 2.86%, VM = 23.34%, and TS = 1.47%.
Coking	Well developed in the north where it attains thickness on over 3 m, but economic potential drops southwards as it converts torbanitic and/or shaly. CV = 22.68 MJ/Kg, Ash = 26.74%, FC = 45.36%, IM = 1.65%, VM = 24.57%.
Targas	0.3 – 1.3 m thick and of good quality where developed.

2.3 Majuba colliery

The Majuba colliery is located in Mpumalanga Province to the south of the town Amersfoot (Figure 2-8). It was commissioned in the early 1980s by Eskom and Rand Coal to supply 12 Mtpa of coal to the 3600 MW Majuba Power Station over a 40 year period (de Oliveira and Cawthorn, 1999). The reserve was estimated at 1 billion tons from the Gus seam that was located at depths of around 250 to 420 m below surface. This was determined from over 400 drill holes in an area of around 32 000 hectares (Chapman and Cairncross, 1992). Recent estimations by (Pershad et al., 2018a) put the resource estimate at 8 billion tons, mostly being classified as undeveloped.

The stratigraphic sequence of the Majuba colliery is given in Figure 2-7 under the Amersfoot column which shows the economic Vryheid formation. A detailed geological study of the coalfield is given by (de Oliveira and Cawthorn, 1999) where the base of the stratigraphic sequence begins with a pink-coloured granitic gneiss comprising of quartz, microcline, plagioclase and biotite, and is capped by a layered ultramafic intrusion which represent Pre-Karoo rocks. The Dwyka rocks overly the Pre-Karoo rocks with a total thickness of between a few centimetres to 36 m and consists of tillite, varved mudstone, fine-grained massive sandstones and conglomerates (Snyman, 1998, de Oliveira and Cawthorn, 1999). The Ecca group overlies the Dywka and has the Pietermarizburg formation at the base. The Pietermarizburg formation in Majuba consists of a massive dark shaley siltstone of around 20 m thick and underlies the Vryheid formation with a gradational contact (Pershad et al., 2018a). The

Vryheid formation overlies the Pietermarizburg formation, also with gradational contact and hosts all the coal seams in the Majuba colliery.

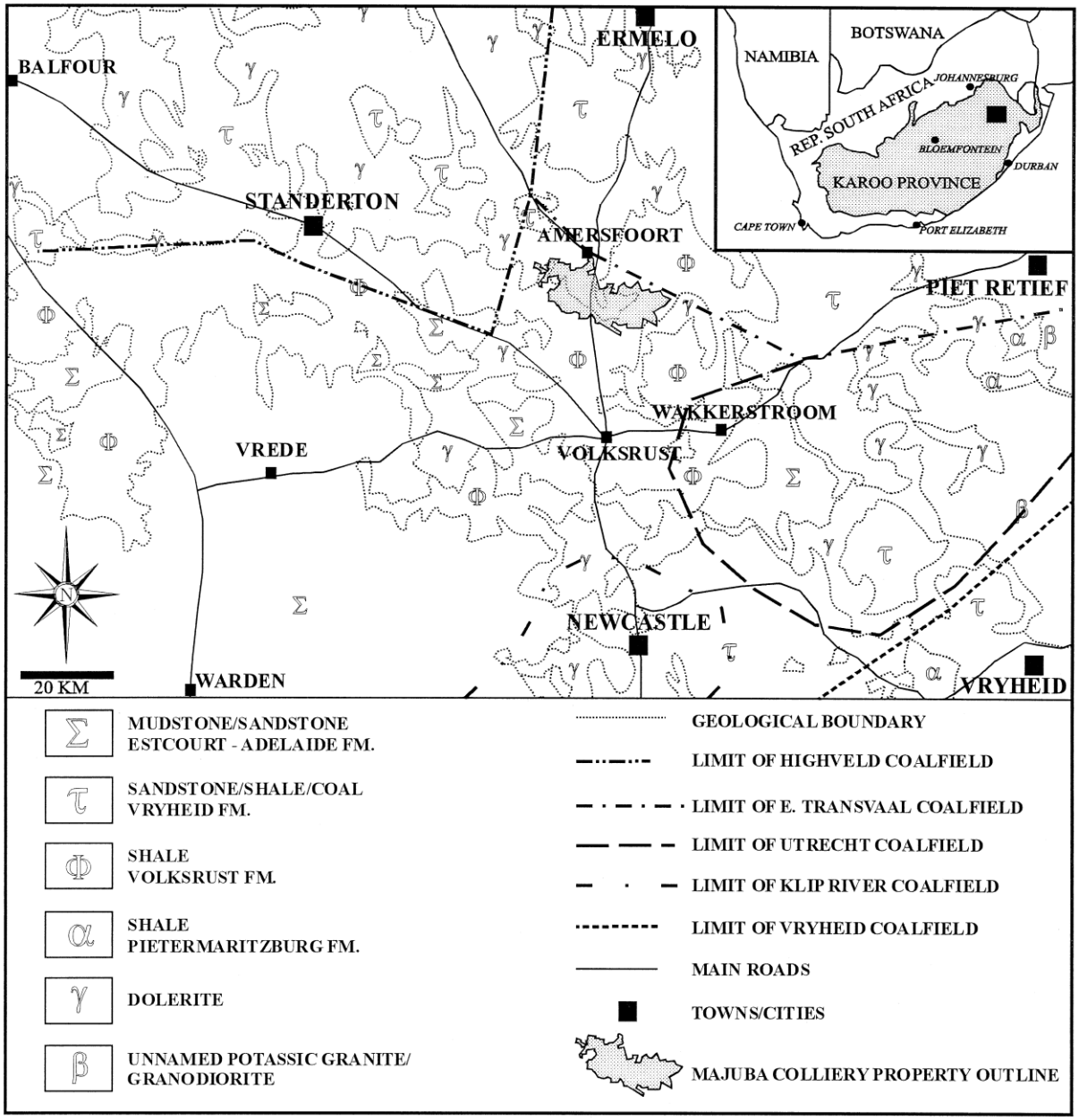

Figure 2-8 Simplified geological map of the Majuba colliery and surrounding area, adapted from (de Oliveira and Cawthorn, 1999)

The coal zone comprises of a few thin (5 – 20 cm) horizontally discontinuous bright coal seams below the Gus seam (de Oliveira and Cawthorn, 1999). Figure 2-7 depicts Targas, Coking and Dundas as the coal seams found underneath Gus seam, with Dundas just a few meters below. The Gus seam fluctuates in thickness from 1.8 to 4.5 m and consists of a lower bright layer (20 to 80 cm), a middle dull layer (over 1 m) and a bright upper layer (30cm) (de Oliveira and Cawthorn, 1999). The floor of the Gus seam is a laminated carbonaceous siltstone and the roof a coarse grained sandstone taken as an abrasive fluvial channel but varies horizontally to a laminated siltstone and finer grained sandstone which represents interchanneled zones (Pershad et al., 2018a). Alfred coal seam is encountered above the Gus seam and varies in thickness from 10 cm to 1.5 m (de Oliveira and Cawthorn, 1999). This seam

is laterally impersistent, meaning it is horizontally discontinuous and it is not found throughout the coalfield. Where it is developed, the Gus-Alfred parting changes in thickness from a few centimetres to over 10 m (Chapman and Cairncross, 1992). A sedimentary sequence dominated by sandstones which fines upwards is prevalent above the Alfred for 30 – 50 m until two thin bright coal seams (Fritz and Eland) are intercepted and are generally less than 2 m apart (Chapman and Cairncross, 1992). Fritz and Eland are on average 40 and 55 cm thick respectively, and are found to be laterally continuous and hence play a key role as markers in the coalfield (de Oliveira and Cawthorn, 1999).

Altogether the sedimentary sequences in the coal zone fine upwards, beginning with coarse grained sandstones and granulestones at the base of each unit, grading upwards into finer-grained sandstones or siltstones eventually being capped by coal formation in some places (Chapman and Cairncross, 1992). There is no coal seams encountered above the Eland and the sequence becomes gradually fine grained and siltstone dominated which suggests that at some point it progressively passes into the Volksrust formation (Chapman and Cairncross, 1992). The Volksrust formation exists in Majuba in dispersed remnants observed in surface outcrops (Figure 2-8) and preserved between dolerite sills in core drills and generally consists of dark grey sandy siltstones with a uniform grain-size (de Oliveira and Cawthorn, 1999). The sedimentary sequence is intruded and disturbed by the Jurassic dolerite units.

2.3.1 Dolerite intrusions

Intrusions of dolerite dykes and sills are regular developments throughout the Karoo Supergroup (Lurie, 2008). These intrusions were controlled by lithostatic pressure and happened along cracks and fissures caused by tension (Pershad et al., 2018a). In the Majuba area (de Oliveira and Cawthorn, 1999) identified four different groups of dolerite intrusions, T1 to T4, as shown in Figure 2-9 and described in Table 2-4. The morphology of these intrusive rocks are classified as near horizontal sheets, transgressive sills and near vertical dikes (Pershad et al., 2018a). T1 and T2 are relatively flat with the former having the upper contact eroded due to proximity to the surface. T2 is a porphyritic homogenous dolerite that is defined by highly altered zone at the base contact due to primary minerals transforming to secondary minerals under hydrothermal action (de Oliveira and Cawthorn, 1999). This causes the dolerite to crumble when exposed to the atmosphere and can be classified as a “sugary” dolerite.

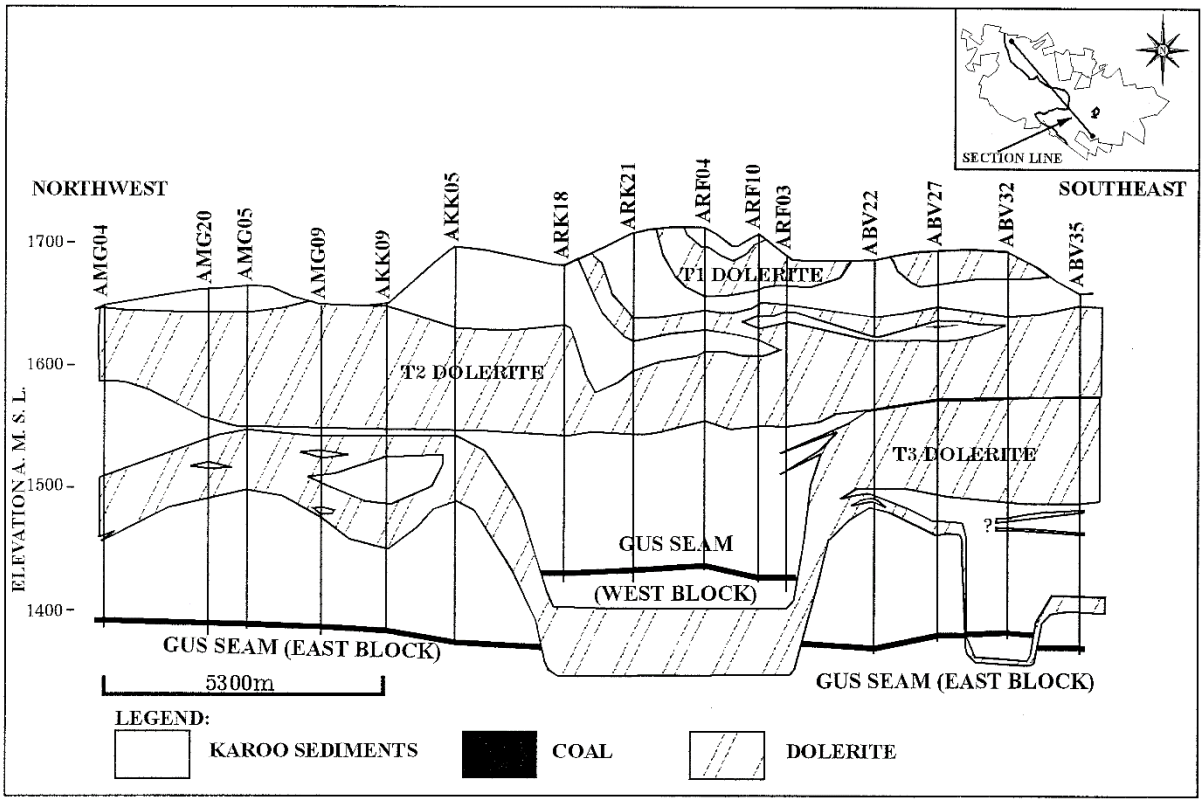

Figure 2-9 Cross section across the Majuba colleiry showing the Gus seam elevation due to transgressive dolerite intrusion that resulted in the area divided into blocks (de Oliveira and Cawthorn, 1999)

T3 and T4 are transgressive with T3 responsible for lifting the sedimentary package by some 70 m as seen in the west block relative to the east block section (Figure 2-9). The dolerite intrusions have left the sedimentary package structurally and metamorphically disrupted which resulted in a complex network within the coal bearing Vryheid formation (Pershad et al., 2018a). These intrusions also devolatilized the coal and in some instances formed natural coke negatively affecting its strength close to the contact zones with the dolerite (Snyman, 1998). This subsequently affected mining in the Majuba Colliery where the original plan of mining the Gus seam using long wall mining method had to be changed to bord and pillar mining but the adverse nature and structural complexity of the dolerite intrusions caused all underground mining to be abandoned with only 611 000 tonnes produced (Hancox and Götz, 2014). Mining through a dolerite that cuts a coal seam results in high mining costs and reduced production because of inaccessible and devolatilized coal. It is therefore imperative to delineate as accurately as possible the thickness and structure of the dolerite intrusions for mine planning purposes (Snyman, 1998).

Table 2-4 Summary of characteristic features of the dolerites in Majuba colliery after (de Oliveira and Cawthorn, 1999)

Dolerite	Description	Morphology and average thickness
T1	Medium-grained and dark grey with calcite and quartz veins running through the rock. Major mineral is plagioclase (± 55%), clinopyroxenes (± 30%), orthopyroxene (± 10%) and minor olivine, apatite and oxides.	Relatively planar > 50 m thick
T2	Porphyritic and highly altered dolerite with a propensity to crumble when exposed to atmospheric conditions. Major mineral is plagioclase (± 65%), clinopyroxenes (± 15%), orthopyroxene (± 15%) and rare olivine and oxides. Ophitic to subophitic texture.	Relatively planar 70 m thick
T3	Light grey to olive green porphyritic rock with a characteristic plagioclase glomeroporphyritic texture.	Transgressive 62 m thick
T4	Seldom recovered intact and is generally crumbly disintegrated material due to fast alteration.	Transgressive 8 m thick

2.4 Majuba underground coal gasification (UCG) site characterization

2.4.1 Background

The Majuba UCG plant was piloted by the South African state owned company Eskom Holdings SOC Ltd (Eskom) in 2007. Eskom generates approximately 90% of electricity is South Africa utilizing a mixture of primary sources of energy including coal, nuclear, hydro, diesel and wind to produce a combined total capacity of about 42 810 megawatts (Pershad et al., 2018a). Most of the electricity is generated from coal with about 36 441 megawatts generated by coal fired power stations. UCG is one of a few clean coal technologies that Eskom is developing in order to meet the energy mix envisaged in the Integrated Energy Plan (IRP) set out by the South African government (DOE, 2016). Dr. Mark van der Riet pioneered the Eskom UCG research in 2002 as part of the Research, Testing and Development (RT&D) of Eskom's Sustainability Division. Eskom sourced and developed UCG expertise from technology provider Ergo Exergy Technologies Inc. (Canada) (Pershad et al., 2018a). Initial groundwork began around 2001 and a pilot plant was successfully commissioned at Majuba coalfield in January 2007 with product gas being co-fired into the nearby Majuba Power station by October 2010. The Majuba pilot plant was successfully operated through to September 2011 when decommissioning commenced with the shutdown of the gasifier (G1). The gasifier was formally declared shutdown in June 2015 (Pershad et al., 2018a). An areal view of the site is given in Figure 2-10.

The successful performance and shutdown of the Majuba UCG pilot plant is a significant step towards full commercialization of UCG technology as this is the first UCG plant in Africa. The successful shutdown of G1 presented an opportunity to investigate some of the key environmental questions regarding groundwater contamination. The project has successfully embarked on a drilling exercise to recover residue samples from the gasification zone through what is termed verification drilling. Verification drilling is diamond core drilling from surface into the gasification zone with the aim of retrieving core samples.

Figure 2-10 An areal view of the Majuba UCG pilot plant, adapted from (Pershad et al., 2018a)

The successful recovery of ash, char and heat-affected strata provides key insights into the geochemistry of the gasification chamber as these products are regarded as potential sources of groundwater contamination. The geological data from the extensive core and percussion drilling on site also provides an opportunity to generate a three dimensional (3-D) geological model of the site which will be used to assess the geological profile and geophysical analysis of the study area.

2.4.2 Locality and site description

The Majuba UCG pilot plant is located in Mpumalanga Province of South Africa, about 35 km north-west of the town of Volkrust and 10 km south-west of the town of Amersfoort. The site is 5 km north-east of the 3 600 MW Majuba Power Station (Figure 2-11). The two sites are linked by a gas pipeline that is designed to convey production gas from the UCG site to the boilers of the Power Station for electricity generation.

The surface area is characterized by regular hills attributed to the erosion of the underlying dolerite sill. The site covers an area of around 60 ha on the eastern bank of the Witbankspruit River (Geelklipspruit in Figure 2-11). The drainage in the area is good and surface water flows through several sporadic streams. Annual rainfall is at an average of ~650 mm with the rainy season usually from October to March where 125 – 150 mm of rain may fall in a single day (Pershad et al., 2018a). The surrounding area is used mainly for agricultural purposes such as sheep and cattle farming and to a lesser extent crop cultivation. The elevation varies between 1660 to 1744 meters above sea level (MASL) with river channels forming cliff features (Figure 2-12).

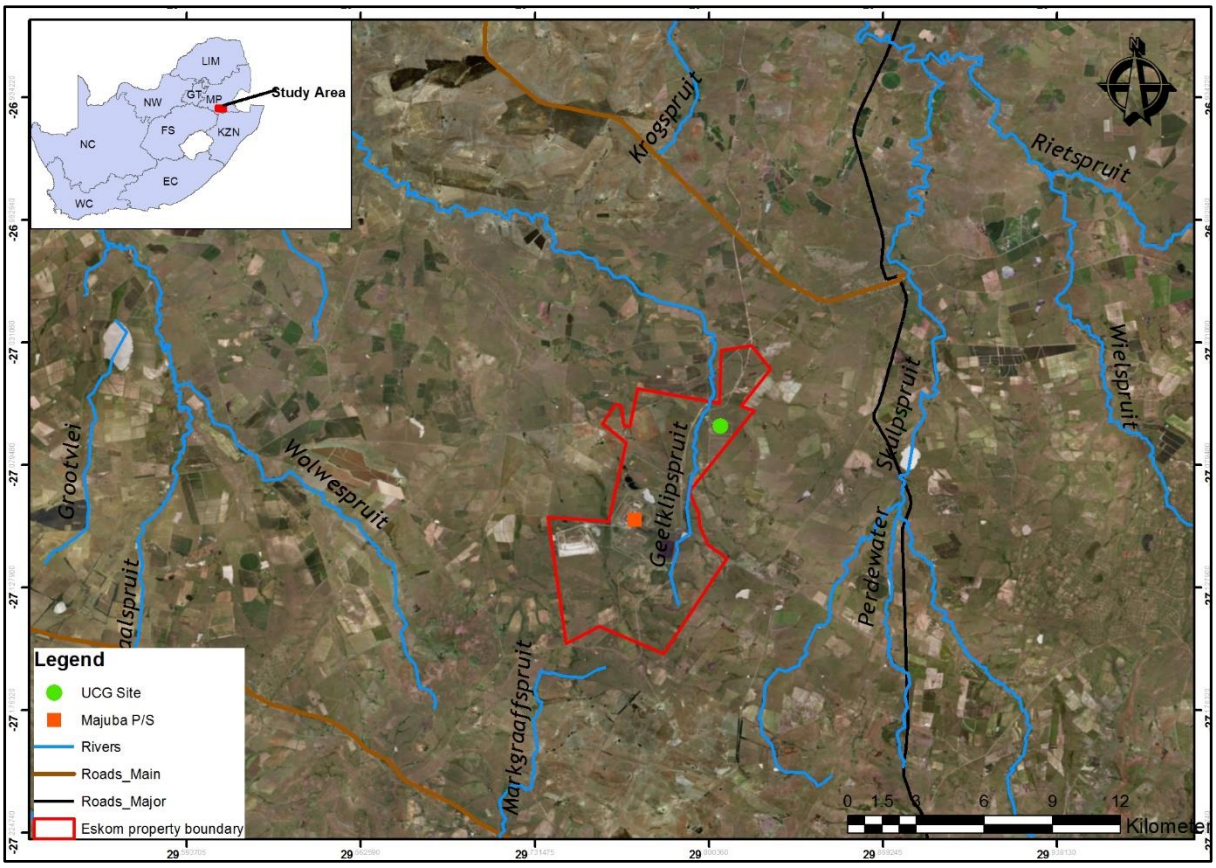

Figure 2-11 Location and surface drainage map of the study area

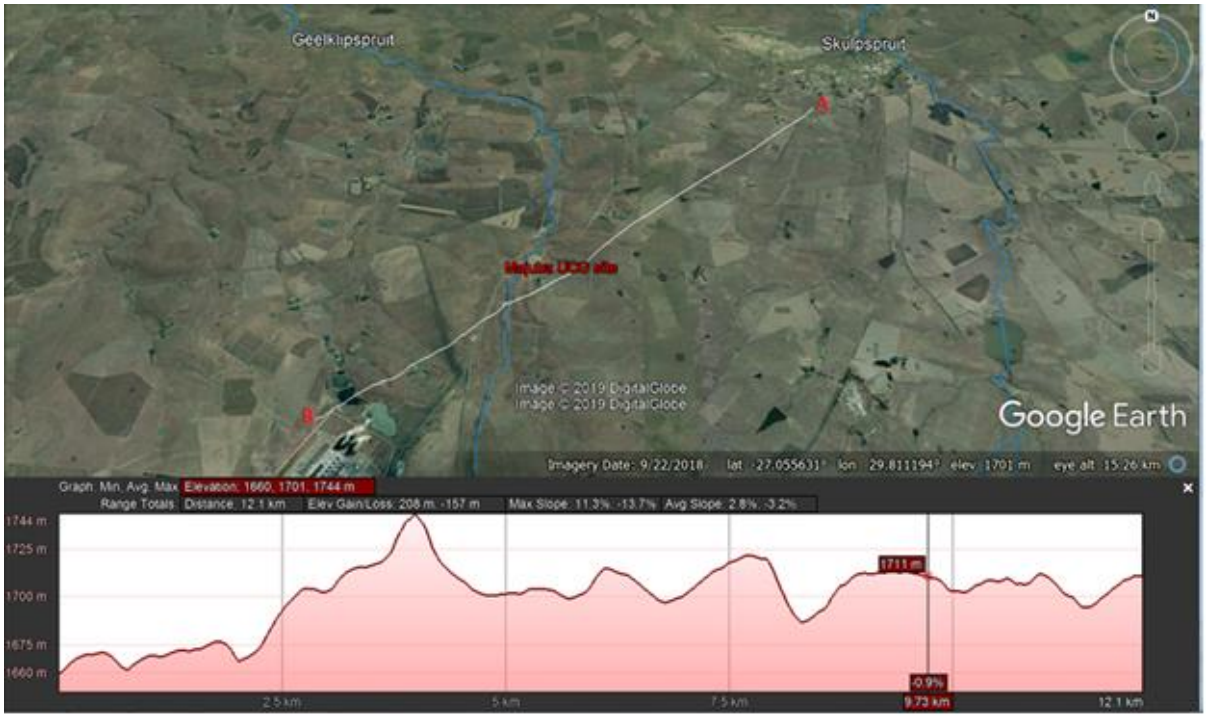

Figure 2-12 Elevation map showing the topography profile of line A-B cutting through the Majuba UCG site

2.4.3 Geology

The Majuba UCG pilot plant is located on the Roodekopjes farm where the intrusive Jurassic dolerite sills are widespread on the surface (Figure 2-13). The sills outcrop in most of the area forming complex networks that transgress the sedimentary package of the Pietermaritzburg, Vryheid and Volkrust formations. The Volkrust formation is also widespread and in the Majuba area is the youngest sedimentary formation outcropping in most areas. There are sporadic outcrops of the Vryheid formation while the Pietermaritzburg formation rarely outcrops.

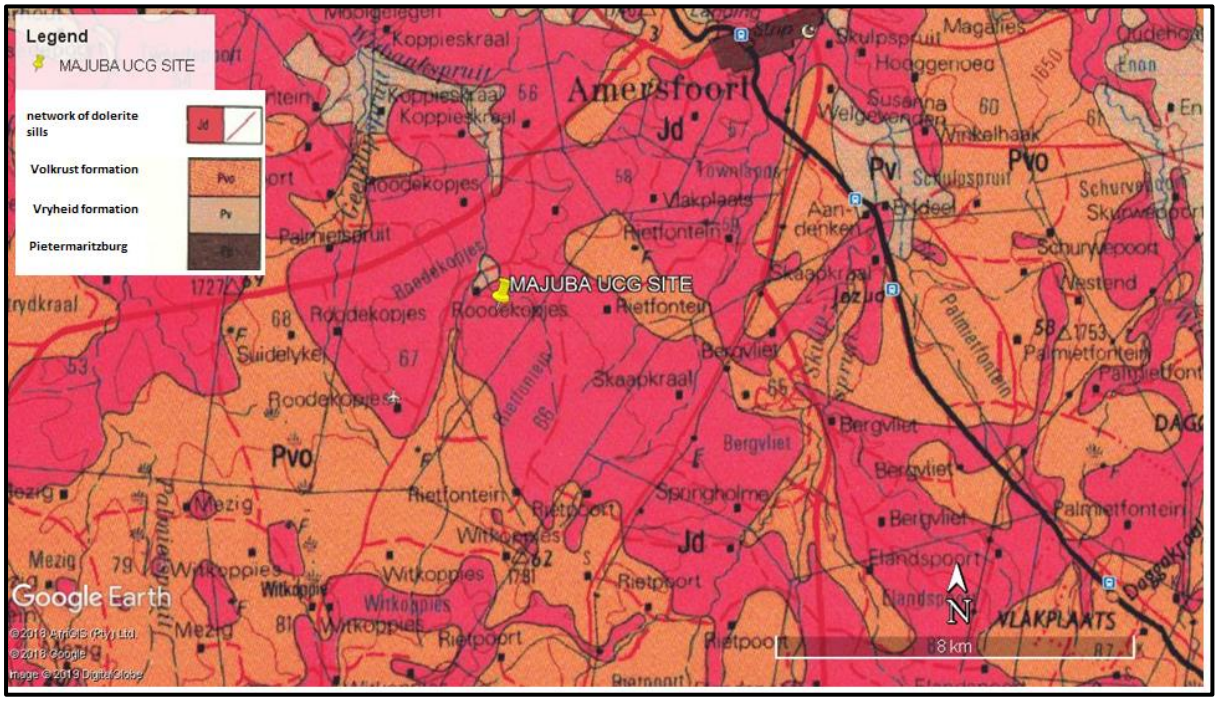

Figure 2-13 Geological map of the Majuba UCG site and surrounding areas

Detailed geological sequence was discussed in section 2.2. The local stratigraphic column of the Majuba UCG site is presented in Figure 2-14.

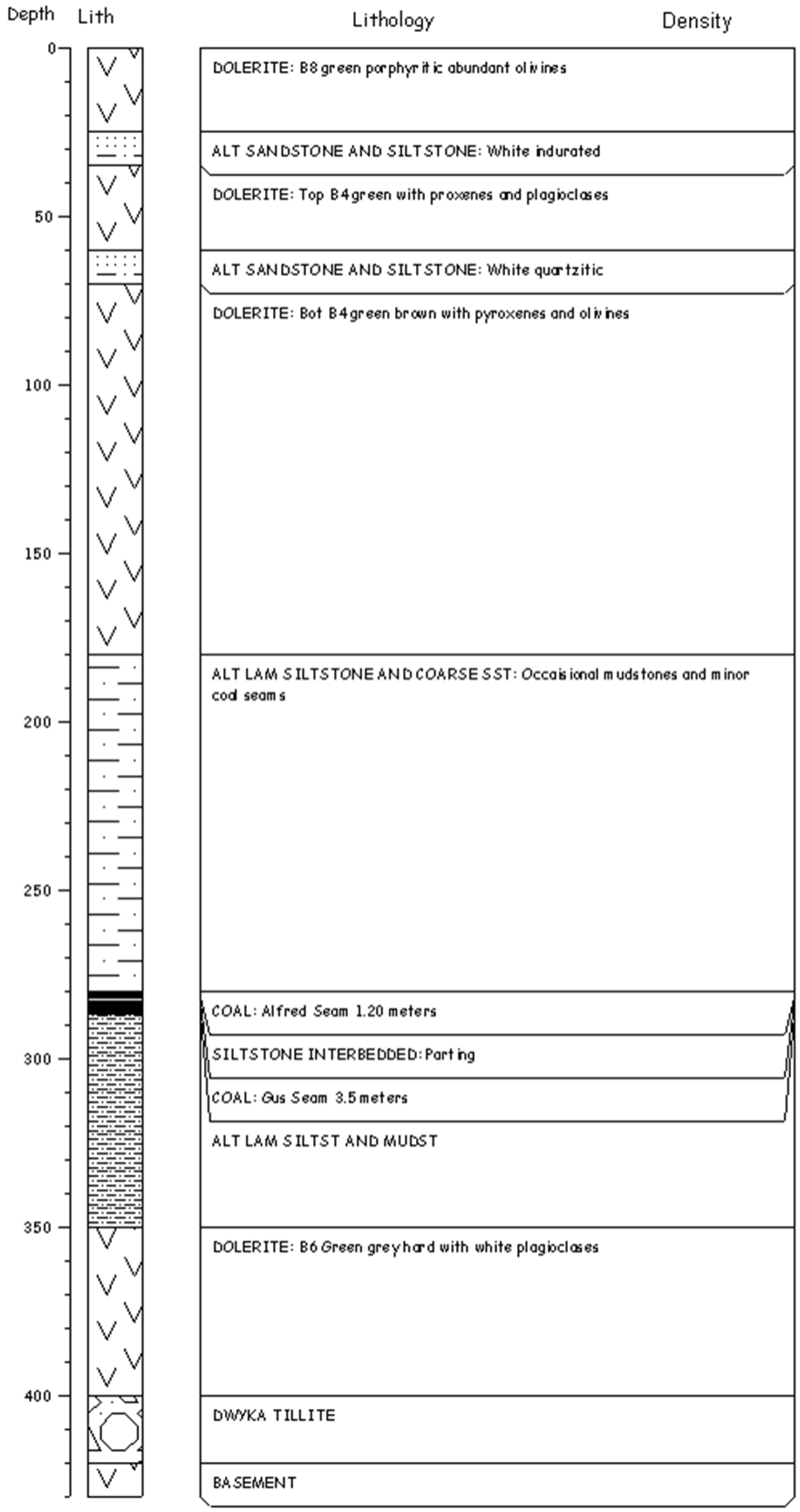

Figure 2-14 Example of local geological stratigraphy of the Majuba UCG pilot site (Pershad et al., 2018a).

The Basement rocks which form the pre-Karoo rocks are found at 400 m below the surface with Dwyka tillite overlying it with a thickness of around 50 m. The upward-coarsening trend of alternating

laminated siltstone and mudstone begins at around 350 m and it is capped by the coal zone with the economic Gus seam located at around 280 m below the surface. A few centimeters above the Gus is the Alfred seam, but it is horizontally discontinuous and therefore is not encountered throughout the Majuba UCG area. The sedimentary sequence continues upwards and is generally characterized by alternating laminated siltstone and coarse sandstones. Thin coal seams, namely Eland and Fritz, are encountered further up around 230 m below the surface. A dolerite sill (T2) is encountered around 170 m and has a thickness of ~100 m. This dolerite sill is susceptible to crumbling when exposed to the atmosphere as seen in Figure 2-15.

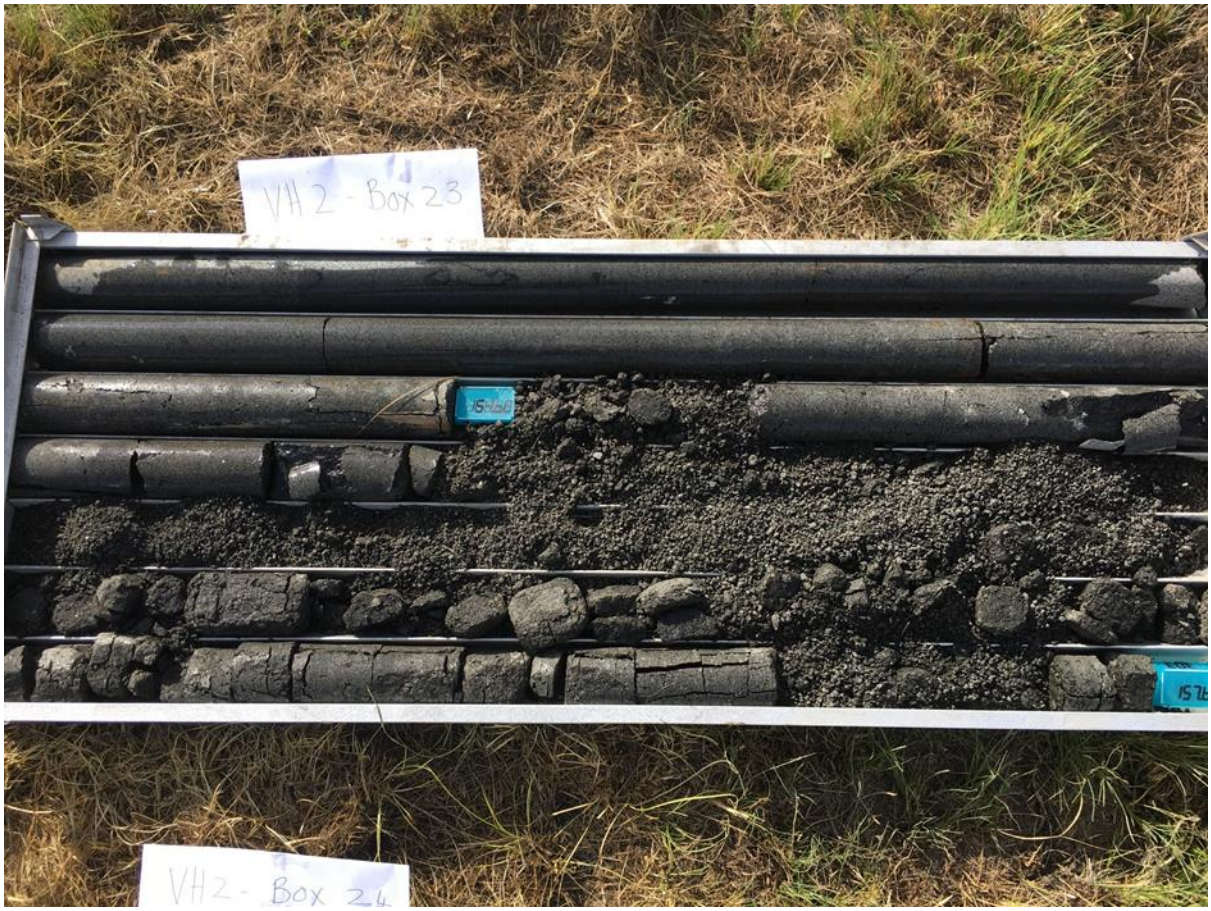

Figure 2-15 Core of the dolerite sill (T2) crumbling when exposed to the atmosphere, "sugary dolerite"

The sedimentary package is further transgressed by the T1 dolerite which at places spits into several transgressive units. The T1 dolerite is heavily weathered and allows flow of groundwater in its matrix.

2.4.4 Geohydrology

A number of distinct groundwater systems are present at the Majuba UCG site, as seen in (Figure 2-17). The upper weathered (shallow) aquifer is low-yielding (hydraulic conductivity (K) range: 1.7 x 10^{-1} – 8.6 x 10^{-3} m/d) owing to its trivial thickness, but the water quality is good due to years of groundwater flow through the weathered strata. It is estimated that the shallow aquifer is present from surface level to around the depth of 70 m. It is underlain by the intermediate aquifer. Correlation between groundwater levels and topography is low, 41.4 %, and therefore groundwater flow does not

follow topography in the shallow aquifer (Figure 2-16), this is possibly due to groundwater flowing in weathered channels within the dolerite instead on vertical percolation that takes place in alluvium. Groundwater data for the shallow aquifer is included in appendix 2-A.

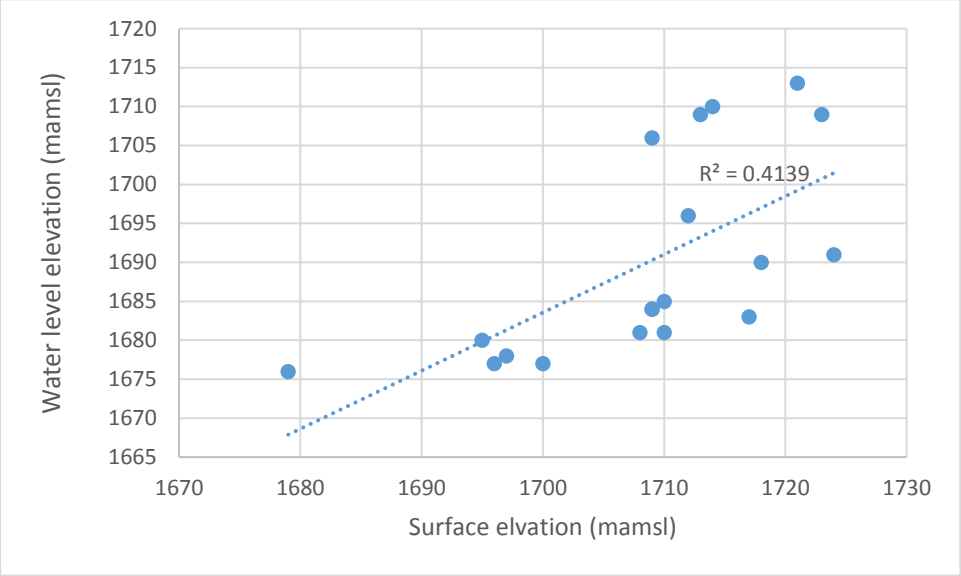

Figure 2-16 Hydraulic head correlation

Groundwater flow through the intermediate aquifer is mainly through fractures, cracks, and joints as the Karoo sediments are excessively cemented, which prevents any substantial infiltration of water. The aquifer can be divided into two zones – the intermediate upper aquifer (IU) and the intermediate lower (IL) aquifer as seen in Figure 2-17. Groundwater flow in the intermediate lower aquifer is mainly through cracks in the lower part of T2 dolerite where the strata can be described as a "sugary dolerite". The coal seam aquifer is at a depth of around 280 m and is underlain by the Dwyka sediments. The groundwater in the coal seam aquifer is of poor quality and can generally be classified as saline water (K ~1.0×10^{-3} – 1.0×10^{-5} m/d) (Love et al, 2014). The groundwater monitoring network had been placed in such a way that all the aquifers are monitored (Figure 2-17).

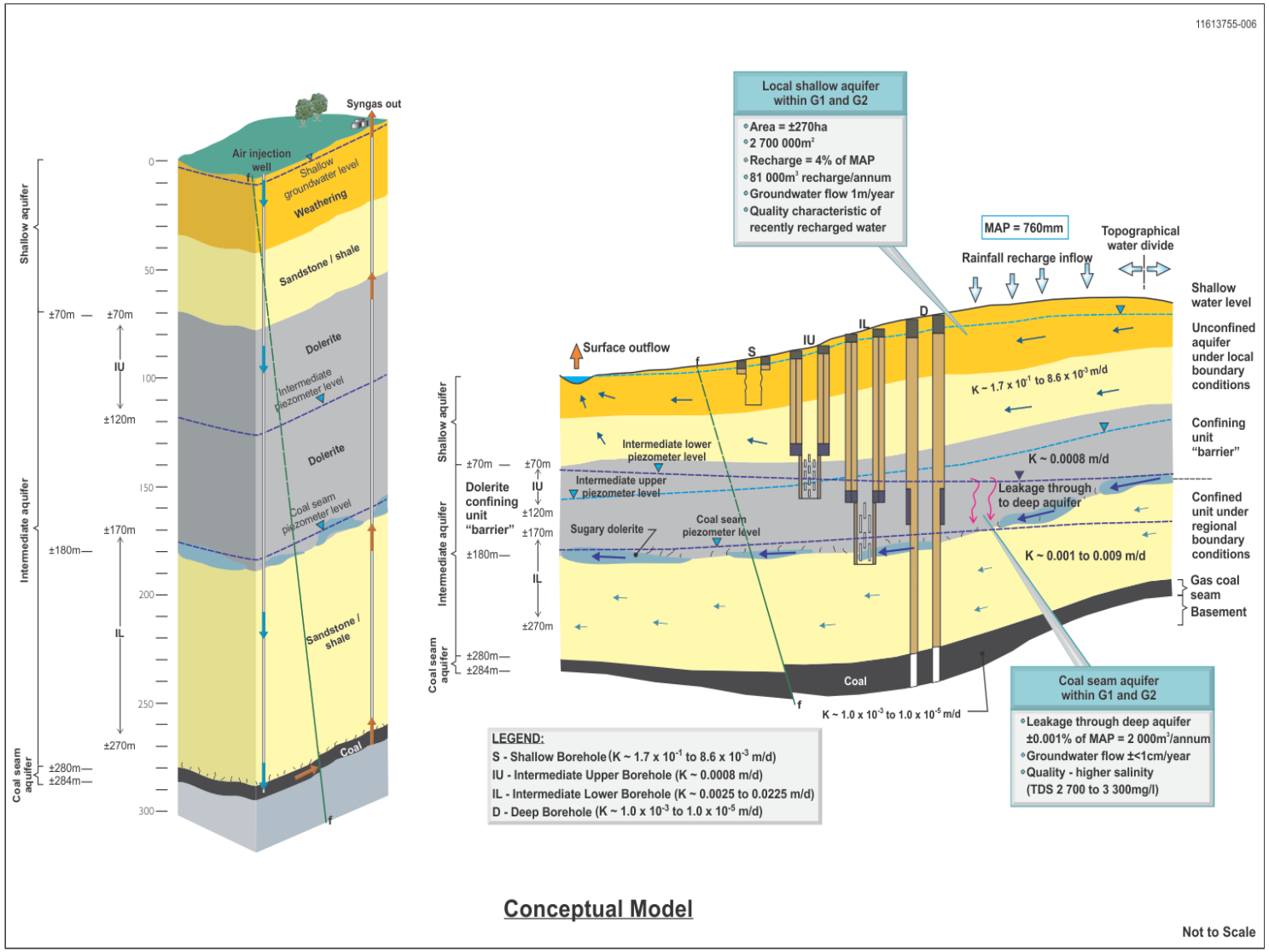

Figure 2-17 Geohydrological conceptual model of the Majuba UCG site (Love et al., 2014)

2.5 Summary

The study area host vast amounts of coal that was originally earmarked for the 3600 MW Majuba Power Station. The coalfield failed to supply coal due to adverse geological conditions that made conventional mining techniques ineffective. The Majuba Underground coal gasification project endeavoured to exploit the economic Gus seam and has successfully fired gas into one of the boilers at Majuba Power Station from Gasifier 1. The decommissioning of Gasifier 1 provides an opportunity to undertake research into the impact of UCG on groundwater, which is the immediate environment that is in contact with the UCG cavity. The question of groundwater contamination from UCG is one that most government authority are seized with and if sufficiently dealt with can enable UCG technology to finally go commercial as pilot studies have been undertaken in most areas around the world however uncertainty around groundwater contamination still remains unanswered.

The literature review in the next chapter takes an in-depth assessment of available resources on UCG technology, especially on the mineralogical changes that the process induces on the coal and surrounding rocks. These mineralogical changes are the potential source of groundwater contamination and needs to be understood at length in order to assess the risk to aquifer contamination. A general review of relevant concepts relating to this study will also be considered and gaps in the literature acknowledged.

3 Literature review

3.1 Introduction

Underground coal gasification (UCG) is an unconventional mining method that permits coal resources to be exploited using high temperature conversion reactions (Perkins, 2018a). An injection well and a production well are drilled into the coal seam and an airflow connection is then created between the two wells before gasification commences. hydro-fracking, Reverse Combustion Linking (RCL), Forward Combustion Linking (FCL), electro-linking, in-seam linking and explosive are various linking methods utilized in UCG (Bhutto et al., 2013). Gasification of the solid coal is initiated by feeding of oxidants (air/oxygen) into the gasification zone via an injection well, with the subsequent transportation of the produced gases to the surface via the production well (Figure 3-1). The gasification process converts *in situ* solid coal into gaseous phases (synthetic gas) composed mainly of methane, hydrogen, and carbon monoxide. The mass transfer of solid coal to gaseous phases creates a channel or cavity in the coal seam which gets partly filled with residue products that include ash and char.

The gasification channel can be separated into three regions: the oxidation zone, the reduction zone, and the dry distillation zone (Figure 3-1). The oxidation zone is dominated by heat generating chemical reactions that involve coal and oxygen. The reduction zone is characterized by an environment deficient in oxygen, which leads to the gasification chamber having a zonal coal progression. The separation depends on key chemical reactions, temperature (related to coal composition), and gas composition occurring in each zone (Bhutto et al., 2013). The main reactions involved in coal gasification zones are drying, pyrolysis, gasification, and combustion (Figure 3-2, Table 3-1). The UCG process begins with heating of wet coal and the moisture is evaporated at around 100°C (R_1), with pyrolysis occurring at much higher temperatures of between 350 - 600°C (Perkins, 2018b). Pyrolysis is the thermal breakdown of volatile compounds at elevated temperatures (Wagner et al., 2018). At the pyrolysis stage (R_2), volatile gases are driven out of the coal and enter the gasification channel, leaving behind char. Bituminous coal can contain up to 45% by mass volatile matter while lignite and subbituminous coal as high as 50% (Bockhorn, 2018). The chemical reactions (R_3 to R_7) occur at the surface of the coal, and the secondary reactions (R_8 to R_{10}) occur in the gaseous phase. The gasification chamber is, therefore, exposed to different chemical and physical processes, leading to a zonal coal profile due to progressive heating that results in different gaseous products (Figure 3-2).

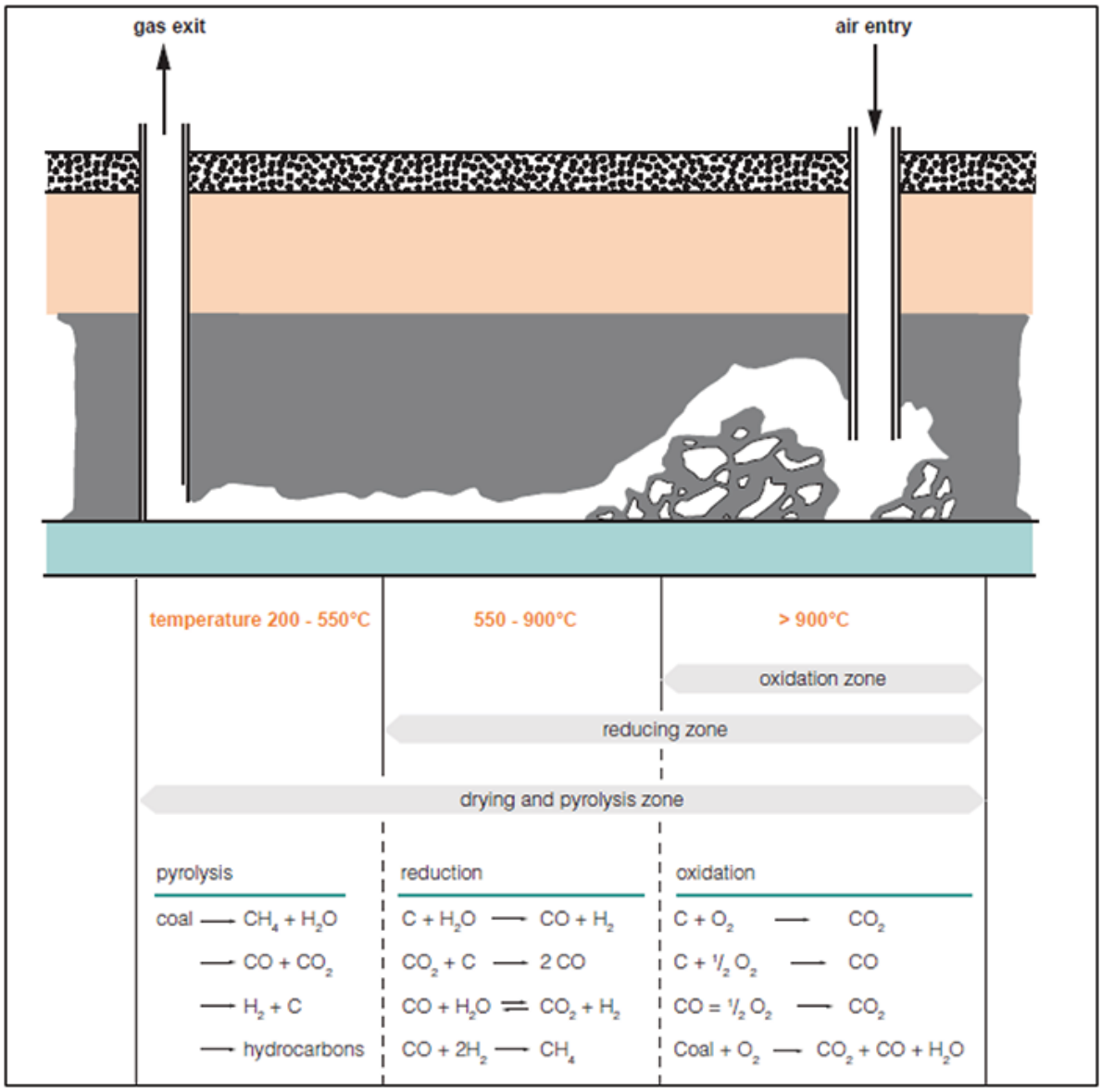

Figure 3-1 Partitioning of the gasification channel into three zones (Pershad et al., 2018b)

Table 3-1: Chemical reactions during UCG (Perkins, 2018b)

Reactions		Stoichiometry	$\Delta H°_{298}$ (MJ/Kmol)
R_1	Evaporation	Wetcoal → Drycoal + H_2O	+20
R_2	Pyrolysis	Drycoal → Char + Volatiles + Tar	0
R_3	Char combustion	C + ½ O2 → CO	-111
R_4	Char combustion	C + O_2 → CO_2	-393
R_5	Steam gasification	C + H_2O → H_2 + CO	+131
R_6	Boudouard reaction	C + CO_2 → 2CO	+172
R_7	Hydrogasification	C + 2H_2 → CH_4	-75
R_8	Combustion	H_2 + ½ O_2 → H_2O	-242
R_9	Combustion	CO + ½ O_2 → CO_2	-283
R_{10}	Combustion	CH_4 + 2O_2 → CO_2 + 2H_2O	-802

An understanding of the chemical, mineralogical, and petrographic properties of the coal, char, and ash (minerals) from the UCG gasification zone is fundamental to a number of investigations needed to assess the effectiveness of the process, and to quantify future risk. For example, post-gasification, the ash (containing sulphur and other potentially toxic minerals and elements) and char (potentially containing heavy molecular weight products such as uncracked or partially cracks hydrocarbons) in the UCG cavity may eventually be leached by the rebounding groundwater into the surrounding aquifers, potentially resulting in groundwater contamination. Furthermore, the cavity can contain elevated levels of CO_2 gas that are free to interact with the incoming groundwater and hence influence the geochemical reactions. Carbon dioxide is soluble in water and produces CO_2(aq) which subsequently reacts with water to form other inorganic carbon compounds including carbonic acid (Deutsch, 1997), which can lower the pH of the groundwater. The petrographic assessment of the char can be used to determine the temperature the gasification zone experienced during the UCG process, hence determining the efficiency of the process.

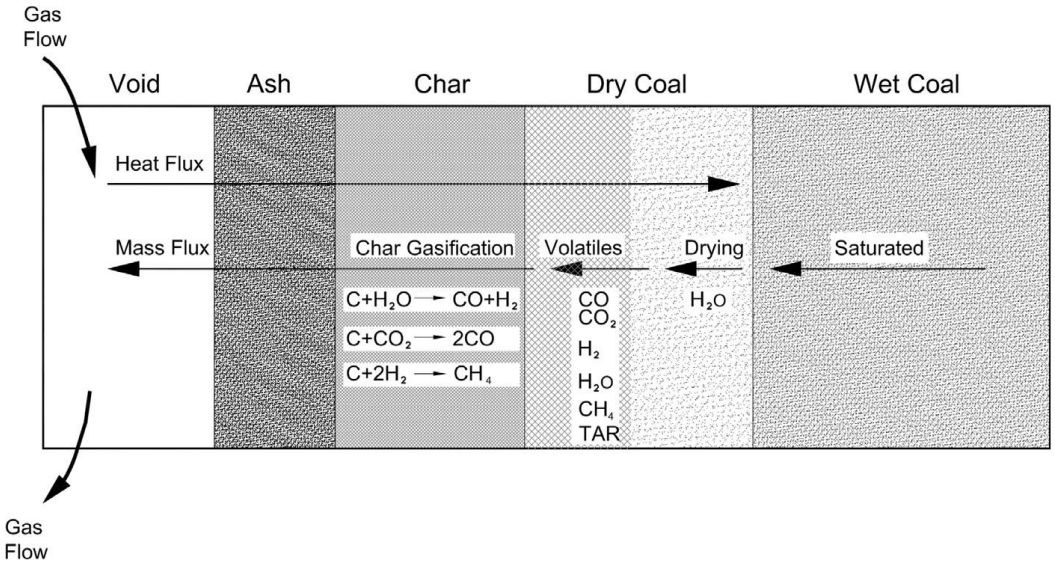

Figure 3-2: Overall illustration of the coal zone of a UCG cavity (Perkins, 2018a)

3.2 Pyrometamorphism

Underground coal gasification utilizes high temperature conversion reactions to alter deep coal seams into a synthetic gas that can be utilized for electricity production. The *in situ* gasification of coal at temperatures in excess of 1000 °C, results in thermal alterations to the sedimentary strata above the coal seam (Kühnel et al., 1993). The term pyrometamorphism or combustion metamorphism is generally used when coal, oil, or gas burns with enough energy to bake or fuse the surrounding rocks (Kristensen et al., 2019). Thermal alterations to the neighbouring rocks occur over a series of time and space (Figure 3-3). The rocks initially become hardened and yellow due to oxidation of iron, and continued heating turns the yellowish colours darker, to more concentrated shades of orange and red, in response to fluctuations in temperature and oxygen supply which affects surrounding areas in the range of a few centimetres to meters in diameter (Grapes, 2011). The majority of the thermal reactions in argillaceous rocks are endothermic and therefore the energy needed for commencing and completing the thermal transformations of minerals must come from the UCG process (Kühnel et al., 1993). As temperatures continue to increase, the surrounding rocks undergo sintering and

recrystallize to produce glazed surfaces while the coal itself turn into ash made up of non-combustible material such as quartz, illite, feldspar, pyrite, kaolinite and carbonates (calcite, siderite, ankerite) that melt from the heat of combustion to form “pools” of slag or paralava (Grapes, 2011).

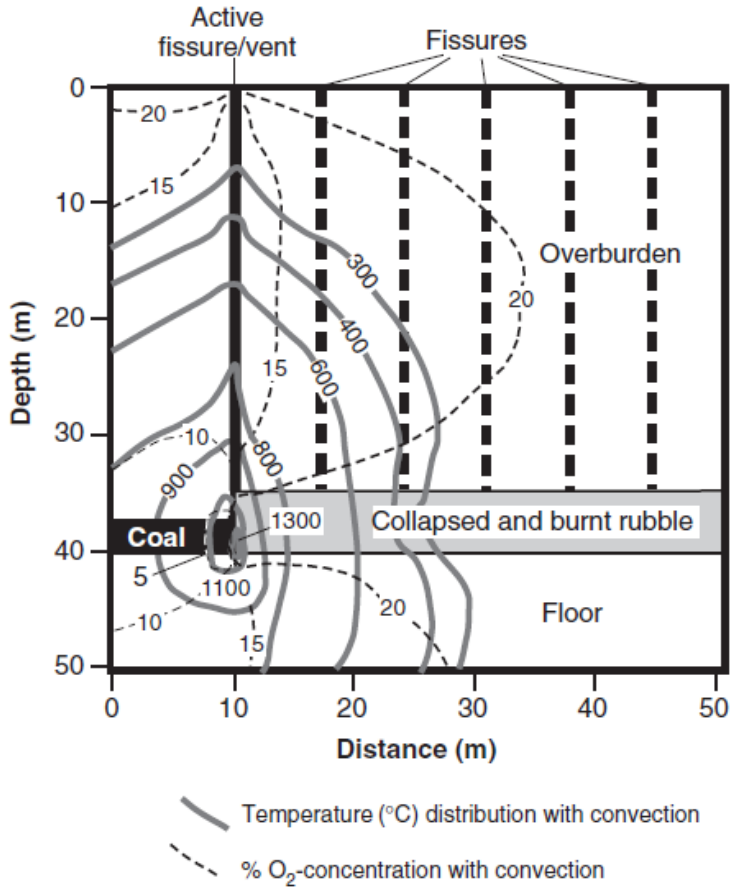

Figure 3-3 Modelled temperature distribution with convection associated with burning coal seam (Grapes, 2011)

The coal seam experiences some of the highest temperatures especially at the burning coal face (1300 °C) where sintering and melting of clastic material is limited to a small area (Figure 3-3). The consumed coal produces a cavity composed partly of burnt rubble and is therefore susceptible to collapse due to lack of support to the overburden. Extreme temperatures in the range of 1500 °C - 2100 °C are also experienced in openings of vents and faults, which partly induces fusion to the surrounding rocks (Quintero et al., 2009). The interaction of underground coal fire and the roof has been modelled by (Wolf and Bruining, 2007).

3.3 Sanidinite facies

Metamorphism in geology is the modifications that a rock experiences due to changes in the rock’s environment (i.e. temperature, pressure and fluid composition) without melting (Philpotts and Ague, 2009). Metamorphism brings forth a wide range of mineralogical or textural changes in rocks, up to the temperatures of crustal melting (800 °C and above) and at pressures of around 4.0 GPa (Blatt et al., 1996). At high temperatures, melting of rocks commences and this can lead to overlapping of metamorphism with igneous activity in a process of partial melting known as anatexis (Frost and Frost, 2014). There are various ways a rock can undergo metamorphism however the most common types

are contact, regional and dynamic metamorphism. The changes that take place in the country rocks during UCG can be classified as contact metamorphism as the heat that metamorphoses the surrounding rocks is localised and adjacent to the gasifier. The UCG process produces heat and makes the coal seam extremely hot with temperature in the region of 900 - 1450 °C (Bhutto et al., 2013). Changes observed in rocks can be described using metamorphic facies. The concept of metamorphic facies was pioneered by Norwegian geologist V.M. Goldschmidt (1911) and Finnish geologist Pentti Eskola (1915) to describe mineral assemblages in metamorphic rocks formed under corresponding temperatures and pressures (Blatt et al., 1996). Sanidinite facies represents high temperature-low pressure metamorphism which can be expected in the country rocks surrounding the UCG chamber (Figure 3-4). The sanidinite facies are distinct from other contact metamorphism in their compositions, crystal habit, textures and preservation of glass which is the effect of high temperature and chemical disequilibrium that is triggered by rapid heating and cooling which is shown by unique pyrometamorphic mineral assemblages (Grapes, 2011). The type of rocks and associated textures synonymous with high temperature contact metamorphism are presented in Table 3-2.

Table 3-2 Common pyrometamorphic rocks that result from natural fusion, adapted from (Grapes, 2011)

Rock term	Features
Buchite	A highly vitrified rock, formed from extreme heat of contact metamorphism. The term buchite implies the presence of glass (quenched melt) from which high temperature phases have crystallized
Clinker	Typically denotes hard, baked, fused, unmelted, reddish rocks that resemble burned paving brick. The rocks may also have a glassy surface due to extensive fusion (i.e. glassy clinker = known as scoria)
Paralava/slag	Normally black to dark grey pyrometamorphic rock with a vesicular, aphanitic texture and has the appearance of artificial slag or ropy basaltic lava. Formed from melted argillaceous rocks (sandstone, shale, marl)

Sanidinite facies provide for distinctive and uncommon mineral groupings and displays features of paragenesis that show merging with igneous rocks whereby in buchites and paralavas, crystallization of high-temperature minerals has taken place from magma (Grapes, 2011). Other high temperature mineral assemblages have been documented in xenoliths in basic lavas and igneous intrusions at shallow crustal levels, in metamorphic aureoles around volcanic and hypabyssal groups of mafic to intermediate composition, and as chips in pyro-clastic rocks (de Souza et al., 2019).

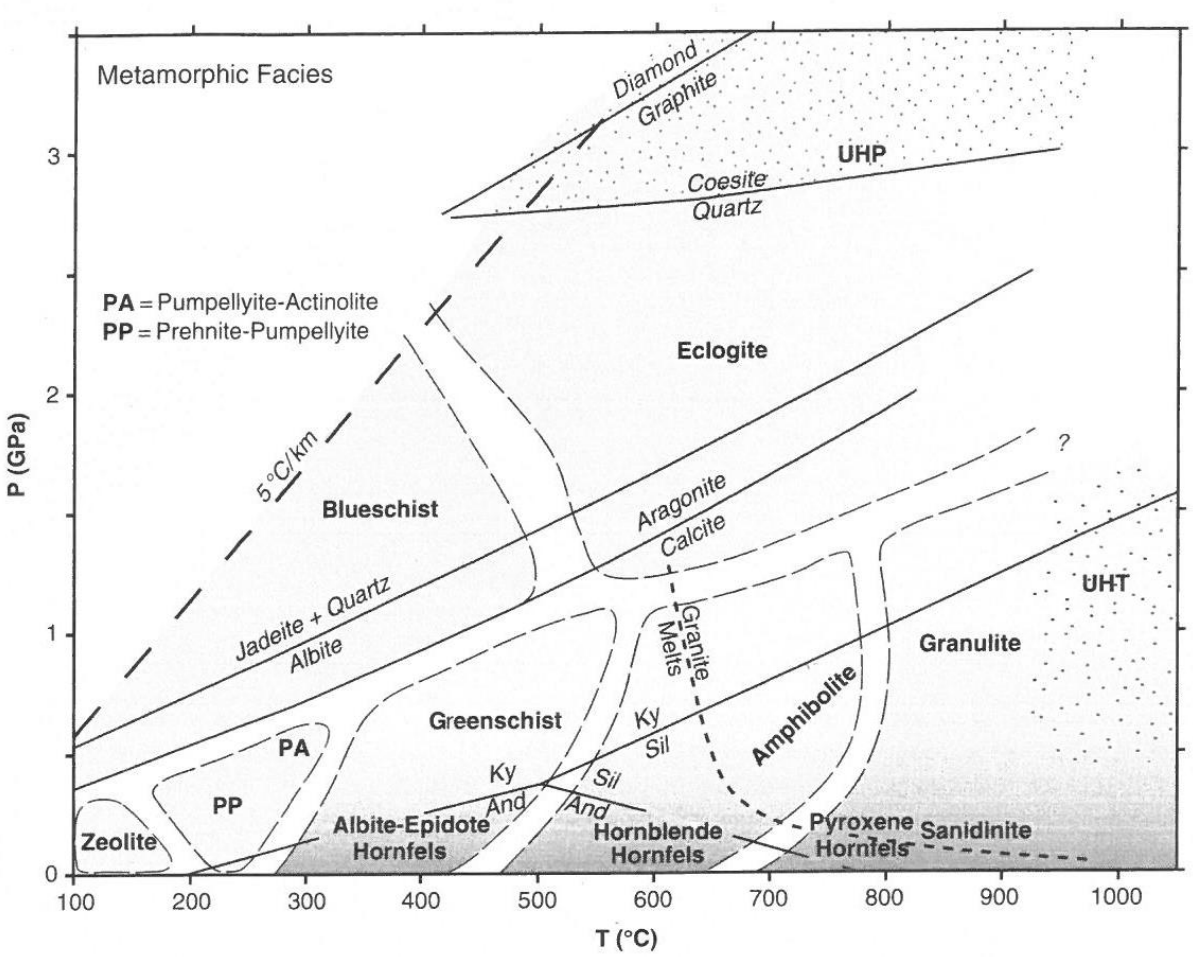

Figure 3-4 Approximate pressures and temperatures for the main metamorphic facies, adapted from (Philpotts and Ague, 2009). Sanidinite facies are high temperature low pressure metamorphism that can be expected also from the ensueing environment of a UCG process, producing distict mineral assemblage.

3.4 Thermal effects

3.4.1 Micro-cracking

Increase in temperature on minerals leads to changes in the mineral structure and if the temperature is high enough melting can take place. Melting reactions usually comprise of a positive volume increase and rapid melting causes the development of high pressures in the melt that leads to hydraulic fracturing and conveyance of the melt along these fractures (Grapes, 2011). These micro-cracks are especially evident in quartz crystals in pyrometamorphic rocks (Figure 3-5). In UCG, clay minerals can be expected to release water from their crystal lattice when the temperature reaches their dehydration and dehydroxylation temperatures. The liberated water moves through pores and cracks from the thermally affected rocks in the direction of the thermal gradient and as pore pressure increases in the gasifier, the pressure pushing the water front ahead into cooler rocks cannot overcome the pore pressure leading to expansion of existing fractures and generation of new cracks (Kühnel et al., 1993).

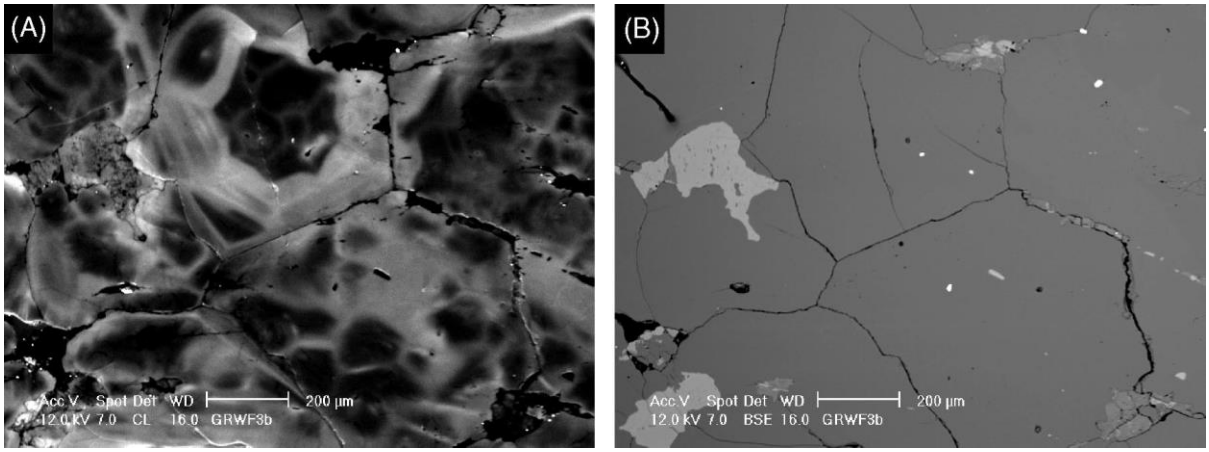

Figure 3-5 Micro-cracking of quartz crystals, back-scattered electron image adapted from (Holness and Watt, 2001)

The initial formation of mirco-cracks in pyrometamorphic events is associated with anisotropic thermal expansion linked with α-β inversion in quartz which occurs at around 590 °C at 600 bars, and this leads to micro-cracks that cut across quartz and feldspar crystals (Grapes, 2011). Cracking and fracturing of minerals leads to spalling of the overburden and this is constructive to the expansion of the gasifier as it provides access for the injected oxygen and steam to the coal ahead of the ignition point (Kühnel et al., 1993). The penultimate stage of micro-cracking takes place with melting at quartz-feldpar grain boundaries and cracks form along grain boundaries and continue inside the gains and outwards across neighbouring grains, and the final stage of cracking occurs during cooling and brings forth cracks that cut across or regenerates coagulated melt-filled fractures (Grapes, 2011). Micro-cracking of mineral grain increases the overall porosity of the lithology and this can increase the interaction of groundwater with the rocks in the vicinity of the gasification zone. Results from Bloodwood Creek Panel 1 UCG project showed that most of the heat transfer was to the overburden with no detectable impacts of temperature in the underburden (Perkins, 2018b).

3.4.2 Glass preservation and glass composition

The heat of combustion is responsible for the transformation of rocks into amorphous (glass) melt in the UCG geo-reactor. Vitrification of clay minerals illite and smectite commences as the temperature of the geo-reactor reaches 800 °C and the initial droplets of melt are formed at grain boundaries (Kühnel et al., 1993). de Souza et al. (2019) suggested that melt generated by igneous pyrometamorphism generally quench and fill pores, micro-cracks and dilation structures in the host rock. Upon cooling the presence of glass in pyrometamorphic rocks can be explained with Figure 3-6. A supercooled liquid is stable at temperatures above the glass transformation range. If the cooling process is at a very fast rate, like during quenching, only glass forms from the melt. When cooling is slower, more crystals form as the melt goes through the glass transformation range. Glass only crystallises if held for a certain period of time above the glass transformation range, that is the temperature at which viscosity is around the order of 10^{13} Pa's, at this viscosity glass devitrify at a fast rate of 10 – 10^3 seconds (Grapes, 2011). At temperatures above 1350 °C much of the melt will cool down into glassy phases as cooling in the UCG reactor is rapid which preserves the glass and minimize the size of the crystals (Kühnel et al., 1993). Once glass has formed, its preservation in the contact aureole depends on whether fluid infiltration takes place during the cooling stage (Grapes, 2011). The residue from UCG is usually rich in glass coupled with high temperature crystals such as mullite

($Al_6Si_2O_{13}$) and cristobalite (SiO_2) that form from the melt (Kühnel et al., 1993). Preservation of the melt as glass presents a new dynamic in the interaction of rocks and groundwater as some of the elements may be easy leached from glass as compared to mineral where they are bounded in chemical bounds within crystal lattices.

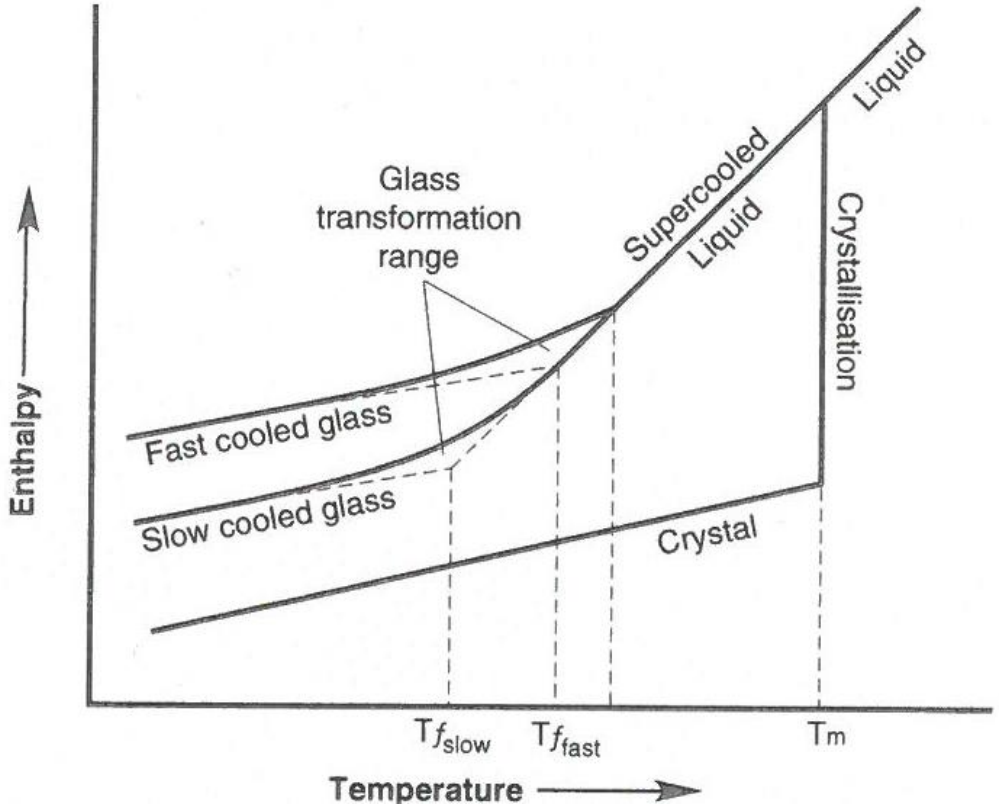

Figure 3-6 The effect of temperature on the enthalpy (or volume) of a glass forming meld (Grapes, 2011)

3.4.3 Columnar jointing

Cooling cracks evolve from the boundaries of solidifying lava or intrusive dykes and usually spread inwards dividing the rock into prismatic columns (Budkewitsch and Robin, 1994). A columnar jointed rock mass is made up of polygonal cross sectional columns cut by numerous sets of joints in various directions (Fan et al., 2017). During heating, there is a possibility of development of contraction stresses which advance the evolution of columnar jointing during cooling of rocks below their softening point (Grapes, 2011). Columnar structures evolve by recurring, step-wise crack advances, creating cm to dm transverse bands on the column face (Budkewitsch and Robin, 1994). Larger columns develop in more massive, thickly bedded sandstones that contain more glass while smaller columns evolve in thin bedded sandstones whereas no columns form in siltstones or beds that have abundant mud pellets (Grapes, 2011).

3.4.4 Dilation

Sediments above a burning coal seam can open up or dilate due to the heat of combustion. The dilation is characterized by open cavities that afford space for vapour phase crystallization of high (sanidinite facies) and low temperature (hydrous) minerals (Grapes, 2011). An example of clay-rich siltstone dilation curve is displayed in Figure 3-7. The dilation increases constantly with temperature

increase from the start of heating until the α-β quartz inversion at 587 °C, where a small sharp increase in dilation is observed. Vitrification at 900 °C does not impact the dilation behaviour however bloating (BL) at 1200 °C results in a sharp increase in dilation (Grapes, 2011). Dilation feature opens up geological strata whereby mineral interaction with groundwater post gasification will be expedited relative to rocks that do not have dilation features or vesicles.

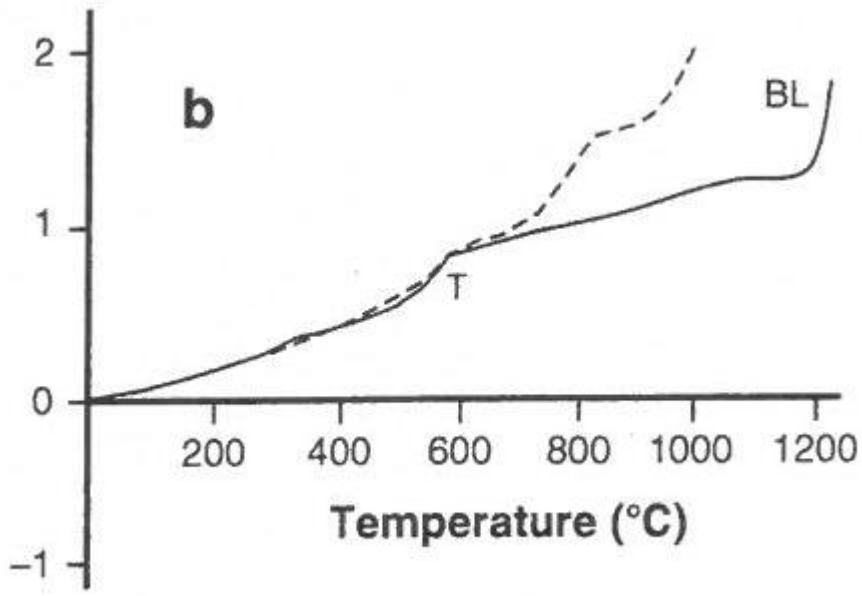

Figure 3-7 Dilation curve of siltstone (Dilation % vs temperature), solid line represents siltstone with clay matrix whilst dashed line represents siltstone with carbonate matrix, adapted from (Grapes, 2011)

3.5 Pyrometamorphosed quartzofeldpathic rocks

Pyrometamorphosed quartzofeldspathic rocks (sandstone, claystone, shale) and sediments (clay, sand-silt, glacial, till, diatomaceous earth), and their metamorphosed counterparts (phyllite, schist, gneiss), are distinguished by the presence of the following mineral assemblages: cristobalite-tridymite, mullite/silliminite, cordierite, clinopyroxene, orthopyroxene, sanidine-anorthoclase, plagioclase (oligoclase-anorthite), corundum, hercynite-rich spinel, magnetite, hermatite, ilmenite, sulphides and native metals (Grapes, 2011). The composition of quartzofeldspathic rocks can be expressed in terms of the mol % of silicate and oxides phases. Typical bulk composition of pyrometamorphosed rocks (sanidinite facies) are presented in a ternary system such as a FMAS diagram (Figure 3-8). A ternary system displays phase relations in which the base is a symmetrical triangle that projects compositional differences in the system with each of the three sides consisting of a binary system (Frost and Frost, 2014). In UCG, the addition of CO_2 to the system from the burning of coal seam allows for the presence of ankerite, calcite, dolomite and siderite which interacts with sulphides (pyrite and pyrrhotite) to produce magnetite-hematite-bearing paralavas (Grapes, 2011). The predominantly reducing environment in UCG coupled with localized overheating enhances the metallization of ferruginous mineral phases and formation of ferroalloys (Kühnel et al., 1993).

The mineral associations in buchites and paralavas can be expressed in terms of alkali-free ternary systems $MgO\text{-}Al_2O_3\text{-}SiO_2$ (MAS), $MgO\text{-}FeO\text{-}SiO_2$ (MFS) and $FeO\text{-}Al_2O_3\text{-}SiO_2$ (FAS) as displayed in Figure 3-9 (Mineral composition and notations (abbreviations) are given in Appendix 3-A). The other major

oxides that usually constitute quartzofeldspathic rocks are CaO and K_2O and their respective ternary systems are displayed in Appendix 3-A. The line A-B in Figure 3-9 represents a pseudo-binary section within the $MgO\text{-}Al_2O_3\text{-}SiO_2$ system between metatalk and metakaolin composition (i.e sections of crystals and melt) and hence represents compositional boundaries of tridymite, cordierite, mullite and orthopyroxene formation (Grapes, 2011). Typical mineralogy of buchites is illustrated by the expanded pseudo binary system of line A-B from Figure 3-9, and is presented in Figure 3-10. The system reveal that mullite, mullite-cordierite, mullite-tridymite, cordierite, cordierite-tridymite, tridymite and tridymite-orthopyroxene buchites can be produced at around the same temperature depending on the composition of the sedimentary protolith (Grapes, 2011).

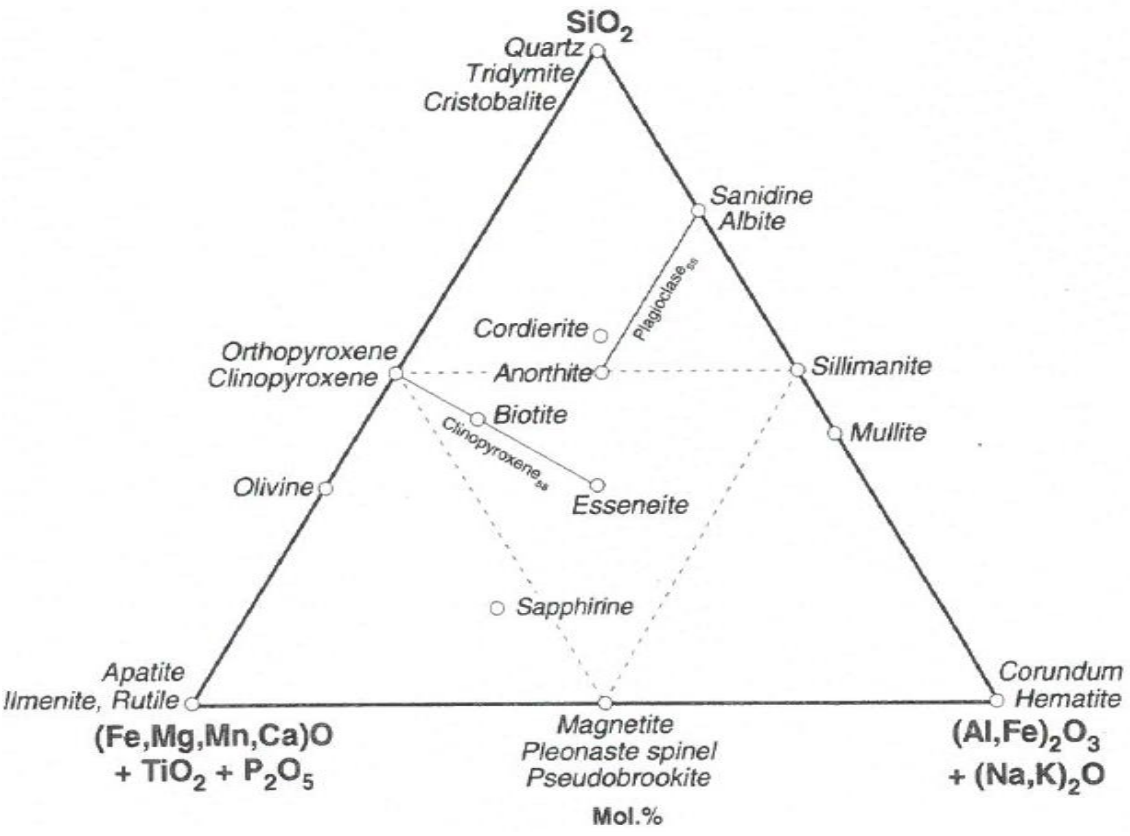

Figure 3-8 Sanidinite facies showing silicate-oxide minerals plotted in terms of mol % [(Fe, Mn, Mg, Ca) O + TiO2 + P2O5] – [(Al,Fe)2O3 + (Na,K)2O3] – SiO2 (FMAS diagram). Adapted from (Grapes, 2011).

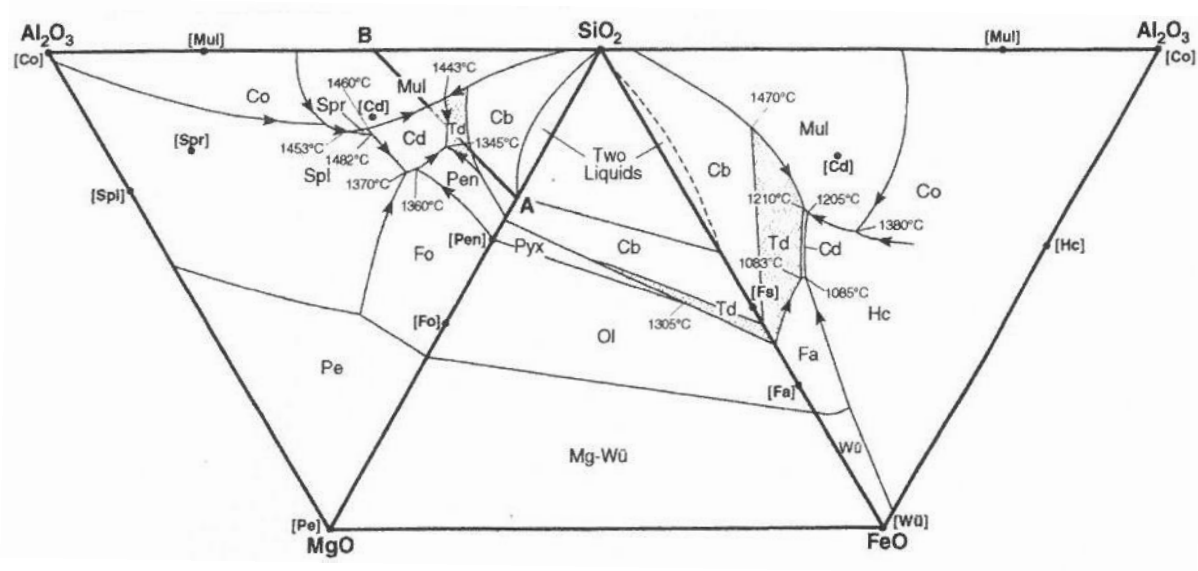

Figure 3-9 Amalgamated phase relations diagram of the atmospheric pressure systems: MgO-Al_2O_3-SiO_2, MgO-FeO-SiO_2, FeO- Al_2O_3-SiO_2, Mineral composition and notations (abbreviations) are given in Appendix 3-A, adapted from (Grapes, 2011)

The pressure-temperature stability fields of pyrometamorphed quartzofeldspathic sedimentary rocks are presented in the petrogenetic grid in Figure 3-11. Buchites and paralavas form over a wide range of temperatures with shared high temperature mineral assemblages. For example, at higher temperatures cristobalite usually forms and persists metastably in the temperature field of tridymite (as seen in paralavas), and at lower temperatures, quartz may occur even when the temperature is above the quartz-trimydite inversion point of 867 °C and continue metastably within the tridymite temperature range (Grapes, 2011).

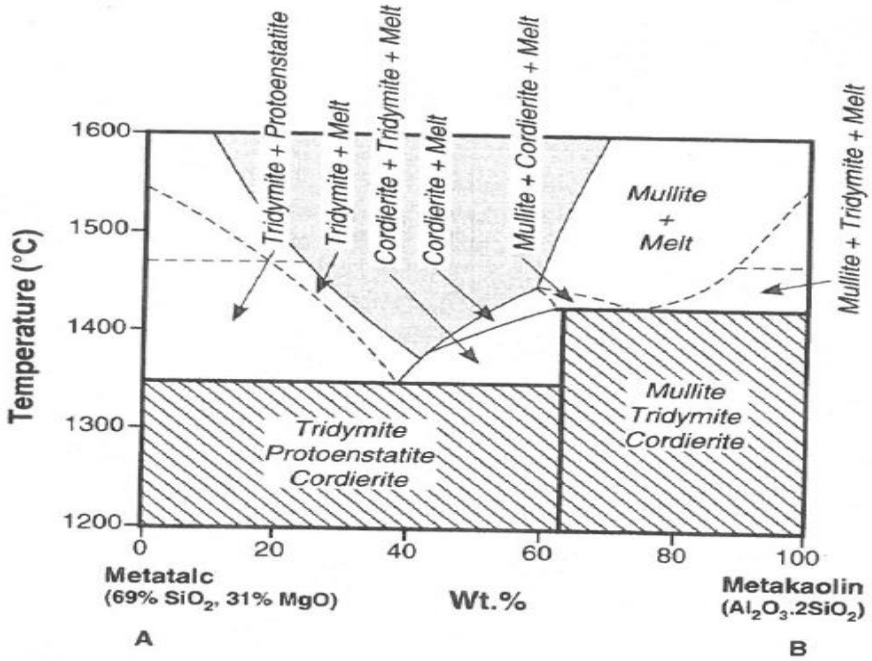

Figure 3-10 Phase diagram for the pseudo binary system of typical buchites produced from compositions between metatalk and metakaolin, adapted from (Grapes, 2011)

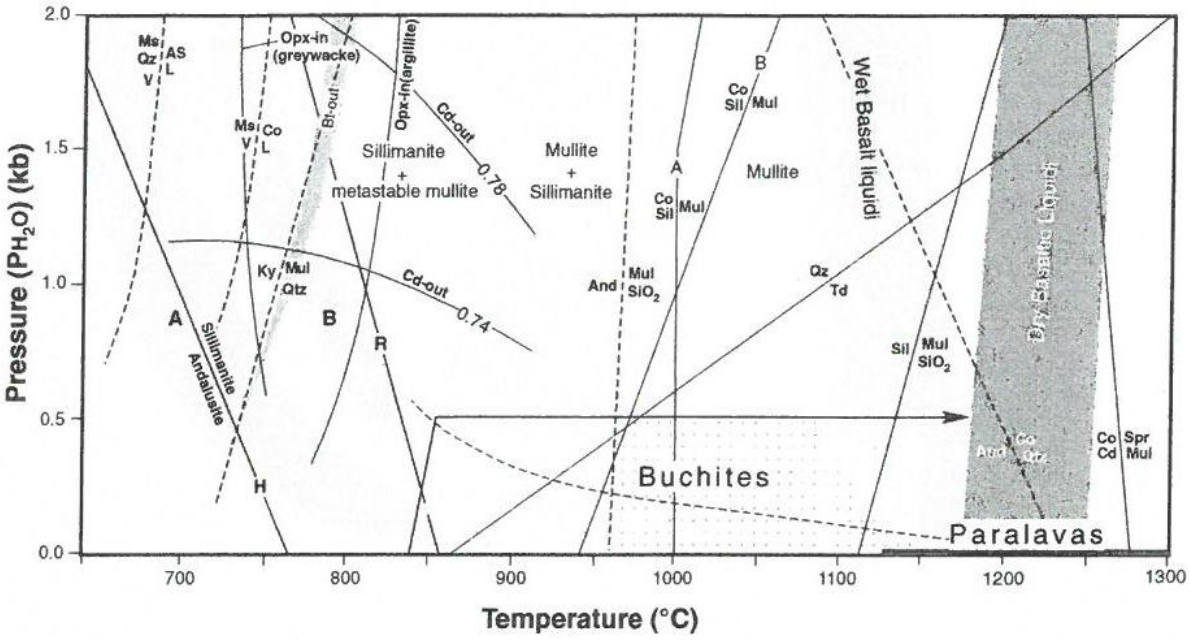

Figure 3-11 Petrogenetic grid of mineral assemblages for pyrometamorphosed quartzofeldspathic, adapted from(Grapes, 2011) Mineral composition and notations (abbreviations) are given in Appendix 3-A.

3.6 Mineral transformation and metastable mineral reactions

Underground gasification of coal results in a cavity which can cause the overburden to collapse due to lack of support. The growth of the cavity can be a complex process but invariably involves spalling and intermediate-scale fracturing coupled with collapse activities (Camp, 2018). All of these actions results in a chaotic rubble-filled cavity characterized by pyrometamorphosed mineral assemblages. A cross section of the UCG cavity along with the reconstruction of the temperature profile in the gasifier is displayed in Figure 3-12. The thermal phase transformation associated with heating and cooling of an argillaceous overburden from UCG field test near Hanna, Wyoming, USA (Kühnel et al., 1993) are presented in Figure 3-13.

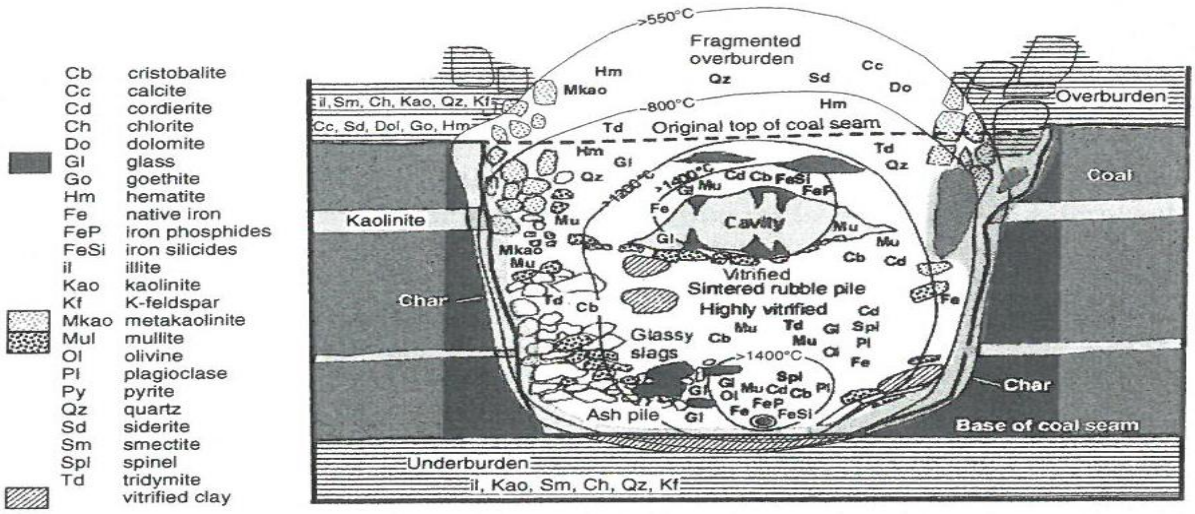

Figure 3-12 Reconstruction of the temperature profile in the gasifier with the aid of high temperature mineral phases formed from argillaceous material in the overburden and phases in the coal seam, adapted from (Kühnel et al., 1993, Grapes, 2011)

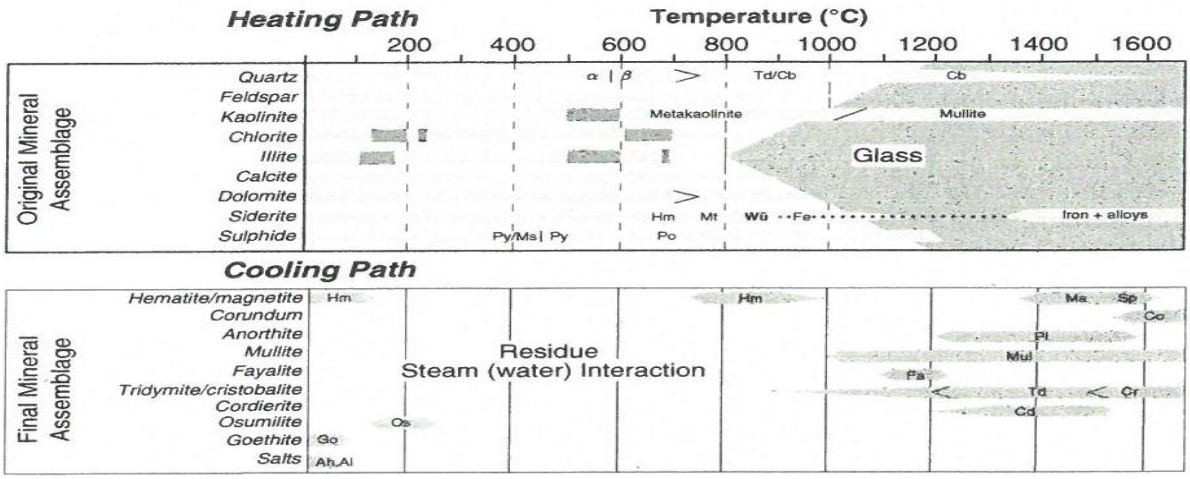

Figure 3-13 Mineral transformations during heating of argillaceous overburden rocks and cooling of UCG products, (the same mineral codes from Figure 3-12 applies) adapted from (Kühnel et al., 1993, Grapes, 2011)

Heating in the UCG chamber results in vitrification of illite as the temperature reached 800 °C (Figure 3-13). As the temperature increases, more minerals begin to melt and at 1200 °C around 80% of the argillaceous rock will undergo vitrification, while at 1350 °C the rock will be totally molten (Kühnel et al., 1993). Mineral assemblages of completely melted (slag) rocks correspond largely to the products of crystallization of dry melts over a widespread range of compositions obtained from laboratory quenching experiments at atmospheric pressure (Grapes et al., 2009). The UCG chamber undergoes rapid cooling which preserves the glass and reduces the size of crystals with the residue products characterized by a range of dendritic, skeletal and hollow crystals which crystallize from the thermodynamically less stable glasses (Kühnel et al., 1993). Quartz are a major component of quartzofeldspathic rocks associated with coal seams and exists as various polymorphs including α-quartz, β-quartz, tridymite and cristobalite. The high-pressure polymorph is coesite. The unquenchable transition of α-quartz to β-quartz takes place at 573 °C (Figure 3-14) which is related to anisotropic thermal expansion that result in micro-cracks that cut across quartz grains (Nesse, 2000, Grapes, 2011). The quartz-tridymite inversion temperature is at 867 °C but metastable quartz can still persist even beyond this temperature, while cristobalite can exist metastably in the tridymite temperature range. Figure 3-13 shows that high temperature crystallization favours anorthite as the plagioclase that is stable at temperatures above 1200 °C. It can therefore be expected that pyrometamorphosed quartzofeldspathic rocks will be enriched in anorthite relative to K-feldspars. Mineral transformations in a gasification zone around a UCG geo-reactor are important as these secondary minerals are expected to interact with groundwater post gasification. There is lack of literature on high temperature mineral phases interaction with groundwater, which has the potential to negatively impacting on the environment. Other mineral transformations are given in the following sections.

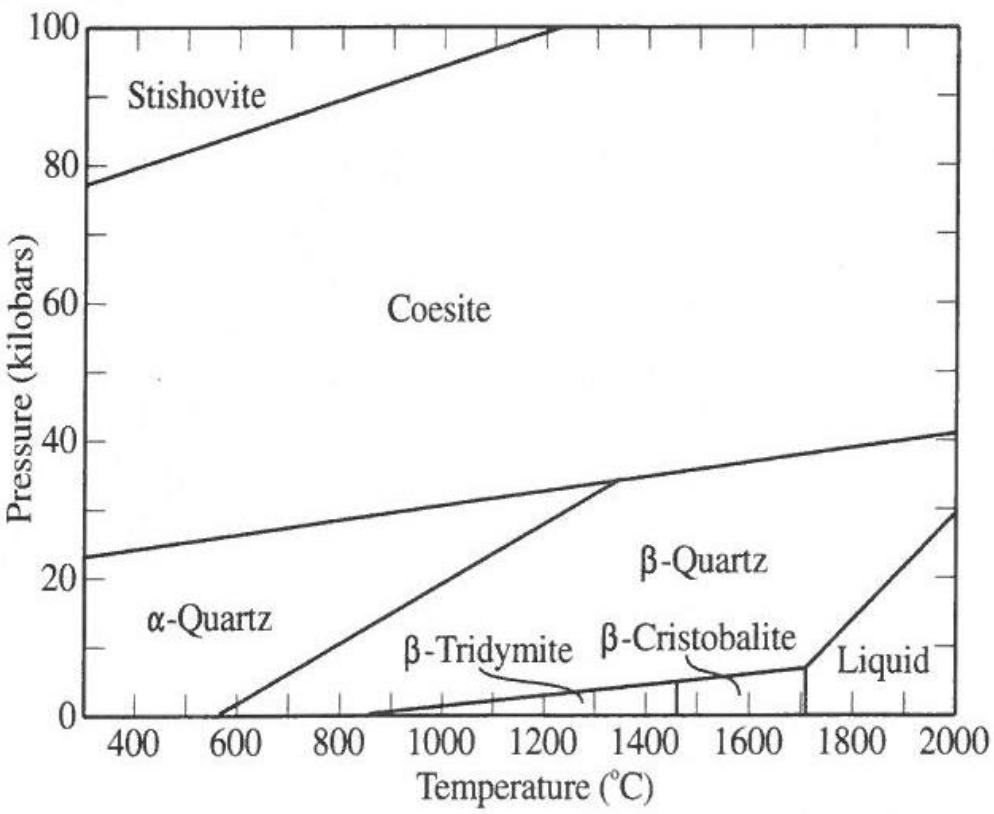

Figure 3-14 Temperature-pressure diagram showing stability field of silica (SiO_2) polymorphs, adapted from (Nesse, 2000)

3.6.1 Pyrite and pyrrhotite transformation

Iron sulphides such as pyrite (FeS_2) occur in coal and associated sedimentary rocks as accessory minerals. Gondwana coals are by and large low in iron sulphide mineral content relative to the Laurasian coals (Wagner et al., 2018). In reducing environments, pyrite changes to pyrrhotite ($Fe_{1-x}S$) which is a non-stoichmetric sulphide with a general formula $Fe_{1-x}S$ (where x < 0.125) by the following reaction (Grapes, 2011):

$$FeS_2 + 2CO_2 = Fe_{1-x}S + 2CO + SO_2$$

The transformation of pyrite during combustion is schematically presented in Figure 3-15. The individual transformation of pyrite (a) produces a pyrrohotite outer shell with some of the pyrite preserved in the core. Fragmentation of the grain and subsequent oxidization results in magnetite formation. Further oxidation produces iron rich melt which eventually crystallizes and magnetite upon cooling. Pyrite occurs in a silicate matrix and (b) represents the transformation of pyrite associated with silicates. A pyrrhotite melt forms as the temperature reaches 1083 °C, which subsequently transforms to iron oxide melt during oxidation. Upon cooling the iron rich melt crystallizes as magnetite with the silicate glass preserved due to the fast cooling.

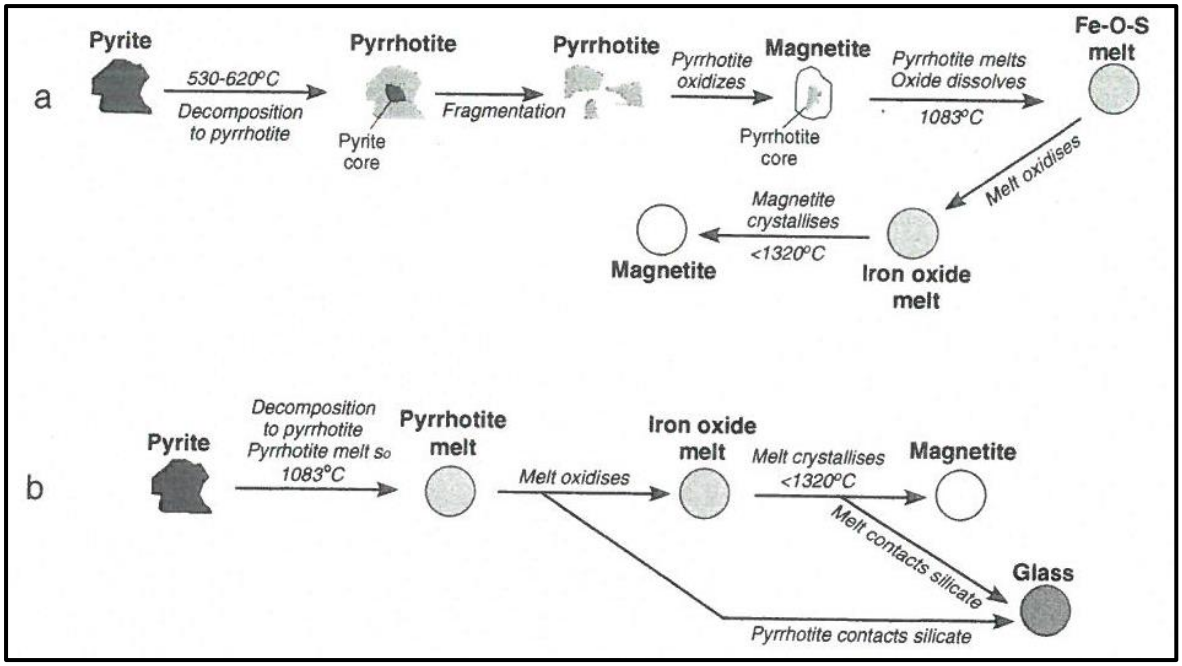

Figure 3-15 Pyrite transformation during combustion. Transformation of individual (isolated) grains of pyrite (a). pyrite with silicate (b) (Grapes, 2011)

3.6.2 Al-silicates

Clay minerals are the most abundant minerals found in coal globally, and in Southern African coals it constitutes up to 80 % of the mineral content (Wagner et al., 2018). Common clay minerals that occur in coal include kaolinite, illite and montmorillonite. The mineral transformation of kaolinite to metakaolin and subsequent crystallization of mullite and cristobalite is illustrated by the phase reactions below (Grapes, 2011):

Loss of structural water at around 500 °C according to reaction:

$$\underset{Kaolinite}{Al_4Si_4O_{10}(OH)_8} = \underset{metakaolin}{Al_4Si_4O_{14}} + 4H_2O$$

Condensation of metakaolin layers to form patterns of Al-Si spinel type phase between 925 °C – 950 °C according to reaction:

$$\underset{metakaolin}{Al_4Si_4O_{14}} = \underset{Spinel}{Al_4Si_3O_{12}} + \underset{Silica}{SiO_2}$$

Transformation to 1:1 type mullite phase and cristobalite between 1015 °C – 1100 °C, and to 3:2 mullite and cristobalite at higher temperatures according to reaction:

$$\underset{Spinel}{Al_4Si_3O_{12}} + \underset{Silica}{SiO_2} = \underset{Mullite}{3Al_2O_2{:}\,2SiO_2} + \underset{Cristobalite}{3.5SiO_2}$$

The reactions above suggest that the thermal decomposition of Al-silicate is associated with a silica melt that can result in polymorphs of quartz such as cristobalite and tridymite depending on the temperature of formation. The Al_2O_3-SiO_2 system is presented in Figure 3-16. In a UCG chamber where rapid cooling can be expected, the mineral grains of mullite, spinel or metakaolin can be expected to

be surrounded by a silica glass. Mullite is not a common Al-silicate in the earth's crust and usually occurs in the sanidinite and corundum-sillimanite facies, at contact areas of super-heated volcanic intrusions, and in post volcanic hydrothermal formations (Brunauer et al., 2001). Sillimanite can also thermally transform to mullite by the following reaction (Grapes, 2011):

$$\text{Sillimanite} = \text{mullite} + SiO_2$$

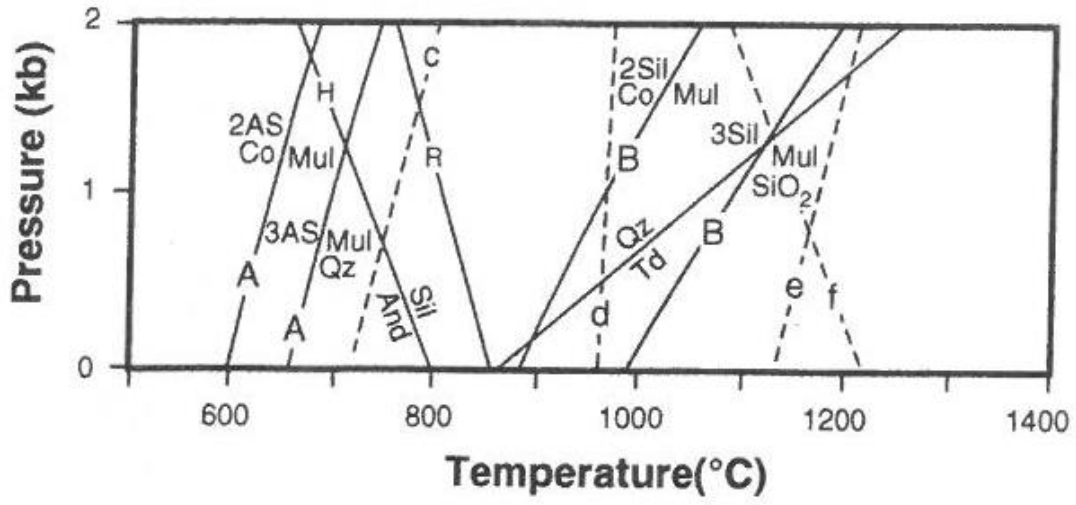

Figure 3-16 Temperature-pressure diagram of the Al_2O_3-SiO_2 system showing phase equilibria, adapted from (Grapes, 2011)

3.6.3 Carbonates and Fe-oxides

Occurrence of carbonate minerals in Southern African coals is associated with hydrothermal fluid precipitation and occur as nodules, veins and cell filling of siderite, calcite, dolomite and ankerite (Wagner et al., 2018). Iron oxides and carbonates are minor constituents in quartzofeldspathic rocks relative to quartz and silicates, however, their thermal decomposition and role in crystallization of secondary minerals is important. The general decomposition reaction of carbonates is as follows:

$$RCO_x = RO + CO_x$$

Where R can be any of the following divalent cations: Ca, Fe, Mg and Mn. An example of Siderite decomposition in reducing conditions is as follows:

$$\underset{Siderite}{FeCO_2} = \underset{Wusite}{FeO} + CO$$

The resultant oxide from the decomposition of carbonates can undergo further oxidation in oxidizing conditions as seen with wusite (FeO) (Grapes, 2011):

$$FeO \rightarrow \underset{Magnetite}{Fe_3O_4} \rightarrow \underset{Hermatite}{Fe_2O_3}$$

Decomposition of siderite during combustion as individual grain and as grains in contact with silicates as in the case with coal/char is given in Figure 3-17. Single siderite grains melt as wustite at around 1370 °C with subsequent oxidation transforming it to magnetite and hematite which melt at around

1590 °C and 1560 °C, respectively (Grapes, 2011). In cases where wustite melt contacts silicates, iron glass (paralava) can be expected.

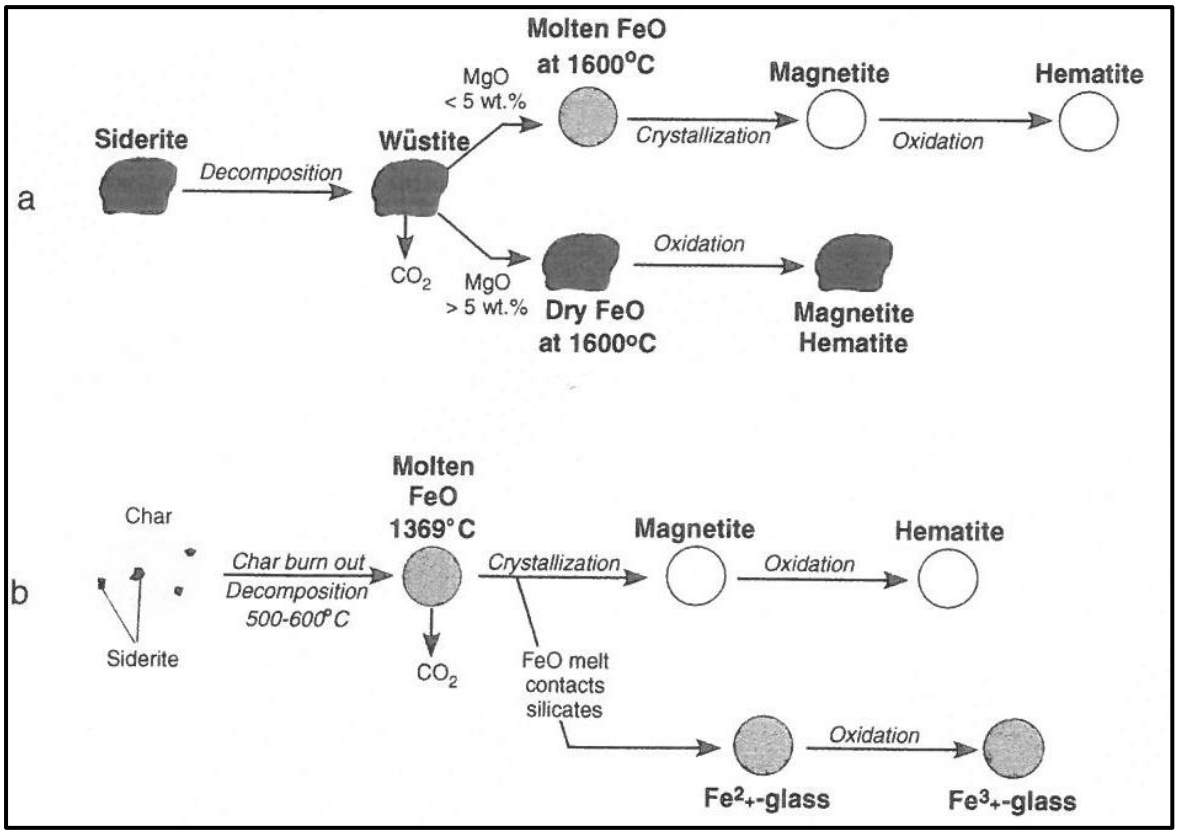

Figure 3-17 Siderite decomposition during combustion, (a) single (excluded) siderite grain transformation, (b) siderite grains in contact with silicates (included) in char particle, adapted from (Grapes, 2011)

3.7 UCG residue and implication on groundwater contamination

Underground coal gasification (UCG) leads to the formation of ash, tars and void spaces in the coal seam (Bhutto et al., 2013). The mineral content of the coal is responsible for the composition of the ash generated by the gasification process. The mineral content of coal is classified into two groupings. The first group is the inherent (syngenetic) inorganic material which was originally contained in the plant matter responsible for the coalification process. This mineral content is found in coal as organo-metallic complexes (siderite, pyrite and colloidal clays) or within the coal matrix as miniscule mineral grains (quartz, clays, feldspars, muscovite, apatite) that precipitated *in situ* or got introduced by water or wind action (Wagner et al., 2018). The second group is the extrinsic (epigenetic) mineral material that was introduced to the coal after the hardening of the peat. These minerals occur as nodules that sometimes cut across bedding planes and intermittently disrupt original layers, and these include marcasite, pyrite, calcite and dolomite, and some trace elements (Wagner et al., 2018).

During high temperature coal conversion (1200 – 1400 °C), minerals contained in coal will undergo transformation into various phases and forms including amorphous glassy masses, round glassy cenospheres, mullite and a range of spinels (Wagner et al., 2018). All this inorganic material resulting from coal conversion is collectively referred to as ash and its composition is dependent on the mineralogy of coal and the gasification conditions. Iron, calcium, magnesium, phosphorus, potassium and sulphur are usually present in ash formed from syngenetic material while iron, calcium,

magnesium and sulphur are found in ash emanating from epigenetic material (Mishra et al., 2016). Overall, based on weight of the dry mass of fuel, coal is composed of major elements (organic portion with contents of the order of a few % by weight), ash-forming elements such as Al, Ca, Fe, Mg, K, Na and Si (in concentrations of around 1000 ppm to a few weight %) and trace elements including As, Hg, Cr, Cd, B, Se, Cl, Se, F and Pb (at concentration below 1000ppm) (Strugała-Wilczek and Stańczyk, 2015).

During combustion and gasification of coal, elements undergo volatilization at different temperatures and stages of the coal decomposition process. These elements can also be released to the environment through condensation and subsequent deposition onto particulates (Llorens et al., 2001). In the UCG chamber condensation occurs in the "colder" parts of the gasifier where elements in the synthetic gas can be deposited as droplets and hence be enriched on surfaces of char and ash in the geo-reactor. The enrichment behaviour can be described using the relative enrichment ratio (RER) factor (Meij, 1994):

$$RER = \frac{element\ concentration\ in\ ash}{element\ concentration\ in\ coal} * \frac{\%\ ash\ content\ in\ coal}{100}$$

Strugała-Wilczek and Stańczyk (2016) classified major and trace element's relative enrichment behaviour during underground coal gasification of lignite and hard coal (Figure 3-18). The classification is as follows:

- Group I – non-volatile elements , RER ≈ 1
- Group II – semi-volatile elements with potential occurrence in the condensate, RER < 0.7
- Group III – highly volatile elements, with limited capacity of condensing on the surface of submicron particles, RER << 1.

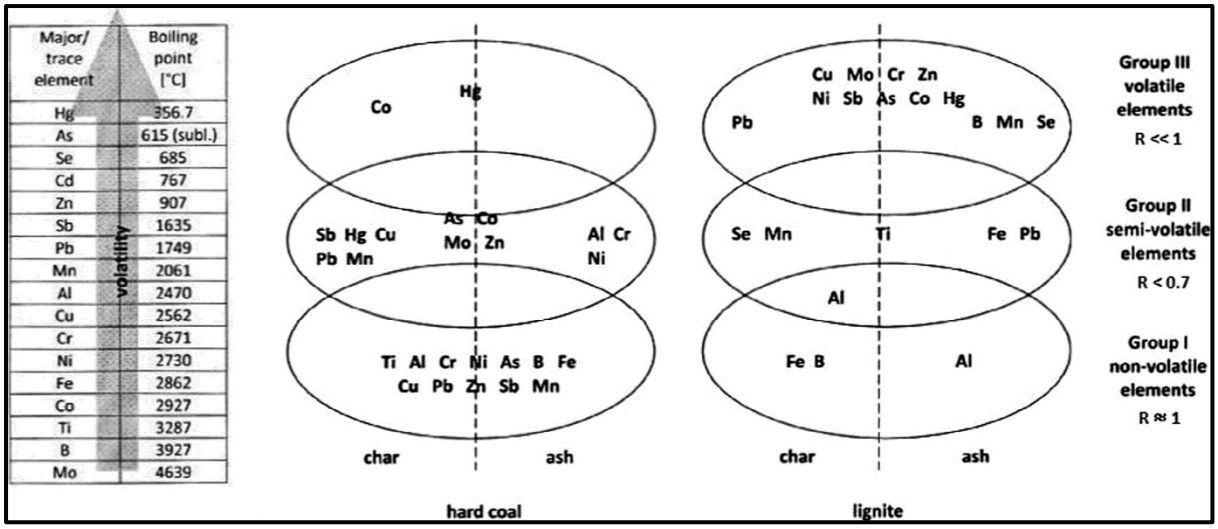

Figure 3-18 Distribution of elements during underground coal gasification of hard coal and lignite (Strugała-Wilczek and Stańczyk, 2016)

At the completion of the UCG process, the geo-reactor shuts down when the injection of oxidants is discontinued and the gasification zone ultimately cools down by natural influx of groundwater. The shutdown process can be expedited by injecting surface water into the gasification chamber. Ultimately the geo-reactor will be flooded with water which interacts with the residue products leading to possible leaching of environmentally toxic material. Leaching of coal ash generated from

surface gasifiers have has been explored quite extensively in a number of studies which show heavy metals and trace elements being leached at rates that pose an environment risk (Jones et al., 2012, Gupta et al., 2017, Zhao et al., 2018). There is however a lack of research into the leaching dynamics of residue products from UCG operations which poses a risk of contamination to the surrounding aquifers. UCG requires a multidisciplinary skill set ranging from mining to geoscience in order to plan, design, operate and rehabilitate a UCG geo-reactor (Pershad et al., 2018a). Post gasification, there is a need to establish if the cavity is environmentally neutral or a potential source of pollution to the surrounding aquifers. This information is especially important to regulatory authorities across the world who are tasked with regulating UCG and other technologies that are seen as clean coal applications.

The potential of groundwater contamination from UCG operations has been previously highlighted by a number of authors (Liu et al., 2007, Imran et al., 2014). However, actual research into this risk is limited. Reference literature from recent studies show some attempt to addressing the risk of groundwater pollution from UCG (Kapusta and Stańczyk, 2011, Kapusta et al., 2013, Kapusta and Stańczyk, 2015, Soukup et al., 2015, Strugała-Wilczek and Stańczyk, 2015, Strugała-Wilczek and Stańczyk, 2016, Xu et al., 2016, Jiang et al., 2018, Wiatowski et al., 2018). However, these studies fall short of providing a definitive solution as most used *ex-situ* UCG products in their analysis to draw conclusions on an *in-situ* based process. In addition, the eluate used in most of the leaching tests was not representative of post UCG cavern conditions. All these inconsistencies do not help authorities in their regulatory duties as these tests fall short of representing UCG field conditions and thus a hindrance for the technology going commercial. Blinderman et al. (2018) stated that a lack of regulatory framework coupled with perceptions of environmental risk emanating from UCG operations must be addressed before the technology can go commercial. The situation is a “catch 22”, as authorities require credible research into the environmental impact of UCG operations in order to regulate the sector, whilst UCG operators require licences for compliance in order to operate commercially. It is therefore imperative to provide research into the environmental impacts of UCG that regulators deem representative of risk factors. This study attempts to address the gaps in literature by analysing the *in-situ* sources of contamination from the UCG gasification zone and to determine the leaching dynamics. This will be done with appreciation of the post gasification field conditions that exist in UCG operations.

Surface waste storage sites such as tailings dams and ash dumps are required by law to chemically profile waste and determine the leaching dynamics as part of the regulatory process. The UCG cavity is a form of waste storage site as it houses the residue products from the spent geochemical process. This waste interacts with groundwater and is subject to physiochemical transformations over time, and hence it is important to device an appropriate elution method that can assess the extent of toxicity and the long term effects of underground storage (Strugała-Wilczek and Stańczyk, 2015). There are a number of leaching tests that are available in literature and some common examples include: batch elution tests that utilize deionized water as the eluent and these tests are designed to provide data on the release of elements without any pH buffering, and column leach tests which provide useful information on the leachability pattern of elements under unrestrained pH conditions (Izquierdo and Querol, 2012). There are also standard leaching test used across the world with varying reagents, contact time and temperature among other parameters. These include the Toxicity Characteristic Leaching Procedure (TCLP), based on US EPA Method 1311, and the Synthetic Precipitation Leaching Procedure (SPLP), based on US EPA Method 1312. These leaching tests use an acidic eluent to

determine the hazardous profile of waste to be disposed on surface waste storage facilities. These standard methods are seen to represent the worst-case scenario, for example, the US EPA does not recommend TCLP for coal combustion products as it provides for inaccurate assessment for this type of material (Izquierdo and Querol, 2012). The geochemical environment in the post-reaction area of UCG is different from the atmospheric conditions that most surface waste is exposed to and hence there is a need to determine the leaching dynamics of the spent geo-reactor under field representative conditions. In literature, deionized water has been the most utilized leaching medium for elution tests on UCG type waste (Strugała-Wilczek and Stańczyk, 2015, Strugała-Wilczek and Stańczyk, 2016). While these studies provide a good base in understanding post-process leaching dynamics, there is a need to test for oxidizing conditions according to the zonal character of the geo-reactor (Figure 3-1). There is also a need to cater for possible development of acidic conditions due to geochemical transformations of the residue especially given the inherent sulphide mineralization in coal that can cause acid rock drainage (ARD).

3.8 UCG impact on groundwater

The UCG process takes place within the targeted coal seam with the coal seam aquifer being consumed as part of geochemical reactions. The gasifier consumes water from the coal seam aquifer together with moisture within the overburden and underburden sections, which then produces a cone of depression in the coal seam aquifer (Pershad et al., 2018b). If there are faults/fractures that link the coal seam aquifer with overlying aquifers then water will be drained from the shallower aquifers as the fractures provide a hydraulic connection (Figure 3-19). The heat from the gasification process can also induce secondary fractures in the surrounding strata. Groundwater monitoring in a UCG facility should cover all the identified aquifers around the gasification zone, before, during and post gasification. The monitoring programme should be both qualitative and quantitative. The quantitative groundwater monitoring of the shallow aquifer can indicate if a change in groundwater levels drops and this might be an indicator that water drainage to the coal seam aquifer is taking place. The deeper aquifer systems may also be confined, leading to piezometric surface that equilibrates within the overlying aquifer. The confined nature of deep aquifers suggests that pollutants can be transported to overlying aquifers if hydraulic connections exists. The groundwater monitoring programme should therefore cover all the overlying aquifers, the coal seam aquifer and the underlying aquifers beneath the gasification zone. A detailed review of groundwater monitoring at UCG sites is given by (van Dyk et al., 2018) which also proposed the frequency of sampling depending on the period of UCG operations.

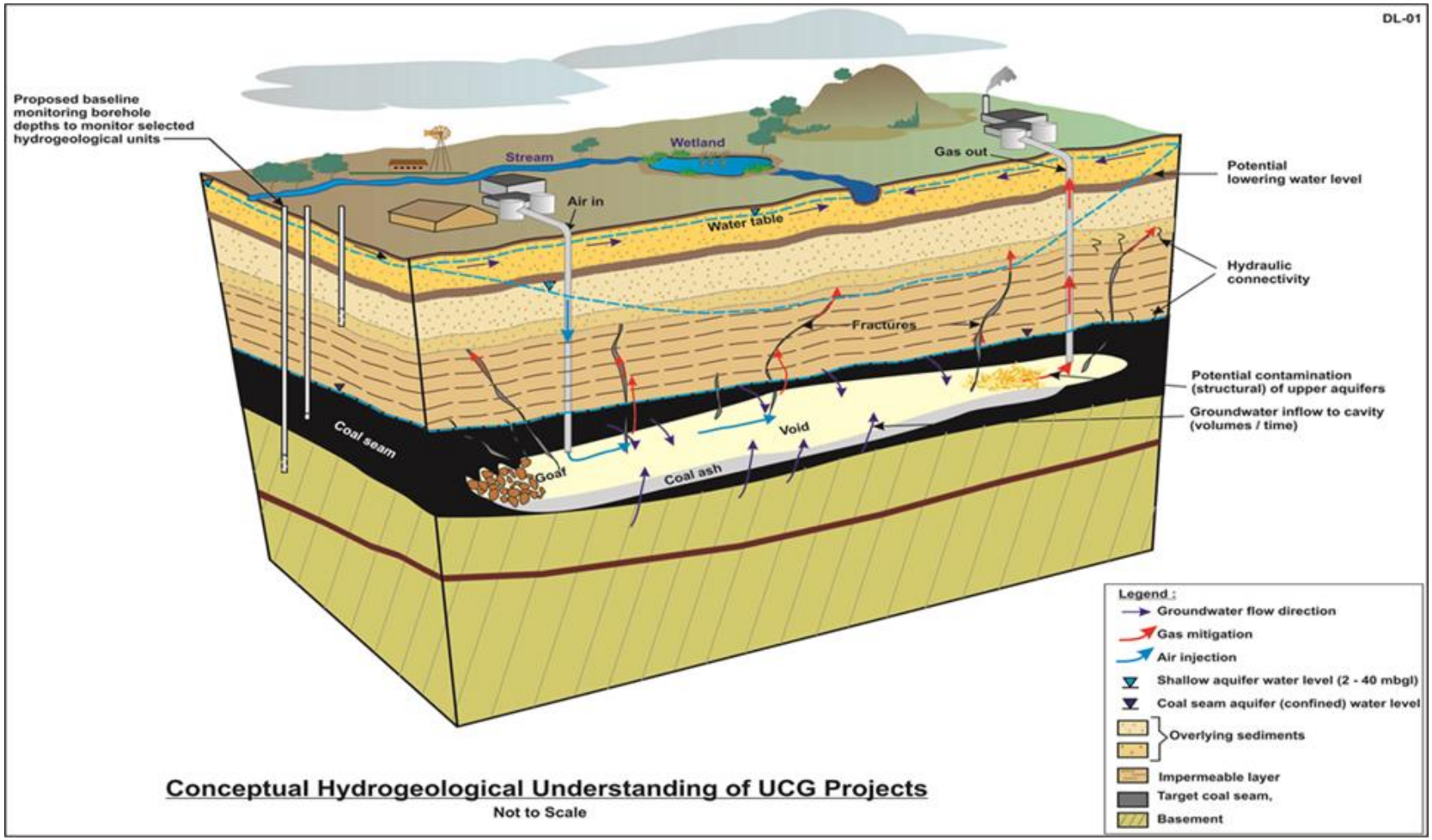

Figure 3-19 Conceptual hydrogeological model of a UCG plant adapted from (Pershad et al., 2018b)

Contamination to groundwater from UCG activities have been documented by a number of authors (Humenick and Mattox, 1978, Liu et al., 2007, Imran et al., 2014, Verma et al., 2014, Xu et al., 2016). Several studies across the world have piloted UCG technology, some with devastating groundwater contamination. Table 3-3 highlights some of the cases of groundwater contamination from UCG activities. UCG sites across the world are summarized in Figure 3-20 .

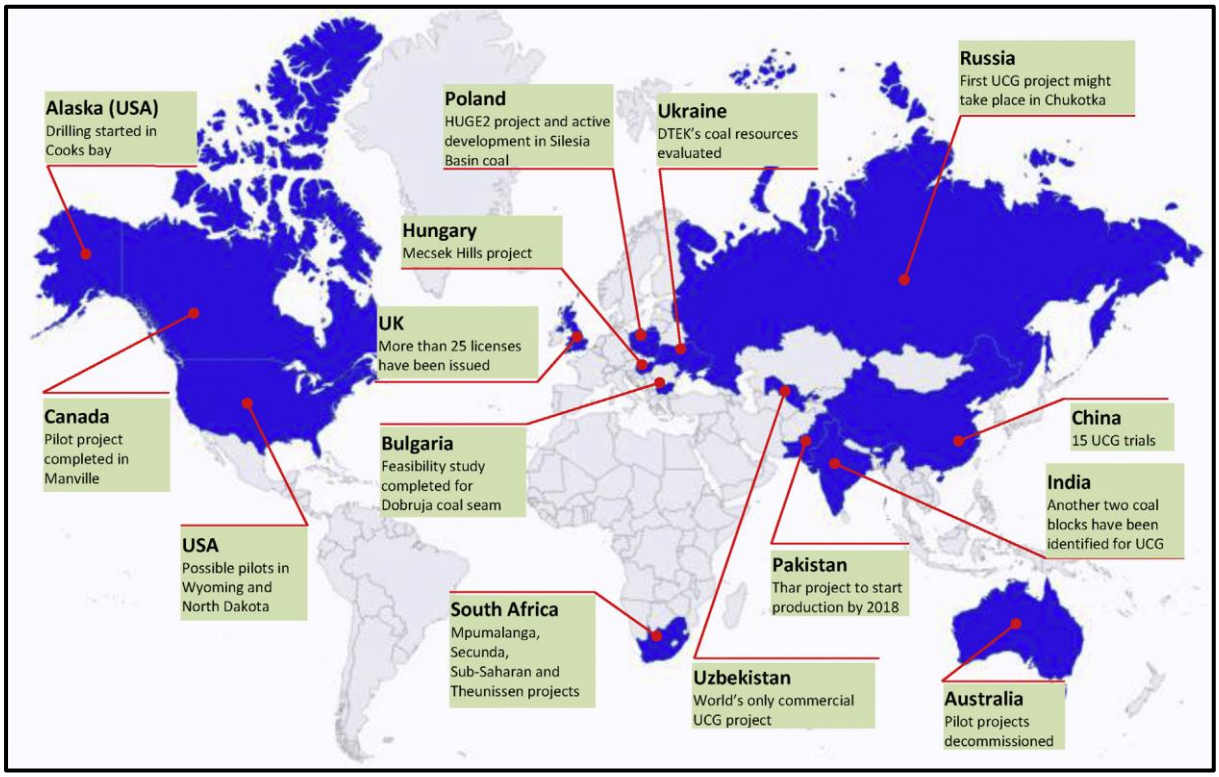

Figure 3-20 Worldwide UCG sites, adapted from (Yang et al., 2016)

Table 3-3 Some of the UCG sites that have reported groundwater contamination, summarized from (Imran et al., 2014, van Dyk et al., 2018)

UCG site	**Groundwater impact**
Hoe Creek I, Powder River Basin, Wyoming, USA	UCG trails were conducted at shallow depths (55 m). 11 boreholes were drilled into the coal seam aquifer and water samples taken during and post gasification. Groundwater analyses data showed that ammonium, calcium, boron, bromide, lithium, magnesium, sulphate, potassium, cyanide, and phenols were five times greater relative to baseline conditions. The majority of the changes in concentrations occurred within 3 m of the gasification zone in all directions.
Hoe Creek II / III	UCG trials were conducted at high pressures which resulted in product gas comprising of phenols and condensable hydrocarbons exiting into the overlying aquifers. In Hoe Creek II, 14 boreholes were drilled into the gasification zone and the overlying aquifer. Groundwater samples were taken before, during and post gasification and the inorganic results showed similar increases in elements as seen in Hoe Creek I.
Rocky Mountain 1 UCG test site in Hanna, Wyoming	12 boreholes were drilled into the coal seam and overlying aquifer. Groundwater samples were taken before, during and post gasification and the inorganic results revealed the following: • Conductivity and temperature were higher in the coal seam aquifer and overlying aquifer relative to baseline • Aluminium concentrations increased nearly 100 times over background values during UCG operation, however reduced to baseline values post gasification • Other elements and compounds that increased throughout gasification were copper, boron, iron, lead, zinc, calcium, sulphate compounds and ammonia. • Sulphate and chloride ionic concentration declined in all wells
Huntley UCG trial, New Zealand	No negative effects on the groundwater quality in the Tauranga Group aquifer by neither depletion of groundwater or contamination. One of the monitoring wells experienced a spike in dissolved organic carbon (DOC) but this trend reverted to baseline values once the pressure was reduced.
UCG test in Fairland, Tennessee	Groundwater monitoring revealed that the following elements all increased in quantity during gasification: calcium, zinc, iron, hydrogen, magnesium, ammonium, manganese, sulphate, mercury, and boron.
Kingaroy project, Australia	The Queensland Department of Environment and Resource Management declared over the media the forced closure of operations, citing detection of traces of benzene above the reporting trigger levels in a monitoring well near the plant and served Cougar Energy with an Environmental Protection Order that halted the development of the Kingaroy project.

Groundwater pollution from UCG activity can be managed if proper mechanism are put in place. The "clean cavern concept" has been implemented in UCG sites like Rocky Mountain I and Chinchilla in which the gasifier is operated using the following notions (Perkins, 2018a):

- Operating pressure is maintained below the neighbouring strata pressure during and post gasification in order to limit the escape of pyrolysis products and guarantee a positive flux of groundwater towards the gasifier.
- Post gasification pyrolysis products are vented out from the cavity
- Cavity temperatures are reduced by groundwater influx or surface water injection into the gasification zone upon shutdown of the gasifier to limit the release of more pyrolysis products.

The clean cavern concept essentially generally covers the organic contaminant risk from UCG operation and does not address the inorganic sources. The organic sources can therefore be reduced by good operational processes while inorganic sources (ash, char, thermally altered overburden) remain in the gasification zone where they pose long term groundwater contamination risk. Potential environmental impacts from UCG operations are summarized in Figure 3-21. Under primary processes, post-process leaching of coal ash by groundwater and post-process leaching of the overburden will be the focus of this study. This study will therefore focus on the exposure medium of groundwater. This study will also include post-process leaching of char and the underburden in an effort to cover all sections of the spent geo-reactor that can be potential groundwater contaminant sources.

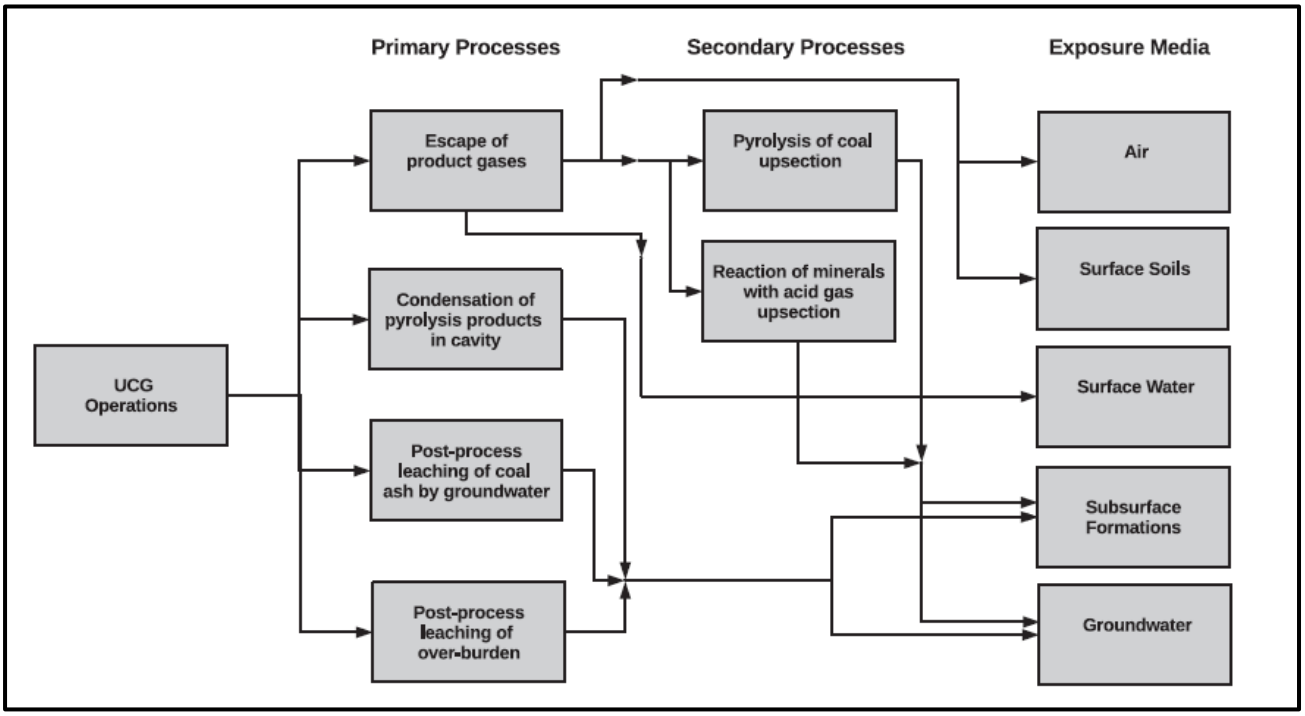

Figure 3-21 Potential environmental impacts from UCG operations, adapted from (Perkins, 2018a)

3.9 Summary

The aim of the study is to determine the potential sources of groundwater contamination from UCG gasification zone and the prospective chemical evolution. The sources of groundwater contamination

are ash, char and the thermally altered surrounding rocks. The mineral transformation that occur within these rocks are important as the secondary minerals are the ones which will be interacting with groundwater post gasification. In some cases there may even be amorphous species instead of minerals due to the rapid cooling in the gasification chamber. The leaching dynamics of all of these UCG products need to be assessed in order to address the question of groundwater contamination. Standard leaching tests may not be appropriate for UCG waste as most of these tests were designed for surface stored waste and not aquifer bound waste. There is therefore a need to assess UCG waste in a way that can address the concern of regulatory authorities taking into account the environment in which this waste exist and the leaching medium its exposed to. This study undertakes to develop a comprehensive leaching testing that takes into account field condition for UCG waste. This research will also undertake to provide predictive mechanisms relevant for UCG type waste.

The next chapter looks at the gasification zone using the Majuba UCG site for samples collection and assessments.

4 Pyrometamorphism and mineralogical assessment of the spent gasifier

4.1 Introduction

The underground coal gasification process inherently produces sufficient heat that bake, fuse and even melt rocks surrounding the gasifier. Burning coal sites are areas associated with substantial mineral transformation due to the high temperature alteration to the sedimentary rocks and the coal itself (Ciesielczuk et al., 2015). These secondary minerals are potential sources of aquifer contamination post gasification, due to the leaching action of the rebounding groundwater as it enters the spent geo-reactor and leaches remnants of UCG. The relics of the gasification process include the ash, char and altered overburden and underburden. Post gasification, groundwater is the only medium that can enter the chamber and carry contaminants to secondary environments. There is therefore a clear need to study the mineralogy of the spent UCG chamber in order to assess the risk to groundwater pollution emanating from UCG activities.

Contamination generated from the UCG chamber will be in the form of dissolved elements in groundwater. Potentially toxic elements exists in mineral phases or amorphous material that form part of the coal and the rocks around a spent geo-reactor. The aim of this chapter is to assess the mineral phases of different types of material contained in a spent UCG chamber. This section of the study aims to address the first objective of the research, which is the characterization of the potential sources of inorganic groundwater contamination from a spent UCG chamber.

4.2 Methodology

Two boreholes (G1VH2 and G1VH3) were core drilled to intercept the gasification chamber at the Majuba UCG pilot plant (Figure 4-1). These boreholes were labelled verification boreholes as they were drilled with the purpose of verifying the extent of the gasification process. For example, G1VH2 represents: G1 = Gasifier 1, V = Verification, H = Hole and 2 means is the second borehole drilled. Two additional boreholes (G1VH4 and G1VH6) were core drilled “off cavity” to retrieve samples from regions unaffected by gasification. The conceptual model of the position of the boreholes in relation to the geo-reactor is shown in (Figure 4-1). The core drills were sampled by cutting out small portions of around 30 mm blocks that were prepared for QEMSCAN (Quantitative Evaluation of Minerals by Scanning Electron Microscopy) analysis. QEMSCAN analysis and sample preparation was done at Eskom Research, Testing and Development centre in Rosherville, South Africa.

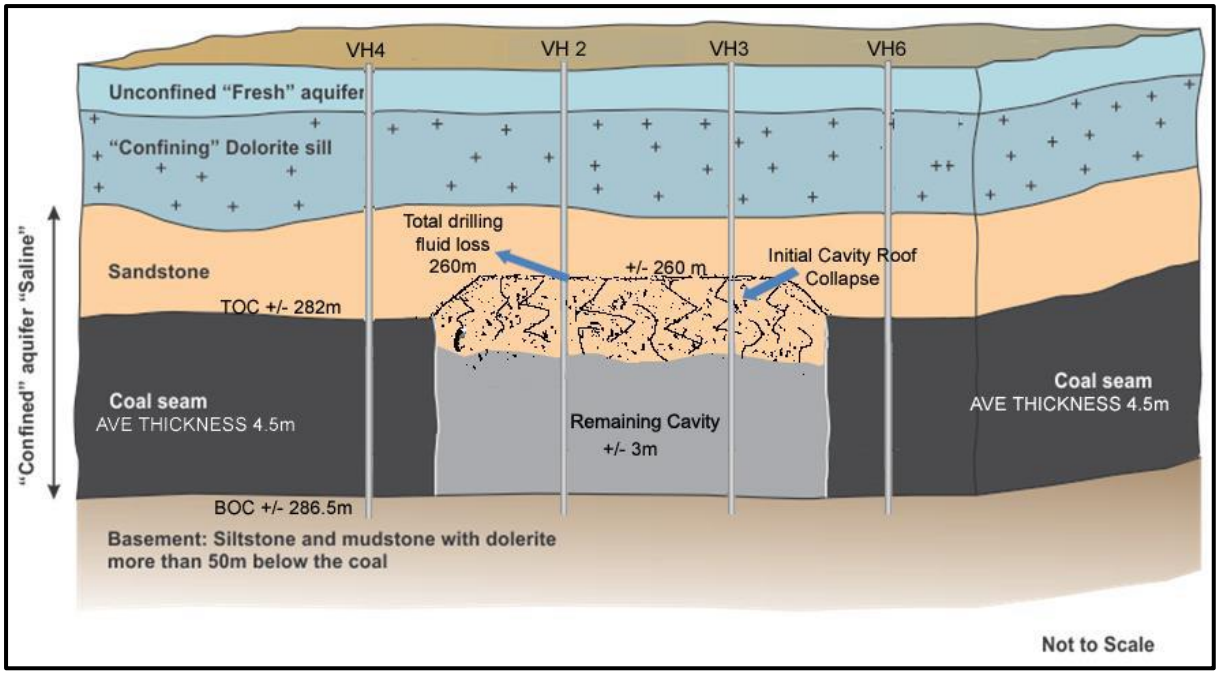

Figure 4-1 Conceptual model of the spent geo-reactor with position of verification boreholes, modified from (Pershad et al., 2018a). Distance between off cavity boreholes (VH6 and VH4) and the cavity intercepting boreholes are presented in Appendix 3-B.

QEMSCAN (FEI Quanta 650F SEM) is an automated scanning electron microscope with three energy dispersive X-ray spectrometers and computer software for data assemblage and image processing (Nazari et al., 2017). QEMSCAN can be used to determine the mineral and phase proportions of any particulate material. A full account of the operation of QEMSCAN is given by (Goodall et al., 2005). Samples taken from drill cores targeted sections of the overburden, gasification zone (Gus seam), ash and the underburden. Sampling depths are presented in Table 4-1. An example of sampling for core drills G1VH3 and G1VH2 are presented in Figure 4-2 and Figure 4-3, respectively. The same sample numbers will be used throughout this document. Visibly cracked sections and alteration spots were also targeted as the thermal effects of gasification were not expected to be uniform. Thermal effects above a burning coal seam are not disseminated evenly and are possibly linked with regions of higher permeability through which hot gases exit to produce fused chimneys (Figure 3-3).

Samples were prepared for QEMSCAN analysis by inserting them into individual sample holders and immersing them in carnauba wax (Figure 4-4). The samples were then placed in a pressure pot set at 2 bars for 6 to 12 hours. This was done to reduce bubbling that typically occurs with unpressurised curing. Once curing was completed samples were then taken out of the pressure container and removed from the mould for polishing. The samples were polished using – Struers TegraPol-21. Polishing was done at a force of 10N/60N with a rotation speed of 300rpm. The samples were then carbon coated using K950x turbo evaporator. Samples were placed upwards and carbon coated in a vacuum. Carbon coating was done to avoid samples getting charged in the chamber when struck by the electron beam. The samples were then transferred to the QEMSCAN machine for analysis.

Figure 4-2 Core sampling of VH3, the same sample numbers will be used throughout this document

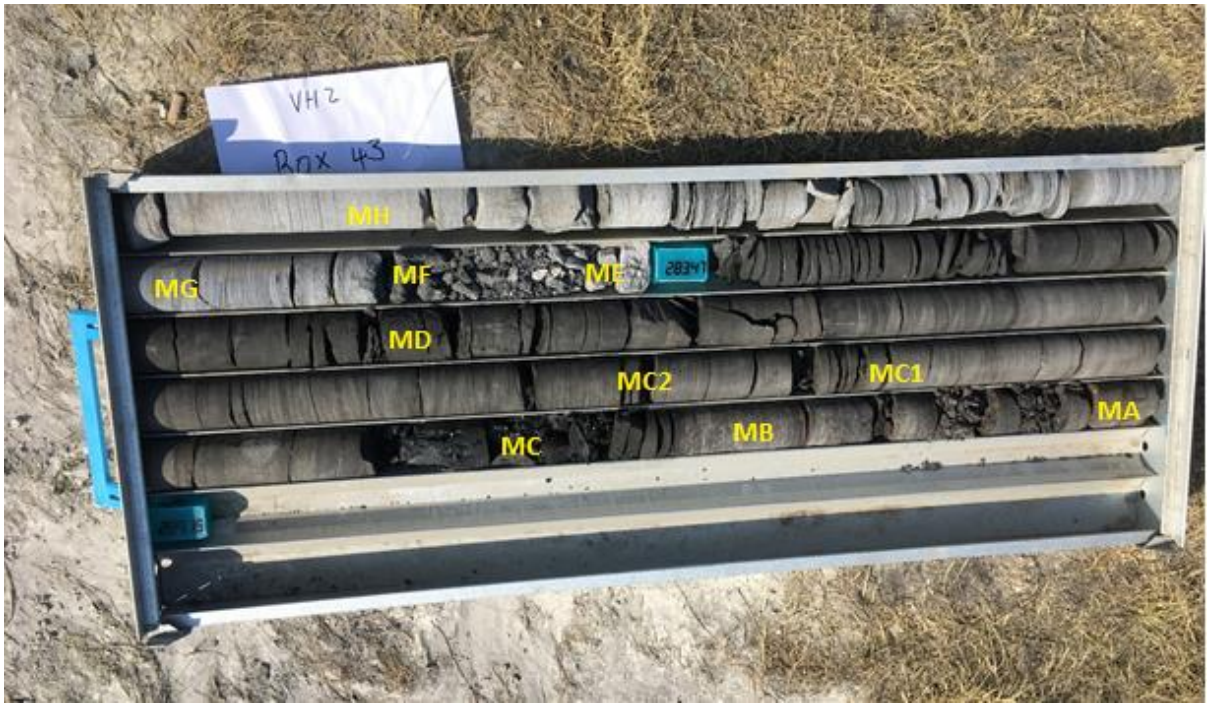

Figure 4-3 Core sampling of VH2, the same sample numbers will be used throughout this document

Table 4-1 Sampling depth with relation to the gasification zone (Gus seam), the sample numbers and same colour coding will be used throughout this entire document. The cavity intercepting boreholes (VH3 and VH2) were sampled more extensively than the off cavity borehole since they presented “new” macro heat affected features that are the subject of this study, while VH4 had pristine sedimentary lithology that has been studies extensively in previous Karoo studies.

Core	Sample ID	Depth (m)	Lithology	Relation to Gus
G1VH2	MA	289	Medium grained micaceous , grey sandstone, reddish tint ("heat affected")	Floor
G1VH2	MB	288.5	Carbonaceous black , shale ,micaceous in places with reddish tint	Floor
G1VH2	MC	288.5	Coal, heat affected, bright banded	Floor
G1VH2	MC1	287.6	Grey siltstones, micaceous/brittle	Floor
G1VH2	MC2	287.1	Grey micaceous siltstones	Floor
G1VH2	MD	286.5	Micaceous, grey siltstones"shaley"	Floor
G1VH2	ME	283	Ash and altered sandstones from "UCG cavity"	Gus
G1VH2	MF	282.5	Light Grey laminated siltstones/shales, heat affected with dark green discolouration	Roof
G1VH2	MG	282	White laminated sandstones, medium grained/micaceous	Roof
G1VH2	MH	279.6	White sandstones, coarse grained	Roof
G1VH3	S0.1	276.1	Sandstone	Roof
G1VH3	S0.2	277.34	Sandstone	Roof
G1VH3	S0.3	278.14	Sandstone	Roof
G1VH3	S1	278.64	Sandstone	Roof
G1VH3	S2	278.92	Sandstone	Roof
G1VH3	S3	279.12	Sandstone	Roof
G1VH3	S4	279.40	Sandstone	Roof
G1VH3	4.1	279.9	Sandstone	Roof
G1VH3	S5	280.24	Sandstone, slaggy	Roof
G1VH3	5.1	280.45	scoria	Roof
G1VH3	S6	280.80	scoria	Roof
G1VH3	6.1	280.90	scoria	Roof
G1VH3	6.2	281.12	scoria	Roof
G1VH3	S7	281.21	Buchite	Roof
G1VH3	S7.1	281.3	Buchite	Roof
G1VH3	S7.2	281.64	Buchite	Roof
G1VH3	S8	281.68	Buchite	Roof
G1VH3	S9	281.71	Ash	Gus
G1VH3	S10	280.80	Char	Gus
G1VH3	S11	282.08	Char	Gus
G1VH3	S12	282.18	Char	Gus
G1VH3	S13	282.30	Char	Gus
G1VH3	S14	282.60	Char	Gus
G1VH3	S15	282.84	Char	Gus
G1VH3	S16	282.87	Char	Gus
G1VH3	S17	283.62	Char	Gus
G1VH3	S18	283.89	Char	Gus
G1VH3	S19	284.12	Carbonaceous black shale	Floor
G1VH3	S20	284.5	Carbonaceous black shale	Floor
G1VH3	S21	285.1	Carbonaceous black shale	Floor
G1VH3	S22	285.5	Carbonaceous black shale	Floor
G1VH3	S23	287.59	Carbonaceous black shale	Floor
G1VH4	T1	274.30	Interlaminated Sandstone and siltstones coarsening downward	Roof
G1VH4	T2	275.00	Sandstone	Roof
G1VH4	T3	276.50	Sandstone	Roof
G1VH4	T4	277.40	Sandstone	Roof
G1VH4	T5	282.00	Interlaminated Sandstone and siltstones carbonaceous	Floor
G1VH4	T6	290.00	Interlaminated Sandstone and siltstones carbonaceous	Floor
G1VH6	T7	290.50	Interlaminated Sandstone and siltstones carbonaceous	Floor
G1VH6	T8	276.50	Sandstone	Roof
G1VH6	T9	277.50	Sandstone	Roof

The QEMSCAN is fitted with a field emission gun (FEG) electron source with an accelerating voltage and beam current. Scanning electron microscope electron beam is situated at predefined points across a particle. At each point a 1000 count X-ray spectrum is acquired in 3 milliseconds and the elemental proportions are used to identify the mineral phase at each point. Selected samples were also analysed

for mineral phases using for X-Ray diffraction (XRD) at the University of Johannesburg. XRD was utilized as a complementary method to QEMSCAN.

Figure 4-4 Sample preparation for QEMSCAN analysis, block samples are put in 30 mm diameter sample holders and carnauba wax is added (right). The mixed sample was placed in a pressure vessel set at 2 bars for 5 to 12 hours (left)

4.3 Results

Some of the QEMSCAN false colour images (simply referred to as QEMSCAN image) presented in this section have been cropped and are not at the true scale. The full-scale images with the average modal proportions and colour key for mineral identification are presented in Appendix 4 -E.

4.3.1 Visual assessment of retrieved cores

The drill core of the Gus coal seam section for the off-cavity borehole, G1VH4, is displayed in Figure 4-5. The Gus coal seam was encountered at 277.81 mbgl and a total of 4.42 m of the coal was recovered. The Gus seam in the Majuba coalfield fluctuates in thickness between 1.8 to 4.5 m (de Oliveira and Cawthorn, 1999) and therefore the retrieved coal corresponds with the upper limit, hence pointing to full recovery of the seam. The overburden contained medium to coarse-grained sandstone alternating with siltstone. Detailed lithology logs are included in Appendix 4-A. The overburden and underburden of G1VH4 had no visible signs of heat exposure and hence confirmed the status of an

“off-cavity” borehole. G1VH4 will be utilized as a reference borehole representing pristine mineralogical assemblages in the study area. G1VH4 is approximately 98 m from G1VH2 (Appendix 3).

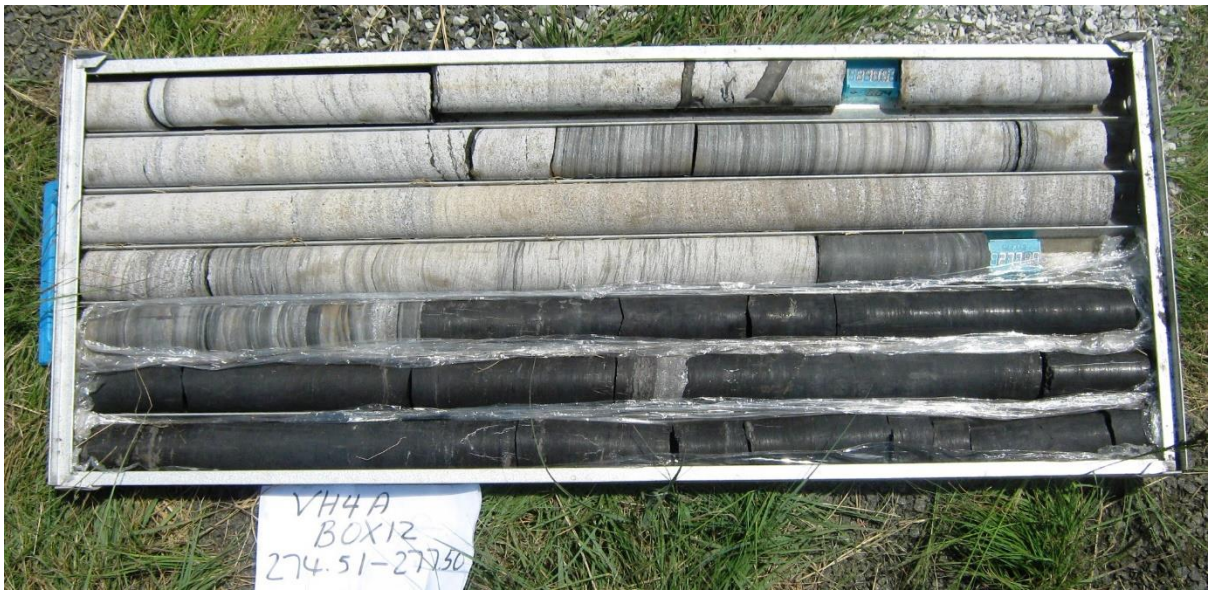

Figure 4-5 Gus seam section of the drill core of G1VH4, the coal seam starts at 277.81 mbg (black core section)

The Gus coal seam sections of the drill cores from the two boreholes, G1VH2 and G1VH3, intercepting the gasification zone are displayed in Figure 4-6 and Figure 4-7 respectively. G1VH2 core drill did not recover any remnants of coal from the targeted Gus seam position however breccia and ash like particles were recovered from the bottommost part of the overburden. During drilling there was a core loss of around 4 meters at the position of the Gus seam before recovery of the carbonaceous shale floor (Appendix 4-A). The overburden did not show any visible signs of slagging or gas release vesicles however there was a small degree of fracturing along bedding planes on the coarse-grained arkosic sandstone. The carbonaceous shale floor showed horizontal orientation fragmentation and this may be due to the platy mica minerals that were visible in this formation which induce flat disintegration in rocks.

Figure 4-6 Gus seam section of the drill core of G1VH2, the coal seam not recovered and bottom of overburden shown by the 283.47 mbg (blue marker). Carbonaceous shale (coal seam floor) begins after the blue marker

G1VH3 drill core retrieved around 2 m of devolatilized coal (char) with the overburden containing an ash layer and an extremely heat-affected sandstone with vast amount of visible vesicles (Figure 4-7). Two meters of the overburden above the char contact showed the most macroscopic pyrometamorphism features. Grapes (2011) showed an example of buchites developing within a maximum of 2 m, more generally < 50 cm, of a sandstone-dolerite contact in the Sterkspruit Valley in South Africa. Selected sections of the overburden with distinct pyrometamorphosed attributes are described in Table 4-2.

Figure 4-7 Gus seam section of the drill core of G1VH3, the ash layer at 281.7 mbg is the bottommost part of the overburden and represents the overburden-char contact.

The contact of the overburden with the char had a thin (2cm) ash layer of soft material (Table 4-2). The sandstone immediately above the ash layer was baked and partly fused with vast amounts of vesicles in a frothy texture (scoria-ceous rock). Bedding planes were barely present and the colour was predominantly white with smaller intersections of dark matrix material. This was characterized as the buchite section of the core, which was typically very light (like chalk). Grapes (2011) also reported a sharp change in specific gravity in the rocks next to the dolerite-arkose contact in an excavation pit at Baksteen, near Heilbron, South Africa. Around 80 cm above the ash layer, the sandstone had a turbid matrix with vitrified smooth glazed surfaces with sharp edges along fracture planes, paralava section.

Table 4-2 Macroscopic features from the heat affected overburden, from core drill G1VH3

Macroscopic features	**Sections of the heat affected metamorphosed overburden**
Ash layer above the coal (char) contact (S9). The ash layer was very soft and crumbled easily	
Buchite (S7): Immensely vesicular white frothy pumice-scoria (scoria-ceous rock), very light (not dense). This section of the core is in the range, 0 to 1.6 m, above the ash layer and can be classified as buchite.	
Paralava (S6): Vesicular vitrified aphanitic rock (fused sandstone), in places had smooth glazed surfaces. Dense and slaggy, has a dark purple matrix (turbid isotropic glass) and basalt like resemblance	

The Paralava section of core becomes progressively more fractured and dense (heavier). The bedding planes became more vertically orientated and slagging was visible with ropy features. The cracks/fractures ware irregular and to some extent seem to follow the “bending” bedding planes. This core section had an aphanitic texture with the scoria rock resembling basalt as the matrix was predominantly dark coloured (dark purple) with vesicles. Above 2 m from the ash layer, the overburden sandstone visibly regained the horizontal bedding planes and the rock gradually resembles the background conditions seen in G1VH4 (Figure 4-5), albeit with more fractures.

4.3.2 Primary mineralization

Detailed geology of the Majuba coalfield and the Majuba UCG site was given in chapter 2. The sedimentary sequence in the roof of the Gus seam is characterized by alternating laminated siltstone and arkosic sandstones in a general trend of fining-upward cycles. The floor of the Gus coal seam comprises of carbonaceous shale and mudrocks. The major minerals that occur in the sedimentary rocks of the coal zone are quartz, feldspar (albite and microcline) and clay minerals (kaolinite and illite). Accessory minerals include calcite, siderite, pyrite and glauconite, rutile, zircon, ilmenite and apatite. A QEMSCAN image of pristine arkosic sandstones of the overburden from drill core G1VH4 is presented in Figure 4-8. The angularity of the minerals is well preserved in a compact assemblage. Most of the interstitial spaces between minerals are filled by clay (kaolinite) which indicates that it was the cementing material during the diagenesis process. A QEMSCAN image of pristine argillaceous siltstone and mudstone from the floor of the Gus seam is presented in Figure 4-9. Both rocks are mica (muscovite) rich which explains the horizontal fracturing that characterize this section of the core drill. Unlike in arkosic sandstones where quartz are dominant, argillaceous rocks have clay (kaolinite) as the major mineral in a dense mineral assemblage.

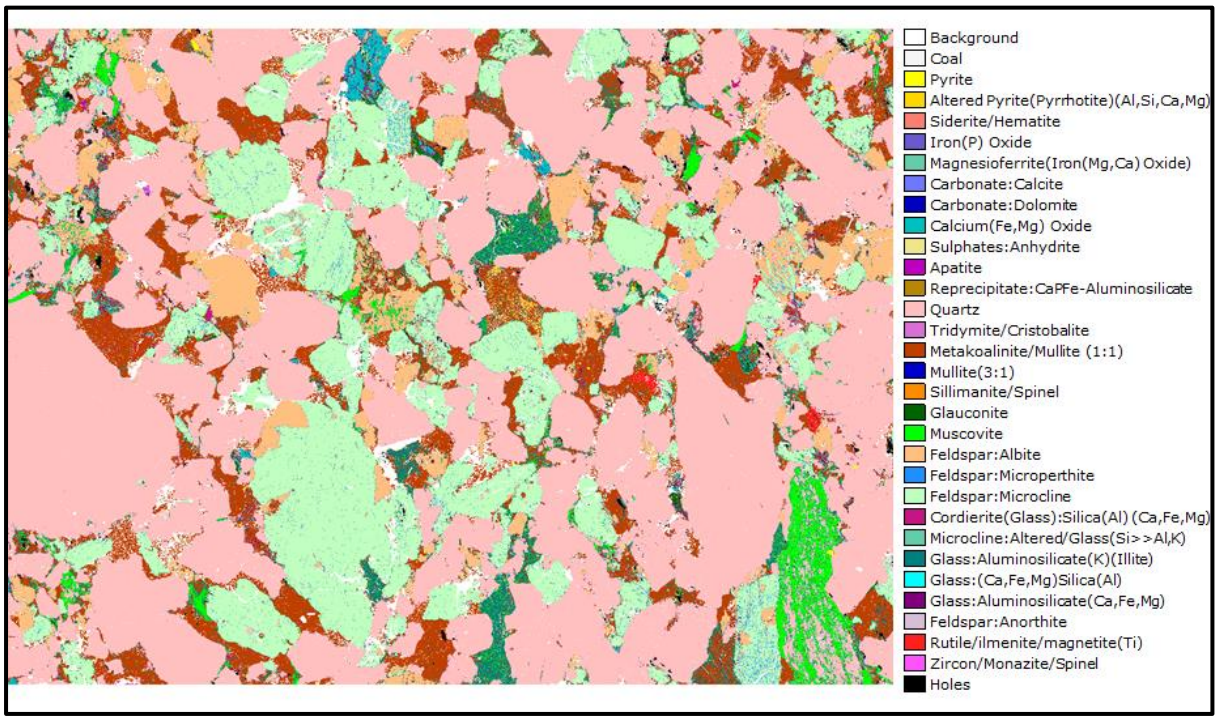

Figure 4-8 QEMSCAN false colour image of medium grained arkosic sandstone from drill core G1VH4 (sample T1), (pink mineral = quartz, bright green = microcline, brown = kaolinite, beige = albite)

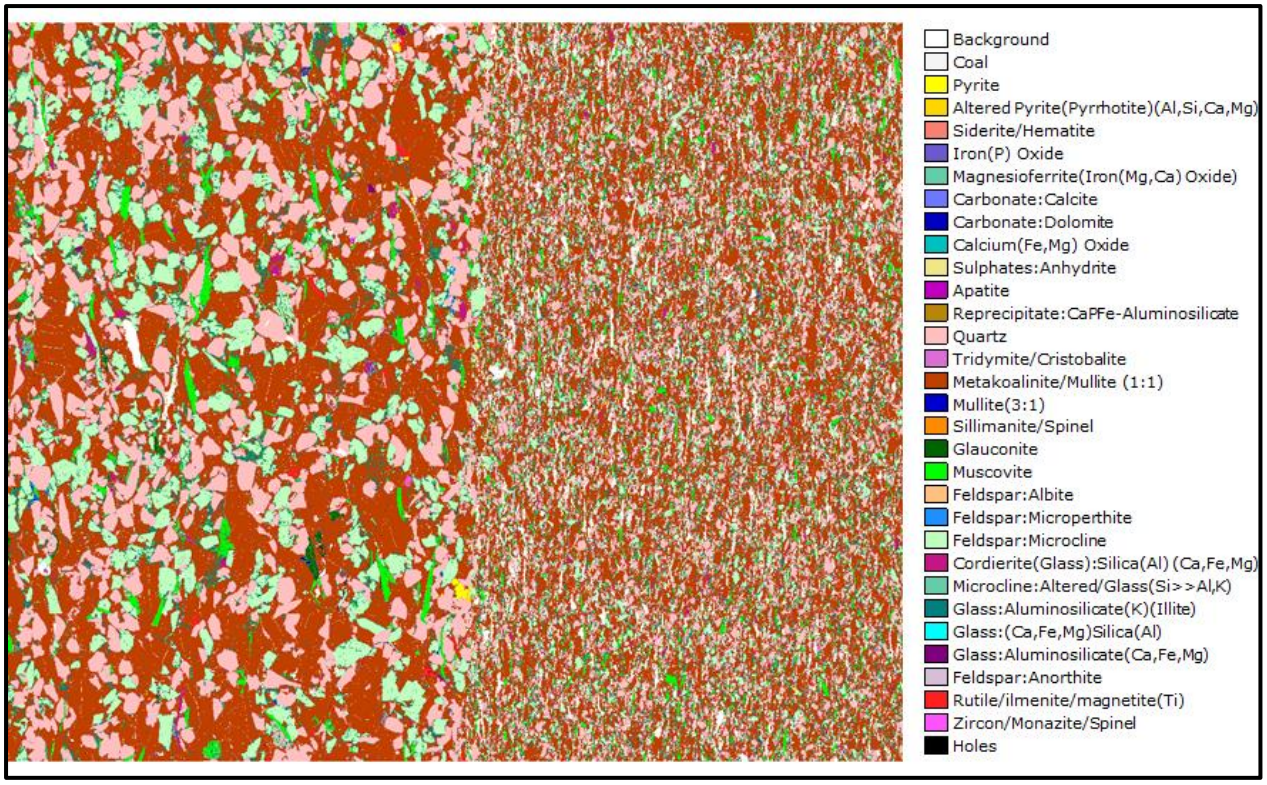

Figure 4-9 A QEMSCAN false colour image of the floor of the Gus seam showing argillaceous siltstone (left) and mudstone (right) with the contact clearly visible in the middle, from drill core G1VH4, (brown mineral = kaolinite, muscovite = bright green)

The average mineral composition of the unaltered rocks of the roof and floor of the Gus seam is given in Figure 4-10. The modal proportions determined by QEMSCAN analysis for all samples are included in Appendix 4-B. The arkosic sandstone roof is characterized by (quartz>microcline>kaolinite>albite>illite) whereas the argillaceous floor is characterized by (kaolinite> quartz> illite> microcline> albite) mineral assemblages. The floor of the Gus seam had very little albite (<0.1 Vol %) with other minerals (e.g muscovite >5 Vol %) occurring at more significant proportions.

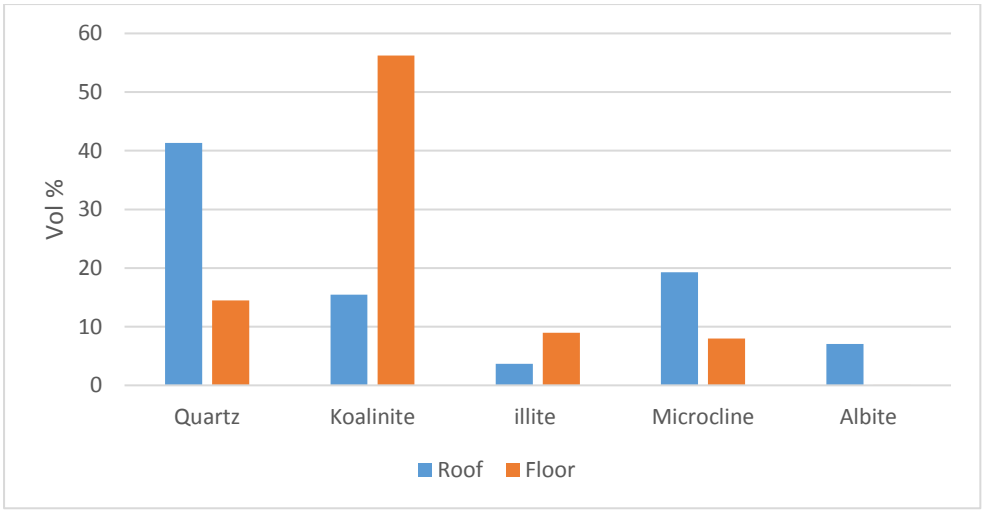

Figure 4-10 Average modal proportions of the unaltered rocks of the roof (T1-T3) and floor (T5-T6) of the Gus seam determined from drill hole G1VH4.

The general mineral assemblage for the unaltered roof and floor of the Gus seam is displayed in Figure 4-11. In this chapter, the thermally altered mineral assemblages from drill cores intercepting the gasification area will be compared with these pristine phases.

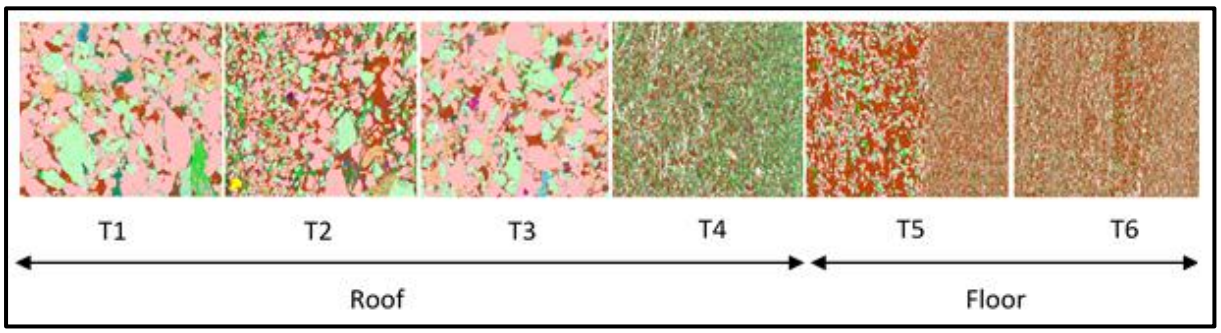

Figure 4-11 general mineral assemblage for the unaltered roof and floor of the Gus seam from drill core G1VH4

4.3.3 Mineral alterations

4.3.3.1 Pyrite and pyrrhotite transformation

Pyrite lenses were found in the interstitial mineral spaces of the unaltered overburden (Figure 4-14). The pyrite profile for the two verification boreholes that intercept the gasification zone (i.e. G1VH2 and G1VH3, simply written as VH2 and VH3) was compared with the off-cavity borehole (i.e. G1VH4, simply written as VH4) in Figure 4-12. The average pyrite proportion in the unaltered overburden of VH4 was 0.09 Vol % while averages of 0.02 and 0.001 Vol % were recorded for the roof sections of VH3 and VH2, respectively. The data is from QEMSCAN analysis and is included in Appendix 4-B. The sharp peak observed in the VH2 profile was for a sample taken from the Dundas coal seam located around two meters below the Gus seam and was included to illustrate the effect UCG has on coal (Figure 4-12).

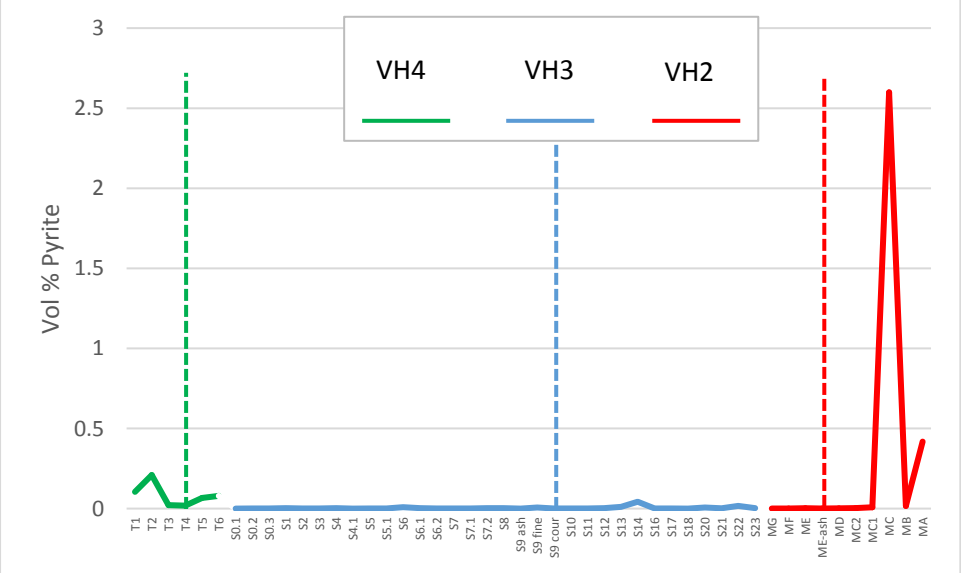

Figure 4-12 Variation in pyrite composition in core drills VH2, VH3 and VH4. Dashed vertical lines represent top of Gus seam in each respective drill core

The devolatilized coal (char samples, i.e. S10 to S18) in VH3 are all relatively poor in pyrite as compared to the Dundas coal seam. The pyrolysis stage of UCG liberates sulphur from sulphide minerals into the gas stream where it escapes in the production boreholes. Pyrite also decomposes to pyrrhotite at 530 – 620 °C (Grapes, 2011) and therefore as pyrite proportions reduce, it is expected that pyrrhotite concentrations would increase. The results therefore confirm that char and rocks near the gasification zone have relatively low pyrite content as compared to the pristine lithology (VH4).

The pyrrhotite profiles are presented in Figure 4-13. The average proportion of pyrrhotite in the overburden of VH4 was 0.16 Vol % while averages of 0.44 and 1.55 Vol % were recorded for the overburdens of VH3 and VH2, respectively. The floor of VH4 recorded an average of 0.12 Vol % while 0.62 and 0.33 Vol % were recorded for VH3 and VH2, respectively. Pyrrhotite mineralization occurred throughout the char section of VH3 with an average quantity of 1.3 Vol % with sample S14 recording the highest proportion of 6.3 Vol %. While pyrite content was relatively higher for the unaltered VH4 overburden as compared to the poorer averages recorded in VH2 and VH3, the recorded averages for pyrrhotite exhibit an inverse behaviour as higher pyrrhotite averages were recorded for the drill cores intercepting the gasification zone (i.e. VH2 and VH3) while the invariable rocks of VH4 were relatively poor in pyrrhotite.

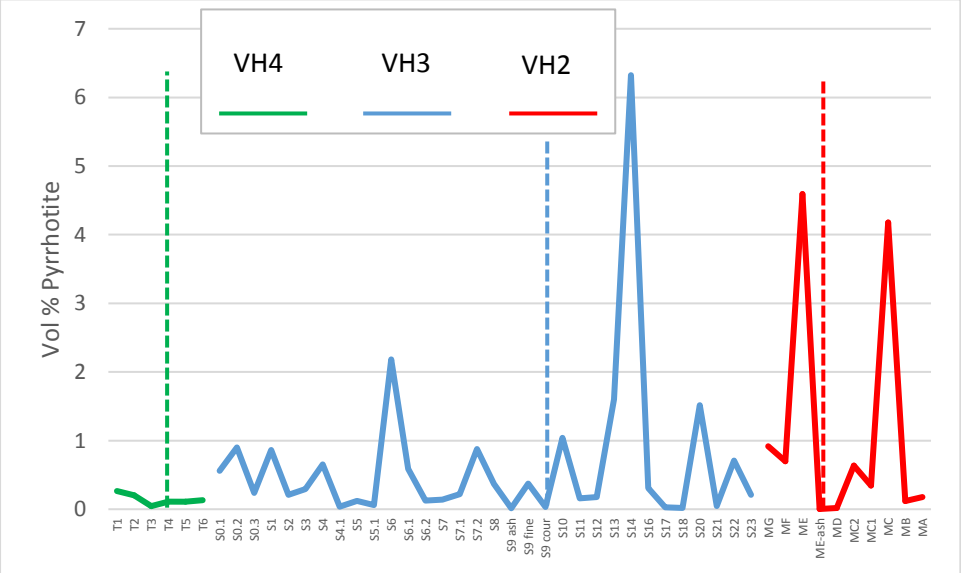

Figure 4-13 Variation in pyrrhotite composition in core drills VH2, VH3 and VH4. Dashed vertical lines represent top of Gus seam in each respective drill core

The absence of pyrrhotite implies that the pyrite decomposition reaction (4.1) has not occurred and therefore the temperature of 760 °C was not reached in VH4 (Grapes, 2011):

$$Pyrite \rightarrow Pyrrhotite + liquid \quad (4.1)$$

Pyrite occurred in the unaltered rocks as part of the rock matrix and located in interstitial spaces (Figure 4-14), however the deportment of pyrrhotite was generally isolated from the rock matrix and formed around the edges of mineral assemblages as droplets/clusters (Figure 4-15). Pyrrohotite was generally associated with high temperature minerals such as cordierite that crystallise from a melt and occurred as droplets mostly rimmed by cordierite and mullite grains which shows crystallization from a melt.

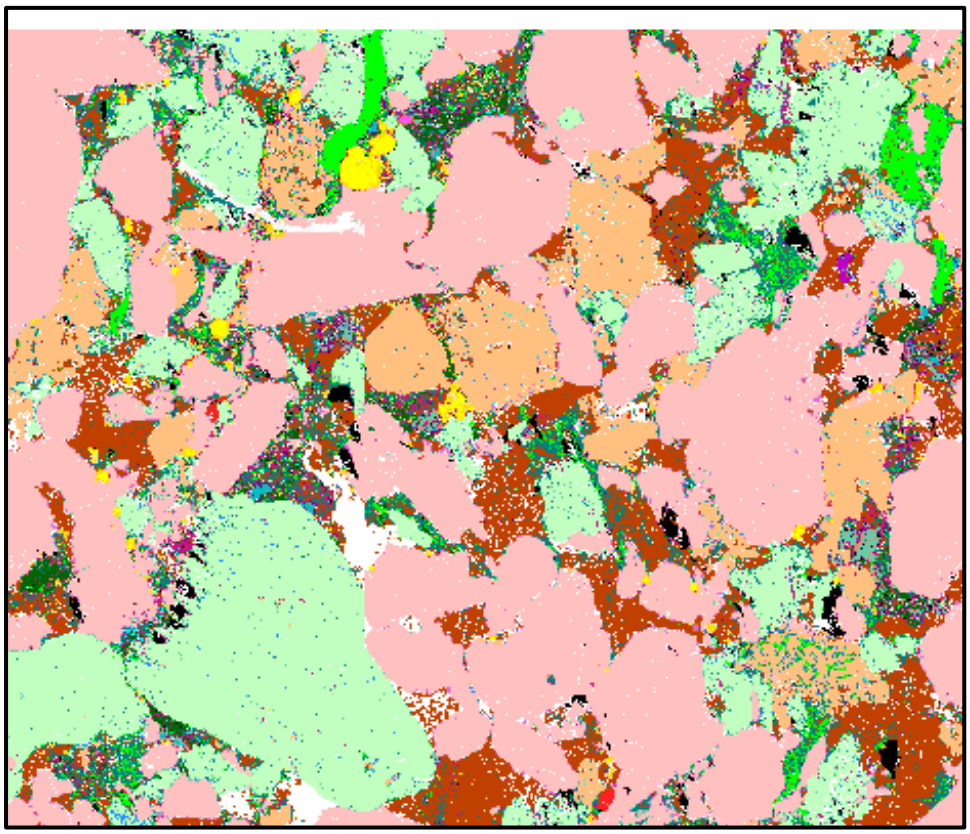

Figure 4-14 QEMSCAN false colour image showing Pyrite (bright yellow) interstitial in unaltered arkosic sandstone (sample T1)

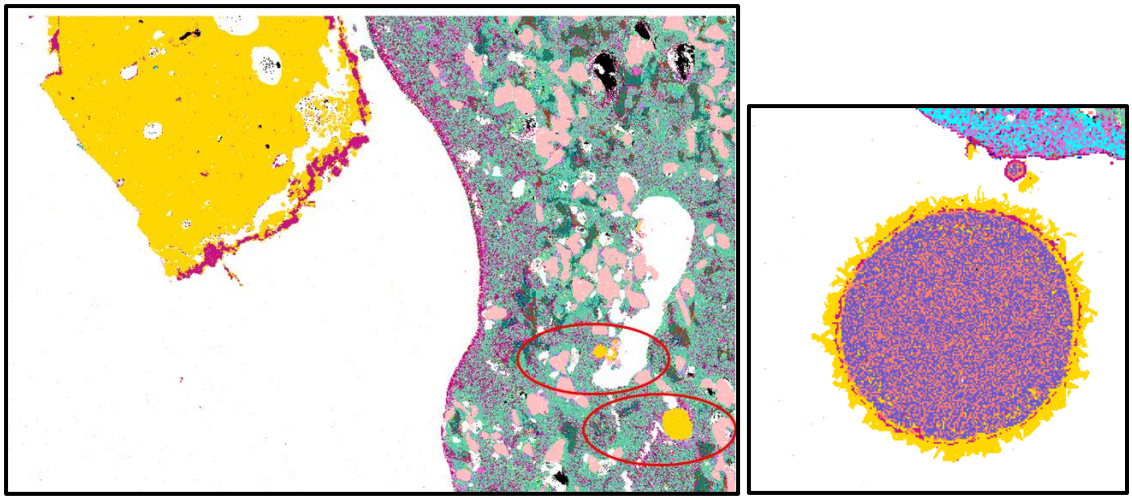

Figure 4-15 (Left picture, S6 from VH3) Altered overburden showing a large anhedral grain of pyrrhotite (yellow) surrounded by cordierite (maroon colour), small droplets of pyrrhotite (encircled in red) also rimmed by cordierite and mullite with the angularity of quartz grains reduced. (Right picture S7.2 from VH3) showing crystals of pyrrhotite on the surface of round molten iron oxide (wustite).

The transformation of pyrite to pyrrhotite and the sequential association with glass was illustrated in Figure 3-15(a). The mineral grains of pyrrhotite on the spherical surface of iron oxide (Figure 4-15) shows that the average enrichment of pyrrhotite seen in the altered overburdens of VH2 and VH3 was generally from the decomposition of pyrite and subsequent crystallization as altered pyrite (pyrrhotite) on surfaces of derivatives of the transformation reaction (i.e. glass and iron oxide) (Figure 3-15). This also explains why pyrrhotite was not observed in the interstitial spaces in rock matrix similar to pyrite occurrence but rather formed anhedral grains on the edges of the thermally altered rocks where it was possibly deposited as droplets from molten material.

Figure 4-16 shows preservation of detrital minerals grains (quartz and microcline) along vitrified material comprising mostly of anorthite, cordierite, mullite, pyrrhotite and silica-glass. There was however lack of pyrrhotite crystallization within the detrital minerals grains except where there was clear signs of slagging and in such instances, it was rimmed by silicate-glass or cordierite. Nesse (2000) stated that masses of pyrrohotite occurring in mafic and ultramafic rocks have crystallized from immiscible segregation of a sulphide melt from a silicate melt. Pyrrhotite was also detected in XRD analysis for sample S8 (Appendix 4-C). Iron sulphides are of environmental concern due to the potential of acid generation when exposed to oxidizing conditions which consequently leads to acid rock drainage.

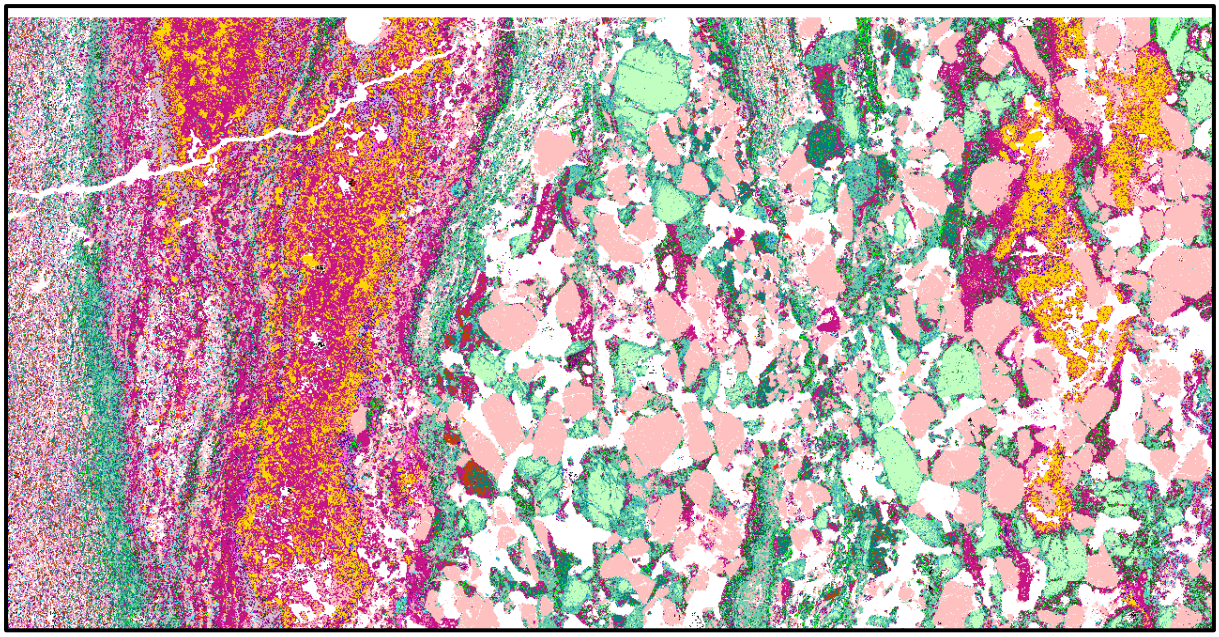

Figure 4-16 Pyrrhotite (yellow) occurring along slag material (glass) and surrounded by anorthite (grey) and cordierite (maroon), sample ME (ash and rubble) from VH2

4.3.3.2 Cordierite

Cordierite $(Fe,Mg)_2Al_4Si_5O_{18}$ is an indicator mineral of pyrometamorphic rocks, mainly in buchites where it has crystallised from a melt and occurs as porphyroblasts or anhedral grains similar in size to quartz and feldspar (Nesse, 2000, Grapes, 2011). The cordierite profile in the Majuba UCG gasification zone (VH2 and VH3) was compared with the off cavity conditions (VH4) and presented in Figure 4-17. The average cordierite proportion in the unaltered overburden of VH4 was 2.6 Vol % while recorded averages for VH2 and VH3 were almost double at 5.05 and 4.2 Vol %, respectively. The minor cordierite detected in VH4 could be relics from the dolerite intrusion. The highest cordierite proportion recorded was 21.2 Vol % (sample S7.1), less than a metre from the roof-char contact. The QEMSCAN image of sample S7.1 is presented in Figure 4-18.

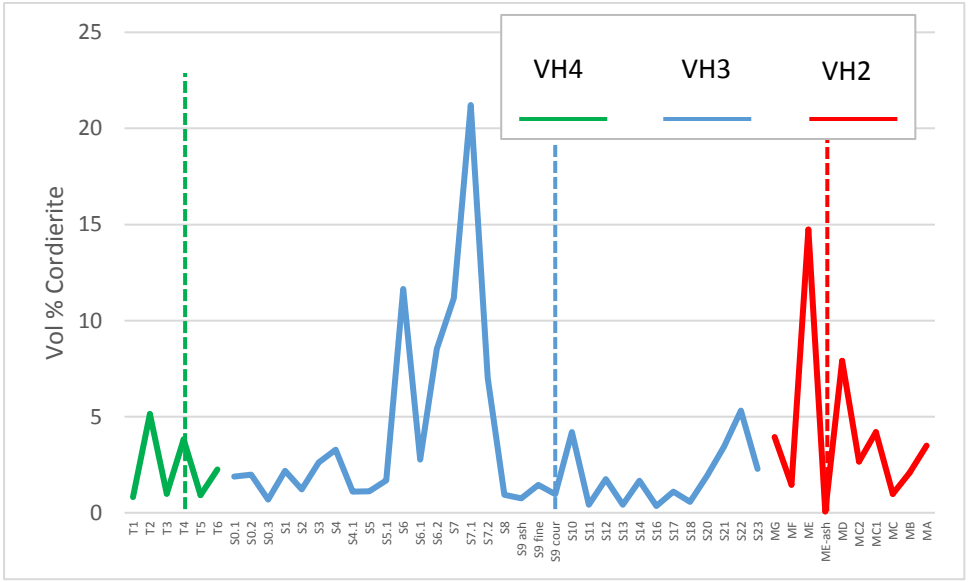

Figure 4-17 Variation in cordierite composition in core drills VH2, VH3 and VH4. Dashed vertical lines represent top of Gus seam in each respective drill core.

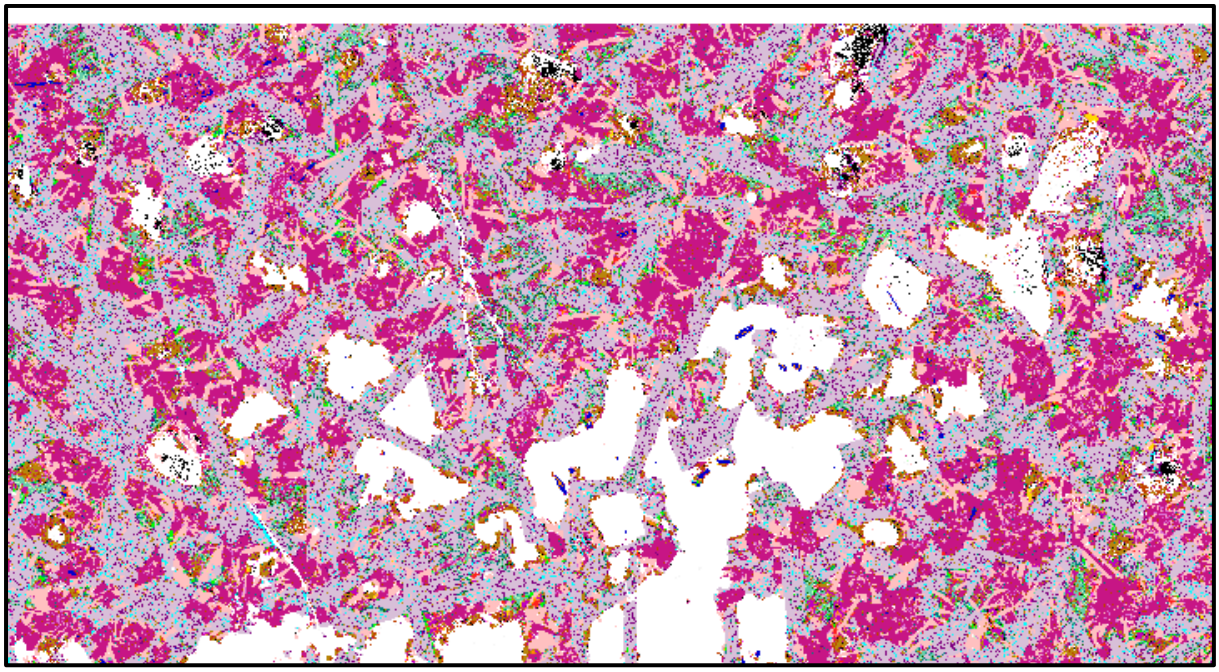

Figure 4-18 Cordierite-anorthite buchite: comprise of anhedral cordierite grains (maroon) in contact and inter-grown within anorthite (grey) and silica rich glass (pink), from drill core VH3 (sample S7.1)

The cordierite was found intergrown with anhedral quartz grains in glass anorthite matrix. The cordierite-anorthite buchite contained numerous vesicles both macroscopic (Table 4-2) and microscopic (Figure 4-18). Cordierite was observed to have crystallized from glass where it occurred rimming grain boundaries and droplets of pyrrhotite (Figure 4-15 and Figure 4-16). The variation in cordierite concentration profile in Figure 4-17 shows that cordierite fluctuates between 0 to around 5 Vol % in the unaltered rocks of VH4. The anomalous sections are therefore the roof section of VH3 from S6 to just before the ash layer at S7.2, which show enriched cordierite crystallization. The anomalous sections of VH2 are the rubble section (sample ME) and the floor (sample MD) with the rest of the profile falling below the 5 Vol % of cordierite. These trends show that cordierite crystallised in the pyrometamorphosed sections that lie close to the Gus seam (i.e. gasification area) and crystallised in slag along with other high temperature phases. The cordierite crystallization can therefore be concluded to be limited to within 1.2 m of the Gus contact. XRD analysis detected cordierite in samples S4, S6, S7 from drill core VH3, and from MF and MG in VH2. Another high-grade metamorphic Fe-aluminosilicate, hercynite ($FeAl_2O_4$), was also detected by XRD in sample MF (Figure 4-19). Cordierite detected in the reference borehole (VH4) may be due to the original heat from the dolerite intrusions.

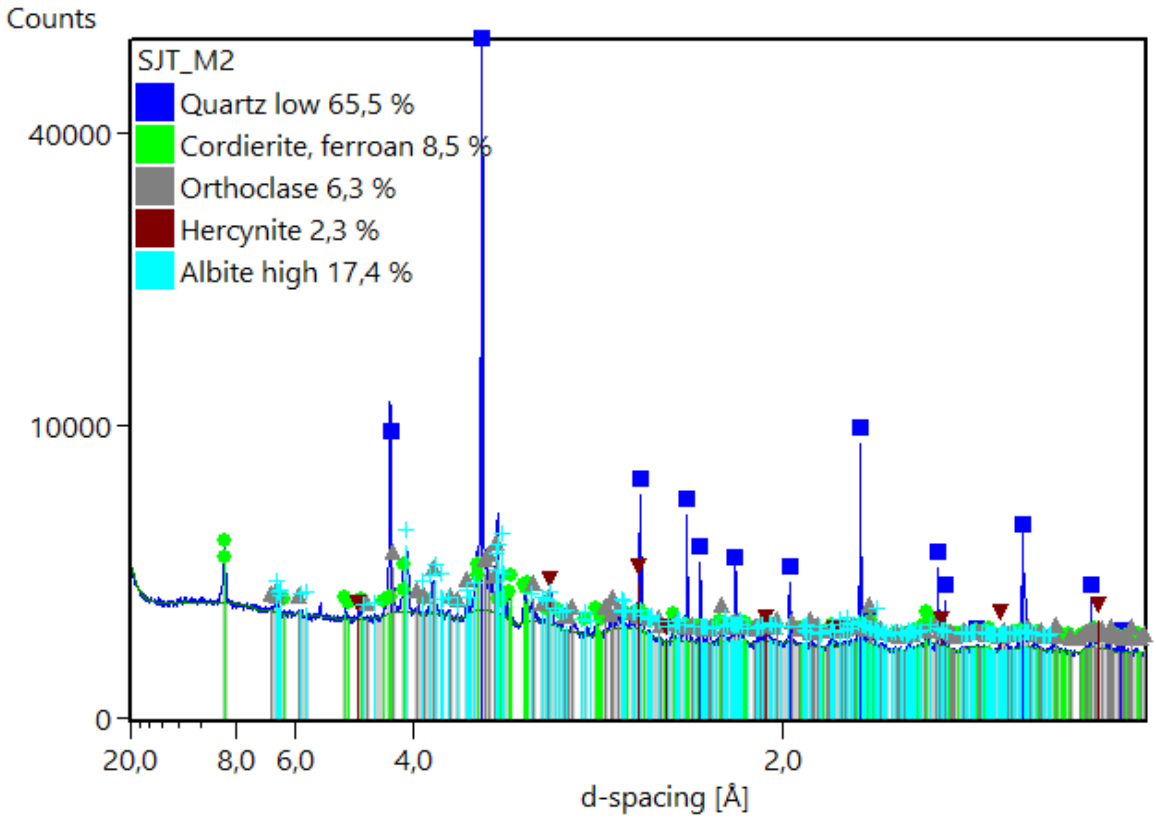

Figure 4-19 Diffractogram of sample MF from drill core VH2, showing mineral formations

4.3.3.3 Tridymite / cristobalite

High temperature altered rocks usually show cracking of quartz crystals as a result of the large volume change caused by the inversion to tridymite/cristobalite at 867 °C (Grapes, 2011). Tridymite and cristobalite are high temperature polymorphs of quartz (SiO_2). Cracking of quartz grains was observed in the medium-grained sandstone samples from S0.1 to S5.1 in the overburden and an example in presented in Figure 4-20. The paralava section of the overburden in drill core VH3 depicted by samples S6 to S 6.3 together with the buchite section (S7 to S8) show silicification. Silicification is the replacement of original mineral grains by SiO_2 mineralization (Ballhaus et al., 2012, Menezes et al., 2019). This results in the reduction in the angularity of the detrital quartz grains. The silicified quartz are characterised by indistinct grain boundaries and form a tridymite/cristobalite matrix due to silica partitioning into the melt (Figure 4-22). Quartz and cristobalite can occur metastably at around 1000 °C with both silica polymorphs and also persisting metastably within the tridymite temperature field (Grapes, 2011). The tridymite/cristobalite profile in the Majuba UCG gasification zone (VH2 and VH3) was compared with the off cavity conditions (VH4) and presented in Figure 25. The average tridymite/cristobalite proportion in the unaltered overburden of VH4 was 0.83 Vol % while recorded averages for VH2 and VH3 were an order of magnitude higher at 2.3 and 5.3 Vol %, respectively.

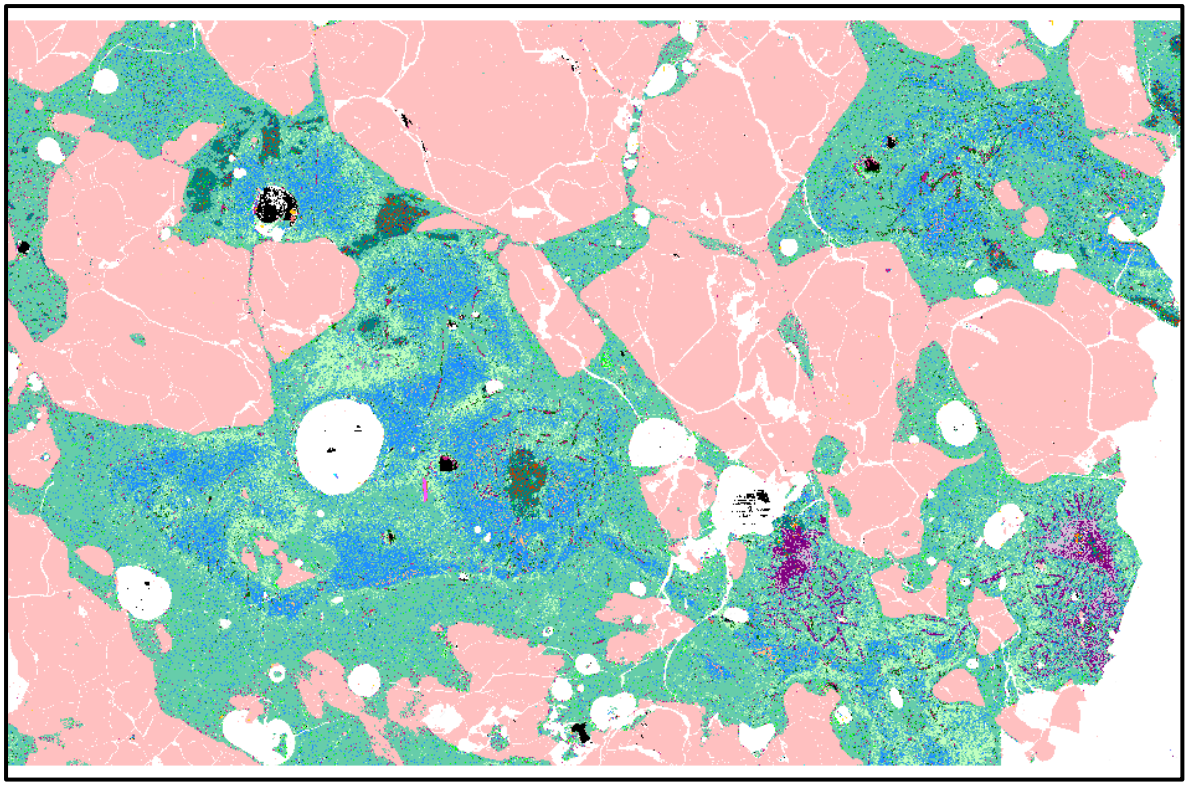

Figure 4-20 cracking of quartz grains, from S 4.1

The highest tridymite/cristobalite proportion recorded was 25.3 Vol % from sample S7.2. From Figure 4-21, it is clear that most of the recrystallization of silica occurred in samples taken from the top of the Gus seam to sample S6 in VH3, while only ME showed slight increase in silica recrystallization in the overburden of VH2 compared to VH4. Figure 4-18 show some of the quartz grains in contact with cordierite and preserved in the highly pyrometamorphosed sandstone. Quartz can persist as unmelted relics in paralavas (Grapes, 2011). Quartz profile is displayed in Figure 4-23. The roof of VH3 becomes progressively deficient in quartz the closer the distance to the char contact. This is the opposite of the trend observed in tridymite-cristabalite profile (Figure 4-21) which shows that silica grains transformed to their high temperature polymorphs.

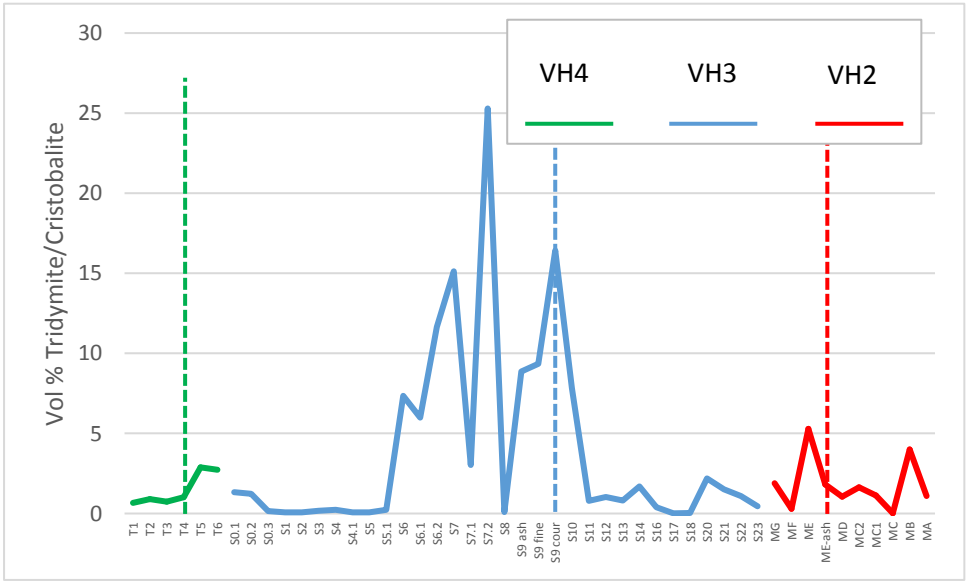

Figure 4-21 Tridymite-cristabalite profiles, Dashed vertical lines represent top of Gus seam in each respective drill core

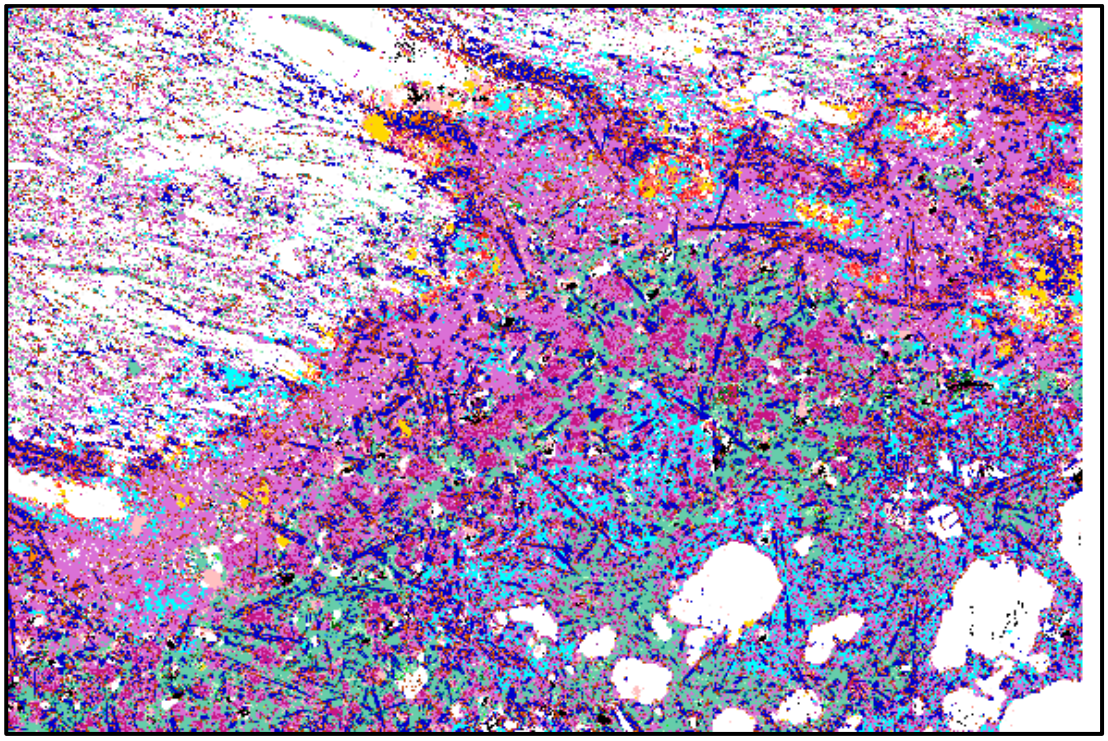

Figure 4-22 Trydimite-cristobalite matrix (purple) with glass (bright blue) and mullite needles (deep blue) from S 7.2

The XRD analysis detected the presence of cristobalite for (S2, S4, S5, S7 and S10) and tridymite for S4 and S18. The diffractogram of S7 is presented in Figure 4-24 and diffractograms of the other samples are presented in Appendix 4-C.

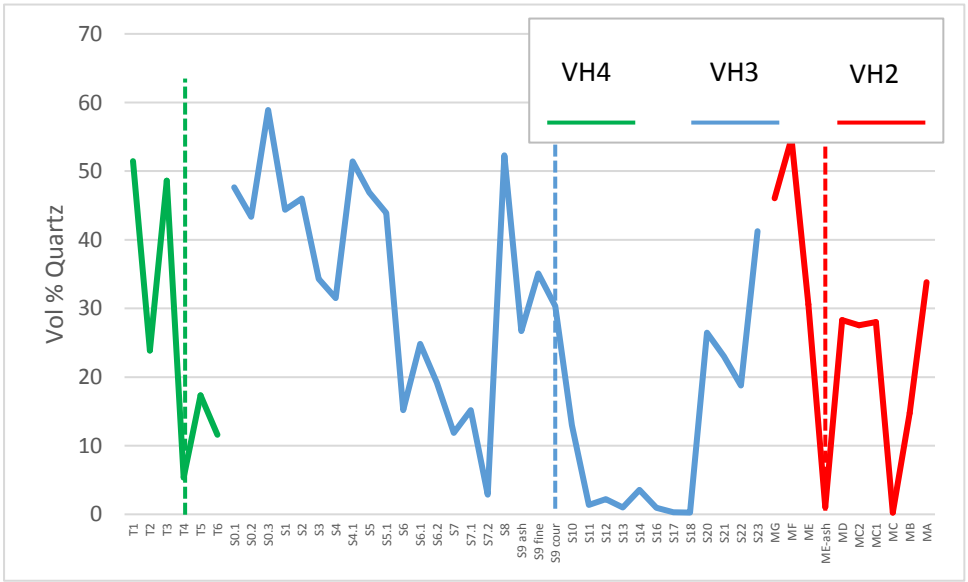

Figure 4-23 Quartz profiles, Dashed vertical lines represent top of Gus seam in each respective drill core

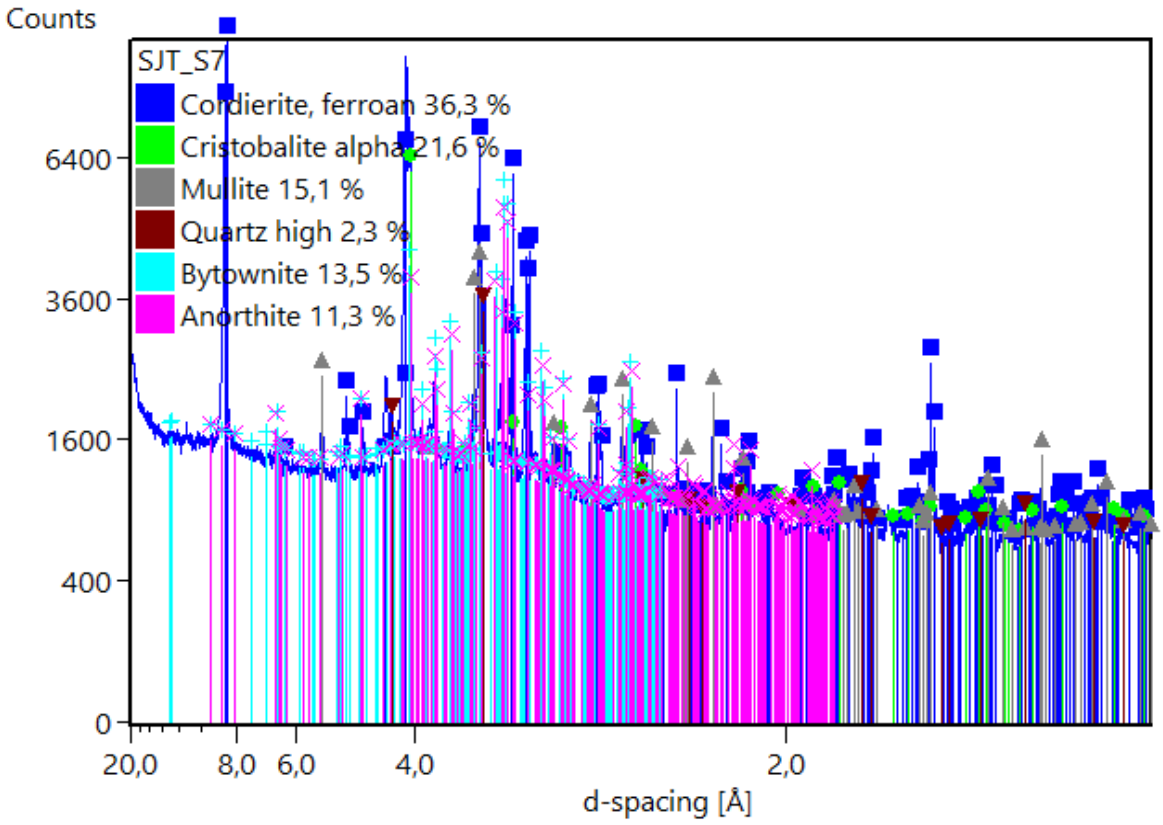

Figure 4-24 Diffractogram of sample S7 showing mineral formations

4.3.3.4 Al-silicates

Mullite ($Al_6Si_2O_{13}$) is a rare almuninosilicate that is associated with high temperature crystallization. The mullite profile for the three core drills is presented in Figure 4-25. The average mullite proportion in the unaltered overburden of VH4 was 0.0007 Vol % while recorded averages for VH2 and VH3 were a three orders of magnitude higher at 0.6 Vol % and 0.7 Vol %, respectively. The highest mullite proportion recorded was 11.5 Vol % for sample S7.2. The QEMSCAN image of sample S7.2 was presented in Figure 4-22. Mullite needles are clearly visible and formed in contact with silica melt. The char section and the underburdens of the three drill wells recorded averages below 0.01 Vol %. Mullite detection confirms that a temperature of above 1000 °C was reached in the gasifier.

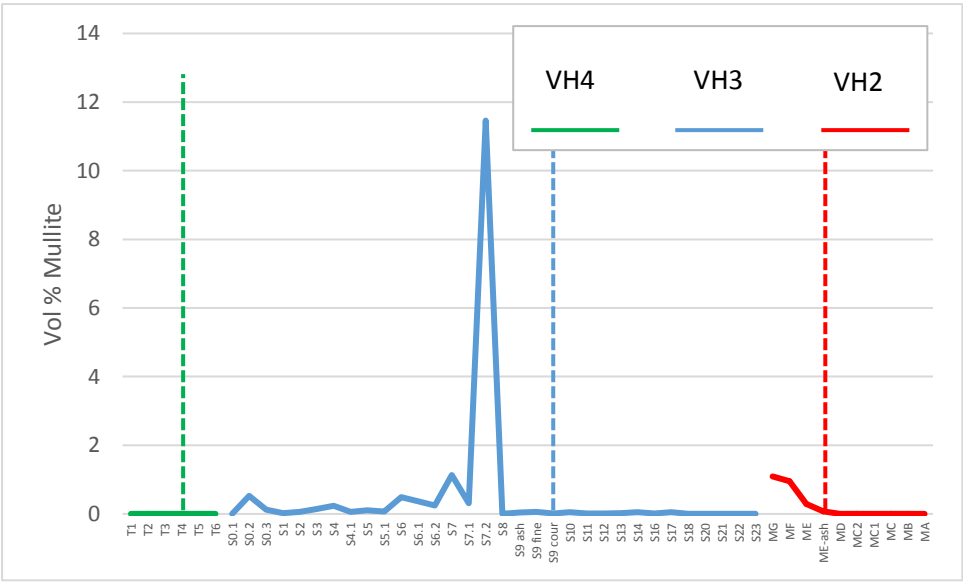

Figure 4-25 Mullite profile

Mullite crystals is characterized by needle grains that are in contact with silica (cristobalite/tridymite) glass. This distinctive mullite texture indicate crystallization from an aluminosilicate melt during devitrification. Features such as spinifex (needles), hopper cystals, radial clusters of mineral in glass and alignment of crystals around vesicles indicate crystallization from a melt (Grapes, 2011).

Another Al-silicate that was profiled from the drill cores was metakaolinite. The metakaolinite profile for the three core drills is presented in Figure 4-26. The average metakaolinite proportion in the overburden of VH4 was 19.6 Vol % while recorded averages for VH2 and VH3 were at 27.3 and 9.1 Vol %, respectively. The highest metakaolinite recorded was 92.6 Vol % from sample M-ash which is at the contact with the gasified Gus seam. The QEMSCAN image of the ash sample is presented in Figure 4-27. The sample shows no quartz or feldspar grains unlike ash samples derived from VH3 which had relics of silica and microcline (Appendix 4-E). This shows that heat distribution within a UCG chamber is not uniform and hence the products of gasification are not uniform throughout the geo-reactor. The ash sample (S9) recorded the highest metakaolinite of all the roof section from VH3, which implies that metakaolinite can be expected to be present in high proportions in a spent UCG chamber as a major mineral in ash.

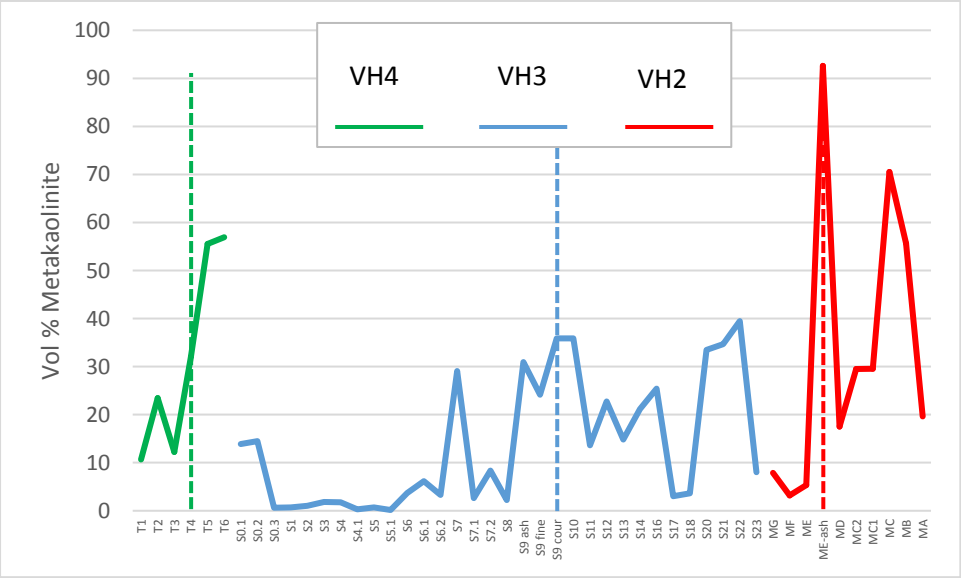

Figure 4-26 Metakaolinite profile

Aluminosilicate polymorphs (Al_2SiO_5) andalusite, sillimanite and kyanite are common mineral phases in pelitic metamorphic rocks (Nesse, 2000). Each of the polymorphs are stable within a specific temperature-pressure range with sillimanite as the high temperature polymorph. The sillimanite profile for the three core drills is presented in Figure 4-26. The average sillimanite proportion in the overburden of VH4 was 0.004 Vol % while recorded averages for VH2 and VH3 were an order of magnitude higher at 0.034 and 0.77 Vol %, respectively. The highest sillimanite recorded was 0.9 Vol

% from sample S7.2. The XRD analysis detected the presence of sillimanite for samples S5 (Appendix 4-C).

Figure 4-27 QEMSCAN image of sample M-ash, which is almost completely composed of metakaolinite (brown).

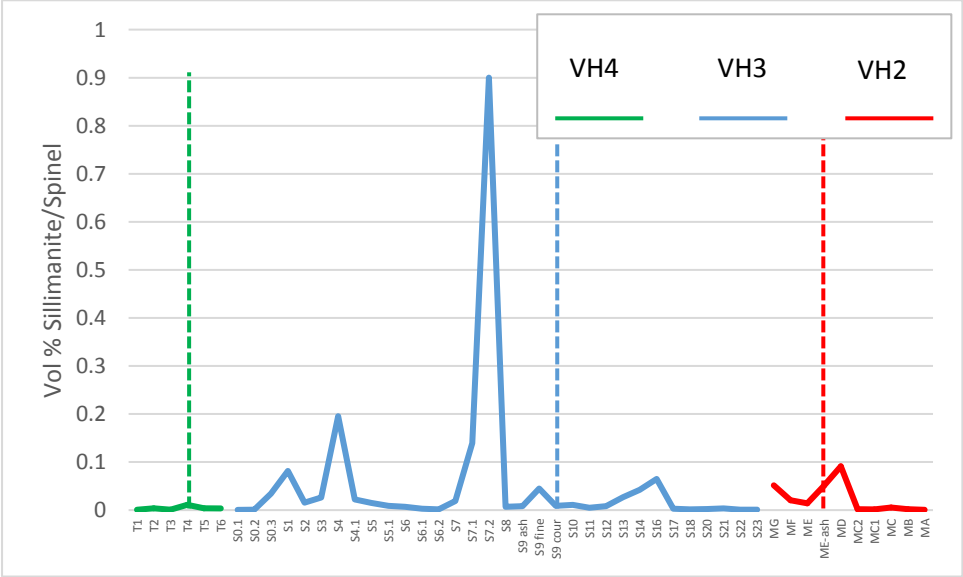

Figure 4-28 Sillimanite profile

4.3.3.5 Alkali feldspar

The feldspar group contains the alkali feldspars (orthoclase/microcline and albite ($NaAlSi_3O_8$)) and the plagioclase series which contains a range of compositions between albite and anorthite ($CaAl_2Si_2O_8$). Microcline and orthoclase are k-feldspar polymorphs with the chemical formula $KAlSi_3O_8$. Anorthite crystallizes from the high temperature sanidinite facies (Figure 3-8). The microcline profile for the three core drills is presented in Figure 4-29.The average microcline proportion in the unaltered overburden of VH4 was 16.3 Vol % while recorded averages for overburdens of VH2 and VH3 were an

order of magnitude higher at 11.9 and 6.5 Vol %, respectively. There was a noticeable decrease in the microcline proportion in the overburden of VH3 especially in the area just above the char contact (i.e. S7 to S8 where the average microcline was 2.7 Vol %) where extreme vitrification has taken place. The char section (i.e. S10 to S18) is also deficient in microcline and this was expected as coal does not contain significant amounts of silicates.

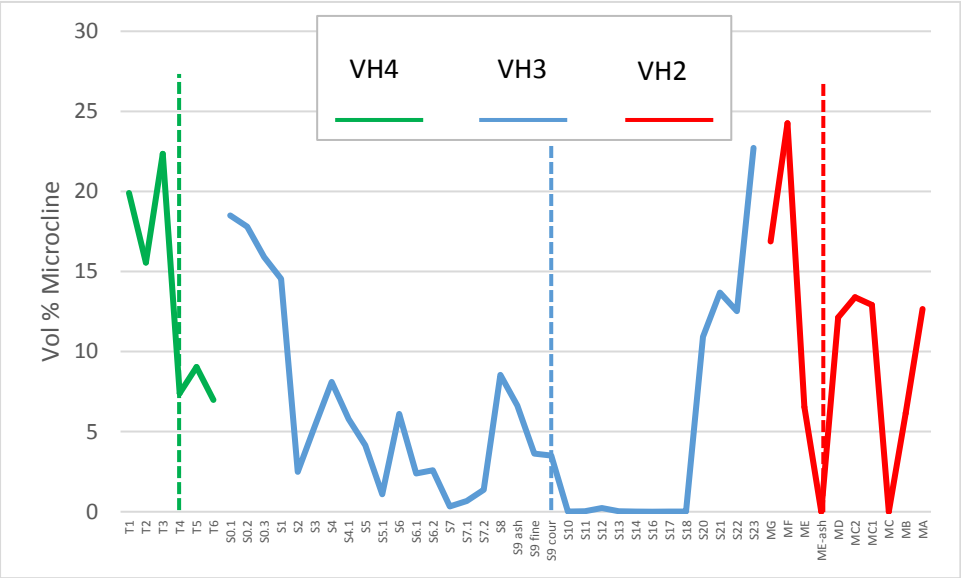

Figure 4-29 Microcline profile

The albite profile for the three core drills is presented in Figure 4-30.The average albite proportion in the unaltered overburden of VH4 was 6.77 Vol % while recorded averages for overburdens of VH2 and VH3 were an order of magnitude higher at 0.55 and 1.1 Vol % respectively.

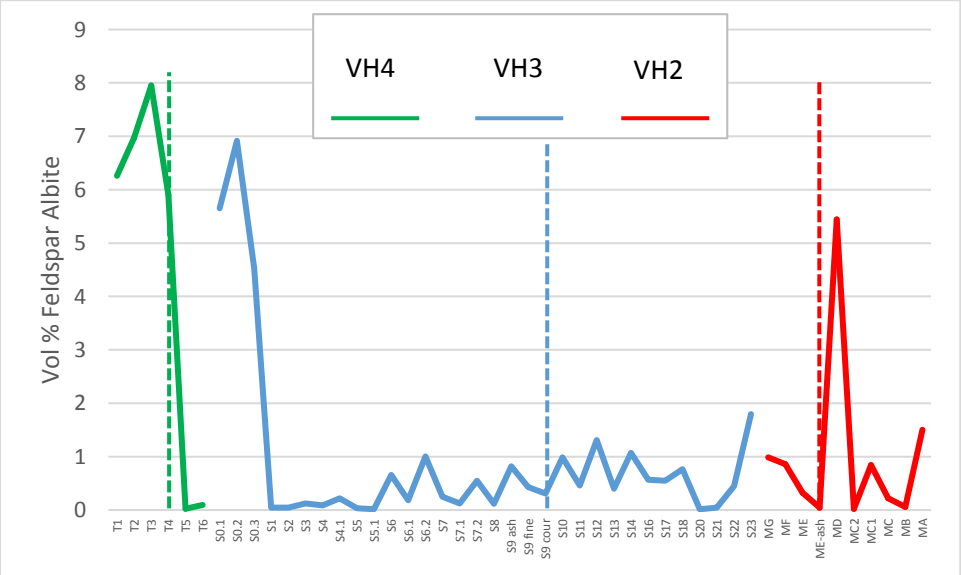

Figure 4-30 Albite profile

There is a general trend of decrease in albite and microcline quantity towards the gasification area (Gus seam) in the overburdens of the two verification boreholes (VH2 and VH3). Figure 3-13 showed

that feldspar melts at temperatures above 1000 °C and plagioclase (anorthite) crystallizes in the temperature range of around 1600 °C – 1200 °C. The profile of anorthite displays the opposite trend seen in microcline and albite where there is a general increase in anorthite quantity in the overburden of the verification boreholes while no change is seen in VH4 (Figure 4-31).

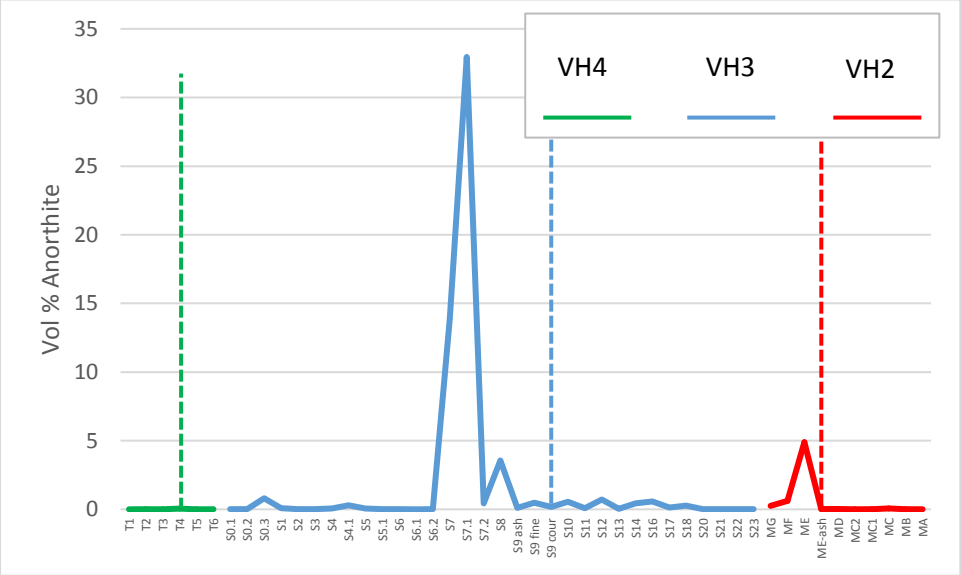

Figure 4-31 Anorthite profile

The average anorthite proportion in the unaltered overburden of VH4 was 0.02 Vol % while averages the roof sections of VH2 and VH3 were two orders of magnitude higher at 1.4 and 2.6 Vol %, respectively. The highest anorthite proportion recorded was 33 Vol % for sample S7.1. The QEMSCAN image of S7.1 was presented in Figure 4-18. The sample shows anorthite crystallized as glass (amorphous) matrix in contact with other high temperature minerals such as cordierite and tridymite/cristobalite. The reduction is primary feldspar minerals seen in Figure 4-29 and Figure 4-30 shows that sections of the overburden close to the gasification area experienced melting/partial melting in which feldspar minerals became molten and during cooling favoured crystallization of calcium rich anorthite as a glassy phase preserved during rapid cooling.

4.3.3.6 Glass

The preservation of glass in pyrometamorphosed rocks was discussed in section 3.4.2. The pyrometamorphic terms, buchite and paralava, denote the presence of glass (quenched melt) (Grapes, 2011). The majority of the glass composition from the QEMACAN analysis on the drill core samples was made up of the following elements: Si, Al, Fe, Mg and K. The profile for the aluminosilicate glass is presented in Figure 4-32. The average aluminosilicate glass proportion in the unaltered overburden of VH4 was 0.65 Vol % while averages recorded for the roof sections of VH2 and VH3 were an order of magnitude higher at 1.45 and 1.12 Vol, % respectively. The highest aluminosilicate glass amount recorded was 6.2 Vol % for S7. The QEMSCAN image of S7 is presented in Figure 4-33. The sample shows all phases existing as slag and no detrital grains were observed. The sample shows widespread dilation features characterized by open cavities.

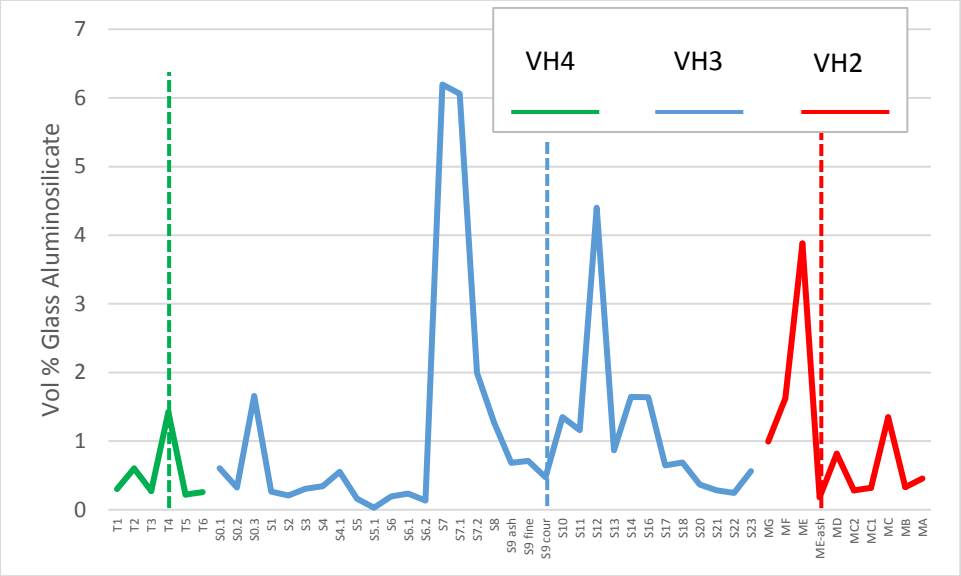

Figure 4-32 Aluminosilicate glass profile

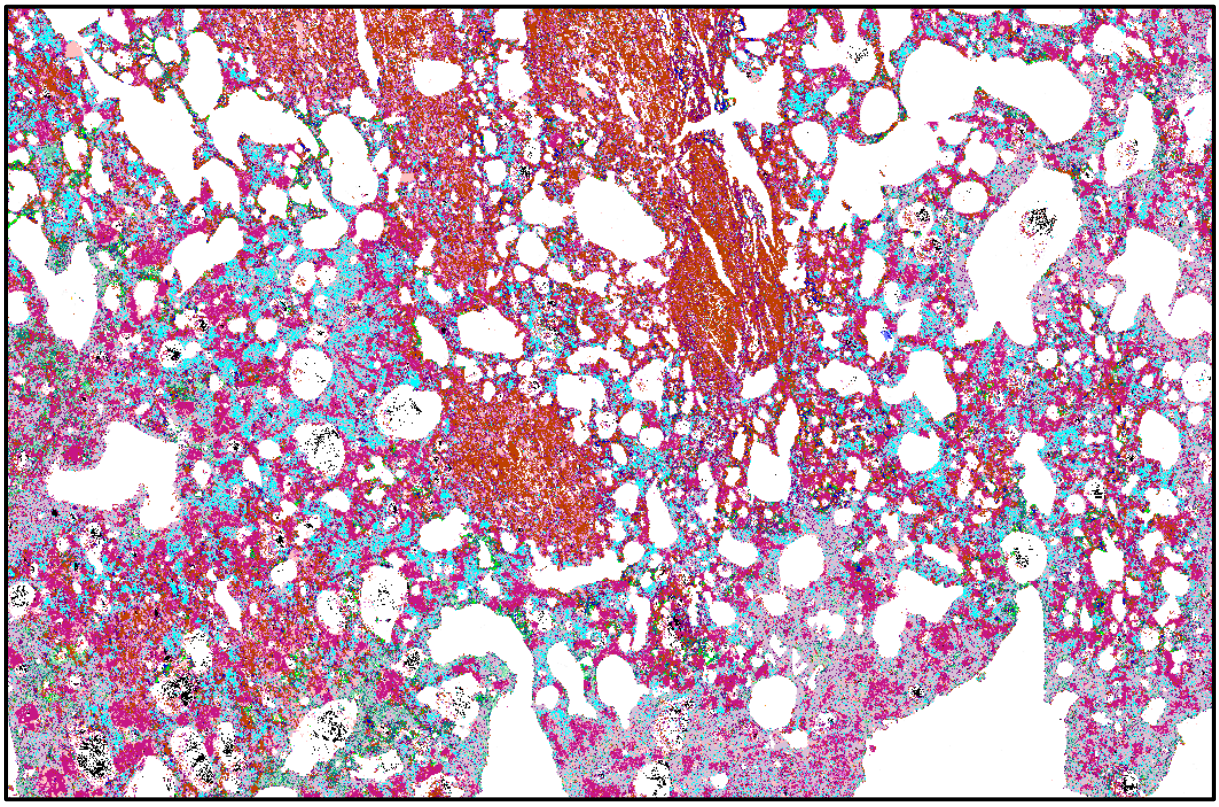

Figure 4-33 Aluminosilicate glass (blue) in contact with high temperature phases: cordierite (marron), anorthite (grey) and metakaolinite (brown). All phases exists as slag and no detrital grains were observed. The sample shows widespread dilation features characterized by open cavities, from sample S7.

The glass fraction also had a silica rich portion associated with major cations (Ca, Fe, Mg and Al). The silica-rich glass profile for the three core drills is presented in Figure 4-34. The average silica-rich glass proportion in the unaltered overburden of VH4 was 0.18 Vol % while averages recorded for the roof

sections of VH2 and VH3 were an order of magnitude higher at 1.0 and 2.3 Vol, % respectively. The highest silica-rich glass quantity recorded was 14 Vol % for S7.2.

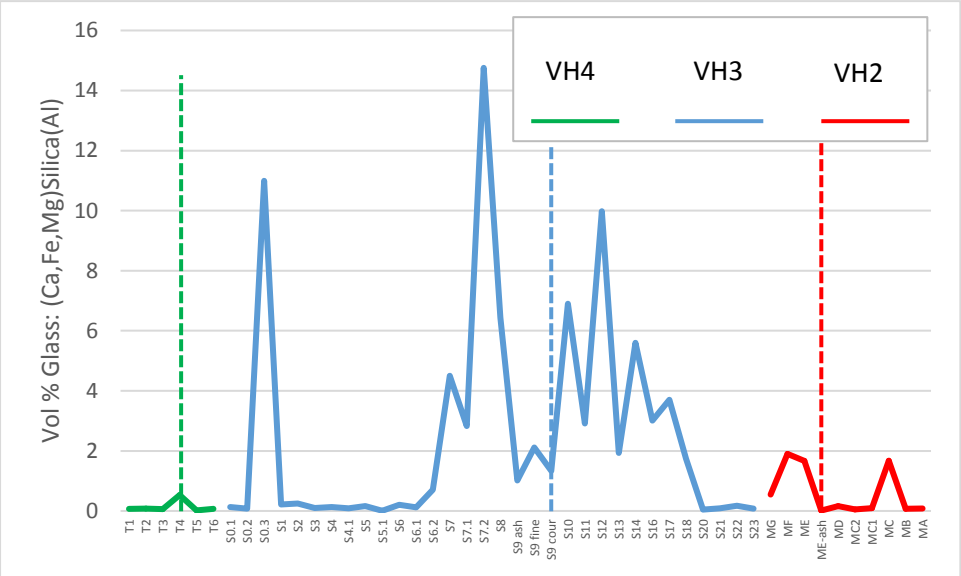

Figure 4-34 (Ca, Fe, Mg) silica glass profile

The trends for the two types of glass material (i.e. aluminosilicate and silica-rich glass) is similar for the three core drills profiled. The original rocks of VH4 were deficient in glass while VH3 and VH2 contained appreciable amounts of amorphous material. The highest recorded volumes of glass was from VH3 (S7 to S7.2) with glass content decreasing with increase in distance from the gasification zone. There was however an anomalous peak at S0.3 which recorded higher levels of glass relative to adjacent samples. This area had visible cracks that may have acted as fissures from which hot gases escaped and therefore vitrified the rock. Char section (S10 to S18) also showed appreciable levels of glass and since coal does not have lot of silicates that could have resulted in these elevated glass percentages, it is possible that this was molten material that was deposited on the char during cooling in the gasification chamber. A QEMSCAN image of the char sample (S11) showing deposits of glass on char is presented in Figure 4-35. The amorphous material is deposited in the devolatilization cavities within the char matrix showing deposition rather than transformation from detrital grains.

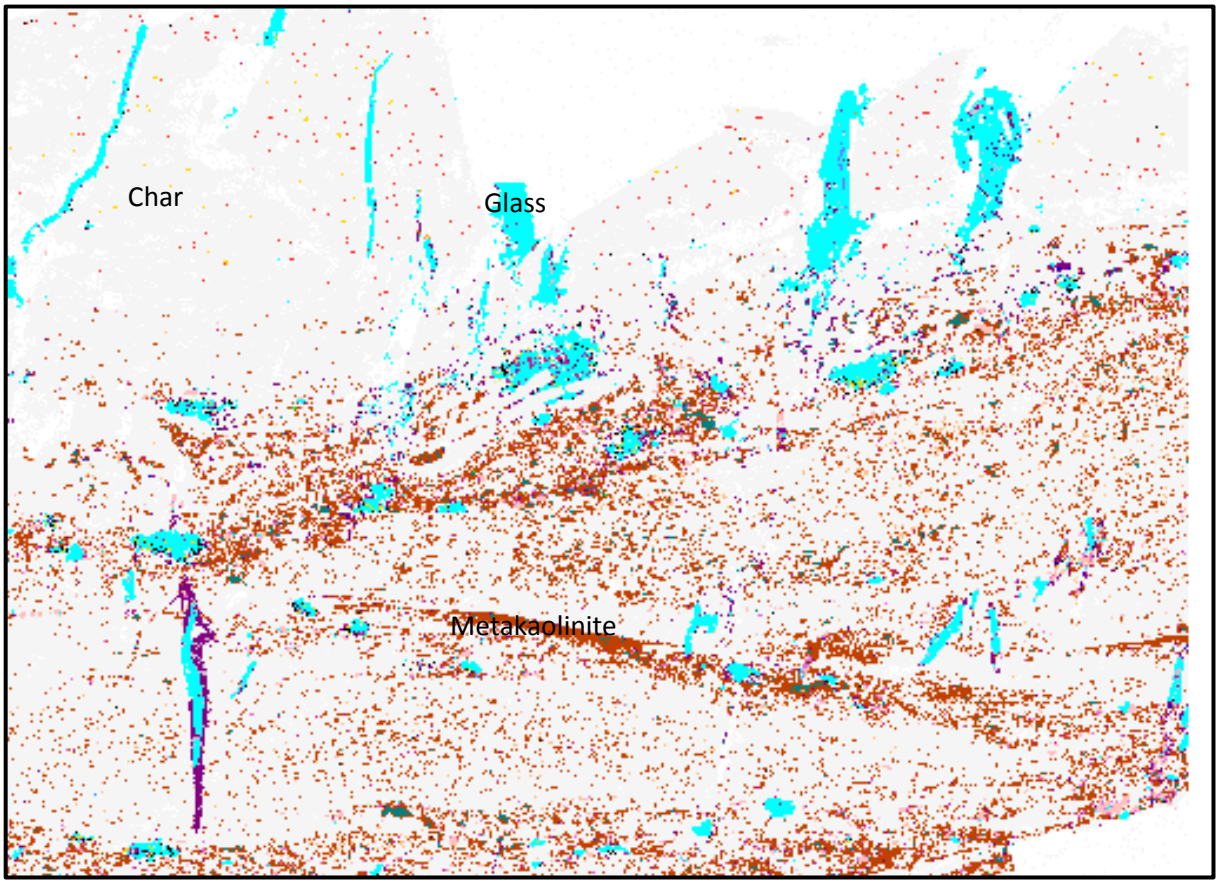

Figure 4-35 Char section showing droplets of glass (blue), the amorphous material is at places deposited in the devolatilization cavities within the char (grey) showing deposition rather than transformation from detrital grains, brown (metakaolinite), sample S11

XRD studies are generally limited in detection of amorphous or non-crystalline phases as this material does not have fixed arrays of atoms that can yield definitive peaks, however a wide "hump" in the diffractogram indicates that a sample has high glass component (Ward and French, 2006). The characteristic glass "humps" were observed in XRD analysis for S11 and the diffractogram is presented in Figure 4-36. The diffractograms of samples taken from VH4 do not exhibit any wide "humps" within the definitive peaks but the profile is moderately flat throughout (Appendix 4-C). The QEMSCAN and XRD analysis show that partial melting of the overburden occurred in rocks that experienced sufficiently high temperatures to generate molten material and during devitrification the glass was preserved due to rapid rate of cooling in the UCG chamber.

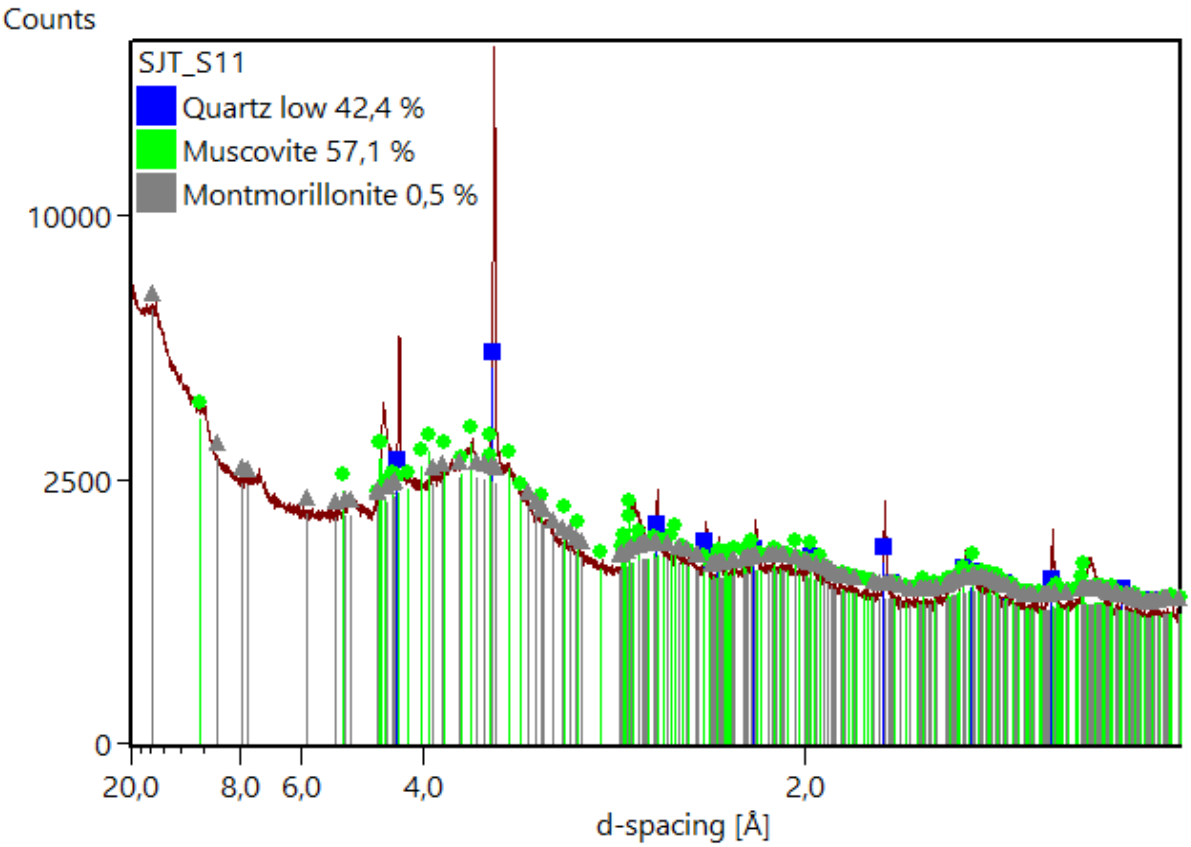

Figure 4-36 Diffractogram of sample S11 from drill core VH3, showing mineral formations and wide "humps" that are characteristic of glass component in a sample

4.3.4 Reconstruction of temperature in the geo-reactor

Changes in mineral assemblages observed in metamorphosed rocks can be used to provide a qualitative estimate of the conditions of metamorphism based on deduced changes in temperature from laboratory experiments (Frost and Frost, 2014). Prediction of the temperature regime in the gasifier through mineral transformation observed from the core drills are summarized in Table 4-3. The reconstruction of the temperature regime is presented in Figure 4-37. Drill core VH3 had the most prominent macroscopic pyrometamorphic features of all the drill cores analysed. The mineralogical analysis though XRD and QEMSCAN detected sanidinite facies phases which included cordierite, mullite, cristobalite, tridymite, anorthite and glass. These high temperature phase were more noticeable from the char contact to around 0.5 m into the overburden. This region of the overburden would have at least experienced a temperature of around 1400 °C. Droplets of slag were detected in char samples, which implies that the overburden was molten at some stage. Drill core VH2 did not retrieve any coal relics however the mineralogical analysis of the overburden detected high temperature minerals such as cordierite, mullite, cristobalite, tridymite, anorthite and glass. While the quantity of these high temperature phases were less than in the roof of VH3, their presence still suggest that at the least 1200 °C was reached.

Table 4-3 Summary of mineral transformations and reconstruction of thermal regime from the Majuba gasifier

Core	Observation and thermal prediction
VH4	T1 to T6 does not show any significant thermally induced mineral alteration. There is however a slight increase (still < 1% Vol) in the glass component at T4. No micro-craking of detrital grains was observed, meaning the α-quartz / β-quartz transition temperature of 573 °C was not reached. There was a small increase in the glass profiles for T4 which is possibly part of the original clastic material or some of the heat travelled through a fissure and affected this section of the core however the other pyrometamorphic attributes were not observed. The floor and roof sections of VH4 was largely unaffected by the gasification process. The mineralogy of VH4 was compared with roof and floor samples from VH6 (i.e. T7 to T9) and the mineralogy was similar (Appendix 4-E). The mineralogy showed that the positioning of the two off cavity boreholes (VH4 and VH6) was accurate in that they were not located in areas near the gasifier. For example the average modal proportions of pyrometamorphic minerals of VH6 and VH4 were similar (e.g. anorthite (0.1:0.2 % Vol), Glass (Aluminosilicate) (0.64:0.65 % Vol), Glass (Silica) (0.19:0.18 % Vol)). Hence VH6 was only included as a reference borehole for VH4 and the QEMSCAN images and modal proportions are included in Appendix 4-E.
VH3	This core displayed the extreme pyrometamorphism features. All samples from the roof section of the core drill displayed micro cracking of quartz grains, which infers that the α-quartz / β-quartz transition temperature of 573 °C was reached for S0.1 to S5.1. Slagging features become prominent from S6 to S9, which means that melting of mineral phases occurred within this region. Pyrrohotite melt and subsequent Fe oxide melt was observed in S6 to S7.2, which means the temperature of 1083 °C was reached (Figure 3-15). Cordierite crystallization is prominent from S6 to S7.2, which implies temperature of 1200 °C to 1500 °C was reached (Figure 3-13). Mullite crystallization is above average for S6 to S7.2 where the highest level was recorded. The eutectic temperature of mullite/tridymite/cordierite is 1400 °C (Figure 3-10), this mineral assemblage characterized most of S7 to S7.2. The eutectic temperature of mullite/tridymite/anorthite is 1350 °C (Appendix 3-A), this mineral assemblage also characterized most of S7 to S7.2. The highest recorded volumes of glass was from VH3 (S7 to S7.2) with glass content decreasing with increase in distance from the gasification zone. There was however an anomalous peak at S0.3 which recorded higher levels of glass relative to adjacent samples. at 1200 °C around 80% of the argillaceous rock will undergo vitrification, while at 1350 °C the rock will be totally molten (Kühnel et al., 1993). Samples taken from the ash layer (S9, fine, course) were dominated by metakaolinite, quartz and minor microcline grains which implies temperatures of 925 °C – 950 °C were reached.
VH2	This core did not retrieve any coal/char. The roof samples (MG and MF) all display cracking of quartz grains which means the α-quartz / β-quartz transition temperature of 573 °C was reached. The second highest proportion of pyrrhotite was recorded for ME which where the pyrrhotite was found occurring with glass surrounded by anorthite and cordierite matrix. The presence of cordierite and anorthite means that 1400 °C was reached. The ash was dominated by metakaolinite with no silica which implies at least 500 °C.

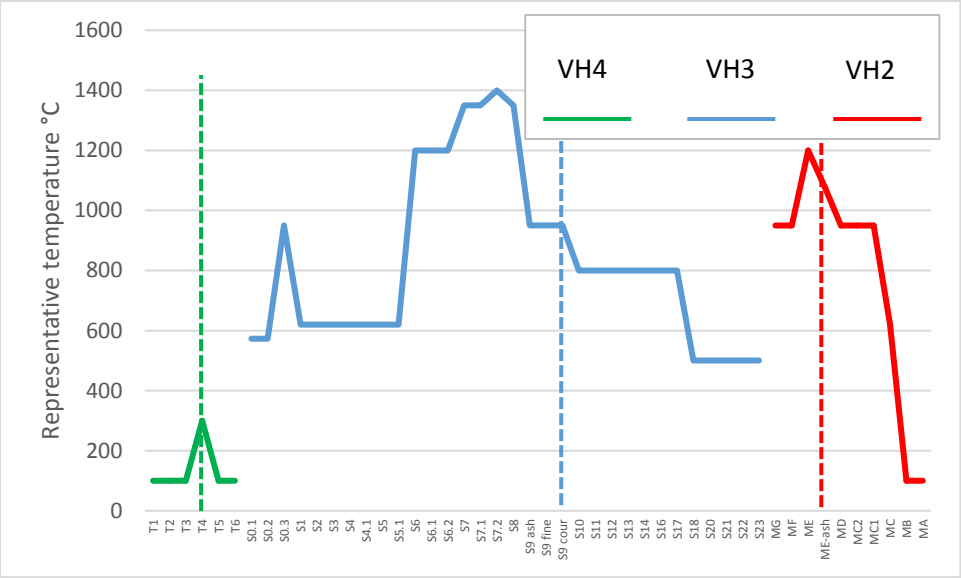

Figure 4-37 Reconstruction of the temperature regime in the Majuba UCG chamber. VH4 is the off cavity borehole and a lower temperature profile was expected

4.4 Summary

The aim of this chapter was to characterize the spent UCG chamber, as this is the medium that the rebounding groundwater will interact with. Two verification cores drilled to intercept the gasification zone were retrieved and compared to an off cavity drill core. The visual analysis of the verification boreholes showed macroscopic signs of extreme heat interaction. These features were more prominent in the overburden of VH3 which contained an ash layer, buchite and paralava sections with vast amount of visible vesicles. These cavities in the overburden will increase the porosity of these strata and hence increase groundwater-rock interactions. The gasification process usually leads to spalling of the roof and the development of macro-fissures in the overlying sediments. The majority of the visible pyrometamorphic features were limited to within 2 m of the overburden-char contact. The QEMSCAN analysis of samples taken from the overburden of VH3 also showed that the majority of thermally altered mineral were limited to 2 m above the char contact. The following mineral alterations or crystallization of secondary minerals was confirmed:

- Pyrite transformed to pyrrhotite. This alteration was seen by an inverse relationship in the profiles of pyrite and pyrrhotite. As pyrite level reduced the pyrrhotite levels increased beyond background as seen in VH3.
- Significantly high temperature mineralization of cordierite was detected in the overburden of VH2 and VH3, which was higher than the background values recorded in VH4.
- Appreciable quantity of high temperature silica polymorphs, tridymite and cristobalite, were detected in the overburden of VH2 and VH3, which was higher than the background values recorded in VH4.

- High levels of mullite were detected in the overburden of VH2 and VH3, which was three orders of magnitude higher than the background values recorded in VH4. The same trend was observed for sillimanite and anorthite
- Significant levels of amorphous material (glass) detected in the overburden of VH2 and VH3, which was considerably higher than the background values recorded in VH4. Glass in rocks points to fast cooling (quenched melt) during devitrification. The amorphous material (glass) of VH6 was similar to VH4 (Table 4-3).

The presence of glass also implies that elements may not be tightly held in crystal lattices, as is the case in mineral phases, and this can lead to enhanced dissolution in groundwater and increased leaching. High temperature crystallization of iron sulphide in the form of pyrrhotite showed crystallization from immiscible segregation of a sulphide melt from a silicate melt as pyrrhotite preferentially formed as individual droplets mostly around silicate rich glass. This can also increase interaction with groundwater post-gasification, as the segregated sulphide will interact more easily with groundwater, other than with pyrite held interstitially in between mineral grains, as would have been the case pre-gasification. In general, there were similarities in mineralogy between VH3 and VH2 however, the extent of overburden alterations were not the same, with VH3 exhibiting the most transformed mineralogy. This shows the heterogeneous nature of gasification in a UCG chamber where different sections experience changing temperatures resulting in a varied temperature profile across the geo-reactor.

The next chapter is the petrographic and chemical characterization of char retrieved from the gasification zone.

5 Petrographic and chemical analysis of coal relics from the spent geo-reactor

5.1 Introduction

One of the most significant environmental risks of UCG is the unavoidable groundwater interaction with residue products post gasification. UCG technology is still in pilot phase in various places in the world and some of the factors impeding the technology from going commercial is the question around groundwater pollution as a result of perceptions that the spent geo-reactor will be largely toxic. The pilot phases of UCG technology present an opportunity to test and try to mitigate some of the problems caused by conventional coal mining. Conventional coal mining has resulted in widespread environmental pollution with over 200 000 acid mine drainage sites in America alone (Hochella et al., 1999). There is therefore a need for comprehensive analysis of coal relics as potential sources of groundwater contamination.

Coal is made up of organic and inorganic constituents, and coal pertrology is the science that deals with the origin, configuration and composition of coal. Coal petrography is a sub-section that describes and classifies coal by use of a microscope. Under the petrographic microscope, the organic fraction of coal, known as macerals, can be quantified with each maceral making an input to the total chemistry and technological behaviour of coal (Wagner et al., 2018). The three main maceral groups that form the foundation of coal petrology are vitrinite, liptinite and inertinite. South African coals are generally medium rank C bituminous coals which are rich in inertinite and have a high mineral content (Malumbazo et al., 2012). In UCG, the reactivity of the coal is a function of the diffusion of the reactants and products. Coal petrography enables the assessment of gasification, combustion, coking and residue products to gain complete understanding of the conversion processes and the thermal maturity assessment via mean reflectance of vitrinite index (RoV) analysis, used in conjunction with other petrological techniques (Malumbazo et al., 2012). The mean reflectance of vitrinite index (RoV) is one of the primary parameters utilized to assess the degree of the coalification of organic substance in coal, and can also be used to estimate the susceptibility of coal to the coking process (Róg, 2018). UCG process involves a varied heat progression, which affects different areas of the coal differently (see section 3.1). Whilst the effect of coal rank on UCG success is fairly well documented (Perkins, 2018a), there is limited information pertaining to the behaviour of coal macerals during UCG. There is a very good understanding of coal particle pyrolysis and gasification of South African coals in surface gasifiers (Bunt et al., 2009, Malumbazo et al., 2013) however very little literature exists in their performance in UCG. There is a recent study on vitrinite reflectance on a laboratory scale geo-reactor by (Róg, 2018) which provides a good basis for temperature reconstruction from char. This research will be referenced in the analysis of the petrographic results.

Proximate analysis of coal is the first basic step in characterization of coal that provides information on the carbon content, ash content, moisture content and volatile matter in coal. The organic components of coal comprise mainly of elements; carbon (C), nitrogen (N), hydrogen (H), oxygen (O) and organically bound sulphur (S), and all these elements make up more than 99% of the organic and inorganic portions of coal (Wagner et al., 2018). Ultimate analysis is the quantitative analyses of all these elements in coal. All this elements exist in chemical bounds or functional groups in coal. Coal contains functional groups such as CH (in aliphatic and aromatic compounds), OH (in hydrogen

bounds), C=O (in humic acids) and –C-C=C-C- in aromatic rings (Wagner et al., 2018). Fourier-Transform Infrared Spectroscopy allows for identification of chemical bond pattern and characterization of the different functional groups in coal. All these chemical and petrographic analysis of coal provide for comprehensive analysis of the environmental risk factor of coal relics from UCG. For example, the total sulphur data determined as part of ultimate analysis can be used in acid base accounting to determined the potential of residue products to generate acid.

The shutdown of gasifier 1 at the Majuba UCG plant provided a chance to derive coal remnants from the gasificaion zone. This chapter attempts to utilize different coal analysis to assess the coal relics from the spent Majuba UCG. Mean reflectance of vitrinite index (RoV) will also be used to assess the temperature profile of the char retrieved from the spent geo-reactor. This section of the study aims to address part of the first main objective of the thesis, which is the characterization of the source of inorganic groundwater contaminants from a spent UCG chamber.

5.2 Methodology

Samples were taken from the G1VH3 core drill from a depth of 281 m. The sampling commenced from an ash layer located immediately below the extensively heat-affected sandstone overburden, and finished at the carbonaceous shale horizon below the coal seam. Core and / or core fragments 1 – 10 cm were handpicked, identified as S9 (ash) to S18 (Figure 5-1).

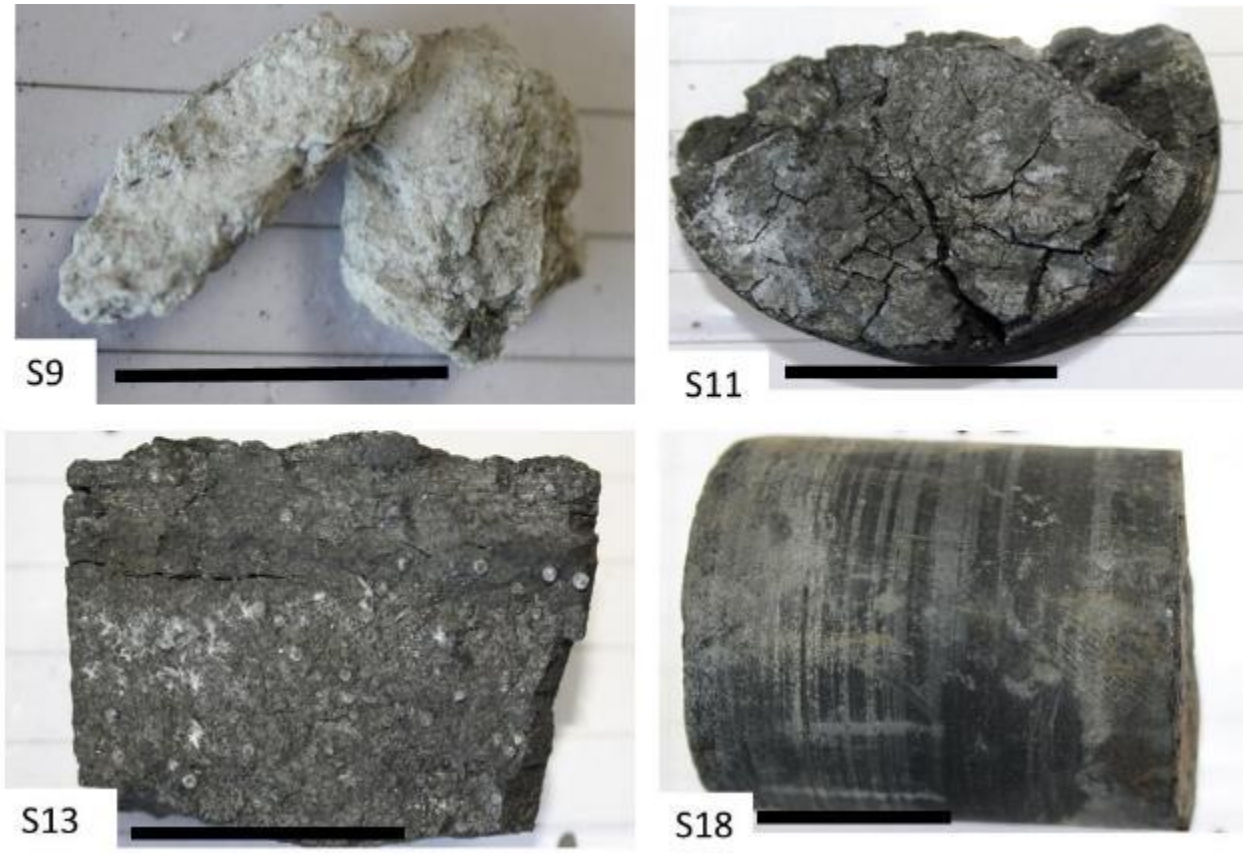

Figure 5-1 Examples of selected core fragments. Scale bar = 2.5 cm

Two sets of epoxy-bound polished blocks were prepared at the University of Johannesburg for each sample in order to: 1) study the *in-situ* lump fragments (prepared perpendicular to the apparent

bedding plane); and 2) statistically determine the reflectance values of the crushed particles and to quantify the maceral composition. Selected fragments from each sample where broken-up using a hammer (where required) in order to fit into the 300 mm diameter mould (Figure 5-2). The rest of the sample was crushed to pass a 2 mm screen (80% -1 mm) and placed in the second mould. The particles were set with epoxy resin and left to cure overnight under vacuum. All samples were polished using a Struers Tegra grinder and polisher with an automated power-head to achieve a final 0.05 micron alumina polish, following SANS 7404-2 (2009).

A Zeiss Axio Imager M2M reflected light petrographic microscope, with a total magnification of x500 under immersion oil, was used for the petrographic assessment of the block- and grain-mounts. Mosaic images of sections of the lump particles were stitched together using the Hilgers Diskus system. The relative proportion of vitrinite to inertinite was determined during the detailed reflectance analysis, reported as % vol.

The reflectance analysis was conducted on the grain-mount samples to determine the impact of the heat on the coal and to gain insight into the gasification process. The Hilgers Fossil system was calibrated using the 5.37 ST, 3.24 CZ, and 0.900 YAG calibration standards, based on SANS 7404-5 (1994). The system was stable throughout the analyses, but the standards were checked before commencing each sample. The Fossil system enables the categorisation of reflectance readings based on the maceral type, and hence reflectance values were recorded separately for vitrinite and various inertinite macerals occurring in the samples. The reflectance reading was taken on the particle falling immediately under the cross hair (or the closest clean surface) in order to prevent bias towards a specific maceral type. Approximately 200 – 250 readings, depending on the available organic matter, were recorded on individual macerals, covering the entire surface of the grain-mount, with a consistent step-size used for all samples.

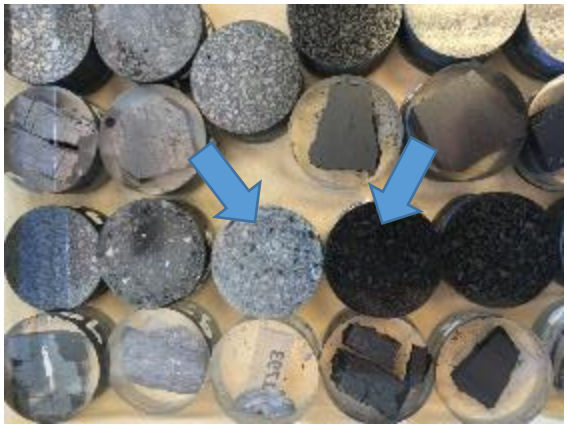

Figure 5-2 : Epoxy-mounted lump and particulate block, 300 mm diameter. The left arrow indicates the ash sample obtained immediately below the heat affected sandstone (S9); the right arrow indicates the coal sample taken immediately below the ash layer (S10).

Proximate and ultimate analyses were carried out at RT&D, using standard procedures (Table 5-1).

Table 5-1 Coal analysis and corresponding standards

Methods	International standards
DETERMINATION OF ASH IN COAL	ISO 1171, SANS 131
DETERMINATION OF VOLATILE MATTER	ISO 562, SANS 50, SANS ISO 562
DETERMINATION OF MOISTURE	ISO 331, SABS-ISO11722, SANS 5925:2007
SULPHUR DETERMINATION	ASTM D4239
CV DETERMINATION	SABS-ISO 1928 DDS Standard Operating Procedure
ASH FUSION TEMPERATURE	ISO 540 (Reducing Atmosphere)
TOTAL MOISTURE DETERMINATION	ISO 589, SANS 589, SABS 0135 part 2 (one or two step)
MAJOR AND MINOR ELEMENTS IN COAL ASH	SANS 408 2007

5.3 Results and discussion

5.3.1 Visual assessment of the char from the geo-reactor

Coal/char was not retrieved from drill core VH2 but approximately 2 m of char was retrieved from VH3. The devolatilized coal (char) section begins immediately below the ash layer which is also signals the end of the sandstone overburden. The sampling depths are given in Table 4-1 and shown in Figure 4-2. The first 40 cm below the ash layer is characterized by dull devolatilized coal that fractures irregularly (i.e. not along any clear path/plane). The char also has small sporadic white tint (S10). The next section, 60 to 100 cm below ash layer, is also predominantly dull devolatilized coal characterized by horizontal fracturing along thin bright vitrinite rich bands (S11 to S13). The cracks along the vitrinite rich layers did not extend into the dull sections of the char and this crack could have played a role in degassing the coal and conveyance of heat and syn gas.

The next section (S14), 100 to 120 cm, is characterized by white spots on the surface of the char. This section also has horizontal cracks along thin bright vitrinite rich bands. The next section (S16) contains widespread blue and white tints on the surface of the char. The last section of the char (S17 and S18) is essentially bright devolatilized coal with bands of dull coal. The fracturing in this section was irregular.

Table 5-2 Visual assessment of the char section of VH3

Sections of devolatilized coal from drill core VH3
Char section below the ash layer (S9), which is essentially the beginning of char column retrieved from VH3. This section is characterized by dull devolatilized coal with sporadic white tints (S10). 
This section of char is characterized by blue and white tints on the char (S11 and S12). The section is generally dull devolatilized coal with thin lenses of bright coal. Blue and white tint on char was also observed in S16. 
This section is characterized by small spherical white spots on char surfaces (S14). 
The section contains widespread white and blue tints on the surface of char (S16). 

5.3.2 Chemical analysis

The chemical properties of coal samples retrieved from core drill VH3 are displayed in Table 5-3, along with data from samples obtained from boreholes drilled away from the gasification zone (VH4 and VH6). These samples were included as reference points for unheated coal composition. All samples originate from the Gus Seam.

Table 5-3: Selected proximate and ultimate data (dry basis) for VH3 samples (S10 – S18), with comparison to VH4 and VH6 samples.

Sample Name	Ash (%)	Volatile matter (%)	Total Sulphur (%)	Measured Carbon (%)	Measured Hydrogen (%)
S10	54.92	2.36	0.75	42.80	0.01
S11	41.20	3.11	0.87	55.81	0.01
S12	46.42	3.22	0.31	50.84	0.01
S13	33.30	2.50	0.49	64.34	0.01
S14	38.37	2.79	1.18	58.35	0.01
S16	20.93	2.42	0.77	76.94	0.08
S17	20.46	3.15	0.48	76.78	0.10
S18	89.65	6.63	0.12	8.90	0.17
VH4 Gus A	19.90	23.90	1.45	61.67	4.50
VH4 Gus B	31.30	21.90	1.55	53.61	3.02
VH4 Gus C	56.10	22.40	1.00	31.26	2.18
VH4 Gus D	43.50	16.10	1.77	44.34	1.99
VH6 Gus	28.80	30.10	3.28	54.70	4.83

The samples from VH3 are depleted in volatile matter relative to coal samples from outside the gasification zone (Figure 5-3); the VH3 samples average 3.24 wt% in terms of the volatile matter content, compared to 21.70 wt% average of samples outside the gasification zone. Therefore, the VH3 samples can be classified as devolatilized coal or char.

The hydrogen fraction in the VH3 samples is significantly depleted compared to the unheated coal samples (Figure 5-4). Hydrogen is highly mobile and H_2 gas is released as part of the gasification process hence groundwater contamination or acidification due to hydrogen in the chamber is unlikely. The sulphur content for Majuba coal as stated by (Snyman, 1998) is around 0.9 %. Sulphur amounts showed depletion for char samples with an average of 0.6 % as compared to the 1.81 % for the coal samples from outside the gasification zone. The general trend shows natural coal has higher sulphur amounts than char. High sulphur content in coal can be a contributing factor to acid rock drainage if it exists as pyrite (Mokhahlane et al., 2018). The chemical results show that the char left in the gasification chamber will most likely be depleted in sulphur and hence environmentally more sustainable as it significantly lowers the risk of acid mine drainage due to sulphide oxidation.

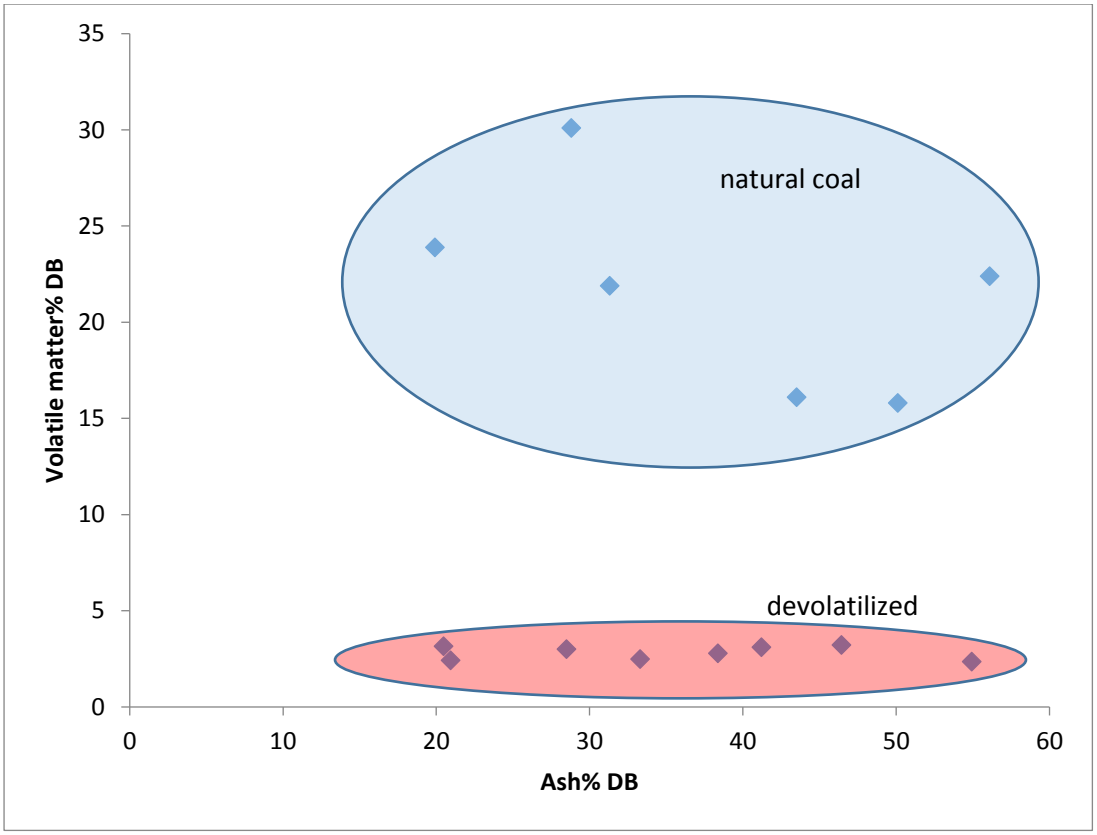

Figure 5-3 Comparison of coal samples from VH3 (gasified) and VH4 and VH6 (not gasified) in terms of the volatile matter content.

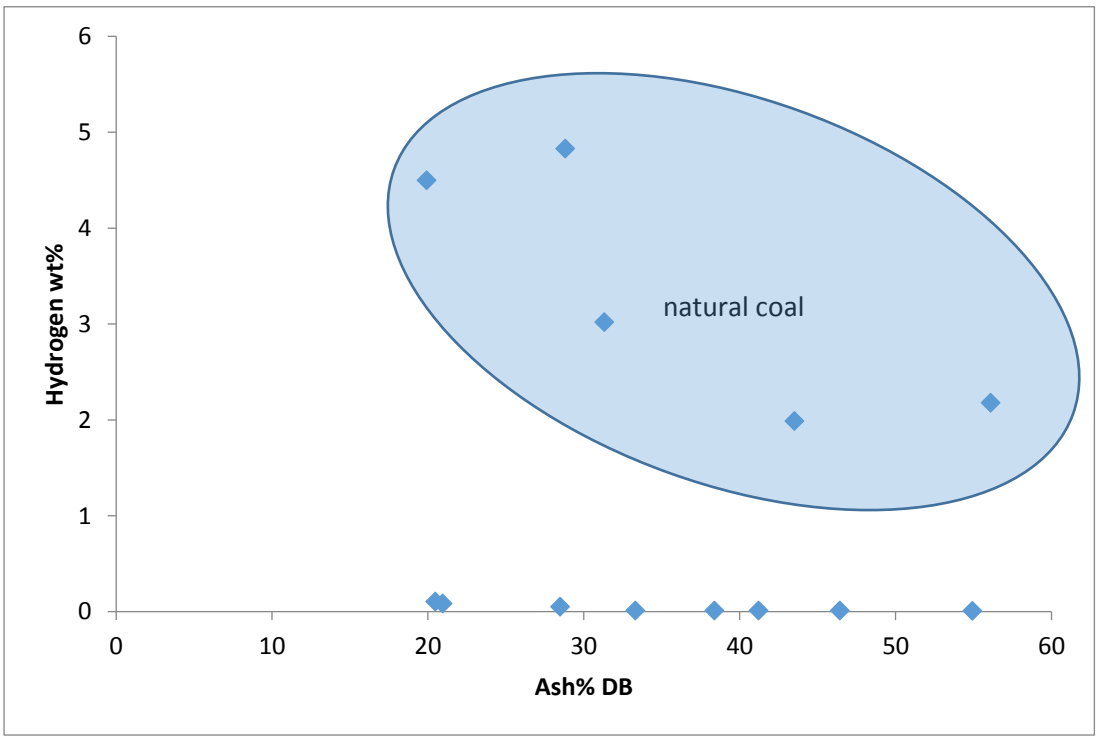

Figure 5-4 Comparison of coal samples from VH3 (gasified) and VH4 and VH6 (not gasified) in terms of the hydrogen content. Hydrogen is highly mobile and H_2 gas is released as part of the gasification process hence groundwater contamination or acidification due to hydrogen in the chamber is unlikely as the spent georeactor will be depleted in hydrogen.

5.3.3 Petrographic analysis

The VH3 samples are dominated by inertinite (inertodetrinite and semifusinite) (Table 5-4 and Figure 5-5), which is typical for coals from South Africa. Snyman (1998) documented a total vitrinite content of 38 %vol. for the Majuba coal, which is higher than the average of 25 %vol. reported for these samples, although two samples do report values of 47 %vol. Three samples (S12 – S13) report extremely low vitrinite contents, which will have affected the overall vitrinite content average from this drill core. The variable maceral composition may influence the total carbon values, as inertinite-rich coals will have a higher carbon content than vitrinite-rich coals of the same rank.

The composite images (Figure 5-5), derived from the block mounts, highlight the banded nature of these Majuba coals, with a predominance of inertinite. The vitrinite bands in S10 (1794) show a degree of swelling in terms of pore development, which was not observed in the samples further away from the ash layer. In the other samples, the vitrinite bands tend to exhibit cracking due to heat stress. Pore development occurs during pyrolysis, when vitrinite softens, forming gas bubbles from the release of volatile matter. Fracturing and pore development will enhance diffusion of the heat and oxidants into the coal seam, and the products out of the coal. Cracking may occur during drying and pyrolysis, with crosslinking of cracks being beneficial to heat and gas transfer through the seam. All the coal in the samples assessed had been converted; no unconverted coal was determined. This suggest that the heat distribution was even through the seam. No spalling was determined, but this may be due to the borehole core.

Syngenetic and epigenetic carbonate minerals were observed, rare pyrite, as well as clays and quartz minerals. Snyman (1998) documented a vitrinite reflectance value of 0.82 %RoVmr for Majuba, indicating that the coal falls into the Medium rank C bituminous range of rank. The reflectance analyses (Table 5-4) confirm that all the samples from VH3 have been exposed to high temperatures. An average vitrinite reflectance value of 5.95 %RoVmr is calculated, with a mean value range of 5.76 – 6.73 %RoVmr, and readings ranging from 5.06 to 7.24 %RoVr (Figure 5-6 and Figure 5-7).

The higher the vitrinite reflectance value, the higher the temperature encountered by the coal. Temperature within the gasification zone affects the quality of the syngas produced, as well as the behaviour of the surrounding rocks and minerals. Róg (2018) used vitrinite reflectance analysis to estimate gasification temperatures for coal extracted from a UCG site in Poland. The Polish coal is comparable to the Majuba coal in terms of rank, but with a higher vitrinite content (Róg, 2018). In the study by Róg (2018), coals were prepared to 700^{o}C, 1000^{o}C, and 1330 ^{o}C in a laboratory, vitrinite reflectance determined, and a profile of vitrinite reflectance along the heating profile was constructed. A mean vitrinite reflectance value of 6.70 was correlated to 1300 °C (range 5.10 – 7.60 %RoVmr); and 1.26 %RoVmr was correlated to 1000°C (range 0.55 – 2.30 %RoVmr). Hence, the coals in the vicinity of the ash layer at the boundary of the UCG cavity at Majuba are likely to have experienced temperatures up to 1300°C, as the vitrinite reflectance readings fall within, or close to, the range documented by (Róg, 2018).

Róg (2018) documents a mean vitrinite reflectance value of 5.38 %RoVmr, with a range of 3.4 – 7.10 %RoV, for the sample at the boundary of the cavity, and value of 7.12 %RoVmr (range 5.2 – above 8.35) for the sample taken from the UCG cavity in Poland. The Majuba sample at the boundary with

the ash layer has a %RoVmr value of 5.76 and a range of readings from 4.98 – 6.80, which is highly comparable to the data produced by (Róg, 2018).

There is a slight decline of reflectance readings through the borehole core across the distance of 2 m, indicating that a slight temperature gradient exists. The lower samples were exposed to slightly lower temperatures, although still well above 1000 ^{o}C when considering Rog's data. The highest volatile matter content and lowest reflectance reading is documented for sample S18. The three samples with vitrinite contents below 7 vol% may produce statistically unreliable reflectance results due to the limited amount of samples available.

Of interest, the samples closest to the ash layer did not provide the highest reflectance values; the third sample has the highest reflectance value. It is possible that the evolving volatile gases have precipitated resulting in vitrinite suppression in the samples closest to the heat source. Alternatively, as the samples closest to the heat source have shown pore development, the heat may be dissipated more rapidly with the evolution of the volatile gases; the samples slightly away from the heat source may contain the heat longer, thus the higher reflectance readings. The UCG process is generally a slow process, providing time for secondary reactions where the heat is high enough (Perkins, 2018a, Perkins, 2018b).

Table 5-4: Mean random vitrinite reflectance (%RoVmr) and maceral group (vol%) on VH3 grain-mounted samples

BH	Seam	Sample	Lab ID	Vitrinite Reflectance analysis			Maceral Group (%vol)	
				%RoVmr	Standard deviation	Range	Vitrinite	Inertinite
VH3	Gus	S10	1794	5.76	0.330	4.98 – 6.80	42.7	57.3
		S11	1795	6.32	0.774	5.15 – 8.05	16.2	83.8
			1796	6.73	0.899	5.07 – 8.92	33.0	67.0
			1797	5.75	0.519	5.03 – 7.51	33.2	66.8
			1798	6.23	0.774	5.25 – 8.52	30.9	69.1
			1799	6.29	0.567	5.26 – 7.51	47.5	52.5
		S12	17100	5.92	0.902	5.00 – 7.83	3.4	96.6
		S13	17101	5.59	0.193	5.15 – 5.85	4.2	95.8
			17102	5.8	0.737	4.92 – 7.86	6.5	93.5
		S14	17103	6.11	0.498	5.41 – 7.73	15.5	84.5
		S16	17105	5.75	0.850	5.03 - 7.51	27.5	72.5
			17106	5.81	0.420	4.94 - 6.82	20.7	79.3
		S17	17108	5.29	0.368	4.56 - 6.22	43.7	56.3
		S18	17109	nd			fragments	fragments
		Average		5.95	0.602	5.06 - 7.24	25	75

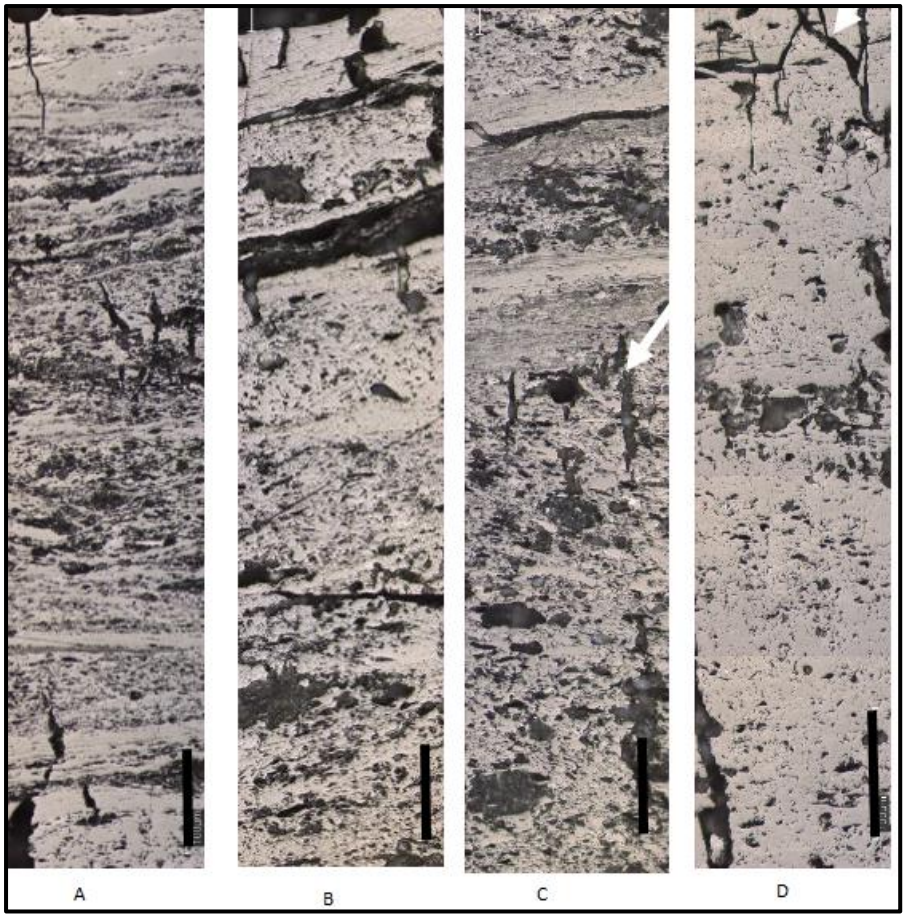

Figure 5-5 Mosaic images of lump VH3 core samples. A) S10 / 1794, note the devolatilisation pores in the vitrinite band towards the top of the image; B) S11 / 1797, note the large cracks in the vitrinite band towards the top of the image; C) S14 / 17103, note the perpendicular, epigenetic carbonate cleats; D) S17 / 17108, note the cracked nature of the vitrinite band towards the top of the image; cross linking of the cracks is evident. (reflected light, x50 oil objective, scale bar is 100 microns).

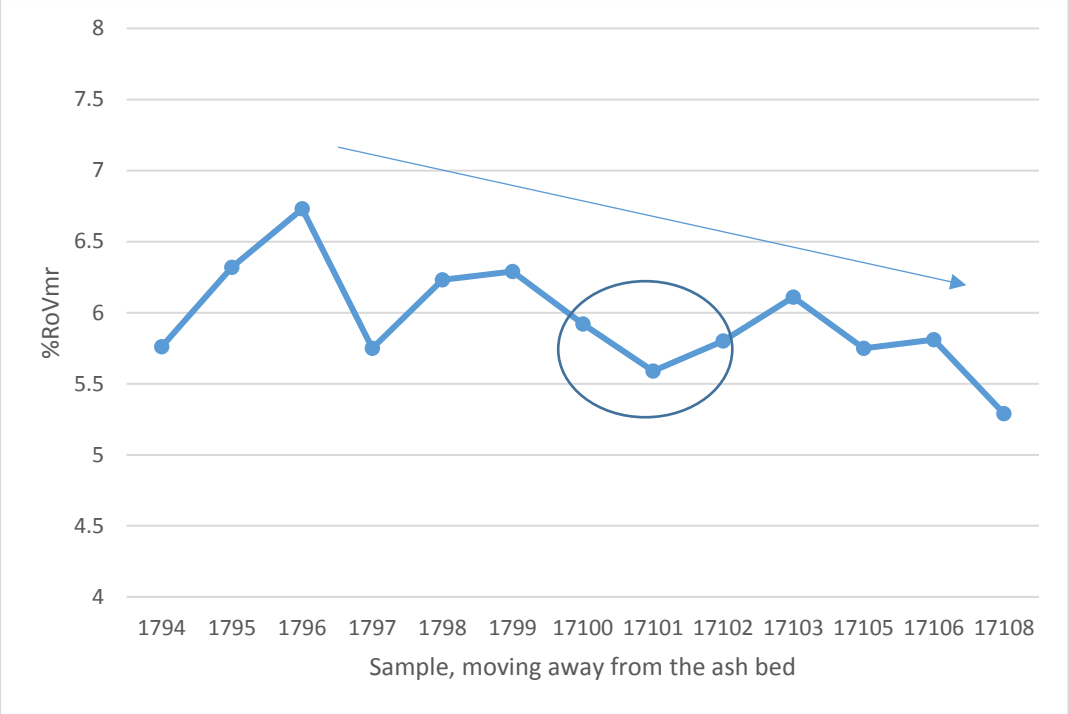

Figure 5-6 Mean random vitrinite reflectance values for the VH3 coal core samples. Whilst the results plot in a zig-zag pattern, there is a general downwards trend in mean reflectance readings, indicating cooler temperatures towards the base of the core. The circled samples contain very low proportions of vitrinite, which is likely to have influenced the vitrinite reflectance values.

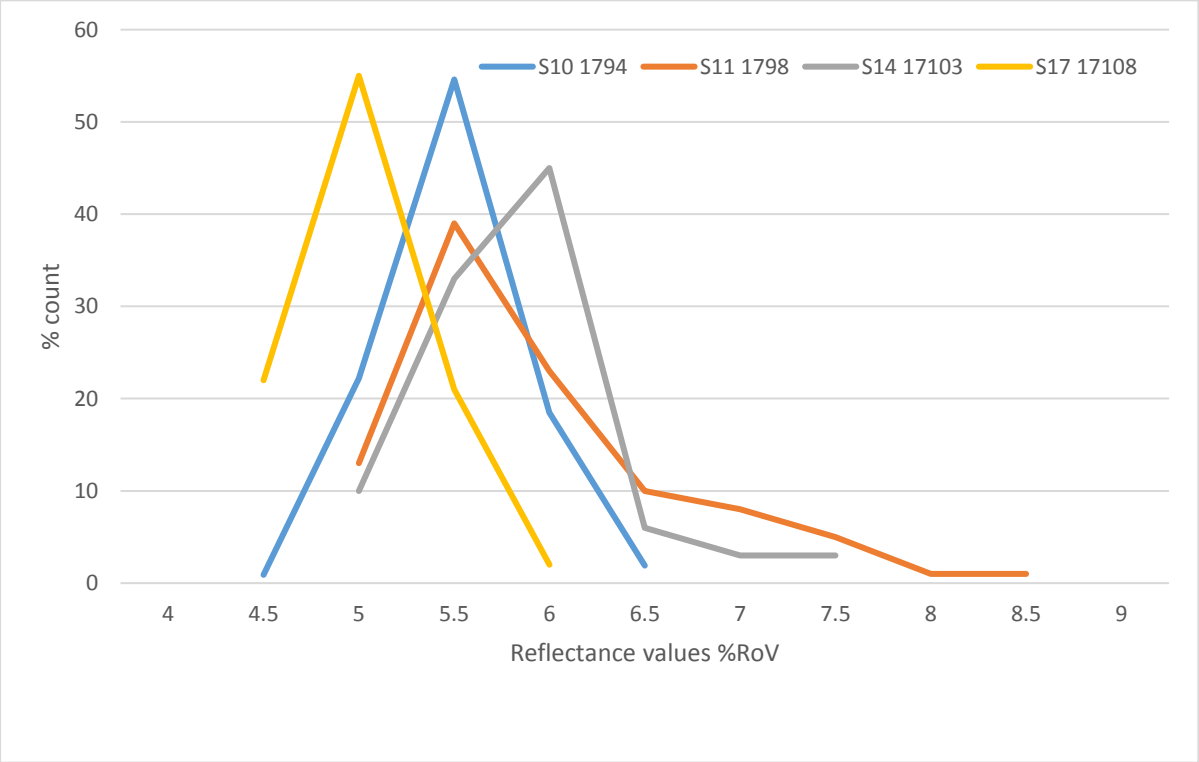

Figure 5-7 Representation of range of random vitrinite reflectance values determined for four samples. S10 1794 was sampled against the ash layer, and S17 17108 at the bottom of the coal seam in the drill core. S11 includes particles with reflectance readings above 8 %RoV, indicative of the highest temperatures the coal was exposed to was over 1000 °C.

5.3.4 Mineralogical analysis

The variation in proportion of minerals phases from the Majuba geo-reactor was assessed in Chapter 4. This section takes an in-depth look at the mineral proportion of char samples retrieved from drill core VH3. The mineral phases were determined using QEMSCAN analysis in conjunction with XRD (see section 4.2). The char section was sampled (S10 to S18) according to Figure 4-2 and Table 4-1. The QEMSCAN false colour image of char samples is presented in Figure 5-8 and full scale images are included in Appendix 4-E.

The QEMSCAN images show widespread cracks within the char samples. These cracks were possibly escape channels for the syn gas that is produced by the gasification process. There is also noticeable filling of the cracks with glass/molten matter as seen more prominently in S11 and S12, where glass (blue) has filled the cracks in the char. The glass profile within char recorded significant amounts of around 10 Vol % in S12 (Figure 5-9). The organic (coal) proportion is lowest in S10 and highest in S18. The char section next to the ash layer (S10) has the lowest organic (coal) proportion and the highest metakaolinite proportion of all the char samples. This shows that the highest coal conversion occurred in the upper sections of the coal seam as retrieved ash was comprised mostly of clay material. The lower parts of the char section is relatively poor in metakaolinite as compared to the other section but high in the coal amount, up to around 90 % for S17 and S18. This shows that the bottom of the coal seam underwent the least coal conversion rate as compared to the upper sections of the coal seam.

There is little presence of pyrite in some of the char samples and the quantities could not be compared to pristine coal samples as this type of analysis was not done previously, however comparison to VH4 was discussed in section 4.3.3.1. Pyrite usually decomposes at temperatures around 195°C and liberates gaseous Sulphur derivatives (Jiang et al., 2018). The presence of pyrite in char suggest that some of the mineral did not decompose into a gaseous phase possibly due to the surface of the mineral not having access to a channel to go into gaseous phases.

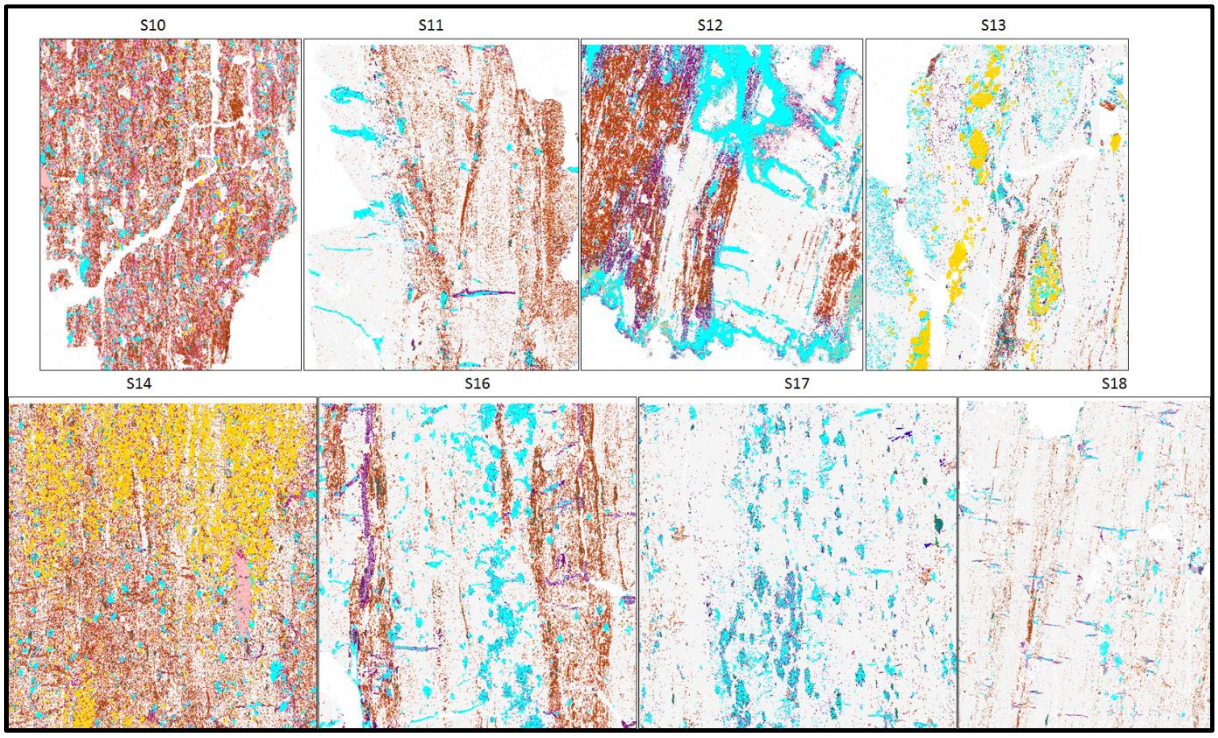

Figure 5-8 QEMSCAN false-colour image of different char sections

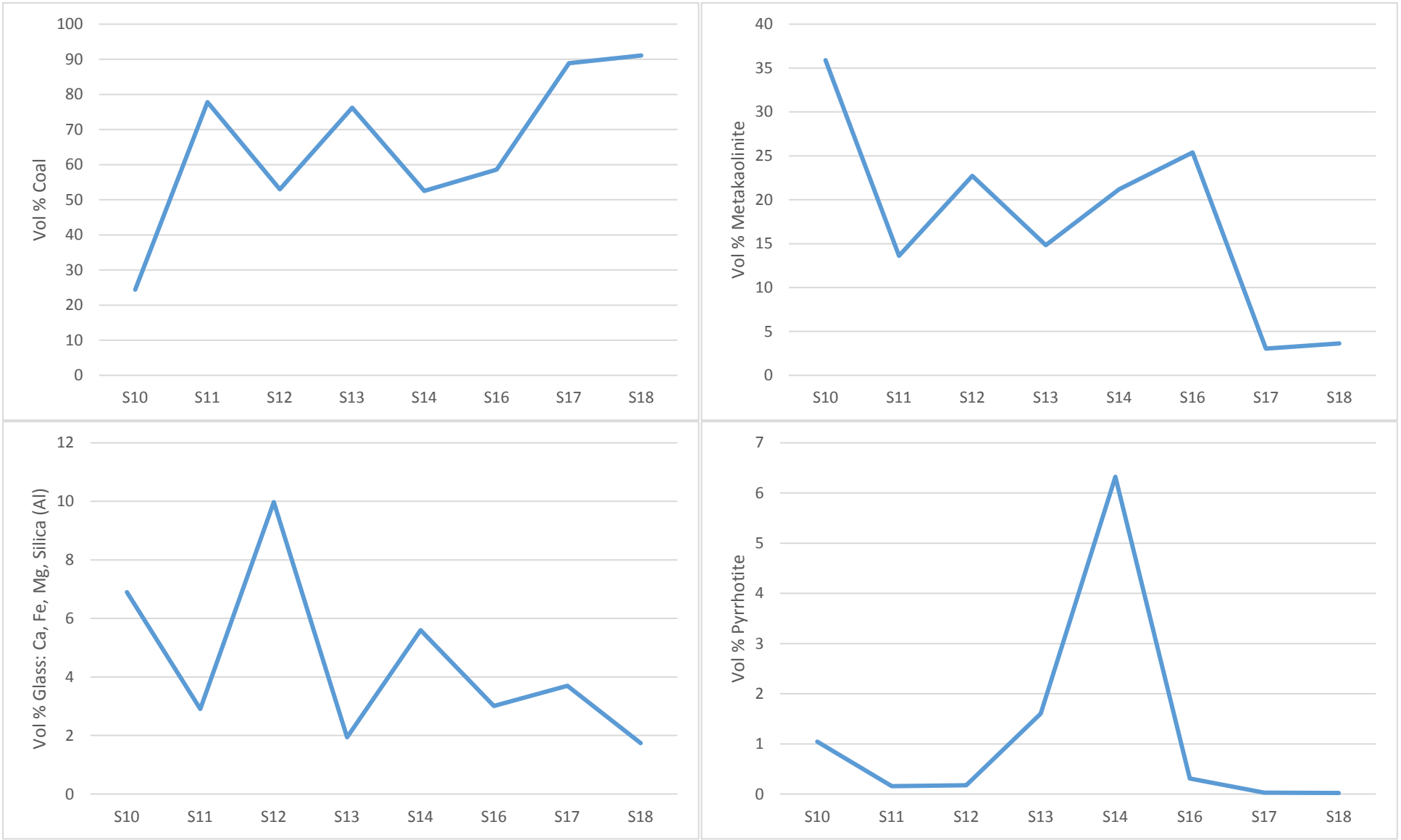

Figure 5-9 Profile of coal and mineral phases in the char section of VH3, pyrite profile is given in section 4.3.3.1

Most of the iron sulphide mineralization is the char samples in pyrrhotite. The pyrrhotite profile shows that S14 contained the highest proportion in the char section of VH3 with 6.3 Vol % (Figure 5-9). Sulphides pose an environmental risk especially to groundwater as they can contribute to acid rock drainage, however the risk occurs under oxidizing conditions.

The ash layer retrieved from VH3 was divided into fine particles (not sieved), coarse particles and whole piece (S9). The QEMSCAN images are presented in Figure 5-10. The mineralogy of the ash retrieved from VH3 was dominated by quartz and metakoalinite (in similar proportion of around 30 Vol %) with microcline and glass in minor proportions. The ash from VH3 has a varied mineralogy as compared to ash retrieved from VH2 where 90 Vol % was metakaolinite. There was negligible sulphide mineralization in ash from both VH2 and VH3.

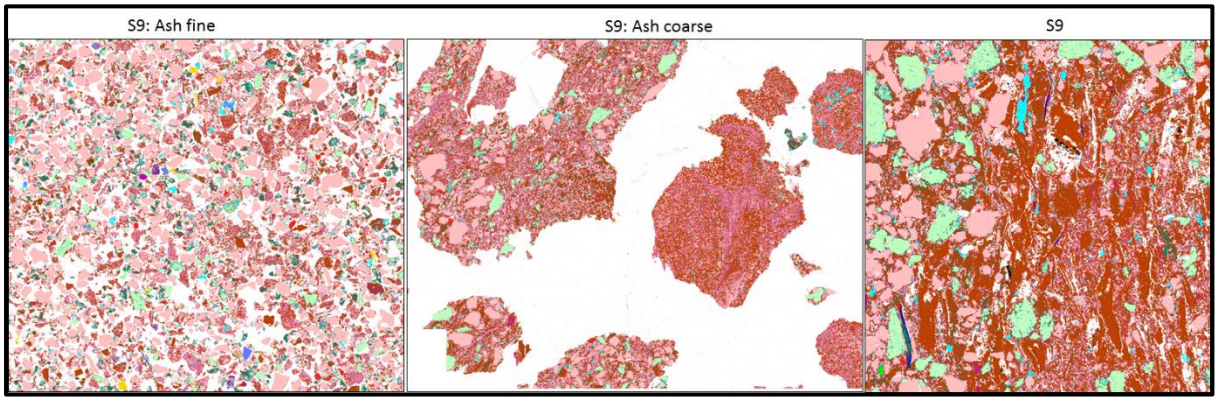

Figure 5-10 QEMSCAN false-colour image of different ash proportions

5.4 Summary

It is evident from the data presented that the coals in the VH3 core drilled in the vicinity of the Majuba UCG cavity were exposed to high temperatures, indicative that the coal was converted. The volatile matter content is very low, and the carbon content is high, clearly different from coals of the same seam from the surrounding area. The vitrinite reflectance data indicates that the coals were exposed to temperatures well above 1000^{o}C, most likely around 1300^{o}C. The samples closest to the ash layer show devolatilisation pores in the vitrinite bands, whilst the samples further away contain stress cracks in the vitrinite bands. The vitrinite reflectance values recorded in this study are comparable to data generated at a Polish UCG site (Róg, 2018). All the coal samples taken from the VH3 core reported high vitrinite reflectance values (above 5.5 % RoVmr), although a slight decrease was observed away from the ash layer, indicative of a very slight heat gradient.

The mineral phases showed sulphide mineralization in the form of pyrrhotite in char samples. Negligible pyrite which suggest that thermal transformations altered iron sulphides to more stable pyrrhotite. The presence of iron sulphide mineralization is an environmental risk especially to groundwater as they can contribute to acid rock drainage. Cracks within the char were filled with molten material which was subsequently preserved as glass. The source of the slag is possibly the spalling overburden which experienced sufficiently high temperature to melt silicate minerals that then dripped into the char below. The preservation of glass could also be an environmental challenge as post gasification, incoming groundwater may readily leach elements from glass more than in tightly held crystal lattice. Devolatilized coal show relatively lower levels of sulphur as compared to natural

coal. This makes the char in the geo-reactor more environmentally sustainable as lower total sulphur content means lower risk of acid rock drainage from sulphur oxidation.

The next chapter looks at the water rock interactions on UCG residue and groundwater. A variety of leaching tests appropriate for UCG waste is explored in order to comprehensively quantify environmental risk. Acid generation prediction is also explored via acid base accounting.

6 Acid base accounting and leaching dynamics of post gasification products

6.1 Introduction

Mining sites are predisposed to release of water containing elevated concentrations of dissolved metals into the environment due to acidic conditions caused by acid mine drainage (AMD). The main source of AMD is oxidation of sulphide bearing minerals due to interactions with oxygen, water and microorganisms. The term acid mine drainage (AMD) is mostly used in mining sites while acid rock drainage (ARD) can be used where material being leached do not necessarily emanate from mining activities (Simate and Ndlovu, 2014). The problem with ARD is the acidification of the leachate which leads to increase solubility of some environmentally toxic metals (As, Cd, Hg, Pb, Zn etc) (Bouzahzah et al., 2015). Even though AMD can occur naturally, it can be enhanced by mining activities that escalate exposure of sulphide minerals to water, air and bacteria (Simate and Ndlovu, 2014).

UCG is an unconventional mining method that produces a cavity with residue products that have the potential to leach into the surrounding aquifer. The potential of ARD from the spent UCG cavity stems from the fact that the overburden, ash, char and the coal seam floor inherently possess sulphide minerals due to the coalification process that occurs in a reducing environment. Sulphide minerals such as pyrite form under reducing conditions where S^{2-} is the dominant redox form of sulphur and since these minerals are not stable when exposed to molecular oxygen, will undergo oxidation and dissolve when exposed to atmospheric oxygen or groundwater with dissolved oxygen (DO) (Deutsch, 1997). The UCG process introduces oxidants in the form of air or oxygen gas during the gasification stage and post gasification surface water can be introduced in the cavity as a form of assisted quenching. The Majuba UCG geo-reactor was extinguished by injecting water from the surface into the gasification zone. This method of quenching is depended on the hydrogeological conditions as high permeable strata may not need assisted quenching. For example, if the coal seam aquifer has high hydraulic conductivity there will be substantial groundwater flow into the UCG cavity after gasifier shutdown and this will assist with cooling of the cavity, however strata with low hydraulic conductivity requires injection of water to quench the gasifier. Post gasification the groundwater gradient will eventually rebound and water will begin to flow through the cavity (Liu et al., 2007). The hydraulic head will re-establish within the coal seam aquifer as the UCG process conditions (pressure and temperature) shutdown with the result that the pre-gasification groundwater regime slowly develops. The geochemical interactions in the cavity have the potential for ARD especially if the sulphide quantities are adequate for acid generation. The reaction below shows the oxidation of pyrite which leads to acid generation:

$$FeS_2 + 15/4O_2 + 7/2H_2O = Fe(OH)_3 + 2SO_4^{2-} + 4H^+ \quad [6.1]$$

The reaction produces the mineral ferrihydrite ($Fe[OH]_3$), sulphate ions and acid. However, oxygen is poor at directly oxidizing pyrite and reaction [6.1] is initiated at low pH by the following two coupled reactions (Deutsch, 1997):

$$FeS_2 + 14Fe^{3+} + 8H_2O = 15Fe^{2+} + 2SO_4^{2-} + 16H^+ \quad [6.2]$$

$$4Fe^{2+} + 7/2O_2 + 14H^+ = 14Fe^{3+} + 7H_2O \quad [6.3]$$

In environments with low oxygen, the ferrous iron bounded to sulphur may not even oxidize to ferric iron in solution therefore reaction [6.2] may dominate (Simate and Ndlovu, 2014). The UCG cavity post gasification is likely to be a low oxygen environment unlike in conventional mining where the coal seam in in constant contact with the atmosphere in open pit mining and some underground mines. The introduction of surface water into the cavity can play a role in the redox potential of the geochemical reactions in that surface water inherently has higher dissolved oxygen (DO) as compared to the coal seam aquifer and groundwater with dissolved oxygen can oxidize sulphide minerals. Surface water from dams or streams is usually introduced in the UCG cavity for assisted shutdown or quenching of the gasification process. This was the case at the Majuba UCG plant where surface water was injected into the UCG chamber to assist with gasifier shutdown (Pershad et al., 2018a).

Oxidation of sulphide minerals contribute to the acidity of rock drainage while dissolution of carbonate minerals (e.g calcite) play a role in neutralizing the acid via the following reaction:

$$CaCO_3 + H^+ = 3HCO^- + Ca^{2+} \quad [6.4]$$

The dissolution rate of dolomite and magnesite are much slower as compared to calcite (White et. al., 1999). Acid generation is hence a dynamic process that needs monitoring over a long period. Non-carbonate minerals like clay can also contribute to the neutralization of acid in solution. For example, kaolinite displays this neutralizing behaviour by the following reaction (Deutsch, 1997):

$$Al_2Si_2O_5(OH)_4 + 6H^+ = Al^{3+} + 2H_4SiO_4Ca^{2+} + H_2O \quad [6.5]$$

The potential for acid generation from disturbed natural strata by mining activities under consideration by the South African's Department of Water Affairs and Sanitation (Best Practice Guideline G4: Impact Prediction, Department of Water Affairs and Forestry 2008). The guideline uses the source-pathway-receptor model for its risk-based approach to impact prediction. Underground mine voids are identified as potential risk source mediums to water bodies. Underground coal gasification creates a cavity or void that contains residue products such as ash, unburned coal and the heat affected surrounding rocks. According to the G4 guideline, all these products will have to undergo geochemical assessment including evaluation of the risk of acid generation and the potential for metal release.

There are two types of laboratory test that can be used for the prediction of acid rock drainage, static and kinetic tests. Static tests like acid base accounting (ABA) are quick and relatively simple to carry out while the kinetic tests, such as leaching tests, usually take longer periods to complete. Kinetic tests also require larger samples and are usually carried out if the ABA test are inconclusive. Acid base accounting described by Usher et al. (2003) as a predictive tool that accounts for the balance between the acid producing potential (AP) and the neutralising potential (NP) of geological material and the difference is calculated as the net neutralising potential (NNP). The acid producing material is generally the sulphide minerals as seen in Eq (1), while the acid neutralising minerals are carbonate minerals such as calcite, dolomite and magnesite, Eq (2). Dissolution of some silicate minerals such as anorthite can also neutralize acid, however their dissolution rates are slower than their carbonate counterparts (White et. al., 1999).

Acid base accounting is a predictive tool used to assess the acid producing capacity of coal mines and rock waste where the acid-neutralising potential (NP) and acid producing potential (AP) of rock

samples are determined and the difference, the net neutralising potential (NNP) is calculated using the equation below:

$$NNP = NP - AP \quad [6.6]$$

The AP is usually based on the theoretical oxidation of all sulphur in the sample to sulphuric acid and is calculated from total sulphur (S_{Total}) or sulphide-sulphur ($S_{Sulphide}$) expressed in wt%. The (S_{Total}) or ($S_{Sulphide}$) is multiplied by the stoichiometric factor of 30.6 in order to express AP in Kg H_2SO_4 per tonne or alternatively by 31.25 to express AP in kg $CaCO_3$ per tonne (Parbhakar-Fox and Lottermoser, 2015). The total sulphur in samples is usually determined using a LECO (Laboratory Equipment Corporation of St. Joseph, Michigan) sulphur analyser. Not all sulphur contained in minerals contribute to acidity in solution as some of the minerals have sulphur already in oxidized form (e.g. gypsum). The inaccuracy in assuming that all sulphur will form acidity can lead to overestimation of AP which then consequently leads to erroneous estimation of NNP. Several attempts have been made to address this discrepancy by several authors (Stewart et al., 2006, Hageman et al., 2015, Dold, 2017).

The dissolution of acid neutralizing minerals such as carbonates contribute towards the neutralization potential (NP). Hydrochloric acid is used to sufficiently digest these minerals and it is expressed in Kg $CaCO_3$ per tonne but can also be converted into Acid Neutralising Capacity (ANC, expressed as kg H_2SO_4/tonne) by multiplying the NP with 0.98.

Negative NNP values indicate the potential for acid to generate while positive NNP values are associated with alkaline conditions but a NNP of +20 is generally needed before non-acid conditions can be concluded. There is therefore a region of uncertainty from -20 to +20 NNP which usually requires kinetic testing if ABA results are inconclusive (Qureshi et al., 2016). The ratio of NP to AP is known as Neutralisation Potential Ratio (NPR) and can also be used to determine the potential for acidic conditions. Material with less than 0.3% Sulphide-S are regarded as lacking enough oxidisable Sulphide-S to maintain acid generation and when assessed in conjunction with NPR the following screening criteria can be applied (Usher et al., 2003):

- NPR ratios of >4:1 are considered to have sufficient neutralising proficiency.
- NPR ratios of 3:1 to 1:1 are regarded as inconclusive.
- NPR ratios below 1:1 and with sulphide-S > 0.3% are theoretically acid-generating.

Net acid generation (NAG) tests can also be used to determine the acid forming potential of material with sulphide bearing minerals. The NAG tests calculate acid forming capacity by reacting powdered material with hydrogen peroxide and then back titrating with NaOH to obtain the acid forming potential (Parbhakar-Fox and Lottermoser, 2015). Hydrogen peroxide is a strong oxidizing agent with a redox potential of 1.77 V (Chirita, 2009). Hydrogen peroxide is used to oxidize the sulphide minerals where S^{2-} is the main redox form of sulphur by the following reaction (Zhang et al., 2018):

$$FeS_2 + 7.5\ H_2O_2 \rightarrow 2\ SO_4^{2-} + H^+ + 7\ H_2O \quad [6.7]$$

After leaching with H_2O_2 the pH of the solution is recorded as final pH or NAGpH, before back titration with NaOH. This final pH serves as a screening criterial for capacity of material to produce acidity using the following thresholds (Usher et al., 2003):

• NAG pH below 3.5 indicates high risk of acid generation

• NAG pH value between 3.5 and 5.5 indicates low risk of acid generation

• NAG pH value larger than 5.5 indicates non-acid generation potential

To avoid overestimating the acid potential, water soluble sulphate can be deducted from the oxidizing sulphide by leaching with deionized water to obtain the concentration of sulphates that is already in oxidized form. Utilizing both NNP and NAG test for potential acid generation of material provides a more reliable evaluation technique than either test alone (Stewart et al., 2006).

This study offers a modified elution method that uses deionized water, hydrogen peroxide, and sulphuric acid as leaching agents. Hydrogen peroxide provides for elution under complete oxidation as it is a strong oxidizing agent that provides for efficient dissolution of even inert sulphides such as pyrite (Antonijević et al., 1997). Elution with deionized water was employed as a reference method since it provided for mild leaching conditions (no pH buffering), while elution with sulphuric acid was utilized for more extreme conditions which are possible in post UCG cavern due to possible ARD (Mokhahlane et al., 2018). The elution tests further incorporated leaching by groundwater taken from the UCG cavern from the study area. The groundwater elution tests were carried out in temperatures recorded from the study site in an attempt to simulate field conditions. The method of UCG residue leaching by groundwater is modified from (Strugała-Wilczek and Stańczyk, 2016) by accommodating varying temperature scenarios.

In UCG, ARD has the potential to weaken the infrastructure around the gasification zone as the production and injection wells were installed using cement and steel casing. If the integrity of these boreholes is compromised, hydraulic connections can develop between the geo-reactor and the shallower aquifers which can lead to cross contamination of contaminants between aquifers or loss of water from the shallow aquifer to the deeper aquifers. The geochemistry of the surrounding aquifers can also be altered as metals become more soluble in acidic conditions leading to widespread groundwater contamination. The aim of this chapter is to explore the leaching dynamics and geochemistry of the residue products from the spent UCG geo-reactor and the potential of acid generation in the gasification zone. This chapter essentially undertakes to address the second main objective of the thesis, which is the determination of chemical evolution of inorganic groundwater contaminants from the UCG process.

6.2 Experimental

Samples were crushed by Retsch KG 5657 Haan BB100, and milled by Giebtechnik Labor Scheibenschwingmmuhle. Elghali et al. (2018) recommends that due to differences in size distribution of waste rocks, samples sizes have to be milled to less than 2mm in order to attain a representative sample for static tests. Major and trace elements were analysed using X-ray fluorescence spectrometry (XRF). Major elements were determined using the Norrish Fusion 1 technique using in-house correction procedures and using a Panalytical PW2404 X-ray fluorescence spectrometer. Milled samples were fused using Johnson Matthey Spectrolflux 105 at 1100°C for major elements determination and raw data corrected using in-house software. Standard calibrations were made up using artificial oxide mixtures and international standards for rocks as well as in-house controls. Sample weight used was 035 gm and flux weight 2.5 gm. Calibration standards were mainly the International Reference Materials USGS series (USA) and NIM series (South Africa). Precision was taken as 1% for elements in abundance of greater than 5% by weight, and 5% for elements in

abundance less than 5%. Trace elements were determined on pressed pellets using a Moviol solution binder. Standardization was carried out by means of International Reference Materials USGS series (USA) and NIM series (South Africa). Accuracy was determined on the basis of counting time and is taken as 5% for elements in abundance greater than 100 ppm, and 10% for elements in abundance between 10 and 100 ppm. The instrument utilized was the Philips PW2404 x-ray spectrometer.

Inductively coupled plasma mass spectrometry (ICP-MS) was also incorporated for analysis of trace elements. 50mg of sample was added to 6ml HF/HNO_3 (2:1) and placed into the microwave digester at 190°C and 450 PSI, for 40 minutes. Samples were then evaporated on a hot plate at 70°C until all liquid evaporated. 2ml of HNO_3 was added and the beakers capped and place on a hot plate at 60°C for 24 hours. The cap was then removed and beakers placed on a hot plate at 70°C until all liquid evaporated. 2ml of HNO_3 was then added and left to evaporate. Once all the liquid is evaporated, 300µl of HNO^3 is added and the sample is ready for the ICP MS.

Samples were leached with groundwater (mine water) obtained from the Majuba UCG drill hole G1VH3 that intercept the gasification zone. Mine water was used instead of the local groundwater because water from the cavity is representative of the UCG void hydrochemistry while local groundwater from adjacent aquifers may have not been affected by the UCG process. The elution method used was adapted from (Strugała-Wilczek and Stańczyk, 2016) which was employed on similar post gasification residue from UCG experiments Poland. Post cavern residue samples were eluted using mine water on a 1:10 ratio. The mixture was placed in a rotating shaker and rotated for 2 hours at 15 revs/min. It was then allowed to stand for 4 hours and then shaken for an additional 1 hour. The mixture was then left static for 16 hours and then rotated for 1 hour. The total experimental time was 24 hours. This experiment was done at 25 °C and at 70 °C. The choice of the experimental temperature was based on field conditions whereby 70 °C was the temperature recorded in the spent UCG chamber three years after gasifier shutdown and 25 °C is the average temperature in the background (“off cavity”) boreholes. All leachates were analysed using inductively coupled plasma mass spectrometry (ICP-MS).

Acid base accounting (ABA) analysis were determined for all samples. ABA is a tool that is designed to determine the acid producing capacity of coal mine wastes in which pyrite is the leading acid-forming sulphide mineral (Parbhakar-Fox and Lottermoser, 2015). The balance between acid-neutralising potential (NP) and acid producing potential (AP) of rock samples were determined and the difference, the net neutralising potential (NNP) recorded. The samples were first eluted with deionized water to obtain the soluble sulphur content. This concentration represents water soluble-sulphur that is already oxidised in samples and hence does not contribute to acidity. The pH of the sample was recorded after the water elution as initial pH. Oxidation products were determined by elution with hydrogen peroxide where only reactive species oxidise and produce acidity in solution which then contribute to dissolution of pH sensitive elements. The pH of the sample was recorded after peroxide elution as final pH. The total reduced sulphur content available for oxidation is calculated from the resultant sulphate concentration and adjusted by subtracting the water soluble sulphate from the water elution test. This then gives the correct sulphur concentration responsible for acid production and hence overestimation of acidity is avoided by using only reactive sulphur in the ABA calculations. The deionized water elution test was carried out over 24 hours using a ratio of 50 ml of deionized water to 5 g solid material. The hydrogen peroxide elution test was conducted over 24 hours at 2 g solid material to 80 ml hydrogen peroxide. An additional elution test using sulphuric acid was

employed to assess the leaching behaviour of the material if acid conditions developed in the UCG cavity. The acid elution test was also carried out over 24 hours using 5 g solid material and 50 ml of 0.1N sulphuric acid. The acid elution test was employed as "worst case scenario" that could develop in the cavity and hence the leaching behaviour of various elements was assessed under this conditions.

Acid-neutralising potential (NP) was determined by subjecting the samples to acid digestion and subsequent back titration with NaOH in order to obtain the NP. The NP represents the carbonate mineral content that is representative of acid neutralising potential in each sample. This procedure is the ABA modified procedure by (Usher et al., 2003) which utilizes hydrogen peroxide to achieve full oxidation of sulphide minerals. All the NP and AP values were converted to kg $CaCO_3$ per tonne and the difference (NNP) recorded.

6.3 Results

6.3.1 Characterization of the UCG geo-reactor

The elemental composition of selected samples from the roof, ash, char and floor of the Majuba UCG geo-reactor was determined using X-ray fluorescence (XRF). The major and minor elements are presented as oxides in Table 6-1. Additionally, the average concentration (AC) is also included in Table 6-1. The major oxide were SiO_2 and Al_2O_3 with Fe_2O_3, CaO and K_2O. Sample S13 (char) was ashed (see Table 5-1) prior to XRF analyses as the equipment gives erroneous readings for samples with high organic content. These results correlate with the mineralogical determinations that show silicates as dominant minerals with calcite and pyrite in smaller proportions.

Table 6-1 Element concentration (wt%) of samples from the Majuba UCG geo-reactor determined from XRF analysis

	SiO_2	TiO2	Al_2O_3	Fe_2O_3	MgO	CaO	Na_2O	K_2O	P_2O_5	SO_3	MnO
H	83.81	0.11	7.88	1.46	0.34	1.22	0.81	3.87	0.01	0.37	0.01
C2	66.08	1.02	21.90	4.08	1.02	0.14	0.25	3.72	0.07	1.58	0.01
E	72.63	0.68	15.34	5.41	0.48	0.88	0.42	3.23	0.08	0.65	0.00
S7	59.47	1.29	25.48	5.42	1.55	2.52	0.70	1.55	0.54	1.13	0.01
S9	74.47	0.01	0.19	1.82	0.00	0.00	0.00	0.02	0.00	0.00	0.00
S13	60.86	1.96	25.48	4.29	0.82	2.43	0.98	1.55	0.05	1.19	0.00
S19	63.82	1.25	27.57	2.76	0.41	0.15	0.14	3.12	0.05	0.56	0.00
AC	68.73	0.90	17.69	3.61	0.66	1.05	0.47	2.44	0.11	0.78	0.00

The trace elements compositions were determined using both XRF (for VH2 samples) and inductively coupled plasma mass spectrometry (ICP-MS) and are presented in Table 6-2. Chromium, Ba, Sr and Zr are present in significant amounts in all the samples with Sc, Co and U on average lower than the other trace elements. The other elements had varied concentrations in all samples. The heterogeneous content of trace elements in coal means that the products of thermal processing also have a diversified trace element content (Strugała-Wilczek and Stańczyk, 2016).

Table 6-2 Trace element composition (ppm) for the Majuba UCG geo-reactor

Sample	Sc	V	Cr	Co	Ni	Cu	Zn	Ga	Rb	Sr	Y	Zr	Nb	Ba	Pb	Th	U
VH2-D	13.2	66.1	105.2	7.7	29.7	22.1	98.1	31.0	94.0	129.4	17.3	146.6	19.9	676.6	29.4	12.8	1.5
VH2-E	8.0	68.9	124.4	3.4	17.8	22.1	29.0	19.5	125.0	383.2	17.0	275.6	14.5	930.9	26.8	9.2	3.1
VH2-F	14.3	129.1	174.7	18.7	44.4	30.8	141.6	33.6	190.4	215.3	50.1	490.5	24.3	882.2	35.1	24.3	3.2
VH3-S7	10.5	74.0	427.5	46.7	124.4	32.0	34.3	23.6	19.7	622.5	33.6	310.5	21.1	660.8	9.4	14.2	5.2
VH3-S8	9.5	93.9	122.2	58.6	23.5	26.8	13.8	36.6	10.6	953.6	26.5	430.1	36.4	512.0	18.3	13.6	10.2
VH3-S9	3.2	15.7	32.4	3.2	11.6	8.1	18.3	12.1	59.5	336.5	12.6	108.8	12.7	623.8	13.6	9.2	4.9
VH3-S13	11.3	107.0	181.2	19.1	19.3	40.2	10.6	26.9	7.2	359.3	37.4	207.2	27.4	796.5	64.4	21.0	5.8
VH3-S19	0.5	53.9	71.6	10.7	31.9	21.1	43.6	20.4	60.1	0.7	0.8	160.3	18.7	18.3	17.5	5.4	1.9
AC	8.8	76.1	154.9	21.0	37.8	25.4	48.7	25.5	70.8	375.1	24.4	266.2	21.9	637.6	26.8	13.7	4.5

6.4 Leaching dynamics of elements from the UCG chamber

The release of various elements from the spent Majuba UCG chamber from the deionized water, hydrogen peroxide and sulphuric acid elution tests are displayed in Figure 6-1 to Figure 6-4. The data and descriptive statistics are included in Appendix 6-A. For simplicity, the discussion and presentation of the results have been categorized according to groupings of elements in the periodic table. Concentrations of elements that were below the detection limit of the ICP-MS were normalized to zero.

6.4.1 Group I/II elements

The leaching behaviour of Ca, K, Mg and Na are displayed in Figure 6-1.

6.4.1.1 Calcium (Ca)

Calcium exist in coal in over 30 different minerals including silicates, carbonates, phosphates, sulphates and oxylates (Finkelman et al., 2018). The Majuba UCG chamber recorded an average calcium oxide content of 1.05 wt% (Table 6-1). The mean mobilization of Ca from peroxide elution was 1.72 Kg\t while a 2.65 Kg\t average was recorded for samples leached with acid (Figure 6-1). The mean release from water elution was two orders of magnitude less at 0.08 Kg\t. The release of Ca is pH sensitive as seen by the negative Pearson correlation coefficient (r = -0.42). Calcium constitutes carbonate minerals such as calcite, which was present in the mineralogical results of the tested samples. Deutsch (1997) tested the solubility of a calcite\water system closed to the exchange of CO_2 gas and found that the speciation of inorganic carbon is pH dependent and prefers the carbonate ion at high pH and therefore the solubility of calcite reduces as pH increases. Even though the acid elution released on average most ions into solution, however some of the highest levels of release were seen in peroxide leaching. The peroxide elution results were the most dispersed as they recorded the highest standard deviation (σ = 2.57). In a spent UCG chamber, Ca can be expected to be released more readily in an acidic environment but under oxidizing conditions more spread-out Ca mobilization can be anticipated. The highest Ca was noticeably released from char samples under all elution methods. Although Ca is generally not regarded as an element of environmental concern, it was one

of the highest released cation in this experiment. The rapid release of Ca can lead to secondary mineral formation (reaction [6.8]).

$$Ca^{2+} + SO_4^{2-} + 2H_2O = CaSO_4.2H_2O \text{ (gypsum)} \quad [6.8]$$

6.4.1.2 Magnesium (Mg)

The mode of occurrence of Mg in coal is in micas, clays, carbonates, silicates and oxides which are included into the coal seam as detrital minerals and rock fragments (Finkelman et al., 2018). The leaching behaviour of Mg is similar to that of Ca albeit to a smaller degree and was present as a minor element with an average abundance of 0.66 wt% (MgO). The mean release from water elution was 0.02 Kg\t while peroxide leaching released an average of 0.26 Kg\t. The acid elution showed the highest mean Mg mobilization at 0.65 Kg\t, however the sample with the maximum release was from the peroxide leaching at 1.9 Kg\t. There acid elution results were the most dispersed as the data recorded the highest standard deviation (σ = 0.44). There was noticeable pH dependency on the leaching behaviour of Mg (r = -0.53), where acidic conditions favoured higher mobilization whilst alkaline conditions showed subdued release. Magnesium has the tendency to be less soluble in water and alkaline reagents while marginally soluble in acidic conditions (Izquierdo and Querol, 2012). The same leaching behaviour was seen also for strontium (Appendix 6-A). In a spent UCG chamber Mg and Sr may be released marginally post gasification but increased mobilization can be expected once the pH drops to acidic levels (<pH 4) due to the observed pH dependent mobilization of these elements.

6.4.1.3 Potassium (K)

Potassium in coal can be precipitated from groundwater or circulating hydrothermal fluids, however it usually emanates from feldspars or clay minerals (Izquierdo and Querol, 2012). XRF analysis reports major elements as oxides and potassium oxide was found in small proportions with an average abundance of 2.4 wt% (Table 6-1). The mean release during acid elution was 0.28 Kg\t while peroxide released the most K with an average of 0.37 Kg\t. The water elution was an order of magnitude lower at an average of 0.03 Kg\t. There was also more variation in the peroxide elution results as the data recorded the highest standard deviation (σ = 0.29). The leaching behaviour of K shows a wide range of pH solubility, as high concentrations were recorded for both alkaline and acidic conditions. Alkaline and acid soluble K is associated with organics or water soluble salts and may have been in ion exchangeable sites in clays (Finkelman et al., 2018). In a spent UCG chamber, K will therefore be released more readily by the incoming groundwater regardless of pH or oxidizing conditions.

6.4.1.4 Sodium (Na)

Sodium is associated with various silicates phases in bituminous coals (Finkelman et al., 2018). The Majuba UCG chamber recorded an average Na_2O content of 0.47 wt%. The mean mobilization of Na from peroxide elution was 0.48 Kg\t, while acid and water released 0.55 Kg\t and 0.22 Kg\t on average respectively. The release of Na produced the negative correlation of pH versus Na concentration (r = -0.41). There was also more variation in the peroxide elution results as the data recorded the highest standard deviation (σ = 0.338). The release of Na was in the same order of magnitude across the different leaching mediums. Therefore the release of Na does not seem to be as pH-dependent as in the other group I/II elements. Interestingly, no Na was mobilized from “off cavity” boreholes (G1VH4 and G1VH6) under peroxide elution even though Na was released from the same samples under water

and acid elution. This behaviour may suggest that the UCG process was able to alter the geochemistry of rocks in the vicinity of the geo-reactor to the extent that Na became more readily available for leaching as samples from this area readily released Na under all experimental conditions. In a spent UCG chamber, Na will therefore be released more readily by the rebounding groundwater head regardless of pH or oxidizing conditions.

6.4.2 Metals

The leaching behaviour of Cu, Fe, Ni and Mn are displayed in Figure 6-2.

6.4.2.1 Copper (Cu)

The abundance of Cu in the Majuba UCG chamber was in trace amounts with an average of 25.4 ppm (Table 6-2). The mean mobilization from peroxide elution was 0.0051 Kg\t, while acid leaching was slightly higher at 0.0058 Kg\t (). The water elution was an order of magnitude lower with an average of 0.00025 Kg\t. There was a noticeable pH dependency in the leaching behaviour as the highest mobilization of Cu was recorded at low pH levels while the smallest release was evident from higher pH levels and this was confirmed by the negative correlation factor (r = -0.36). The acid elution results were the most dispersed as they recorded the highest standard deviation (σ = 0.058). Copper occurs in most coals as a sulphide mineral, typically chalcopyrite, and can also be found to be organically bound particularly in low-rank coals (Finkelman et al., 2018). According to Izquierdo and Querol (2012), Cu displays appreciable degree of mobility in acidic conditions, irrespective of form of occurrence. Even though there was varied release of Cu across the pH range, in general, the mobilization was noticeably low with 0.056 Kg\t as the highest recorded concentration. It is possible that during the gasification process, Cu was not volatilized into the gaseous phase but remained in solid phase due to its high boiling point (2562 °C), which suggests that it infuses into a water-insoluble phase (Strugała-Wilczek and Stańczyk, 2015). In the UCG chamber, no significant Cu can be expected to leach unless the pH of the geo-reactor drops to below 4.

6.4.2.2 Iron (Fe)

Iron occurs in coal in a variety of mineral phases including sulphides (pyrite, chalcopyrite, pyrrhotite, arsenopyrite, bornite), micas (biotite, glauconite), carbonates (siderite, ankerite), clays (vermiculite, chlorites, montmorillionite), silicates (garnet, amphibole, epidote, olivine), oxides (hematite, magnetite, goethite, chromite) and several sulphates (Finkelman et al., 2018). The Majuba UCG chamber recorded an average iron oxide content of 3.6 wt%. The average release of Fe from water elution was 0.0036 Kg\t, while peroxide elution was an order of magnitude higher at 0.69 Kg\t and acid was two orders of magnitude higher at 4.22 Kg\t. The acid elution results were the most dispersed as they recorded the highest standard deviation (σ = 4.18). There was an obvious pH-dependency in Fe release as determined by the negative correlation factor between pH and Fe concentration (r = -0.49), showing that as pH decreases more Fe is mobilized. The highest recorded mobilization was 19.2 Kg\t at pH 1.83, and at around pH of 2 there is a sharp decrease in Fe concentration. There is poor mobilization of Fe above pH of 3, as Fe concentrations remained below 0.2 Kg\t. A similar trend of Fe release was recorded by Izquierdo and Querol (2012) on fly ash leachate. The rebounding groundwater in the UCG cavern can be expected to release negligible amounts of Fe however if aggressively acidic

conditions develop and the pH drops to below 2, then significant amounts of Fe will be mobilized into solution.

6.4.2.3 Nickle (Ni)

Occurrence of Ni in coal is mostly related to the organic portion but Ni can also be inorganically bound with sulphides and clays (Finkelman et al., 2018). The abundance of Ni in the UCG chamber was found in trace amounts with an average of 37.8 ppm. Nickle can be expected to occur in UCG residue products as it only volatilizes into the gaseous phase at temperatures above the UCG operating conditions (Strugała-Wilczek and Stańczyk, 2015). The mean release of Ni from acid elution was 0.03 Kg\t while for peroxide was an order of magnitude lower at 0.041 Kg\t. Water elution recorded the lowest average mobilization of 0.00007 Kg\t. The release of Ni is pH sensitive as seen by the negative correlation factor (r = -0.32), for pH versus Ni concentration. There is a sharp decrease in the concentration of Ni around pH of 2 and above this pH there is poor release of Ni into solution. The acid elution results were the most dispersed as they recorded the highest standard deviation (σ = 0.058). Only 4 samples out of 52 from the water elution test recorded Ni detectable concentrations. Furthermore, all peroxide elution samples that recorded a final pH above 5 had below detection levels of Ni. Interestingly, no Ni was leached from the "off cavity" samples under both water and peroxide elution tests. It is possible that the high temperatures and the subsequent mineralogical alterations are responsible for increased release of Ni in areas in the immediate vicinity of the geo-reactor. The rebounding groundwater in the spent UCG chamber is not expected to leach any appreciable concentration of Ni unless the pH drops to below 2.

6.4.2.4 Manganese (Mn)

Manganese in coal is mainly found in carbonates, particularly siderite, or in pyrite and clays in carbonate-deficient coal (Finkelman et al., 2018). The abundance of manganese oxide in the Majuba UCG chamber was at an average of 0.004 wt%. The mean release of Mn from acid elution was 0.05 Kg\t while from peroxide elution was in the same order of magnitude at 0.01 Kg\t. The water elution test released two orders of magnitude less Mn with an average of 0.0002 Kg\t. The solubility of Mn is noticeably sensitive to pH as seen by the negative correlation factor (r = -0.37). The acid elution results were the most dispersed as they recorded the highest standard deviation (σ = 0.083). Most of the water extracts have concentrations below the detection limit while acid elution produced the highest concentrations. All the "off cavity" samples recorded below detection limit concentration under peroxide extraction even though some of the same samples showed mobilization under water elution. This suggest that oxidizing conditions would not readily release Mn from pristine sedimentary rocks while mobilization can be expected in the geochemically altered strata of the spent geo-reactor. In general, Mn is poorly mobilized and should not be an element of great environmental concern in spent UCG geo-reactors.

6.4.3 Trace elements

The leaching behaviour of V, Zn, Co and Cr are displayed in Figure 6-3.

6.4.3.1 Vanadium (V)

Occurrence of V in coal is mostly linked to the organic portion but can also occur in clay minerals (Finkelman et al., 2018).The average recorded V concentration in the Majuba UCG geo-reactor was 76.1 ppm. The mean release of V from acid elution was 0.049 Kg\t while for peroxide was an order of magnitude lower at 0.0073 Kg\t. Water elution recorded the lowest average mobilization at 0.00027 Kg\t. The solubility of V is noticeably sensitive to pH as seen by the negative correlation factor (r = -0.32). The highest concentration of V released was 0.59 Kg\t at a pH of 1.83 and there was a sharp decrease in the mobilization of V at around pH of 2. In general V was leached in low concentrations from all the leaching methods and no V was released from the 'off cavity' boreholes under peroxide leaching. In a UCG chamber the incoming water can be expected to poorly mobilize V into solution.

6.4.3.2 Zinc (Zn)

Zinc in coal is mainly found in sulphide minerals, particularly pyrite, but can also be organically bound in low-rank coals (Finkelman et al., 2018). The average recorded Zn abundance in the Majuba UCG geo-reactor was 48.7 ppm. The mobilization of Zn from peroxide and acid elution was similar with average concentrations of 0.0080 Kg\t and 0.0090 Kg\t respectively. Water elution released an order of magnitude less Zn with an average of 0.00017 Kg\t. The solubility of Zn is noticeably sensitive to pH as seen by the negative correlation factor of pH vs concentration (r = -0.37). In general, Zn was released in low concentration and can be expected to be poorly released by in incoming groundwater in the spent UCG geo-reactor.

6.4.3.3 Cobalt (Co)

Cobalt in coal is mainly found in sulphide minerals, clays and linnaeite group mineral (Finkelman et al., 2018). The average recorded Co abundance in the Majuba UCG geo-reactor was 48.7 ppm. The mean release of Co from acid elution was 0.032 Kg\t while for peroxide was an order of magnitude lower at 0.0015 Kg\t. Only three samples from the water elution had concentration detectable by the instrumentation and subsequently recorded the lowest average mobilization of 0.000044 Kg\t. The solubility of Co is noticeably sensitive to pH as seen by the negative correlation factor of pH vs concentration (r = -0.36). Just like in zinc and vanadium, Co is expected to be released in low concentration by the rebounding groundwater in the UCG chamber.

6.4.3.4 Chromium (Cr)

Occurrence of Cr in coal is associated with clays and spinel group minerals (Finkelman et al., 2018). The average recorded Cr abundance in the Majuba UCG geo-reactor was 154.9 ppm. Chromium was not detected from the water elution tests and from the peroxide elution only 4 samples out of 52 mobilized appreciable concentrations of Cr. The mean release of Cr from acid elution was 0.0084 Kg\t. The solubility of Cr is noticeably sensitive to pH as seen by the negative correlation factor of pH vs concentration (r = -0.21). At circumneutral pH, Cr (III) forms low solubility minerals (O'Connor et al., 2015), therefore Cr levels in the incoming groundwater are expected to stay low if the pH remain above acidic levels. Deutsch (1997) reported that divalent Cr can be expected to form low solubility minerals such as $Cr(OH)_3$ at pH above 5.5 which limits Cr concentration in solution.

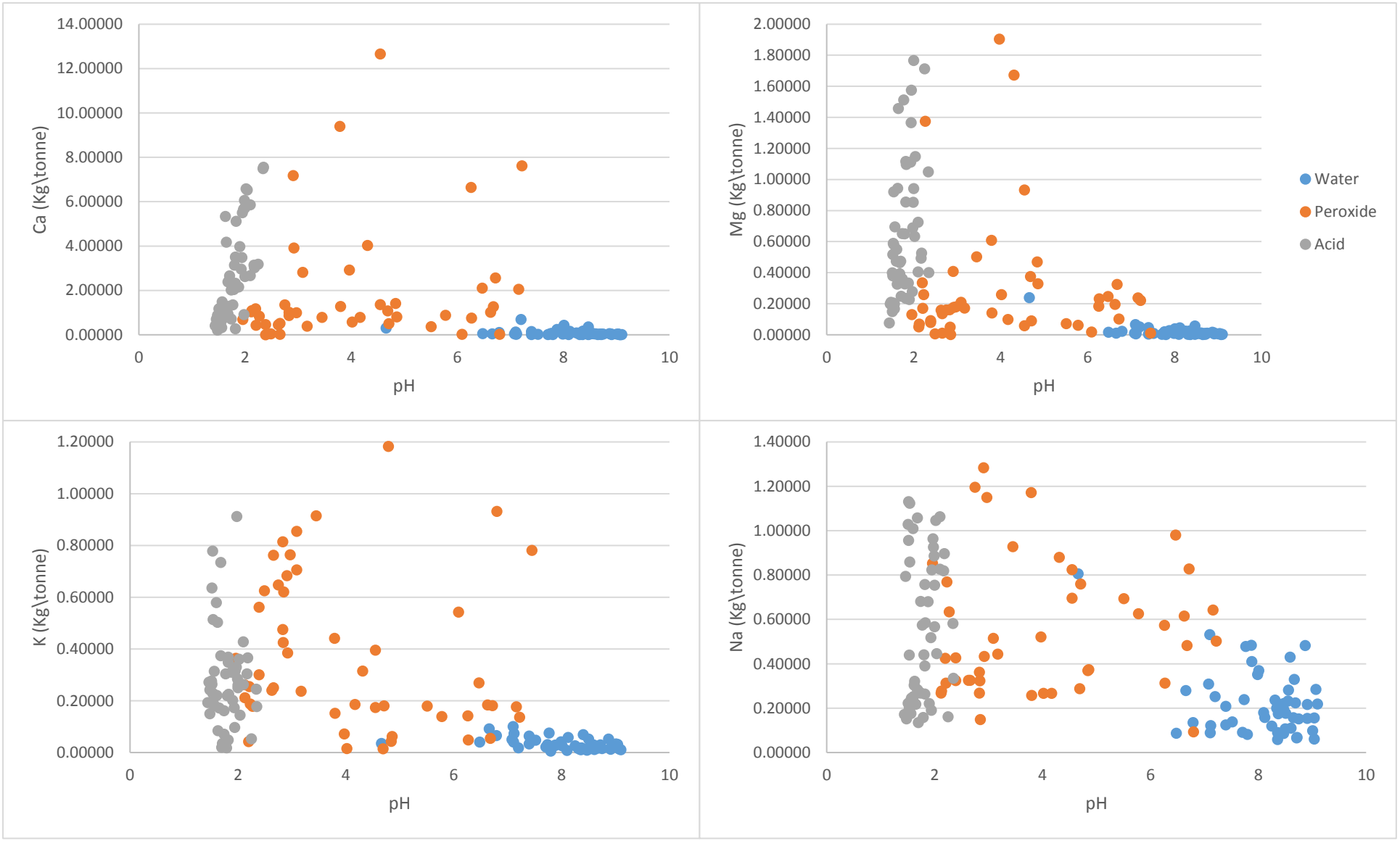

Figure 6-1 Mobilization of group I/II elements from the spent Majuba UCG geo-reactor via deionized water, hydrogen peroxide and sulphuric acid elution tests

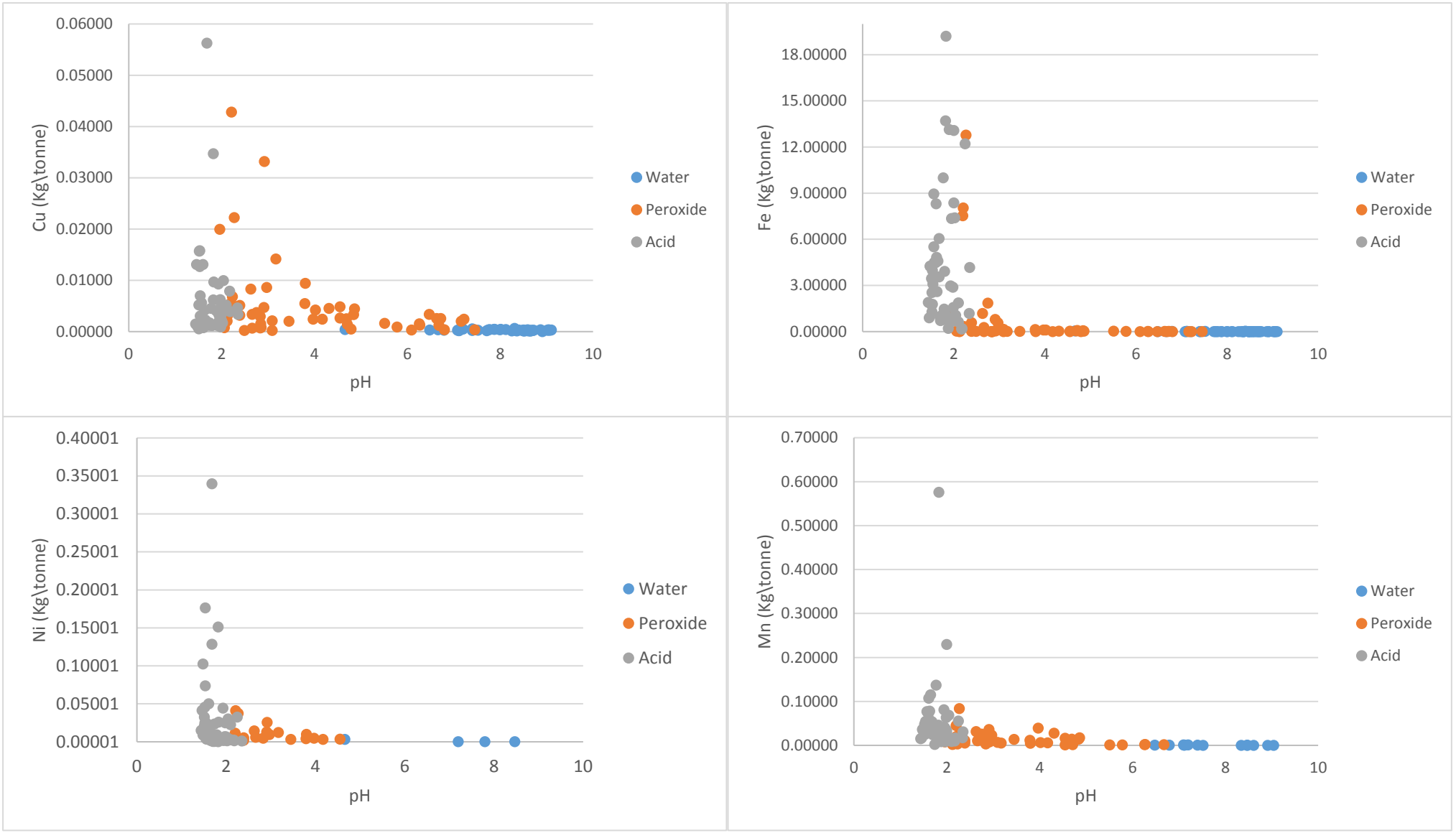

Figure 6-2 Mobilization of heavy metals from the spent Majuba UCG geo-reactor via deionized water, hydrogen peroxide and sulphuric acid elution tests

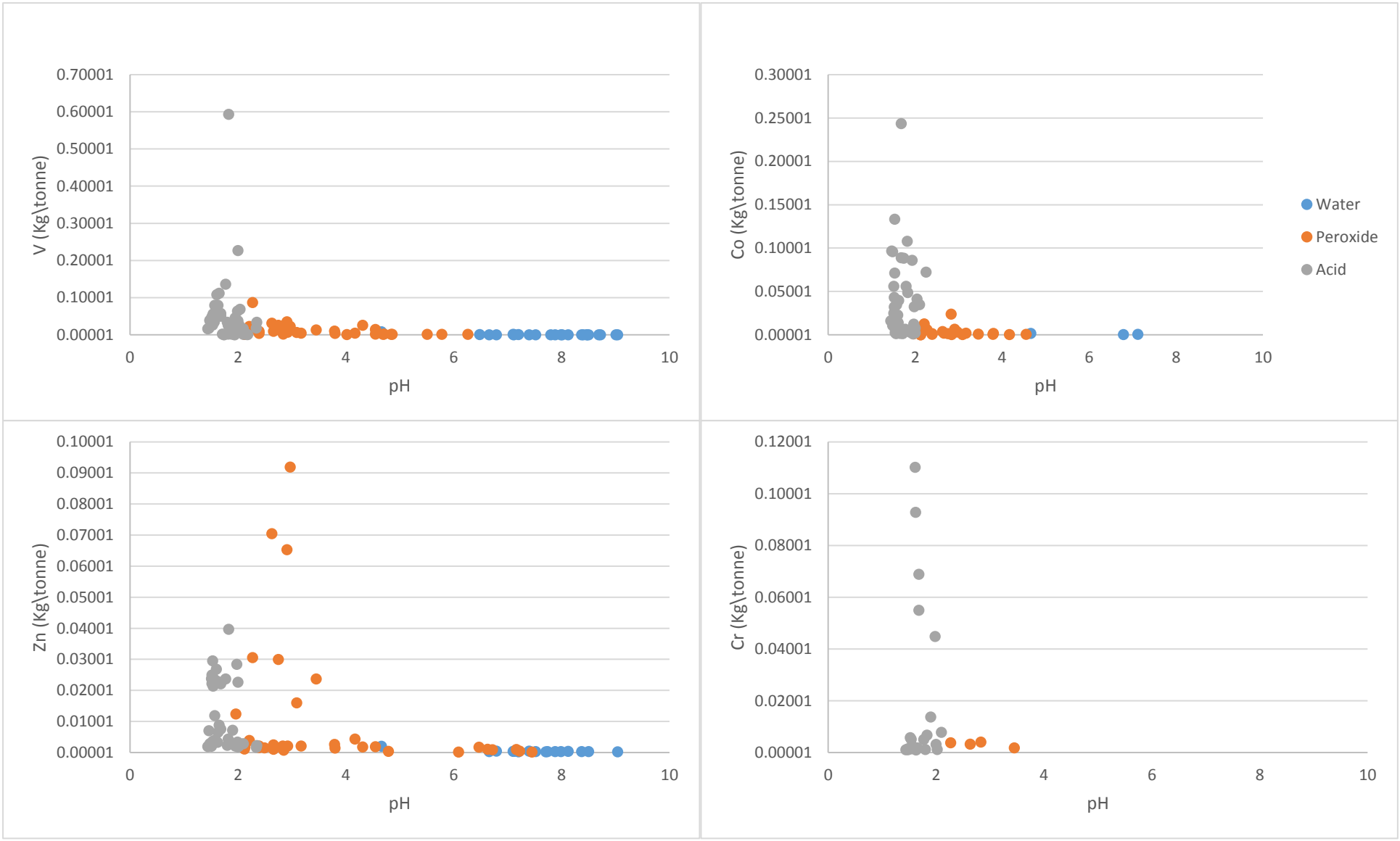

Figure 6-3 Mobilization of heavy metals from the spent Majuba UCG geo-reactor via deionized water, hydrogen peroxide and sulphuric acid elution tests

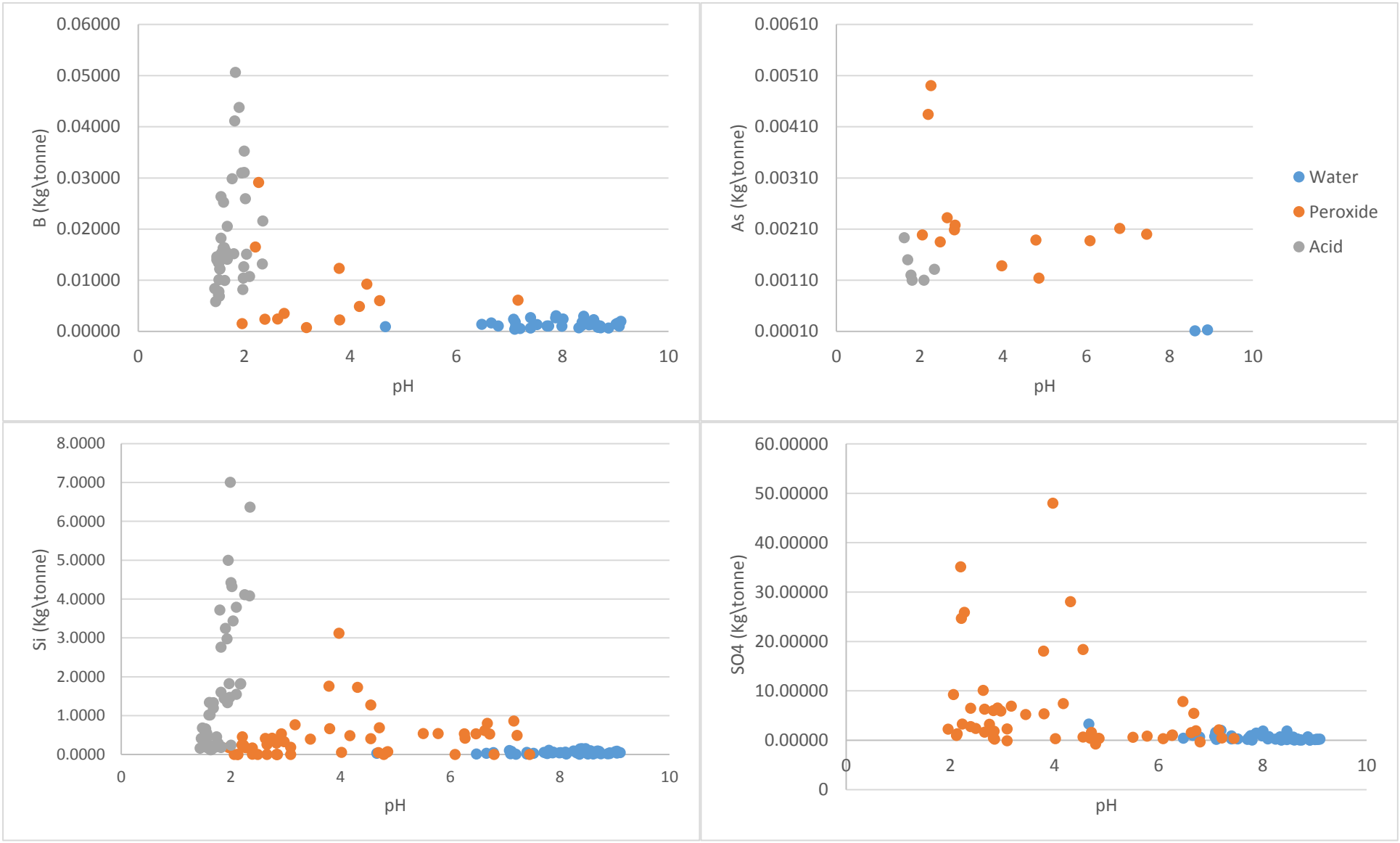

Figure 6-4 Mobilization of metaloids and non-metals from the spent Majuba UCG geo-reactor via deionized water, hydrogen peroxide and sulphuric acid elution tests

6.4.4 Metalloids and non-metals

The leaching behaviour of B, As, Si and SO_4 are displayed in Figure 6-4.

6.4.4.1 Boron (B)

Occurrence of B in coal is mostly related to the organic portion but can also occur in illite or in the exceedingly refractory tourmaline (Finkelman et al., 2018). The mobilization of B from water and peroxide elution was in the same order of magnitude with an average concentration of 0.0014 Kg\t and 0.0026 Kg\t respectively. The release of B from the acid elution was an order of magnitude higher with an average concentration of 0.018 Kg\t. There is an apparent pH-dependency in B release as determined by the negative correlation factor between pH and Fe concentration (r = -0.54), showing that as pH decreases more B is mobilized. Boron was poorly mobilized across all leaching mediums and will not be an element of environment concern in the spent UCG chamber.

6.4.4.2 Arsenic (As)

The XRF analysis parameters did not have As as part of the trace elements analysis therefore total rock As levels were not recorded. Coal combustion is one of the leading causes of As pollution in the environment (Wang et al., 2018). Arsenic occurs in coal mostly as arsenate, pyrite and organically bound As (Finkelman et al., 2018). Arsenic was poorly mobilized under water elution with only 2 samples out of 52 recording detectable concentrations of 0.00013 and 0.00011 Kg\t respectively. The mean release under peroxide and acid elution was 0.00058 and 0.00016 Kg\t respectively. Only one sample from the gasification zone recorded any detectable As concentration under peroxide elution and whilst almost all the samples from the "off cavity" sedimentary rocks released As into solution. Acid elution also showed the same leaching behaviour where As mobilization was predominantly from coal samples taken from "off cavity" coal seams and almost none from the residual char samples from the spent UCG geo-reactor. This was expected as As undergoes sublimation at 615 °C (Strugała-Wilczek and Stańczyk, 2016) and therefore UCG products are expected to be deficient in this environmentally toxic element. Since As volatilizes at temperatures below the UCG operating conditions and is therefore not expected to be an environmental risk in the spent geo-reactor. Wang et al. (2018) reported that 40 – 80% of the initial As in coal volatilizes at below 1150 °C.

6.4.4.3 Silicon (Si)

Silicon is one of the major elements in the earth's crust and 68.8 wt% was the recorded average of the Majuba UCG geo-reactor (Table 6-1). The average release of Si from acid elution was 1.6 Kg\t while for peroxide was an order of magnitude lower at 0.42 Kg\t. Water elution recorded the lowest average mobilization of 0.054 Kg\t. The release of Si is pH sensitive as seen by the negative correlation factor (r = -0.40), for pH versus Si concentration. Even though Si is found in high abundance in the rocks around the UCG chamber it is generally poorly mobilized. The "off cavity" samples did not yield any detectable Si concentration under peroxide elution however the same samples released Si under both water and acid elution.

6.4.4.4 Sulphates (SO_4)

Sulphur is one of the elements of great environmental concern in coal utilization. The main forms of sulphur in coal are pyritic, sulphate and organic (Liu et al., 2001). The average abundance of SO_3 in the Majuba UCG geo-reactor was 0.78 wt% (Table 6-1). The average release of SO_4 from water elution was 0.57 kg\t, while peroxide elution was an order of magnitude higher at 6.3 kg\t. The SO_4 concentrations under acid elution is not included in Figure 6-4 because sulphuric acid was the leaching medium in the test and hence the results for acid elution are not representative of the SO_4 released from the samples. The water soluble sulphates from the water elution test represent sulphide in oxidized form and this SO_4 does not contribute to acidity unlike the S^{2-} that contributes to acid producing reactions under oxidizing conditions. This reduced form of sulphur is oxidised and released into solution when leached with the oxidising agent, hydrogen peroxide, and hence contribute to acidity in solution. The average pH for all samples recorded from water and hydrogen elution tests was 8.09 and 4.04 respectively, which indicate that the samples had acid producing minerals that contributed to reduction in pH. The implication of S will be dealt with in detail under the acid generation section below.

6.4.5 General discussion

Group I/II elements are found in major to minor quantities in the spent Majuba UCG geo-reactor. These elements show a pH-dependent solubility as seen by the negative correlation factor for each element. The water elution tests (no pH buffer), generally released the lowest concentrations of these cations into solution and had an alkaline final pH in most cases. The water elution results were in the main, one or several orders of magnitude lower than the other elution tests results. Although deionized water is not representative of the site groundwater chemistry, it provides a good base for understanding the leaching dynamics in a spent UCG geo-reactor as it does not impose pH conditions on the samples. Acid elution generally mobilized more elements into solution however there were exceptions like in the case of potassium where the highest mean release was under peroxide elution. The same leaching behaviour was also recorded for barium (Appendix 6-A), where the peroxide elution results were two orders of magnitude more than acid and water elution results. Deutsch (1997) reported that simple sulphate salts such as barite ($BaSO_4$) do not form strong complexes with hydrogen and hydroxyl species at normal groundwater pH levels and therefore the pH does not significantly affect their solubility.

Hydrogen peroxide elution represent rock-water interactions that can be expected if a highly oxidizing environment prevails in the spent geo-reactor. Oxidants are injected directly into the gasification zone during the UCG process and post gasification the oxygenated water can be injected from the surface for assisted quenching. At the Majuba UCG pilot plant, surface water from a river (Witbankspruit) was injected into the spent geo-reactor to assist with quenching at the rate of 333 m^3/d for over 3 months. The pH of the final solution is influenced by the oxidation of sulphide minerals which then induces acidity in solution. This leads to more elements dissolving due to the pH solubility dependency that elements undergo. The data from the peroxide elution was in the main the most varied as seen by the high standard deviations recorded by this leaching method. It is therefore expected that under oxidizing conditions, the UCG chamber can have some areas of high and some areas of low release for group I/II elements. For example, the highest calcium mobilization was recorded in char samples as compared to other areas in the gasification zone. This can be from the presence of calcite cleats that are known to transverse coal seams (Busse et al., 2017). Under peroxide elution, sodium was not

released from “off cavity” samples while it was readily released from boreholes drilled within the gasification zone. It is possible that the UCG process has geochemically altered some of the minerals to a degree that some of the elements have become susceptible to mobilization under oxidizing conditions. Similar behaviour was seen for barium and to a lesser extent in Strontium. There was also poor Lithium (Li) mobilization from “off cavity” samples under all the leaching tests, however, Li was released from samples taken from the roof section next to the gasification zone but samples taken further away from the geo-reactor in the roof did not show any Li mobilization. These samples may have been less affected by the heat from the gasification zone. In summary, poor mobilization of group I/II elements can be expected by the rebounding groundwater in a spent UCG reactor. However if there is a prevailing oxidizing environment, some of the elements can be released at marginally higher levels. The acid elution represents the “worst case scenario” and on average most of the elements are released at significant levels under these conditions. It is therefore recommended that any spent UCG geo-reactor must be periodically monitored to ensure that the pH does not drop below 4. Beyond this pH, chamber rehabilitation must be considered to avoid detrimental groundwater contamination.

Metals were found in minor to trace amounts in the spent Majuba UCG geo-reactor. These elements also show a pH-dependent solubility as seen by the negative correlation factors (pH vs concentration). The water elution tests released the lowest concentrations of these metals and in some cases had below detection limit quantities. The following elements recorded below detection limit concentrations for all 52 samples under water elution test: Cd, Cr, Sb, Se, Sn and Pb. Only 4 samples out of 52 under water elution test recorded nickel at detectable levels while chromium and arsenic only had 3 and 2 samples at detectable levels respectively. The general trend from the results show the acid elution data as the most dispersed as compared to the other leaching tests and hence recorded the highest standard deviation. The following elements recorded below detection limit concentrations for all 52 samples under peroxide elution test: Cd, Se and Sn. Furthermore the “off cavity” samples recorded below detection limit for the following elements under peroxide elution: Cr, Co, Mn, Si, Li, Na, Mo, Ni and V. It is possible that the high temperatures and the resultant mineralogical alterations are responsible for amplified release of these elements in sites at close proximity to the geo-reactor. Whilst peroxide elution generally leached more metals into solution as compared to water elution the quantities leached were still low for samples with a final pH of above 4 due to the pH dependency of mobilization. More sulphates were dissolved under the oxidizing conditions as compared to the water soluble sulphates released in water elution test. This indicates that the samples had reduced forms of sulphur (S^{2-}) which contribute to acidity under oxidizing conditions. The average final pH from the water elution was much higher with the average value of the peroxide elution at 8.09 as compared to the peroxide leaching which was at an average of 4.04. The average pH from the acid elution was 1.79 which represents the “worst case scenario” that the geo-reactor can be subjected to and was used to observe the leaching behaviour if acidic conditions developed in the UCG cavity. On average most of the elements were released at significant levels under these acidic conditions. The results show that a decrease in pH will lead to more release of potentially toxic elements into groundwater in the UCG cavity, therefore pH monitoring should form an integral part of the hydro-chemical analysis post gasification to avoid decreasing in pH (especially below 4). Below this pH, chamber rehabilitation must be considered to avoid detrimental groundwater contamination. However the following elements still recorded below detection limit concentrations for all 52 samples under acid elution test: Sb, Se and Sn, which indicate that the solubility of some elements was either not affected by pH or simply that these elements were not present in the samples.

6.5 Mine water leaching

The mine water elution results are displayed in Figure 6-5 to Figure 6-7. The chemistry data is presented in Appendix 6-B. The water chemistry of the mine water is also included in Appendix 6-B

6.5.1 Group I/II elements

6.5.1.1 Calcium

The concentration of Ca in the original mine water was 67.3 mg\L. The temperature effect provided a mixture of observations as ash, floor and roof samples had a reduction in concentration when the experimental temperature was increased from 25 to 70 °C, whereas char recorded a small increase in concentration. The mine water elution tests generally resulted in concentrations lower than the original mine water concentration except for the ash sample at 25 °C which recorded the highest concentration of 68.1 ml\L. The average Ca concentration released from the spent geo-reactor was 45.5 mg\L which was still 32% lower than the original mine water concentration. The results show that the overall interface between mine water and the spent geo-reactor will lead to the solution decreasing in Ca concentration. This decrease can be attributed to precipitation between the mine water and clay minerals in the rocks of the geo-reactor. Deutsch (1997) simulated Ca behaviour in groundwater using geochemical models which showed that as temperature increases there is a decreased Ca concentration from solution due to precipitation. Higher leachate temperatures decrease the concentration of Ca in solution because of the low solubility of gypsum at higher temperatures (Ahern and Frazier, 1982) (see also equation [6.8] in section 6.4.1.1).

6.5.1.2 Magnesium

The concentration of Mg in the mine water was 9.5 mg\L. The floor samples recorded the highest release of Mg with 16.9 mg\L and 12.0 mg\L for elution at 25 and 70 °C respectively. There was a general trend of reduction in Mg concentration as experimental temperature increased across all sections of the geo-reactor. The average Mg mobilized from all sections of the geo-reactor was 10.8% lower than the concentration in the original mine water. The results show that the carbonaceous shale floor of the UCG chamber releases relatively more Mg ions into solution however general mine water interactions with other areas of the geo-reactor will result in a decrease concentration in solution regardless of temperature up to 70 °C.

6.5.1.3 Potassium

The concentration of K in the mine water was 91.7 mg\L. The results show small concentrations increases as the experimental temperature increased for all samples except for the ash samples where a marginal decrease was recorded. All samples recorded a final K concentration that is below the original mine water concentration except for one roof sample (S7 at 70 °C), which was at 107.7 mg\L. The results show that higher temperature generally released more K into solution, however the average K concentration released from all the samples was 77 mg\L, which was still 16% lower than the original mine water concentration. The two char samples produced the lowest K concentrations as compared to the other sections of the geo-reactor and this could be due to complexation with organic compounds in the solid phase of the char. (Deutsch, 1997) suggested that strong competition for organic ligands by major cations (such as K) can limit organic complexation of trace metals.

Potassium is not expected to be an element of environmental concern in the spent geo-reactor as interaction with mine water generally leads to concentration decrease and temperature difference shows negligible impact.

6.5.1.4 Barium

The concentration of Ba in the mine water was 0.05 mg\L. Char and one roof sample (S7) recorded an increase in concentration as the experimental temperature increased whilst the rest of the samples showed a decrease in concentration at higher experimental temperatures. All samples released more Ba into solution than was originally in the mine water regardless of temperature which translated into a 63% increase in the average Ba concentration. Barium had the highest average abundance of all the trace elements as shown in Table 6-2, and the leaching behaviour shows that these Ba ions are readily released into solution regardless of temperature. Interaction with incoming groundwater will therefore mobilize Ba into solution from all sections of the geo-reactor. Deutsch (1997) reported that barite (BaSO4) precipitation can limit Ba concentration due to the presence of sulphate in solution.

6.5.2 Metals

6.5.2.1 Nickel

The concentration of Ni in the mine water was 0.34 mg\L. The results show small concentrations decreases as the experimental temperature increased for all samples except for the ash samples where a marginal increase was observed. Increased concentrations of Ni relative to the background concentration of the mine water was recorded in all samples released. The average mobilization from all samples was 31.5% higher than the concentration in the original mine water. This was expected as Ni goes into gaseous phase at temperatures above the UCG operating conditions and hence its occurrence in all sections of the spent geo-reactor was expected. The rebounding groundwater in the UCG chamber is expected to leach higher concentrations of Ni into solution even though the pH of the mine water was just above 8, however, Ni showed poor mobilization under alkaline condition and displayed pH-dependent leaching in section 6.4.2.3. The temperature effect shows that as the geo-reactors cool down, slightly more Ni ions will go into solution.

6.5.2.2 Copper

The concentration of Cu in the mine water was 0.018 mg\L. The results show a trend of increase in concentration as the experimental temperature increases except for one roof sample (S7) which recorded slight decrease. The average Cu mobilized from all samples was 78% higher than the concentration in the original mine water but in spite of this, Cu was generally released in low concentrations as 0.032 mg\L was the highest recorded concentration. The rebounding groundwater in the UCG chamber is not expected to leach significant amounts of Cu as the pH of the mine water is around 8 and Cu showed a pH dependent leaching in section 6.4.2.1. Strugała-Wilczek and Stańczyk (2015) suggested that since Cu has a relatively high boiling point, it is unlikely to transition into the gaseous phase during gasification but rather remains in the solid phase where it remains immobile due to incorporation into a water-insoluble compound.

6.5.2.3 Manganese

The concentration of Mn in the mine water was 0.323 mg\L. The results show a trend of decrease in concentration as the experimental temperature increases. The average mobilization from all samples was 0.122 mg\L, which was 62% lower than the concentration in the original mine water. Decrease in concentration of Mn as compared to the concentration in the leaching medium can be as a result of Mn oxidation reactions and precipitation as oxides (Strugała-Wilczek and Stańczyk, 2016). Under oxidizing conditions and at pH above 5.5 a divalent Mn forms relatively insoluble minerals such as MnO_2 which limit Mn concentration in solution (Deutsch, 1997). The results show that the overall interaction between mine water and the spent geo-reactor will lead to a decrease Mn concentration in solution.

6.5.2.4 Iron

The concentration of Fe in the mine water was 1.5 mg\L. The results show a trend of decrease in concentration as the experimental temperature increases. Increased concentration of Fe relative to background concentration of the mine water was recorded for ash sample at 25 °C of 1.87 mg\L however the average mobilization from all samples was 0.028 mg\L, which was 82% lower than the concentration in the original mine water. This decrease in concentration is as a result of Fe undergoing oxidation and subsequently precipitating as iron oxide (Strugała-Wilczek and Stańczyk, 2016). Just like Mg, Fe is redox sensitive and forms relatively insoluble minerals such as $Fe(OH)_3$) under oxidizing condition and at pH values above 5.5 (Deutsch, 1997). The results show that the overall interaction between mine water and the spent geo-reactor will lead to a decrease the Fe concentration.

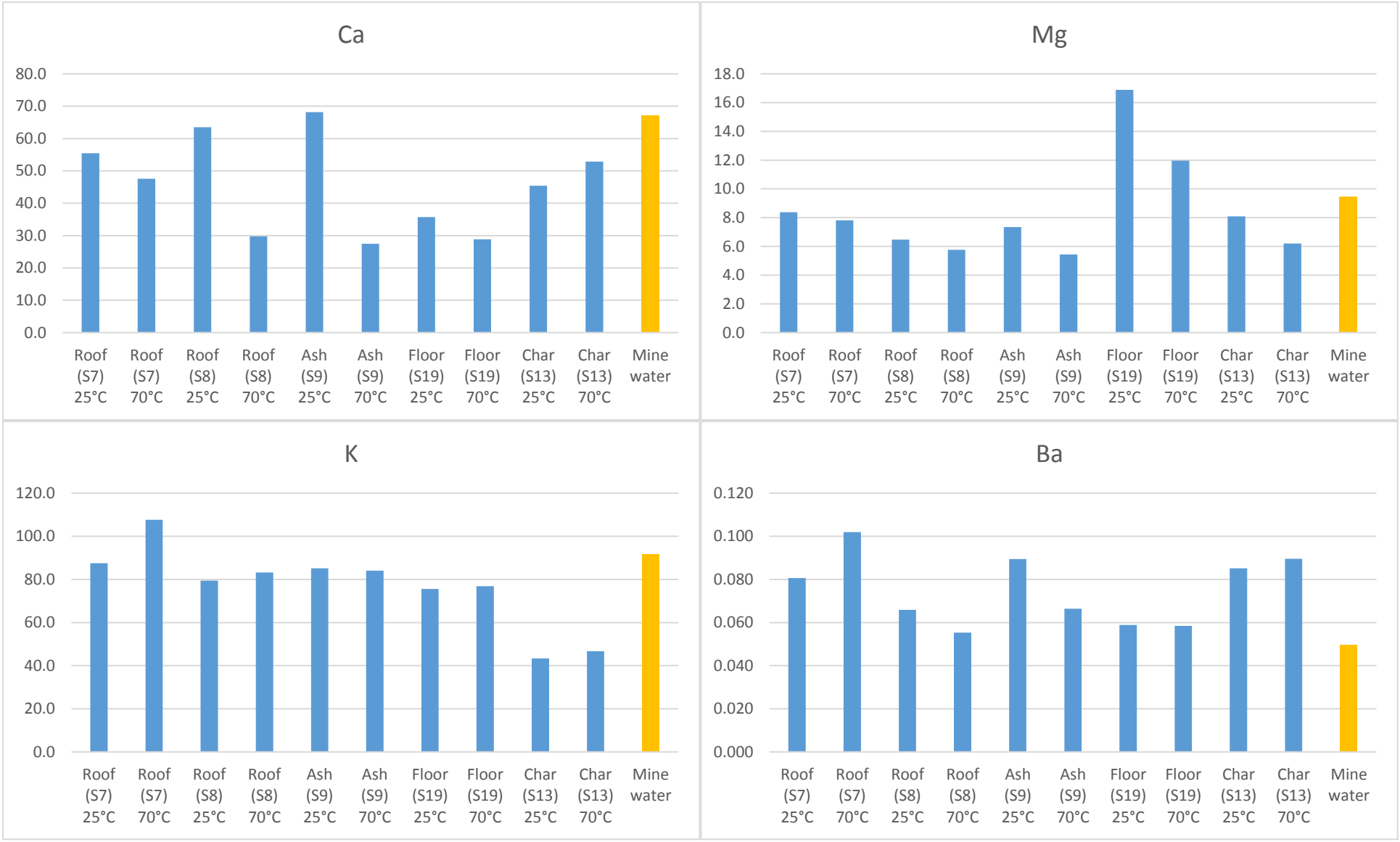

Figure 6-5 Mine water elution results for calcium, potassium, barium and magnesium (in mg\L)

Figure 6-6 Mine water elution results for nickel, copper, manganese and iron (in mg\L)

Figure 6-7 Mine water elution results for calcium, potassium, boron and magnesium (in mg\L)

6.6.1 Metalloids and non-metals

6.6.1.1 Aluminium

The concentration of Al in the mine water was below detection limit of 0.021 mg\L. The char and floor samples recorded a decrease in concentration as the experimental temperature increased whilst the rest of the samples displayed an increase in concentration. Although Al was below detection limit in the original mine water, the solvent was still an effective leaching medium as it mobilized Al in all the samples albeit in small proportions, as the average mobilization was 0.11 mg\L. Deutsch (1997) demonstrated that Al is limited in solution by the presence of minerals like kaolinite which favour dissolution of silica rather than Al thereby increasing silica concentration in solution and precipitating Al in secondary minerals. The incoming groundwater in the spent UCG geo-reactor can be expected to mobilize Al ions into solution but in small concentrations (i.e. < 0.5 mg\L).

6.6.1.2 Arsenic

The concentration of As in the mine water was below detection limit of 0.021 mg\L. Only three samples recorded detectable As concentration, one of which is the roof sample (S8) which also mobilized As under acid elution. The highest mobilization was from ash at 25 °C with a concentration of 0.035 mg\L but generally As was poorly leached. Deutsch (1997) suggested that As can be expected to be present in low concentration in polluted areas as it is affected by adsorption/desorption processes in that the anionic form of As dominate in groundwater where it is easily adsorbed by anion adsorbers such as ferrihydrite or exchanged in clay minerals. In the spent UCG geo-reactor arsenic is not expected to pose any significant environmental risk as the gasification zone is expected to be deficient is arsenic as it sublimes in at around 615 °C and it showed poor leaching behaviour.

6.6.1.3 Boron

The concentration of B in the mine water was 8.5 mg\L. The results show a trend of increase in concentration as the experimental temperature increases. All samples released B at higher concentration than in the original mine water with the average concentration recorded as 14.8 mg\L which then translates into an average increase of 57%. Boron has a boiling point of 3927 °C (Strugała-Wilczek and Stańczyk, 2015) and was therefore expected to be present in UCG residue products. The incoming groundwater in the spent UCG chamber can be expected to mobilize B ions into solution from all sections of the geo-reactor.

6.6.1.4 Sulphate

The concentration of SO_4 in the mine water was 980 mg\L. The results show a trend of increase in concentration as the experimental temperature increases. The mobilization SO_4 ions from all the samples were at lower concentration than the original mine water. The average concentration recorded from all samples was as 317.8 mg\L which is 68% less than the concentration in the original mine water. The decrease in overall SO_4 concentration can be explained by the possible formation of

gypsum as Ca also experienced a general decline of 32 % (see equation [6.8]). The results show that the overall interaction between mine water and the spent geo-reactor will lead to the solution decreasing in SO_4 concentration.

6.6.2 General discussion

The following elements showed general decrease in concentration with increase in temperature (some had at least one sample area behaving contrary): Mn, Fe, Ni, Sr, Ca, Mg, V and SO_4. Manganese recorded a decrease in concentration with increasing experimental temperature across all sections of the geo-reactor. Vanadium also showed the same leaching behaviour (Appendix 6-B). Sr had the similar behaviour except for char samples. The dissolved concentrations of the major elements in silicate rocks are usually restricted in groundwater by the formation of secondary minerals of low solubility (Deutsch, 1997). The following elements showed a general increase in concentration with increase in temperature (some had at least one sample area behaving contrary): B, K, Cu, and SO_4. The following elements showed a mixture of responses whereby two or more samples showed an increase in concentration with increase in experimental temperature and vice versa: Al and Ba. The equilibrium constant for all minerals are temperature dependent (Deutsch, 1997). The following elements had below detection limit concentration after elution with mine water from all sampled parts of the geo-reactor: Cr, Cd, Zn and U.

The mineralogical composition of leached samples is important in understanding the solubility behaviour of elements. Some mineral portions form complexes with other dissolved species in solution with the result that the effective dissolved concentrations of those components are reduced in solution and therefore need more of the mineral do dissolve to attain equilibrium concentration levels (Deutsch, 1997). Calcium, Mg, K, Mn, Fe and SO_4 all recorded a reduction in concentration in the eluate after the mine water elution. These elements are contained in the various carbonate, silicate, and sulphate phases contained in the samples. The divalent (Ca^{2+}, Mg^{2+}, SO^{2-}_4, CO^{2-}_3) and trivalent (Fe^{3+}, Al^{3+}, PO^{3-}_4) form sufficiently strong complexes with each other and hence their existence in solution can increase the solubility of minerals containing there components (Deutsch, 1997).

6.7 Metal mobility

The result of contaminant migration due to dissociation of a contaminant between groundwater and the surface of the solid in an aquifer can be demonstrated by the distribution coefficient (Deutsch, 1997). The distribution coefficient (K_d) is the ratio of the amount of contaminant adsorbed on the surface of the solid phase to the dissolved concentration of the contaminant. The metal mobility was estimated on the basis of the distribution coefficient K_d and calculated according to the following equation (Strugała-Wilczek and Stańczyk, 2016):

$$K_d = \frac{Ci,s}{Ci,r}$$

Where

Ci,s – the content of substance in the solid phase [mg\kg]

Ci,r - the concentration of the substance in solution [mg\l]

Higher distribution coefficient indicate low relative mobility of the dissolved element, while lower values indicate high relative mobility. The elements can be divided into three groups after logarithmization (Strugała-Wilczek and Stańczyk, 2016):

- Group I - poorly mobile elements where a small quantity is mobilized, $\log_{10}(k_d) > 4$
- Group II - moderately mobile elements, $3 < \log_{10}(k_d) < 4$
- Group III – mobile elements with great affinity for release into solution $\log_{10}(k_d) < 3$.

The relative affinity of elements to leach into the water phase after the calculated distribution coefficients are presented in Appendix 6-C and displayed in Figure 6-8. The metals have been divided into three groups:

- Group I – poorly mobile metals: Fe, Al and Ba
- Group II – moderately mobile metals: Ba, Ni, Cu, Mn, V
- Group III – metal with great affinity to leach into water phase: Sr, V, Co, Mn, Cu, Ba, Pb

The borderline cases (i.e. K_d = 3 or 4) occupy the intersection areas in Figure 6-8. The heat affected roof released the most metals into solution at 25 °C. These metals mostly belong to group III (mobile elements). The highest number of metals mobilized into solution at 70 °C were from the roof and char samples.

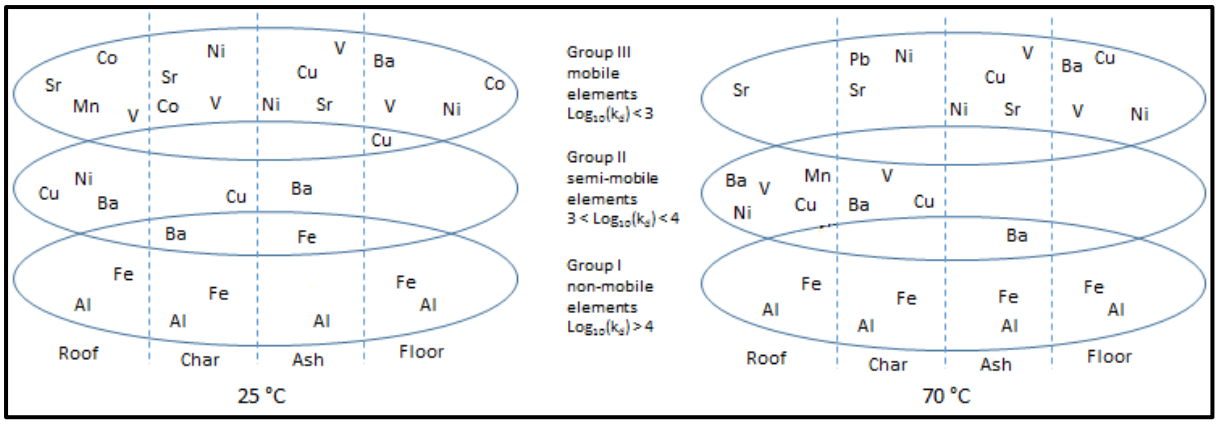

Figure 6-8 Distribution of the elements into solution after mine water elution

Aluminium and Fe were the main non-mobile elements across all sections of the geo-reactor and their relative mobility was not affected by change in experimental temperature. The two elements form part of many mineral assemblages including silicates and sulphides minerals. Whilst these group I elements had a higher distribution coefficient (K_d) as compared to the other metals, their average release was relatively similar to the other metals. For example, Ni was released at an average concentration of 0.11 mg\L across all the sampled areas and Al was also released at the same average concentration of 0.11 mg\L. The K_d value is partly dependent on the abundance of the element in the solid phase and since Al was several orders of magnitude higher than Ni in the solid phase, the K_d value is thus different even though the average release concentration is the same. Group I elements affinity to remain in the solid phase during interaction with mine water renders them environmentally neutral in terms of groundwater contamination. Barium was also classified in group I for char (25 °C) and ash (70 °C) samples.

The roof section of the geo-reactor had four mobile metals (group I) at 25 °C and just one metal at 70 °C. The semi mobile elements (group II) had the same metals (Cu, Ni, Ba) appearing under both experimental temperatures however at 70 °C two more metals (V and Mn) emerged for the roof section. The results show that if the geo-reactor temperature remains around 70 °C, there will be less of the highly mobile metals (group III) whereas at background temperatures of 25 °C more group I metals will emerge. The semi mobile metals from the roof section show the opposite leaching behaviour where at higher experimental temperatures more metals were encountered than at lower temperatures.

Char samples at 25 °C had only Cu as the semi mobile metal with Ba borderline between group I and group II. There were four group III metals (V, Co, Sr, Ni) at 25 °C while only 3 (Pb, Sr, Ni) at 70 °C. Noticeably, Pb appeared only for this char section as it was below detection limit in all other experimental conditions. The relative mobility of metals from char samples is similar to the roof section in that more metals with a higher capacity for elution to an aqueous phase (group III) are observed under lower experimental temperatures whilst the moderately mobile metals emerge more at higher temperatures. The higher elution ability of Pb from char samples at higher temperatures is an environmental concern as generally this element was not mobilized from other sections of the geo-reactor from both deionized water and mine water eluates, which indicates that temperature plays a role in dissolving this element from the organic surfaces. Strugała-Wilczek and Stańczyk (2015) suggested that the presence of Pb in UCG waste products despite having a low boiling point shows that the metal is subject to only partial sublimation. There is also a possibility that condensation of the syn gas in the colder parts of the UCG chamber deposited Pb on char surfaces.

The ash samples have the same group I (Cu, Sr, Ni, V) and group II (Ba) metals under both experimental temperatures. Iron is borderline between group II and group I under 25 °C. The floor also have the same group I elements (Ba, V, Ni, Cu) at both experimental temperature with Cu borderline with group II and Co emerging at the 25 °C conditions. The leaching behaviour of the floor and ash is therefore expected to remain the same even as the temperature drops in the spent geo-reactor.

6.8 Acid generation potential

The data analysed for potential acid generation was taken from 52 sampling points which included the char, ash, roof and floor of the spent UCG geo-reactor. The results of the acid base accounting are presented in Table 6-3. The initial pH column represent the final pH after elution with deionized water. The final pH column records the final pH after elution with hydrogen peroxide where reactive species are oxidised. The neutralising potential (NP) is recorded as base which represents the back titration using NaOH. The NNP (net neutralising potential) was calculated for both a closed and an open system using the respective acid producing (AP) values. This analysis utilized both the acid base accounting (ABA) and net acid generation (NAG) methods of predicting acid generation. All values with a final pH of below 3.5 are classified as high risk acid generating under NAG and have been highlighted in red. The range 3.5 to 5.5 is classified as low risk acid generation and is highlighted in orange. All samples with a final pH above 5.5 are classified as non-acid generating. All values with a final NNP below -20 kg/t $CaCO_3$ are classified as acid generating under ABA and have been highlighted in red. The values with a final NNP above 20 kg/t $CaCO_3$ are classified as non-acid generating and have been highlighted in green. The uncertain region is between -20 to +20 kg/t $CaCO_3$ and samples in this region may require further investigation to determine their acid potential.

Prediction of acid generation based on both NAG and NNP provides a more consistent screening practice than either test conducted alone which increases the confidence in the acid potential classification and detecting of deceptive contradictory data that requires further investigation (Stewart et al., 2006). For example, some of the data that would have been classified in the uncertain region under NNP, is actually clearly defined as high risk acid generating under NAG with the final pH below 3.5. Using both NAG and NNP can therefore help avoid performing kinetic tests which require large samples (>1kg) and take a long time (months) to conduct. Kinetic tests also provide leaching rates and show lag times to acid formation. For example, the roof section of borehole G1VH3 (S1 – S8) recorded NNP values that lie in the uncertain region except for S6 which was classified as acid generating, but the same samples were clearly classified as high risk acid generating under NAG with the final pH below 3.5 after oxidation.

The UCG chamber lies around 280 meters below surface and is therefore taken as a closed system flooded with mine water and as such for NNP the focus will be on NNP closed system. Only 7 out of 53 samples were clearly acid generating (13.2%) while only 4 (7.5%) were classified as non-acid generating. The uncertain region constitutes 80%. Research and experience has revealed that samples between -20 to +20 kg/t $CaCO_3$ can develop acidity or stay neutral, however when NNP is used together with other methods this uncertainty can be eliminated (Usher et al., 2003). A more stringent classification provides the following:

- NNP = NP - AP < 0, the sample has the potential to generate acid. Then 55% of samples qualify.
- NNP = NP-AP > 0, the sample has the potential to neutralise acid produced. Then 46% qualify.

Application of NAG classified 26 samples (49%) as high acid generating while only 13 (24.5%) was categorized as non-acid generating. The low risk acid generation constitutes 26.9% of the samples.

Table 6-3 Acid base accounting cells for each sample area (kg/t $CaCO_3$ where applicable)

Sample ID	Initial pH	Final pH	Acid (Open)	Acid (Closed)	Base	NNP (Open)	NNP (Closed)
S1	8.50	2.39	6.78	13.56	0.62	-6.17	-12.95
S2	9.01	2.84	1.92	3.84	2.33	0.4	-1.52
S3	8.71	2.12	1.04	2.08	-0.48	-1.52	-2.56
S4	8.72	2.39	2.90	5.79	1.55	-1.34	-4.24
S5	8.36	2.13	1.40	2.80	-0.58	-1.98	-3.38
S6	6.48	2.21	25.70	51.41	-1.19	-26.89	-52.6
S7	7.40	3.17	7.22	14.45	7.71	0.49	-6.74
S8	9.04	3.8	5.59	11.17	21.55	15.96	10.38
S9	8.98	4.47	31.61	63.22	3.48	-28.13	-59.74
S10	8.67	6.72	2.00	4.00	12.36	10.35	8.35
S11	8.55	6.63	1.61	3.22	23.42	21.81	20.2
S12	8.59	6.47	8.19	16.39	30.66	22.46	14.27
S13	7.88	4.31	29.23	58.46	37.63	8.4	-20.84
S14	8.01	4.55	19.15	38.29	27.71	8.56	-10.59
S16	7.87	3.79	18.83	37.65	18.39	-0.44	-19.26
S17	8.37	7.22	0.49	0.98	26.77	26.28	25.79
S18	8.56	7.16	2.19	4.38	24.85	22.66	20.48
S19	7.71	3.09	2.39	4.77	-1.58	-3.96	-6.35
42-H	7.52	2.63	10.54	21.08	2.58	-7.96	-18.5
43-A	9.04	2.75	3.36	6.72	2.36	-1	-4.37
43-B	9.10	1.96	2.36	4.73	0.78	-1.59	-3.95
43-C	7.20	2.27	27.01	54.02	12.07	-14.95	-41.96
43-C1	7.99	2.91	6.83	13.67	0.39	-6.44	-13.28
43-C2	7.74	2.97	6.16	12.32	0.42	-5.74	-11.9
43-E	8.40	4.17	7.75	15.51	13.15	5.39	-2.36
43-F	6.66	2.92	6.55	13.10	-0.54	-7.09	-13.64
43-G	7.11	2.66	6.59	13.17	2.00	-4.58	-11.17
Up Roof #3	7.12	2.83	6.29	12.58	1.52	-4.77	-11.06
Roof #2	7.08	3.45	5.45	10.90	-4.22	-9.67	-15.12
Floor #5	6.79	2.83	0.51	1.02	5.00	4.49	3.98
Bottom #1	8.65	2.85	0.23	0.47	2.26	2.03	1.79
T1	8.12	6.8	-0.33	-0.67	14.97	15.3	15.63
T2	7.10	4.79	-0.76	-1.53	10.45	11.22	11.98
T3	7.40	3.09	-0.11	-0.21	4.62	4.72	4.83
T4	8.87	7.45	0.40	0.80	142.51	142.11	141.7
T5	9.07	2.66	1.74	3.49	2.84	1.1	-0.65
T6	8.31	2.49	2.51	5.02	1.52	-0.99	-3.5
T7	7.77	6.09	0.36	0.72	19.42	19.06	18.7
T9	4.66	2.06	9.64	19.27	-5.29	-14.92	-24.56
5.2	8.91	2.23	3.46	6.91	4.84	1.39	-2.07
12.8	8.25	6.27	1.13	2.26	5.51	4.38	3.25
5.3	8.36	4.69	0.46	0.91	11.07	10.61	10.15
6.2	8.75	4.84	0.38	0.76	17.81	17.43	17.05
12.6	8.34	6.68	5.68	11.35	21.91	16.24	10.56
12.5	7.80	4.55	0.68	1.36	1.58	0.9	0.22
12.4	8.47	5.51	0.66	1.32	9.54	8.88	8.22
12.2	8.10	4.71	1.69	3.39	7.10	5.41	3.71
6.3	8.61	4.02	0.33	0.66	12.35	12.02	11.69
6.1	8.91	4.86	0.38	0.75	14.58	14.2	13.83
5.1	8.51	2.2	36.56	73.13	14.44	-22.13	-58.69
12.7	8.47	3.97	50.01	100.03	36.25	-13.76	-63.78
12.1	8.69	6.26	1.06	2.11	18.30	17.24	16.18
12.3	8.47	5.78	0.88	1.75	9.43	8.56	7.68

The initial and final pH versus NNP (net neutralising potential) is presented in Figure 6-9. The initial pH values were recorded after elution with deionized water and this pH is influenced by water soluble sulphates from inactive species (e.g. gypsum), which do not contribute to acidity as they already exist in oxidized form and hence the majority (98%) recorded above 5.5 pH values, classifying them as non-acid producers. The final pH values were recorded after elution with hydrogen peroxide where reduced sulphur species underwent oxidation and became soluble adding to the acidity of the solution and hence the majority (75%) recorded below 5.5 pH values rendering them acid generators. The NNP values were adjusted to account for the non-acid producing sulphur species determined from the deionized water elution test.

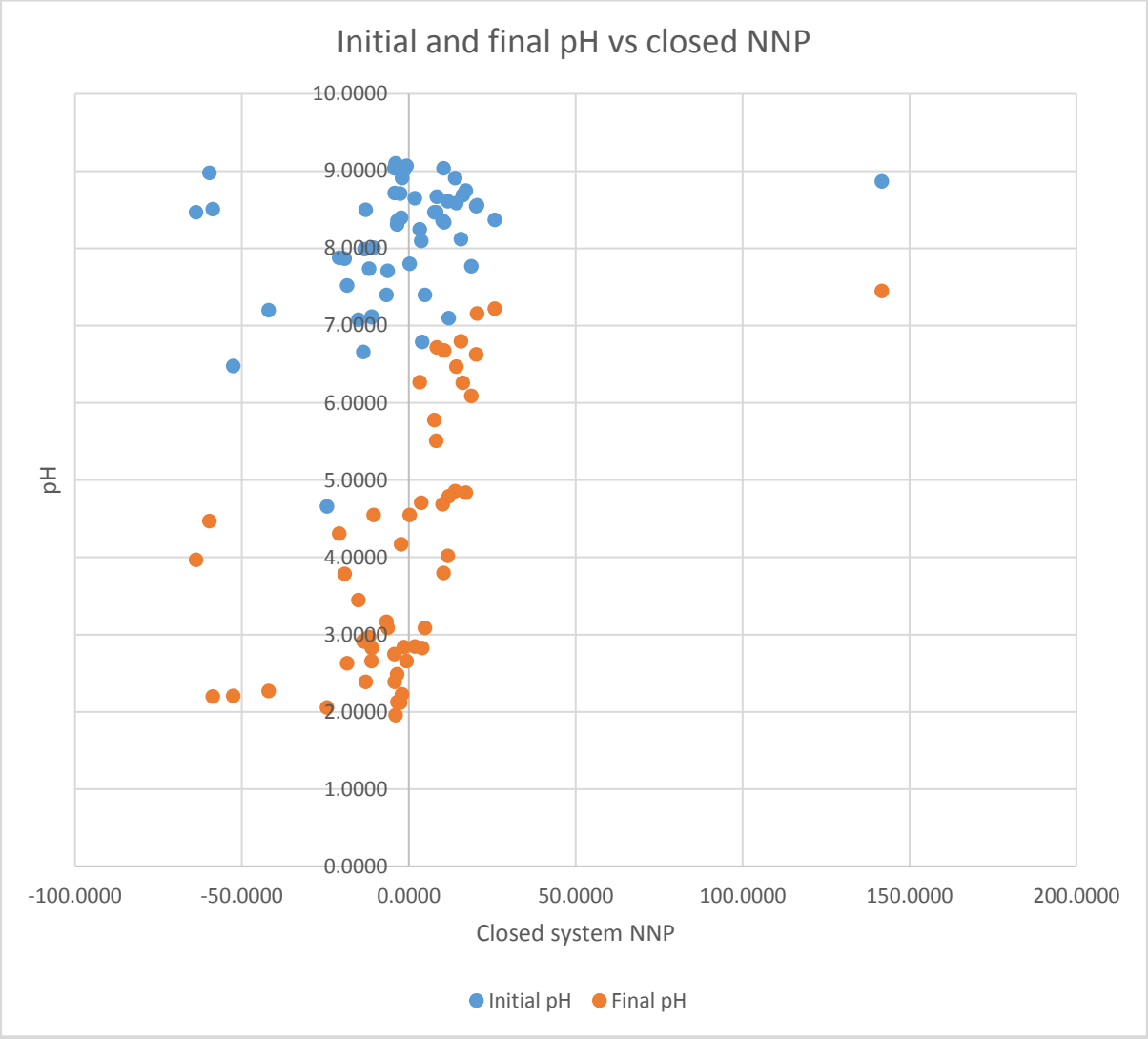

Figure 6-9 Initial and final pH vs closed NNP

The Neutralisation Potential Ratio (NPR) results are presented in Figure 6-10. Neutralisation Potential Ratio was used to determine the long-term acid production potential of the samples. Samples with less than 0.3% Sulphide-S are regarded as lacking enough oxidisable Sulphide-S to maintain acid generation (Usher et al., 2003). The graph is divided into regions representing the likelihood for acid generation. The “very low” region represents samples that are non-acid producing while the “very high” region represents acid generating samples. The uncertain region is represented by the blue region under the “very low” region. The NPR larger than 4:1 normally points to non-acid generation,

whilst NPR less than 1:1 indicates acid production if the sulphur content is also above 0.3 wt.%. Samples with less than 0.3% Sulphide-S are regarded as lacking enough oxidisable Sulphide-S to maintain acid generation (Usher et al., 2003). About 20% of samples had a Neutralisation Potential Ratio (NPR) ratio of ≤ 1:1 which is considered as potential acid generating. About 40% of samples had a NPR ratio of >4:1 which is considered non-acid producing and around 40 % of samples were in the uncertain region of 3:1 to 1:1.

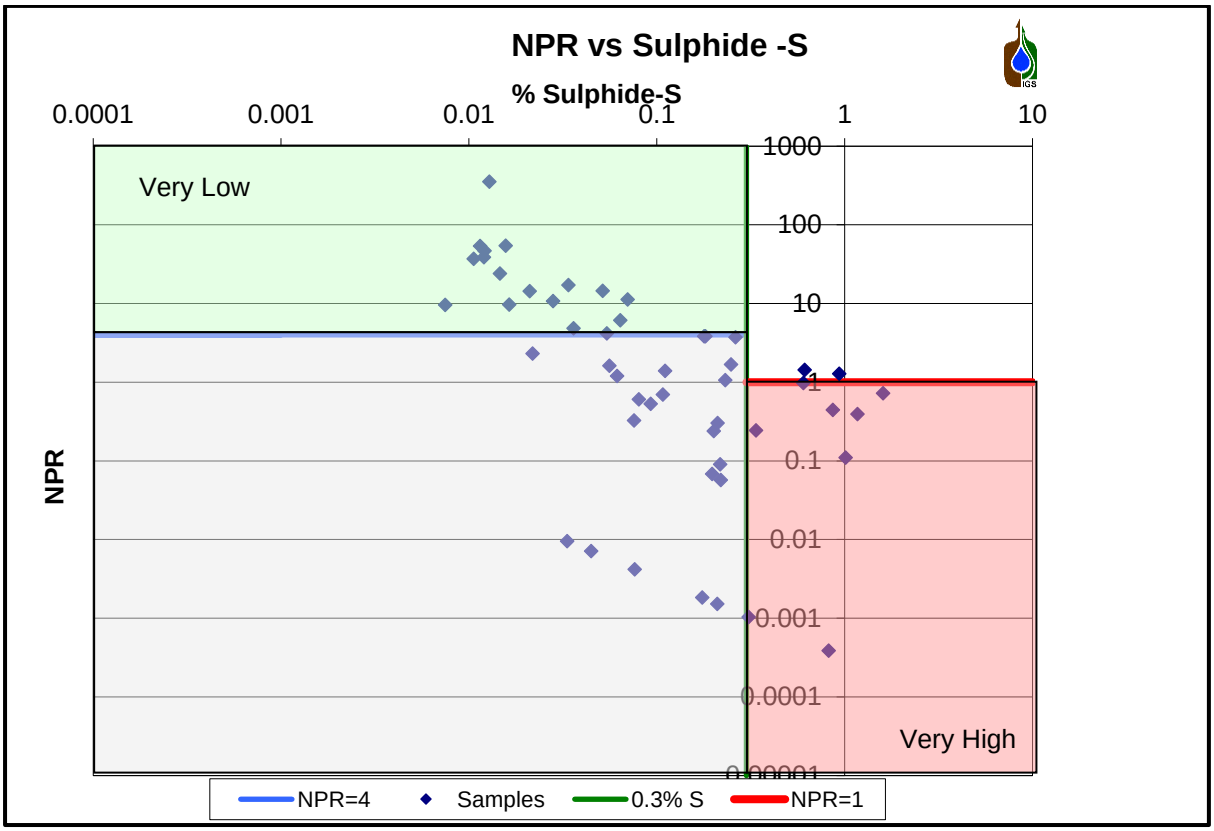

Figure 6-10 Neutralising potential ratio versus Sulphide-S

6.9 Summary

The aim of this chapter was to assess whether interaction between groundwater and the spent UCG geo-reactor will lead to leaching of inorganic elements. The leaching mediums used were deionized water, hydrogen peroxide, sulphuric acid and mine water elution at two different temperatures. The samples from the geo-reactor were subjected to these various leaching tests to determine the immediate environmental risk and also predict any possible future risks due to chemical evolutions in the UCG chamber. The water elution results generally released one or several orders of magnitude lower concentrations of elements than the other leaching mediums. The final pH for water leaching was mainly alkaline which can be attributed to the dissociation of major elements like calcium which buffer solutions to higher pH levels especially if reactive species like S^{-2} remain un-oxidized. Under peroxide elution the average pH in solution decreased and consequently the solubility of elements increased. Peroxide elution induces full oxidation and this is the basis for acid rock drainage associated with coal mining. The decrease in pH is attributed to oxidation of sulphide minerals which acidify the solution thereby increasing the solubility of metals and non-metals. Acid elution was incorporated to assess the leaching dynamics in the spent UCG geo-reactor if ARD conditions developed. The average

pH recorded was 1.79 and the highest mobilization of elements were recorded under this leaching medium which represents the “worst case scenario” that the geo-reactor can encounter. Chemical breakdown of silicate minerals of the spent geo-reactor failed to buffer or counter the acidity by consuming the hydronium that is responsible for the low pH as seen in the acid elution test. However static tests are rapid as compared to conditions expected in the UCG cavity where chemical equilibrium between the rocks and groundwater is expected and lower rates of sulphide oxidation are anticipated which can lead to silicate minerals contributing to acid neutralization. It is therefore recommended that any spent UCG geo-reactor must be periodically monitored to ensure that the pH does not drop to acidic levels (below pH of 4) to avoid rapid release of environmentally toxic elements.

The mine water elution was incorporated to assess the leaching dynamics under field conditions as water/rock interactions were subjected to experimental temperature of 25 and 70 °C. The following elements showed general increase in concentration with decrease in temperature: Mn, Fe, Ni, Sr, Ca, Mg, V and SO_4. As more groundwater flows into the UCG void, the temperature is expected to decrease with time hence these elements can be expected to increase in solution. The dissolved concentrations of the major elements in silicate rocks are usually restricted in groundwater by the formation of secondary minerals of low solubility. The following elements showed general increase in concentration with increase in temperature: B, K, Cu, and SO_4.

The result of contaminant migration due to dissociation of elements between groundwater and the surface of the solid in an aquifer was demonstrated by the distribution coefficient. These results do not show contaminant migration away from the cavern. The heat affected roof released the most metals into solution at 25 °C while the highest number of metals mobilized into solution at 70 °C were both from the roof and char samples. Aluminium and Fe were the main non-mobile elements across all sections of the geo-reactor and their relative mobility was not affected by change in experimental temperature. The semi mobile metals were Ba, Ni, Cu, Mn, V while metals with great affinity to leach into water phase were Sr, V, Co, Mn, Cu, Ba, Pb. The higher elution ability of Pb from char samples at higher temperatures is an environmental concern as generally this element was not mobilized from other sections of the geo-reactor from both deionized water and mine water eluates, which indicates that temperature plays a role in dissolving this element from the organic surfaces.

Acid base accounting was used as a predictive tool to assess the acid producing capacity of the spent geo-reactor. The NNP (net neutralising potential) was calculated in terms of the acid producing (AP) and neutralising potential (NP). The analysis utilized both the acid base accounting (ABA) and net acid generation (NAG) methods of predicting acid generation. Utilizing both NNP and NAG test for potential acid generation of material provides a more reliable evaluation technique than either test alone. NNP classified about 13% of samples as acid generating while only 7.5% were non-acid generating. Application of NAG classified 26 samples (49%) as high acid generating while only 13 (24.5%) was categorized as non-acid generating. The low risk acid generation constitutes 26.9% of the samples. About 20% of samples had a Neutralisation Potential Ratio (NPR) ratio and enough oxidisable Sulphide-S to maintain acid generation. The UCG process therefore decreases the overall acid generating capacity of the coal seam. However, the spent UCG chamber shows potential of leaching of some environmentally sensitive inorganic species from char, ash, roof and floor.

7 Qualitative hydrogeological assessment of aquifers surrounding an underground coal gasification site

7.1 Introduction

Heat penetration can alter the overlying rocks and create fractures that result in the coal seam aquifer becoming hydraulically connected to the shallow aquifer, which then leads to the draining of the shallow aquifer into the gasification zone (Figure 7-1). The confined nature of the coal (deep) seam aquifer allows its water levels (head) to stabilize at shallower levels above the coal seam depth (Dvornikova, 2018). The hydraulic connections can ultimately transmit water contaminated with inorganic and organic UCG products from the gasification zone to the shallow levels where subsequent contamination of pristine aquifers can occur. UCG operatives have to ensure the site is well characterized and that the coal seam has limited connectivity with other water sources (Imran et al., 2014).

Subsidence of the overburden above the UCG burn void can also result in serious groundwater contamination via fractures that result in aquifers cross connections. This can result in the transmission of pollutants generated from the burn zone to overlying aquifers (Liu et al., 2007). Overburden failure can create joints and fractures (Ghasemi et al., 2012), similar to the ones seen in Figure 7-1, and this can be pathways for contaminants to migrate from the UCG cavity to the shallower aquifers. The environmental risks to groundwater pollution from UCG activities are mostly site specific. Appropriate site selection can mitigate most of the potential risks to groundwater contamination as factors such as depth of cover and competency of overlying rock play an important role in roof collapse (Ghasemi et al., 2012, Imran et al., 2014). If there is no hydraulic connection between the shallow aquifers and the coal seam aquifer, from which gasification is undertaken, there remains little risk of groundwater contamination. Usually the coal seam aquifer is of poor quality and not used for any domestic or agricultural use. However if faults and fractures exists within the natural strata, a hydraulic connection can be created between the coal seam aquifer and the shallow aquifer as seen in Figure 7-1.

Stratification is the vertical distribution of salinity, pH and temperature of groundwater into a stepwise or layered dissemination (Ryuh et al., 2017). Stratification within an underground cavity associated with coal mining is common in the Karoo coal-bearing formations (Johnstone et al., 2013). UCG creates an underground cavity as a result of coal being gasified in situ and upon completion of the gasification process, groundwater levels are expected to rebound in the gasification zone and groundwater flow to resume. The geochemical evolution of the UCG cavity will be a result of interactions between groundwater and the various residue products contained in the cavity including ash, unburned coal, heat affected surrounding strata and hydrocarbons. Assessment of stratification in the UCG cavity is an important aspect as it may point to chemical processes such as diffusion which may influence the evolution of contaminants. Johnstone et al. (2013) reported stratification in the cavity of coal mines in Ermelo Mpumalanga, which showed groundwater quality evolves from sulphate type water to sodium type water due to sulphate reducing bacteria. This stratification led to the scrapping of the planned water treatment plant for decanting groundwater from the mine void, this was due to the water quality on top of the cavity being better than water at the bottom of the cavity.

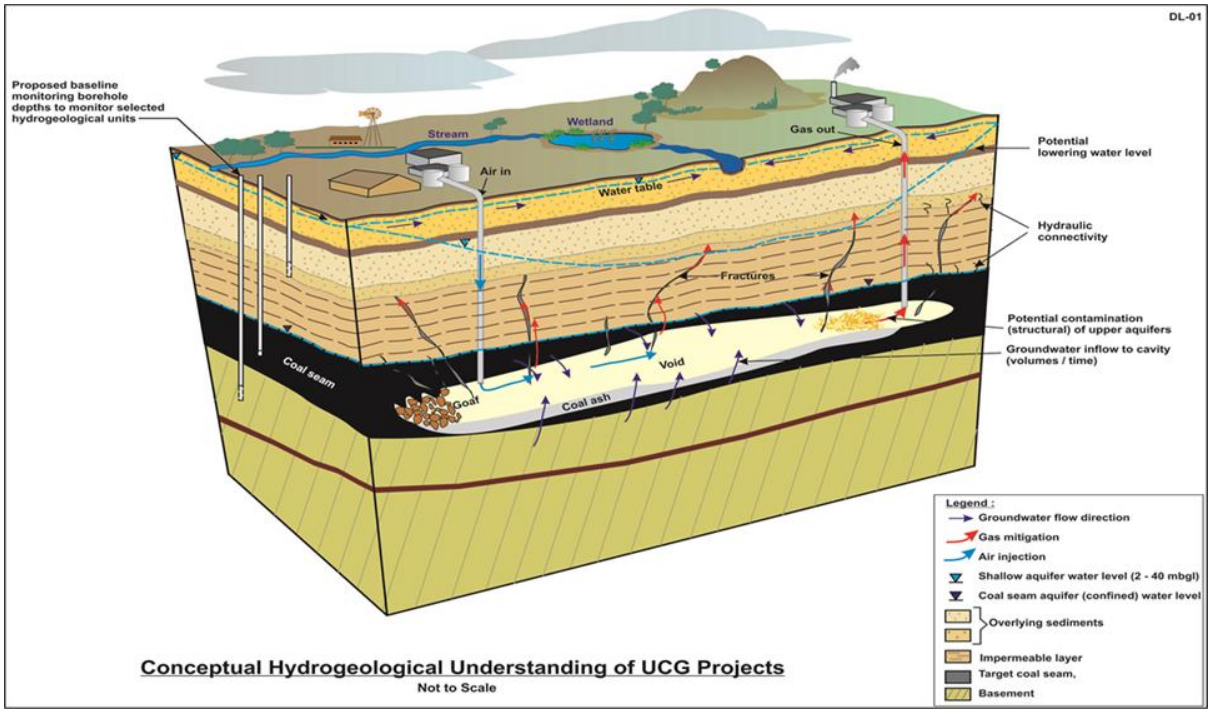

Figure 7-1 Conceptual hydrogeological model of a UCG plant adapted from (Pershad et al., 2018a)

Water is made up of Oxygen and Hydrogen atoms that exists in various stable isotopes. In natural waters the isotopic ratio of oxygen and hydrogen varies due to chemical, biological and physical processes. For example in cooler regions the equilibrium water vapour would have an isotopic composition of $\delta^{18}O$ = -10.6‰ and $\delta^{2}H$ = -93‰ whilst over high latitude seas the isotopic signature is as low as $\delta^{18}O$ = -11.6‰ and $\delta^{2}H$ = -106‰ (Clark and Fritz, 1997). These variations in isotopic fractions caused by isotopic effects during phase transitions such as condensation and evaporation are also dependent of temperature changes. For example during evaporation, water that is taken up into the gaseous phase and is enriched in the lighter isotopic fractions of $\delta^{16}O$ and $\delta^{1}H$ leaving behind water that is concentrated in $\delta^{18}O$ and $\delta^{2}H$. The interpretation of evaporation can lead to quantitatively identifying the admixture between various surface water bodies and subsurface waters. This provides a tool to determine the conditions during groundwater recharge by determining the $\delta^{18}O$ and $\delta^{2}H$ compositions in borehole samples (Clark and Fritz, 1997).

Groundwater contamination can be assessed using the source-pathway-receptor model in which polluted groundwater travels through a flow path in order to impact a receptor or user of the resource. This chapter aims to assess the pathway section of the model using a borehole that intersects the gasification zone or cavity (source), and two other boreholes are used for comparison and as background boreholes. The water quality will be assessed using electrical conductivity (EC). Temperature will also be assessed as an additional parameter but does not necessarily relate to the EC. The second aim of this chapter is to study groundwater hydraulic connections across various aquifers at the UCG site in Majuba, using hydrochemistry and stable isotopes ($\delta^{18}O$ and $\delta^{2}H$) tools, in order to assess the environmental risk to groundwater post the first gasification phase. A 3D geological model of the site will be developed and used to analyse the environmental risk. The third aim of this chapter is to analyse groundwater time series data in order to assess the evolution of chemical species on a field scale.This chapter essentially undertakes to address the second main objective of the thesis, which is determination of chemical evolution of groundwater contaminants from the UCG process.

7.2 Methodology

7.2.1 Stable isotopes

Groundwater samples were taken from Majuba UCG site using bailers and analyzed for isotope fractions, D/H ($^{2}H/^{1}H$) and $^{18}O/^{16}O$, at iThemba Laboratories in Gauteng using a Thermo Delta V mass spectrometer. Equilibration time for the water sample with hydrogen was about 40 minutes and CO_2 was equilibrated with a water sample in about 20 hours. Laboratory standards, calibrated against international reference materials, ware analysed with each batch of samples. The analytical precision is estimated at 0.2‰ for O and 0.8‰ for H. Analytical results are presented in the common delta-notation:

$$\delta^{18}O = [(^{18}O/^{16}O_{Sample} \,/\, ^{18}O/^{16}O\ v_{\text{-SMOW}}) - 1] \times 1000 \qquad [1]$$

These delta values ($\delta^{18}O$ and $\delta^{2}H$) are expressed as per mil deviation relative to a known standard, in this case standard mean ocean water (SMOW). The samples were taken from all the identified aquifers; shallow, intermediate lower, intermediate upper and the coal seam aquifer. Hydrochemistry data from the UCG site groundwater monitoring was also used to analyze hydraulic connections at the study site. Groundwater was sampled on a monthly basis from all identified aquifers using bailers and all samples were preserved and transported to the laboratory for chemical analysis. Major and minor elements were analyzed together with pH and electrical conductivity. The groundwater monitoring chemical data was plotted on diagnostic plots for geochemical analysis of the groundwater status.

7.2.2 Electrical conductivity and temperature profiling

Three boreholes at depths of around 290m were selected for this study. Two of these boreholes were groundwater-monitoring boreholes (G2WMD2 and G2WMD1) within the production zone that is monitoring the coal seam aquifer. The other was the verification borehole (G1VTH1) that was drilled after the gasification process was concluded and intersects the UCG cavity. The monitoring boreholes were used as background as they are not within the gasification zone and hence the geochemistry is not expected to be influenced by the gasification process or its products. The verification borehole intersects the UCG cavity and hence provides useful information on the geochemical evolution on the gasification zone. Down-the-hole profiles of temperature and Electrical Conductivity (EC) were taken in order to investigate the stratification of the coal seam aquifer and UCG cavity. Stratification in old coal mine voids in the region has been reported by Johnstone et al (2013). This has resulted in dilution of polluted water thereby eliminating the need for water treatment. A Solinst TLC (Temperature, Level and Conductivity) meter similar to the one in Figure 7-2 was used to profile EC down the borehole. Water level measurements can be read off the marked flat reeled tape made of Polyvinylidene fluoride (PVDF) material. EC and temperature measurements were taken with depth. The probe was lowered to the bottom of the borehole and depending on measurement interval selected, dual measurement of Temperature and EC were recorded simultaneously at each depth.

Figure 7-2 Solinst TLC meter (Left) and measurement arrangement (Right)

7.3 Results and discussion

7.3.1 Generation of geological model

3D geological modelling serves as a qualitative and quantitative method of efficiently estimating mineral resources and delineating subsurface bodies (Jiskani et al., 2018). It uses available geological information from drill holes, geological maps and rock properties with the aim of processing and interpolated the data to produce a 3D visual representation of the geological conditions from the field (Zhang and Zhu, 2018). Various software packages are available on the market for geological modelling and for the Majuba UCG site, Leapfrog Geo version 4.4 was used. As part of this study a 3D geological model was generated and completed for the study site.

The lithological data used was from 25 boreholes of varying depth, drilled in the vicinity of the gasification zone. The location and distribution of the boreholes is given in Figure 7-3. Detailed well log data that include the collar, survey and lithology intervals are included as Appendix 7-A. Starting from surface, the lithology identified as “cover” is the sum total of all unconsolidated material that rests on top of the dolerite. The T1-dolerite is the first rock strata encountered closer to the surface in the Majuba UCG site and is characterised by widespread weathering features, and is assigned “Dolerite 1” in the lithology table. The “Karoo sediments” are the main geological strata on the site and have been transgressed by the dolerite sills. This lithology is therefore encountered in various depths in the drill hole logs. This lithology is made up of various sedimentary rocks including mudstones, shales and sandstones of varying grade. For simplicity, the lithology has been summed up as “Karoo sediments”. The T2 Dolerite is encountered deeper into the subsurface and carries the name “Dolerite 2”. This lithology has a thickness of over 100 m in places and has a fairly consistent lateral extend over the study area. The Gus seam is encountered at around 280 m depth from the surface and is assigned the name “coal” in the lithology table. The other thin coal seams in the study area were not delineated as they were not the target of the geological model and indeed the gasification process. The delineation of the Gus seam was the main objective of generating the geological model.

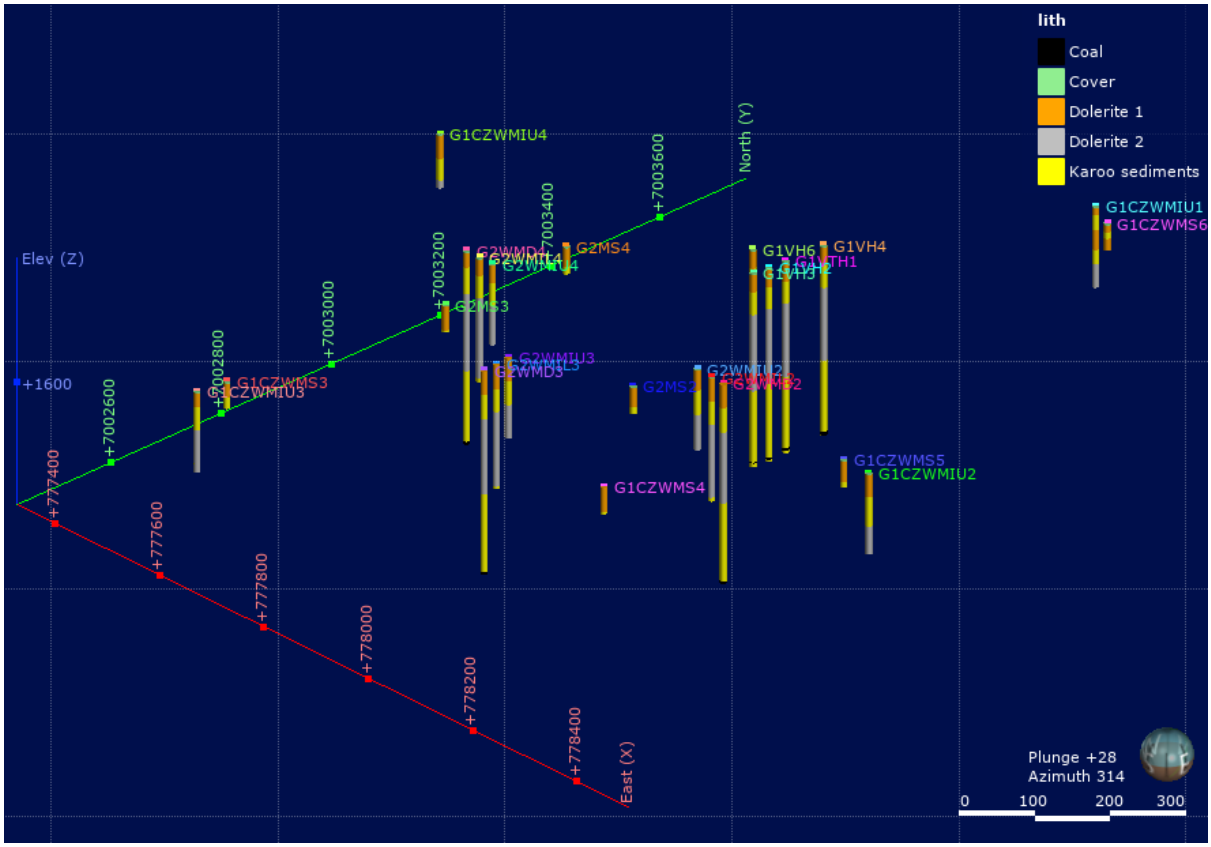

Figure 7-3 3D multilog displaying borehole distribution at the Majuba UCG site

The boreholes that intersected the Gus seam contained all the geological units used to generate the geological model (Figure 7-4). For simplicity, the other coal seams encountered in the study area were profiled as part of the "Karoo Sediments" lithology. The 3D geological model displaying interpolated lithology is presented in Figure 7-5. The model was calibrated by correlating the Gus seam to the density log obtained from downhole geophysics. In downhole geophysics, a probe is send down a borehole where geophysical properties (e.g density) of the rocks are recorded. In this study a geophysical contractor was appointed by Eskom UCG to gather the data. Coal is naturally low in density as compared to other sedimentary rocks and this makes it easy to distinguish when mapping coal seams from downhole geophysical surveys (Hatherly, 2013). The correlation of Gus seam (at around 280 m deep) to the "coal" lithology for four selected boreholes is displayed in (Figure 7-6). The Gus seam has a deviant density profile from the consistent profile observed for the "Karoo sediments", this anomalous profile is characterized by a lower density with varying spikes profiles. This erratic contours are as a result of the outline of the Gus seam which consists of a lower bright layer (20 to 80 cm), a middle dull layer (over 1 m) and a bright upper layer (30cm) (de Oliveira and Cawthorn, 1999). It is this irregular trend that is matched to the "coal" lithology in the core drills as a calibration of the model (Figure 7-6). The other thin coal seams are also presenting atypical trends in the density log which shows their limited thickness compared to the targeted Gus seam. The Eland and Fritz seams are encountered close to each other at around 230 m and are depicted as singular spikes in the density profile. The two seams are encountered in all four boreholes, hence they can act as marker seam as they are continuous throughout the coalfield. The Alfred seam is encountered at around 270 m also as a thin seam depicted by the single spike. The seam is however only encountered in boreholes G1VH4 and G1VH6 and thus is characterized as laterally impersistant in the Majuba coalfield. This

geological profile is consistent with previous geological work (Chapman and Cairncross, 1992, de Oliveira and Cawthorn, 1999) done in the vicinity of the study area as seen in the cross section (Figure 7-7). The delineation of aquifers in the study area was presented in section 2.4.4.

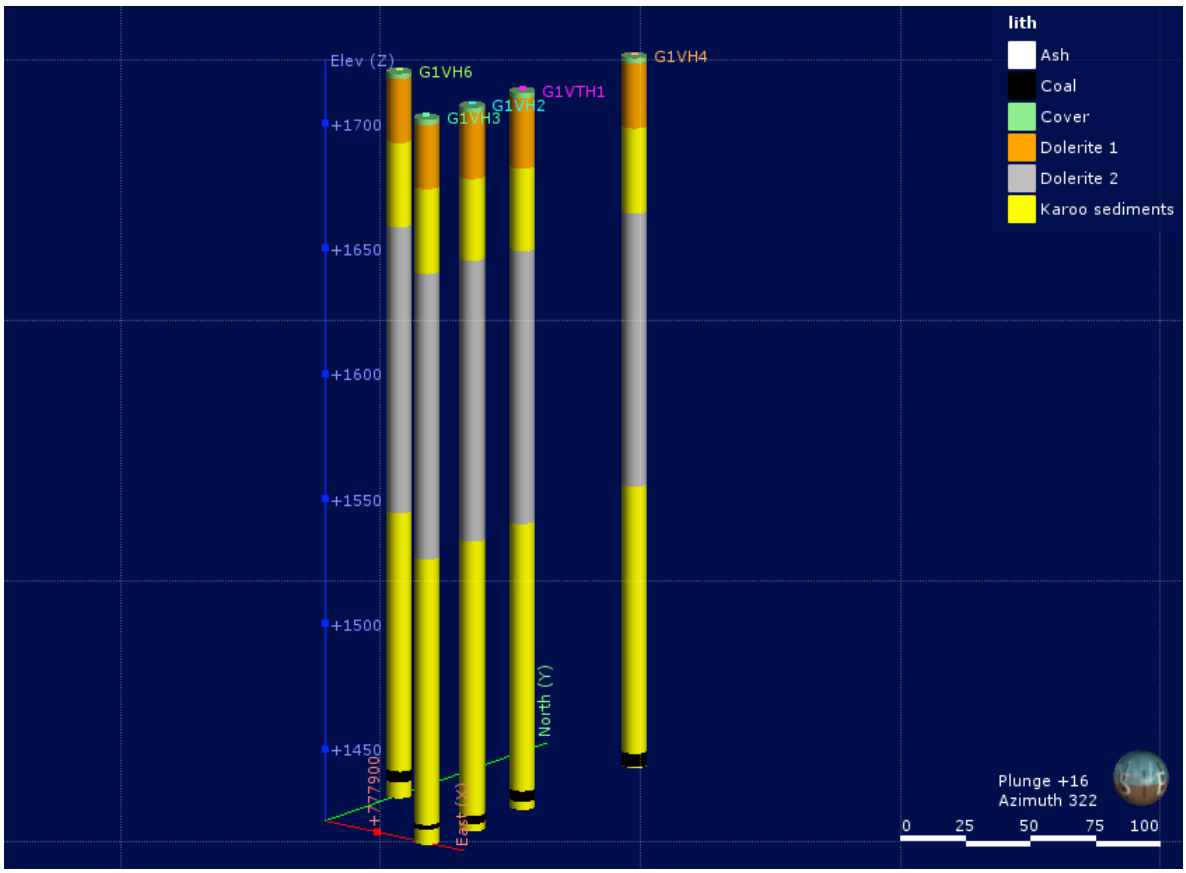

Figure 7-4 Profile of deep drill hole logs showing lithologies used in the profiling of the geological model. The coal represents the Gus seam. All other coal seam were profiled as part of the Karoo sediments.

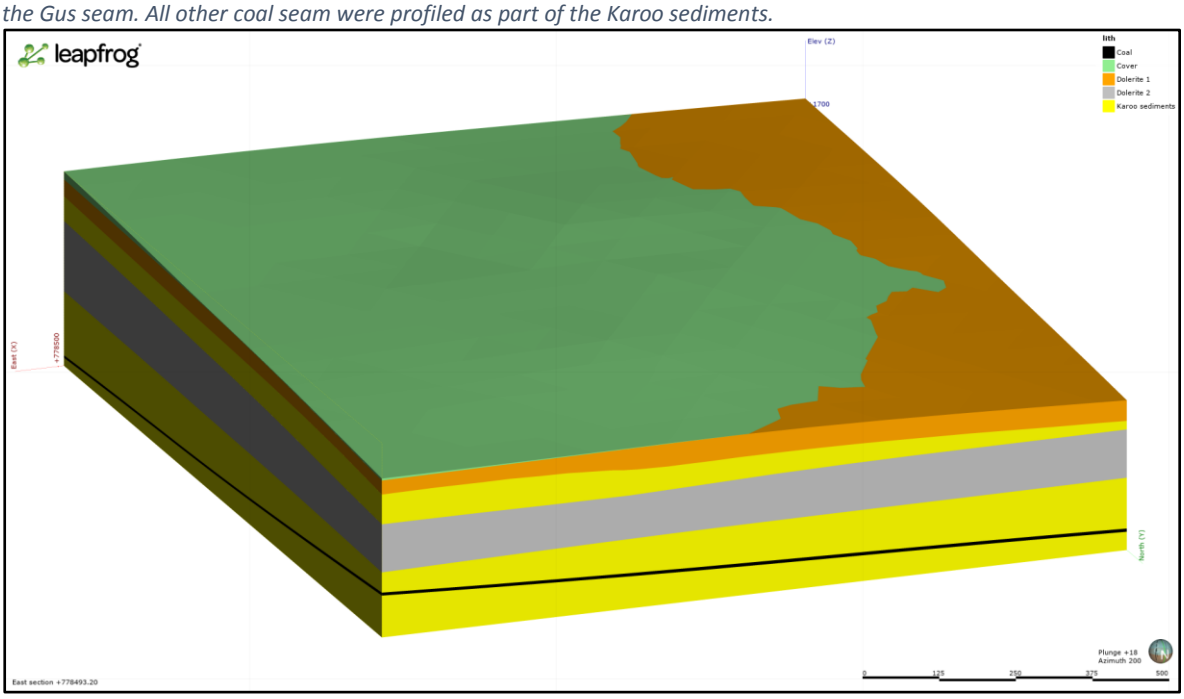

Figure 7-5 3D geological model of the Majuba UCG site, cross section is provided below in Figure 7-7.

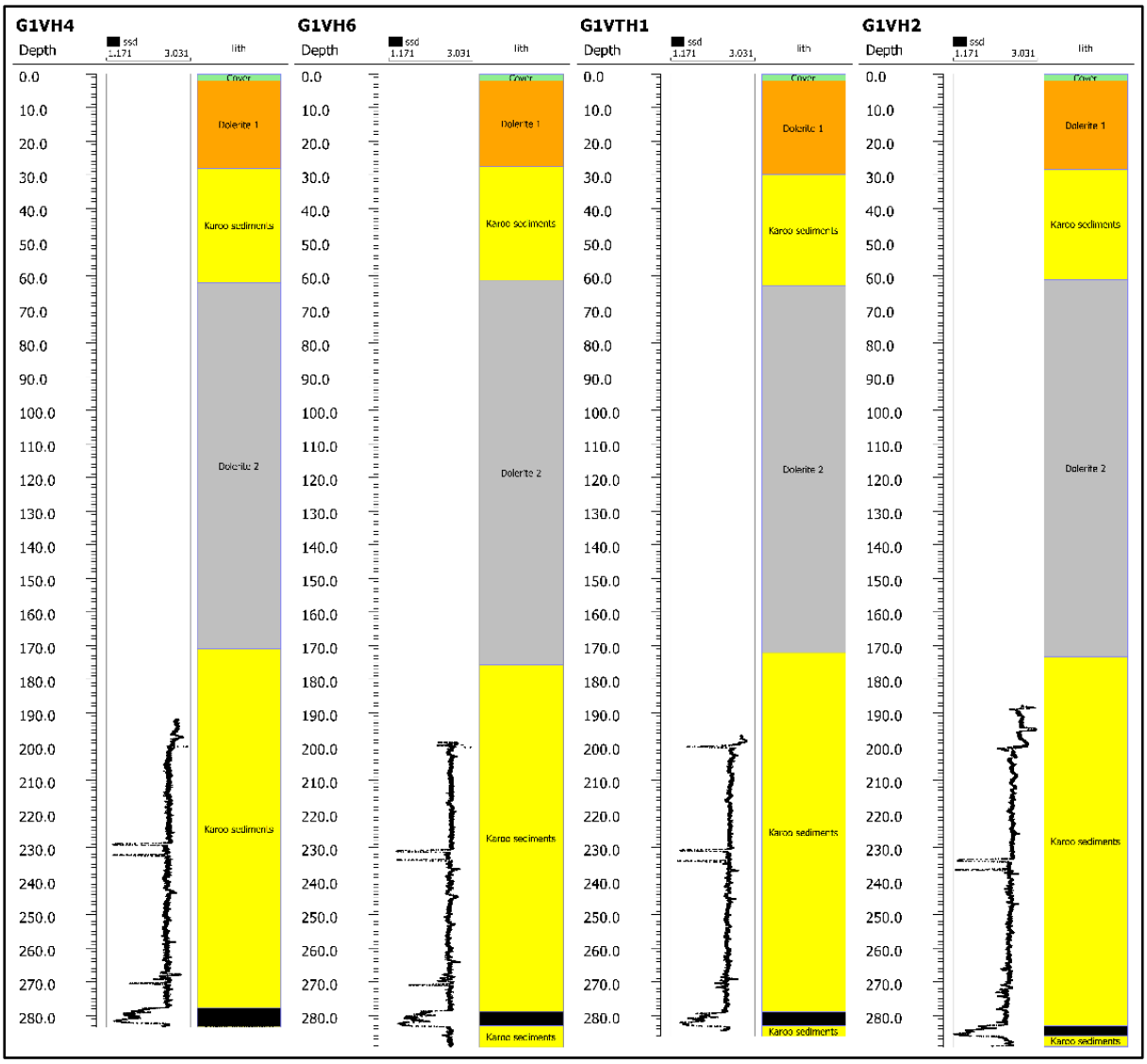

Figure 7-6 Drill core lithology correlation with density log profile from downhole geophysics

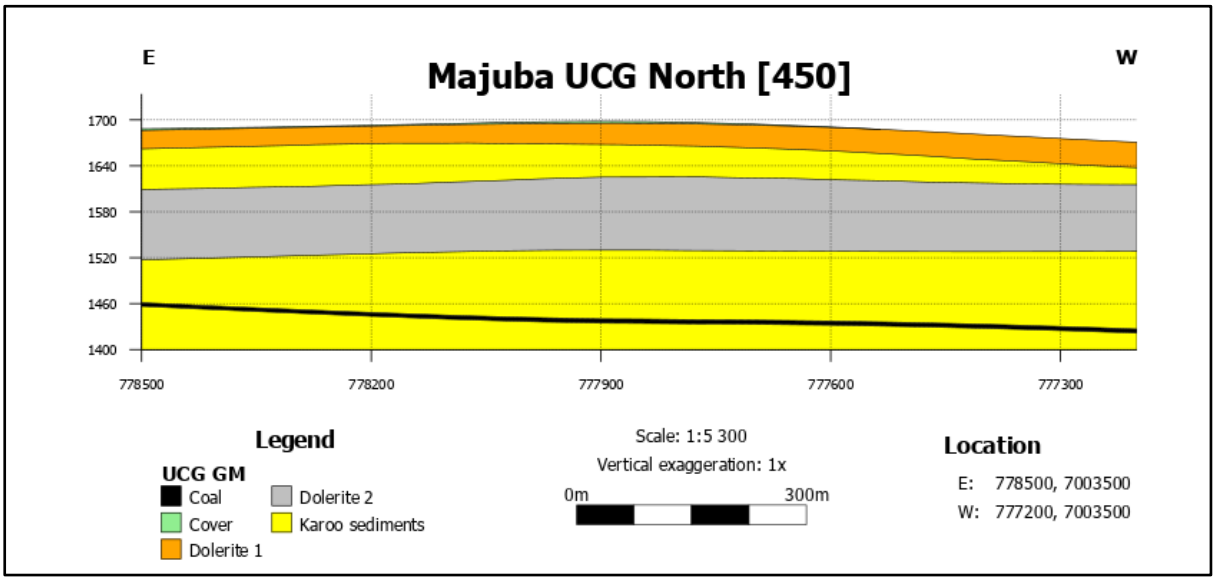

Figure 7-7 East-West lithology cross section of the study area

7.3.2 Isotopic analysis

The isotopic data of the environmental isotopes $\delta^{18}O$ and $\delta^{2}H$ is presented in Table 7-1. The $\delta^{18}O$ values ranges from -7.08‰ to 4.15‰ whilst the $\delta^{2}H$ ranges from -42.2‰ to 14.91‰. The stable isotopes data plotted in a $\delta^{18}O/\delta^{2}H$ diagram (Figure 7-8) with respect to Global Meteoric Water Line (GMWL). The lack of historical rainfall data for $\delta^{18}O$ and $\delta^{2}H$ in the study area prompted the addition of the Pretoria Meteoric Water Line (PMWL) from a Pretoria station, which is situated approximately 267 km from the study area. This station collects and record isotopic rainfall data that is kept in the Global Network of Isotopes in Precipitation (GNIP) database managed by the International Atomic Energy Agency (IAEA). The recorded monthly precipitation data, resulted in the following relationship isotopic trend: $\delta^{2}H = 6.5\ \delta^{18}O + 6.4‰$.

Table 7-1 isotopic data of groundwater in the study area

Borehole Identification and aquifer association	**d D (‰)**	**$d^{18}O$ (‰)**
GWMD2 Deep aquifer	-42.2	-7.08
GWMD3 Deep aquifer	-40.9	-6.98
GWMD4 Deep aquifer	-42.0	-7.01
GWMIL2 Intermediate Lower	-23.5	-4.52
GWMIL3 Intermediate Lower	-27.1	-4.95
GWMIL4 Intermediate Lower	-29.1	-4.79
GWMIU1 Intermediate Upper	-16.3	-2.55
GWMIU2 Intermediate Upper	-25.7	-4.54
GWMIU3 Intermediate Upper	-5.4	-0.24
GWMIU4 Intermediate Upper	-13.6	-2.06
GWMS2 Shallow	-19.1	-2.93
GWMS3 Shallow	-19.7	-3.34
GWMS4 Shallow	-20.5	-3.63
Dam	14.9	4.15

The $\delta^{18}O$ and $\delta^{2}H$ values trended along the GMWL and are divided into two clusters, suggesting the possibility of two aquifer systems of groundwater at Majuba UCG site. The samples that were enriched in $\delta^{18}O$ and $\delta^{2}H$ were from the shallower aquifers (shallow and intermediate upper) confirming that the water was subjected to the influence of evaporation. The samples showing depletion in $\delta^{18}O$ and $\delta^{2}H$ are the deep aquifer samples which confirms that they are not affected by evaporation and that recharge may have occurred at high elevation where heavy isotopes had been reduced from rainfall due to altitude/elevation effect. The variability in water isotopic composition between the shallow and the deep aquifer points to dissimilar recharge events, runoff conditions, sampling period salinity and altitude effect (Ayadi et al., 2018). The less negative values were obtained from the upper and lower intermediate aquifers as well as the shallow aquifer. These waters may be more enriched in the stable isotopes since they have a shorter residence time in the ground than the deep aquifer waters.

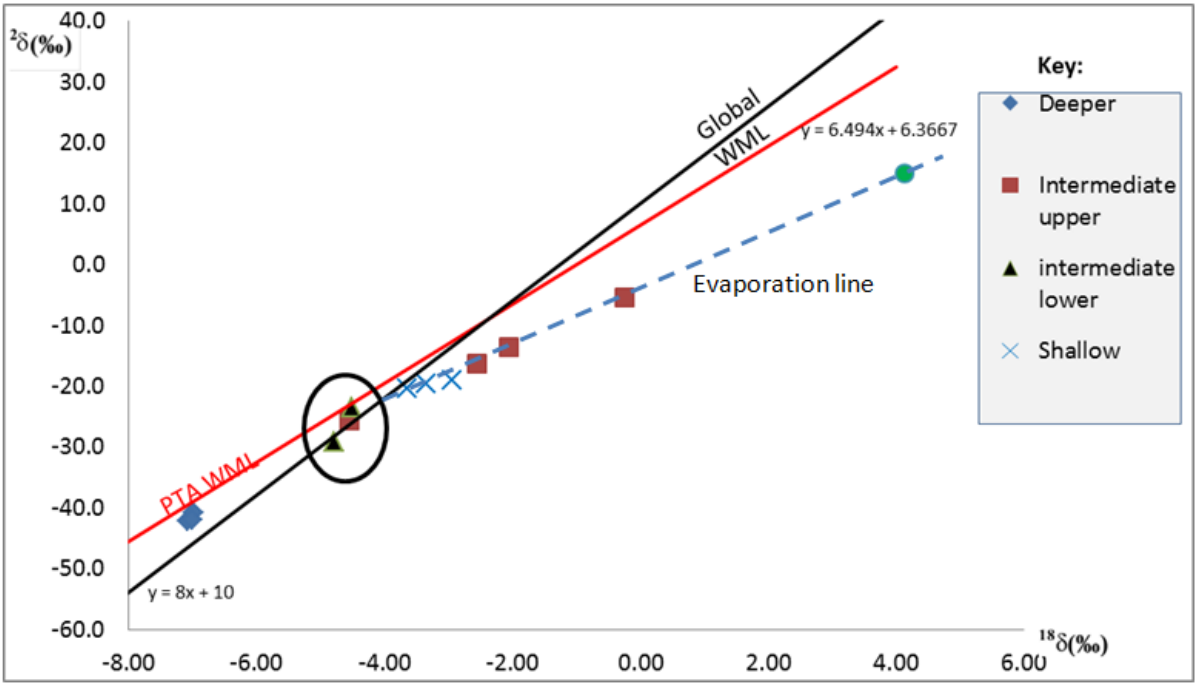

Figure 7-8 The Craig plot for Majuba UCG site, dam sample is plotted in green

The deep aquifer is represented by average values of -42 and -7.02 for $\delta^{18}O$ and $\delta^{2}H$, respectively. These values are significantly different from the mean values observed in other aquifers. The deep aquifer samples are clustered separate from the other aquifers. The positioning of the deep aquifer samples are consistent with the position of paleo-waters that have equilibrated with surrounding rocks, where little or no evaporation transpires. The deep aquifer is expected to receive little local recharge during precipitation events as compared to other aquifers. It is an isolated aquifer from the rest of the other aquifers with no evidence of mixing.

A clear distinction can be seen in the isotopic signature of the different aquifer systems depicted in Figure 7-8. This is particularly portrayed in the deep and shallow aquifer where the clustered points are closely packed for each aquifer system. One sample from the intermediate upper aquifer plots in the position dominated by the samples from the intermediate lower (encircled in Figure 7-8), which confirms mixing between the two aquifers through the T2 weathered dolerite but not mixing with the deep aquifer. The deep aquifer and the dam sample are most distinctive and isolated as compared to the other aquifers.

The evaporation line in Figure 7-8 has a slope of 4.6, which is in line with the global range of 4 to 8, for example GMWL has slope close to 8 (Clark and Fritz, 1997). The slope depends on the relative humidity, temperature and concentration in the atmospheric moisture (Yurtsever and Payne, 1978). Relative humidity is fairly constant at 80% in Mpumalanga Province during the summer season (Govere and Durrheima et al, 2001). Craig-Gordon (1965) model has established the relationship between the evaporation line slope and the relative humidity. The 4.6 slope value relates to a relative humidity value within the 50% to 75% range as described by (Gordon et al, 1993). This deduced range corresponds with the 80% relative humidity in the Mpumalanga area. The isotopic signature for the shallow aquifer plots along the evaporation line which suggests that the water from the surface point (dam) and the shallow aquifer originated from similar precipitation. The shift in isotopic signature of the dam to more positive $\delta^{18}O$ and $\delta^{2}H$ values is due to constant evaporation in the dam favouring the enrichment of water vapour in the lighter isotopes and the heavier isotopes remaining in the dam. The shallow aquifer plots along the evaporation line but with more negative $\delta^{18}O$ and $\delta^{2}H$ values as

compared to the dam. This is due to the isolation of groundwater from the atmosphere upon aquifer recharge that leads to isotopic signature being unaffected by fractionation due to evaporation.

The three points from the intermediate upper aquifer also plots along the evaporation line, which suggest that recharge was from the same water source as the shallow aquifer. The more positive isotopic signature of these three points as compared to the shallow aquifer suggest that fractures in the dolerite sill preferentially transmit groundwater which drains some of the water from the shallow aquifer and transmit it quicker than in the sandstones in the shallow aquifer. This means that groundwater that is recharged in the shallow aquifer, with a more positive isotopic signature, will travel slower (longer residence time) through the sandstone matrix. However if the water encounters fractures at the contact zone of the dolerite sill with the sandstone (where the intermediate upper aquifer is located (Figure 3-19)) then water flows faster and undergoes less isotopic fractionation due to rock-water interactions. This leads to some of the intermediate upper aquifer points having a more positive isotopic signature than the shallow aquifer. This also shows that there is possible mixing between the shallow aquifer and the intermediate upper aquifer.

7.3.3 Hydro-chemical analysis

Monthly groundwater monitoring data over a two year period of monitoring was used to characterize the water type of each aquifer system identified on the Majuba UCG site. The groundwater chemical data was also plotted in an Expanded Durov plot as seen in Figure 7-9. The distinct appearance of the deep aquifer can be seen under the chloride section, where water with high chloride concentration plot. The deep aquifer plots in the square section of natural saline waters in the Expanded Durov plot. This was expected as deep aquifers contain high levels of sodium chloride salinity due to the marine depositional environment (Clark and Fritz, 1997). Outliers (red dots) were experienced in only one month, this is likely a sampling or analytical error as this trend did not persist. All the other aquifers plot in the bicarbonate section of the diamond section of the Expanded Durov plot and also plot in the irrigation return water block in the square section of the Expanded Durov plot. However this water is not likely from irrigation but rather weathered aquifers. Whilst other aquifers may have relatively similar chemistry it is clear that the deep aquifer maintains its discrete hydro-chemical signature. All the samples were taken post gasification, and from the chemical analyses, no link can be established between the deep aquifer and its shallower counterparts. The hydrogeological conceptual model (Figure 3-19) shows that the three upper most aquifers may be linked through fractures in the lithology. Fractures and the weathering of the intrusive dolerite rocks can also make flow to be more rapid in these aquifers as compared to the deep coal seam aquifer. This can lead to a higher ion exchange in the aquifers which may support a Sodium-bicarbonate water type dominating.

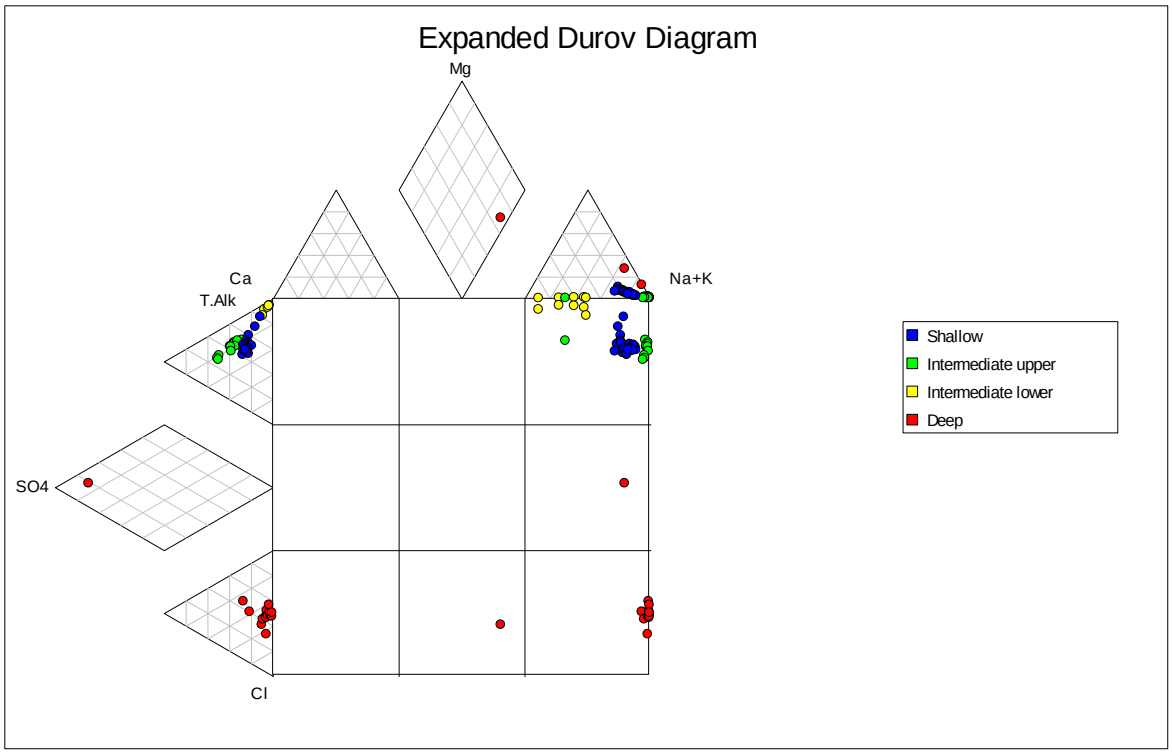

Figure 7-9 Expanded Durov Plot of average groundwater data from different aquifers, more detailed analysis using other diagnostic plots including standard Durov are presented below in section 7.3.5.

The STIFF diagram in Figure 7-10 was used to analyse the chemistry of selected groundwater average data from boreholes from each aquifer system. The G2WMD2 (Coal seam aquifer) has a distinct chemical profile with relatively elevated levels of; Na, K, Cl and SO_4. This is typical of deep mine water that has low flow rate in the aquifer. The other boreholes from the shallower aquifers have high carbonate-bicarbonate quantities synonymous for fresh aquifer water.

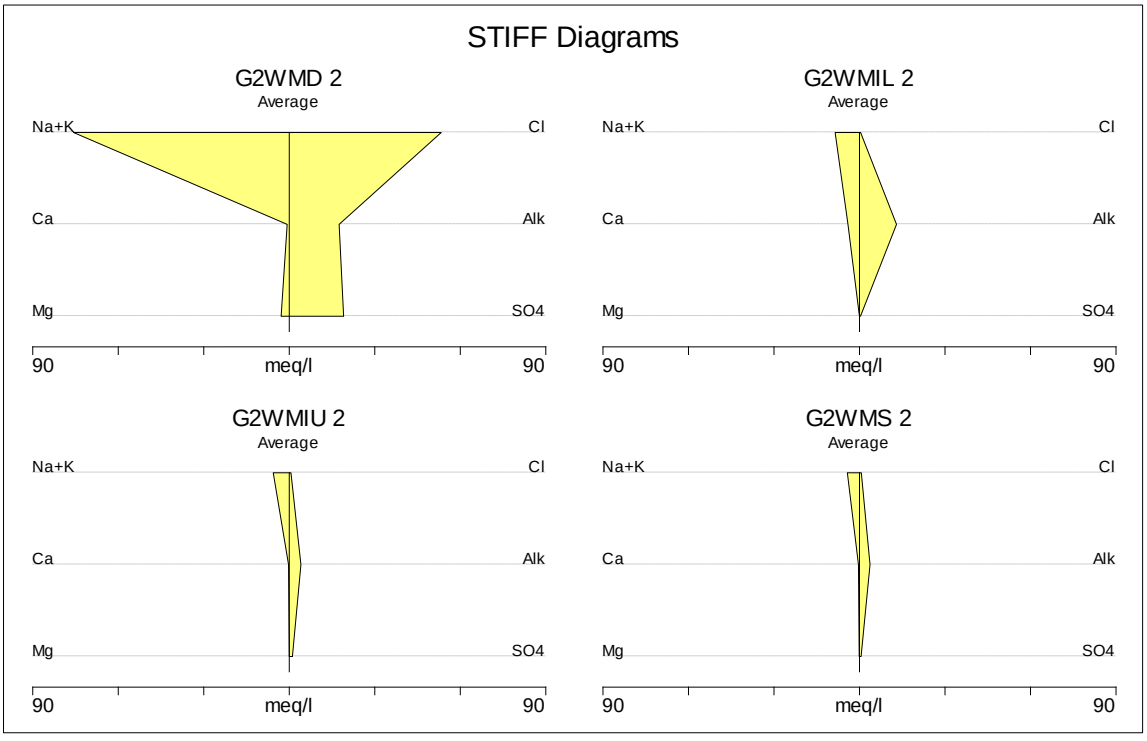

Figure 7-10 STIFF diagram of selected boreholes

The general trend from the isotope and chemistry data indicate no link between the deep coal seam and the shallow aquifer. The deep aquifer is represented by an isotopic signature that is depleted in the heavy isotopes with average values of -41.7‰ and -7.02‰ for $\delta^{18}O$ and $\delta^{2}H$ respectively, while the shallow aquifer is enriched with average values of -19.9‰ and -3.3‰. Hydro-chemical data also indicated a sodium-chloride water type for the deep aquifer and a sodium-bicarbonate water for the shallow aquifer.

7.3.4 Stratification

All electrical conductivity (EC) and temperature profiles presented in this section all commenced at the static water level (SWT) and the data displayed in appendix 7-A. The EC and temperature profiles for the groundwater monitoring borehole, G2WMD2, are presented in Figure 7-11. G2WMD2 is a monitoring borehole within the production zone that is used to monitor the coal seam aquifer (deep aquifer). The borehole is solidly cased from surface to 279 mbgl (meters below ground level), at the depth of the Gus coal seam. The EC of groundwater increases with depth with the maximum of 780 mS/m measured at the depth of 294mbgl. The temperature also increases with depth until 244 mblg where it levels off at around 21.5 °C. The EC profile shows an erratic behaviour around 283 mbgl, which is approximately where the casing ends and this possibly represents a groundwater flow zone. Deeper than this point the general trend of stable EC readings were seen in the profile.

The EC and temperature profiles for the groundwater monitoring borehole G2WMD1 are presented in Figure 7-12. A similar trend of increasing EC and temperature profiles with depth to that observed in G2WMD2 was also seen in G2WMD1. There was a drop in EC at greater depths from 283mblg and this coincides with the depth where the casing ends, and possibly represents an area where fresh aquifer water is flowing. The drop in EC suggests that fresh aquifer water is of a better quality than the stagnant water in the well. In contrast to G2WMD1, the temperature increases with depth without coming to a constant but highest recorded temperature was 22.8 °C at 280 mbgl. The EC and temperature profiles for the G1VTH1 are presented in Figure 7-13.

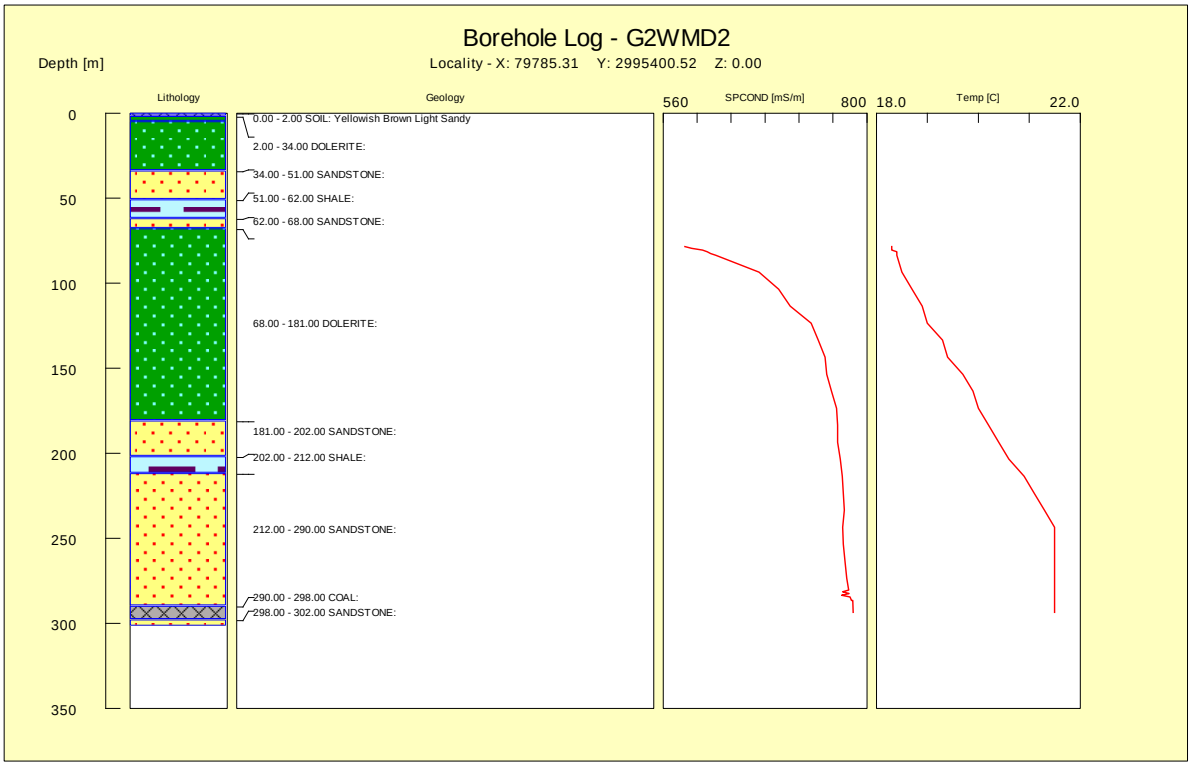

Figure 7-11 EC and temperature profile of G2WMD2, which is solid cased from top to depth of 279mbgl

G1VTH1 is a verification borehole drilled into the UCG cavity, post gasification and hence the EC and temperature profiles covers the gasification area (cavity). The EC profile shows an erratic behaviour while the temperature increases with depth. A maximum temperature of 70°C was measured at a depth of around 250 m. The maximum temperature in G2WMD2 was 21.5°C, while in G2WMD1 it was 22.8°C, which suggest heat from the gasification zone is affecting the temperature of groundwater in G1VTH1 especially from 250 mbgl. The erratic behaviour of the EC in G1VTH1 may be due to groundwater flow zones or fractures intersecting the well as this borehole was not cased from around 200 mbgl to the end of well at around 290 m. There is a general trend of increasing EC with depth despite the erratic behaviour seen in the EC profile, and water at the bottom of the borehole has much higher EC as compared to water at the static water level (SWT).

The three boreholes represent a fracture (or hole) in the natural strata and can therefore be utilized as pathways in the source-pathway-receptor model. The results show that the chemistry of the groundwater (i.e. represented by EC) at the coal seam (or gasification) level does not carry throughout the length of the boreholes. This is in spite the fact that all these boreholes tap the confined coal seam aquifer and their peizometric surfaces are quite shallow. The stratification in EC is an indication that whatever groundwater chemistry is experienced in the coal seam (gasification zone), this groundwater chemistry will not affect the shallow parts of the water in the borehole. One of the critical questions regarding UCG solid residue in the cavity, is the ability of groundwater to transmit it to shallower levels. The results do not support the idea that any contamination will be translated to overlying aquifers through the influence of the piezometric surfaces (confining pressure). The temperature profile also supports this localization of water chemistry as heat was not carried throughout the length of the boreholes in all profiled wells. Both temperature and EC were stratified in all boreholes.

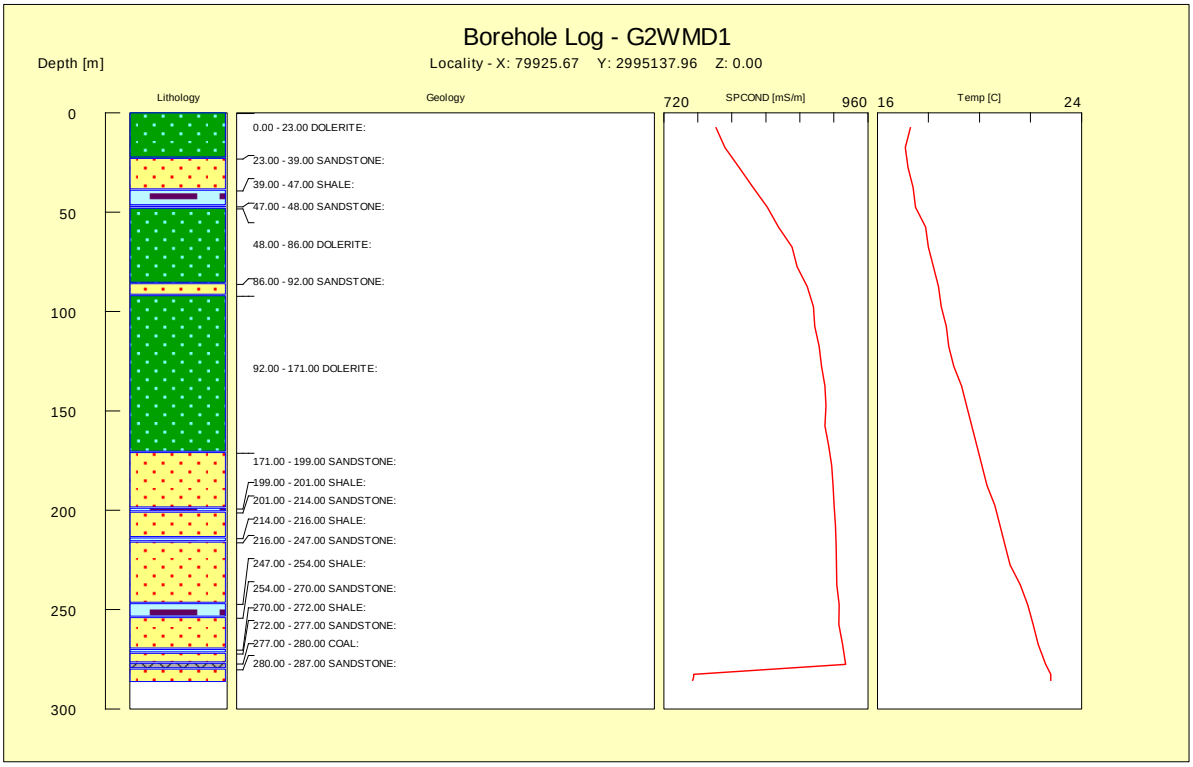

Figure 7-12 EC and temperature profile of G2WMD1, which is solid cased from top to depth of 280mbgl

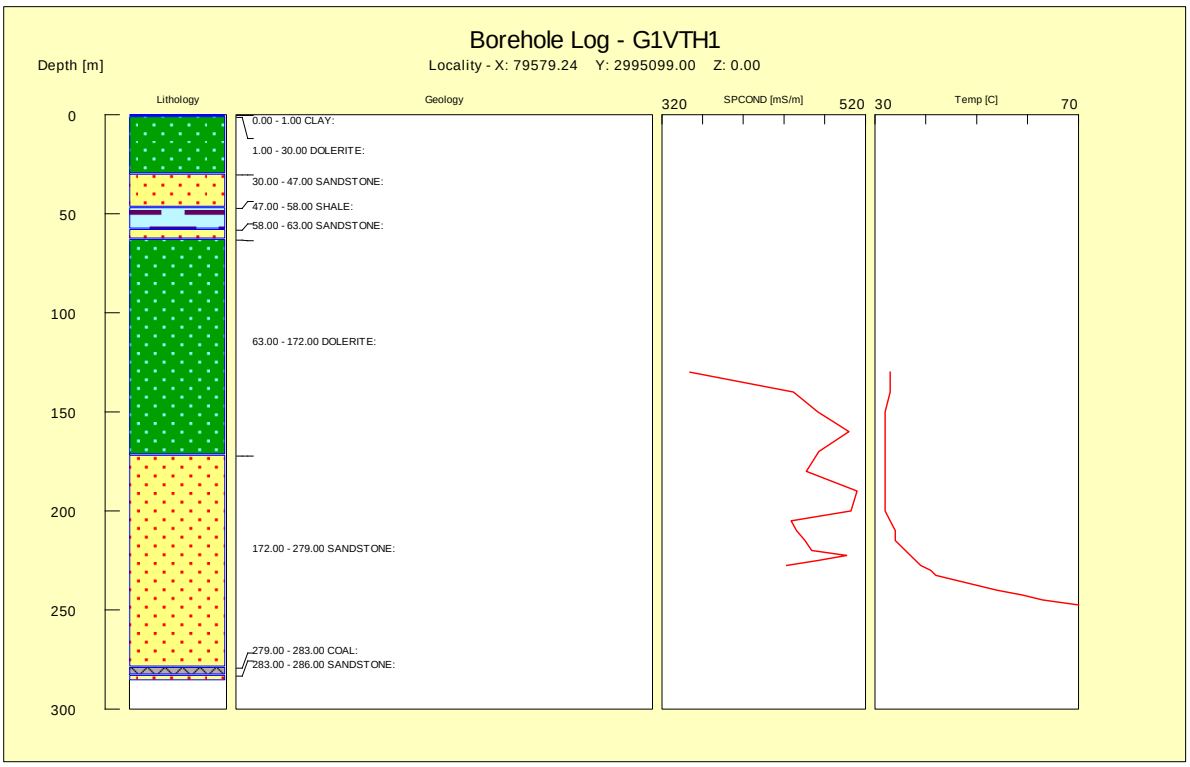

Figure 7-13 EC and temperature profile of verification borehole G1VTH1, which is solid cased from top to depth of 200mbgl and the borehole extends to around 286mblg

7.3.5 Time series data

This section presents time series data from the coal seam aquifer and the data is presented in Appendix 7-A. The data presented covers four groundwater monitoring boreholes (G2WMD1, G2WMD2, G2WMD3, G2WMD4) five verification boreholes with three intercepting the gasifier (G1VTH1, G1VH3, G1VH2) and two off cavity (G1VH4 and G1VH6) and one background (WMD1). All these boreholes that were drilled to the coal seam aquifer depth (280 m). The gasifier was officially declared shutdown in June 2015, which represents the post gasification time series in the data presented. The first verification borehole was drilled after this period and hence the chemistry data begins from 2015 for G1VTH1. All the other verification boreholes were drilled after that and sampling commenced as soon the borehole development was completed for each respective well. The groundwater monitoring boreholes and the background well were sampled before gasifier shutdown and provide a good basis for comparative analysis of the groundwater chemistry of the spent geo-reactor.

The Ca, Mg, Al and Mn time series data is presented in Figure 7-14. The Ca profile shows that most of the boreholes recorded data below the SANS 241:2005 standard except for the groundwater monitoring borehole G2WMD1. The elevated Ca values however dissipated with time and normalised to the levels seen in other wells. There was a single spike (anomalous) value in G2WMD2 in 2014, however this trend did not persist which can be a result of human error or equipment malfunction in the analysis. The magnesium profile is similar to the calcium trend with G2WMD1 the only well with chemistry above the SANS standard. The aluminium profile show several boreholes (G2WMD1, G2WMD2, G2WMD4 and G1VTH1) that breached the upper SANS 241:2005 limit. All of these elevated Al values were once off spikes for the boreholes except for G2WMD1, however the levels of Al were still below 1 mg/l. Manganese profile shows once off spikes for G1VTH1 and G1VH2, however this trend dissipated with time and normalised to the levels seen in other wells which was below the SANS 241:2005 standard.

The Na, Cl, Fe and SO_4 time series data is presented in Figure 7-15. Sodium and Cl recorded very high values for most boreholes. This was expected as the coal seam aquifer is a deep aquifer with saline waters. The trend for the verification boreholes is relatively lower as compared to the background and monitoring boreholes. This is due to the surface water introduced during borehole development and which would have diluted the natural groundwater. Surface water was also introduced to the geo-reactor during quenching, therefore it is expected that wells intercepting the gasification zone will have lower levels of saline elements. The trend however shows a steady recovery to background conditions as most of the verification boreholes recorded higher Na and Cl levels with time. Sulphate trend is similar to Ca and Mg where G2WMD1 recorded relatively high levels with the rest of the boreholes generally trending below the SANS 241:2005 standard. The off-cavity verification boreholes G1VTH1 and G1VH4 had slightly higher value than the SANS 241:2005 standard whilst the verification boreholes intercepting the geo-reactor were generally within the standard. This is possibly due to gasification process which removes sulphur from the coal while the off-cavity boreholes would still contain natural bound sulphur in the unaltered coal seam. The Fe profile shows relatively high levels in G2WMD1 and G1VTH, however this trend dissipated with time and normalised to the levels seen in other wells.

The average major cation/anion proportions for the period 2013 to 2018 are presented on the STIFF diagram in Figure 7-16. The profile of G2WMD1 is anomalously different from all the other coal seam boreholes and is relatively enriched in cations Na/K and anion SO_4. This trend is attributed to the natural conditions within the borehole and not to UCG activities as most of the anomalously trend persisted with time (e.g. Na and SO_4). The water type of G2WMD1 was characteristically isolated from the other boreholes as seen in the Piper diagram and plot in the saline region (Figure 7-16). Other wells that show sodium chloride type water are G2WMD2, G2WMD3, G2WMD4 and G1VH6 while WMD1 is mixed between saline and sodium bicarbonate type water. The other verification boreholes G1VTH1, G1VH3, G1VH2 and G1VH4 are sodium bicarbonate type water due to the surface water influence. There is noticeable anionic clustering for the background borehole (WMD1), which shows slight enrichment in Cl on the Piper diagram (between 40 – 60 %), while G2WMD2 and G2WMD3 show an even higher Cl enrichment of around 80 %. This trend shows that these boreholes are highly saline because of the marine depositional environment.

The Durov plot shows similar trends, and the EC section of the Durov plot is empty since EC was not included as a parameter for water analysis. It is recommended that future groundwater monitoring at the Majuba UCG site include EC to provide a holistic hydro-chemistry profile. The pH trend shows all wells are alkaline and fall within the SANS 241:2005 standard except for the G2WMD2 and G2WMD3 which are highly alkaline (> pH 9.5). This trend is consistent with time and therefore is a result of natural groundwater conditions in two wells. The two cavity boreholes (G1VH3, G1VH2) have a distinct circumneutral pH profile. The pH of the mine water derived from the cavity was 8.06 and the mine water elution tests generally mobilized less alkaline species (e.g. calcium) into solution than the original concentration in the mine water. It was therefore expected that the pH of the boreholes intercepting the cavity to be strongly influenced by the neutral surface water introduced during quenching and therefore have a more neutral pH as compared to the other coal seam boreholes.

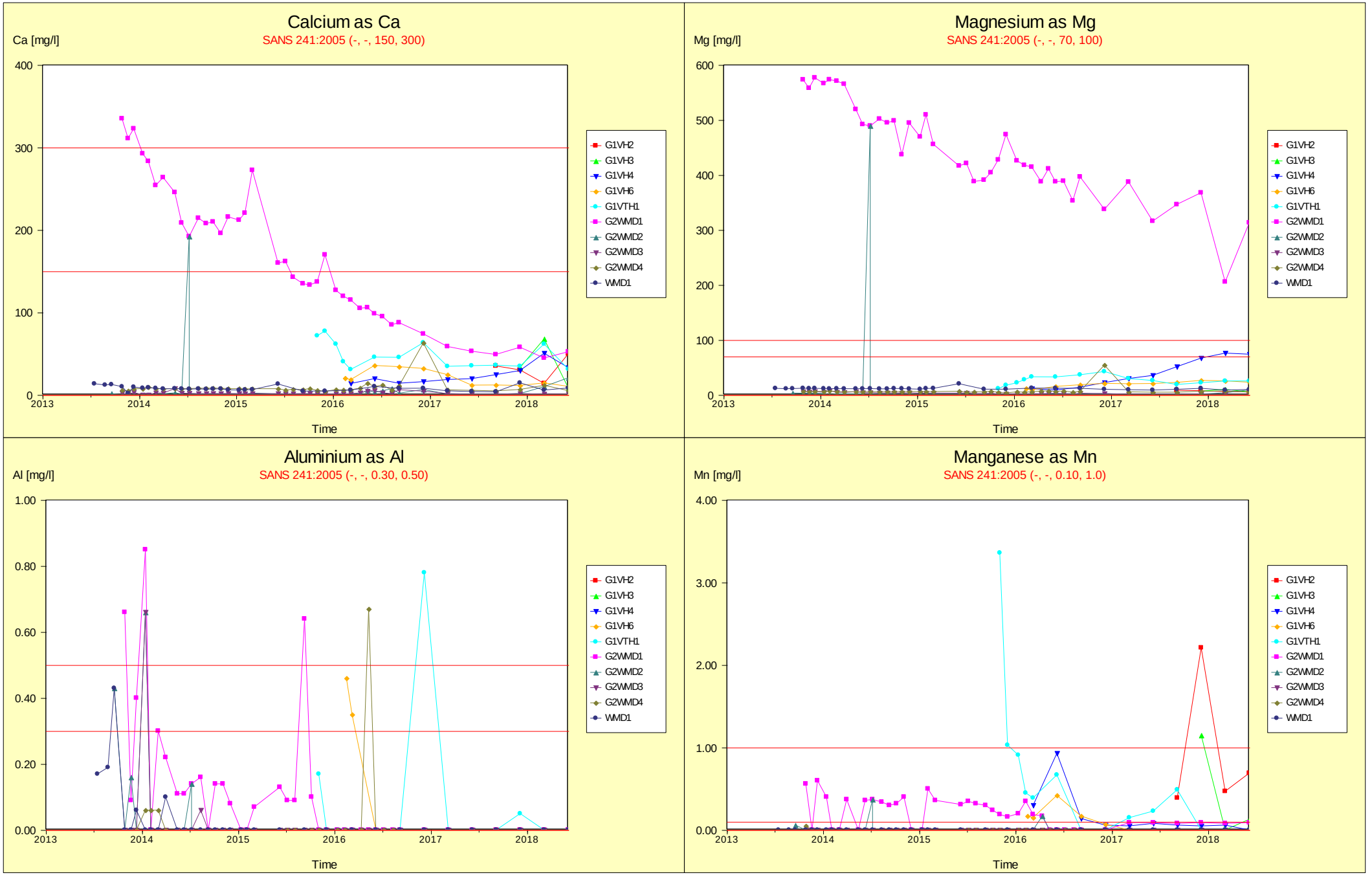

Figure 7-14 Time series data for the coal seam aquifer (Ca, Mg, Al and Mn)

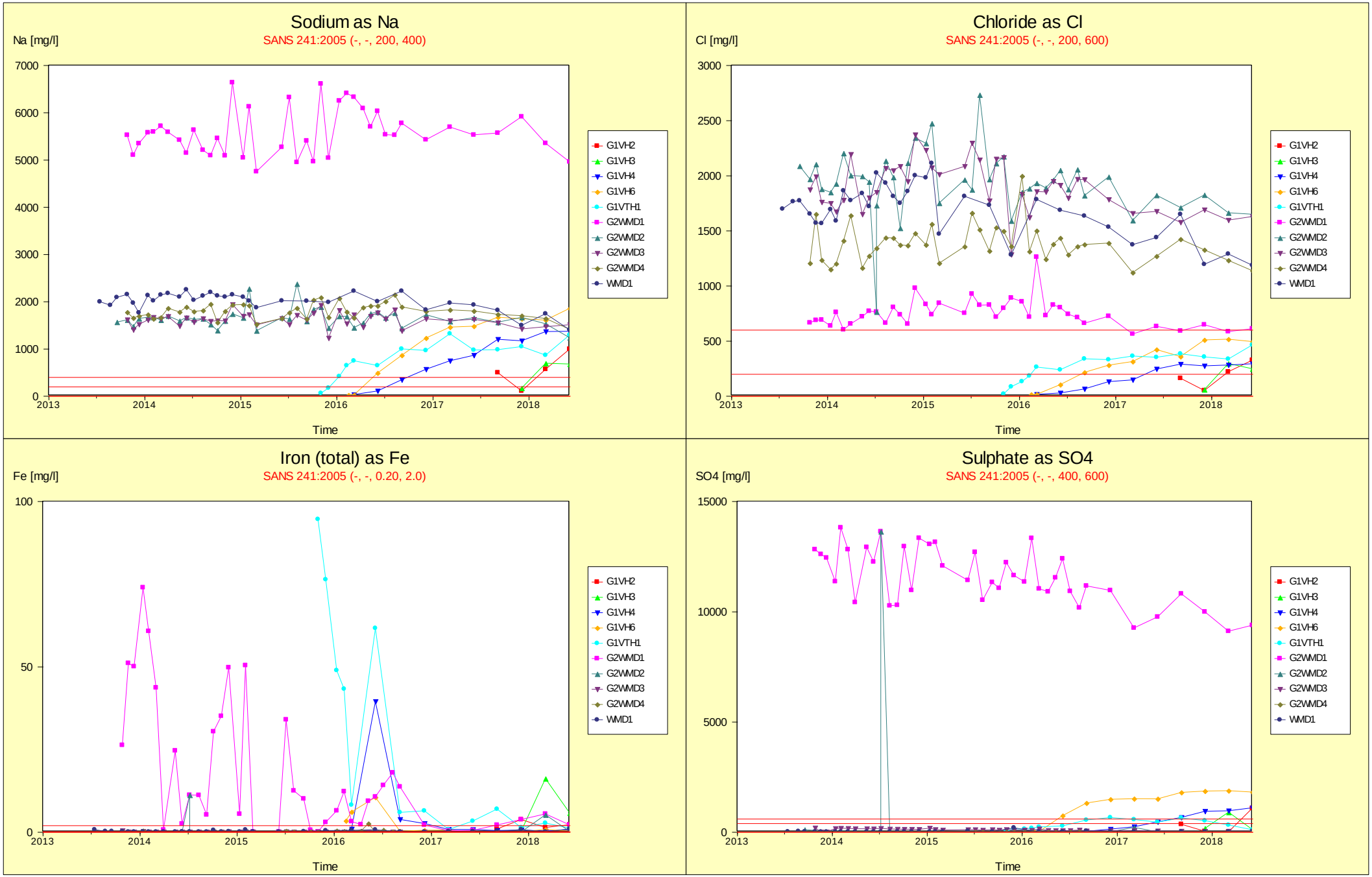

Figure 7-15 Time series data for the coal seam aquifer (Na, Cl, Fe and sulphate)

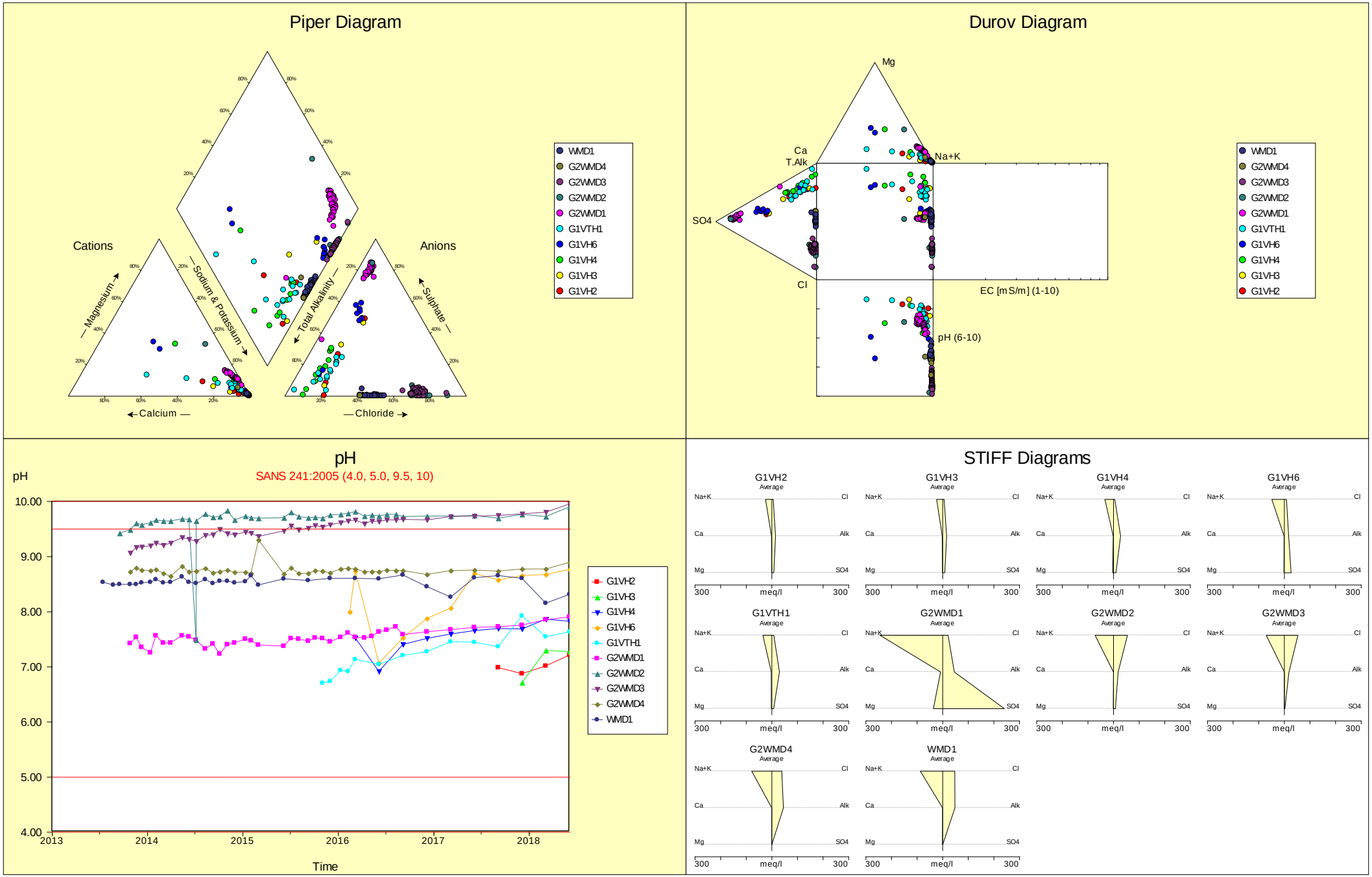

Figure 7-16 Diagnostic plots and pH time series profile, EC was not part of the hydro-chemical parameters analysed from groundwater as displayed in Durov plot.

The time series data does not show any trend that indicates contamination from UCG activities in both the verification boreholes and the groundwater monitoring boreholes. The anomalous trends seen in G2WMD1 are attributed to natural conditions. The groundwater chemistry of the verification boreholes initially signalled surface water chemistry but with time the geochemistry of the groundwater in the geo-reactor is reverting back to background conditions.

7.4 Summary

The conceptual model of the site is supported by the stable isotope and hydrochemistry results. The water from the intermediate upper and intermediate aquifer lower aquifers had a mixture of signatures for the stable isotopes. This corresponds to the leakages depicted in the conceptual model that is associated with a weathered dolerite that is found in the intermediate upper and intermediate aquifer lower aquifers. The deep aquifer is represented by an isotopic signature that is depleted in the heavy isotopes with average values of -41.7‰ and -7.02‰ while the shallow aquifer is enriched with average values of -19.9‰ and -3.3‰ for $\delta^{18}O$ and $\delta^{2}H$ respectively. Therefore the deep aquifer has a distinctive isotopic signature for stable isotopes from the shallower aquifers which confirm that there is no groundwater mixing in these aquifers. Hydro-chemical data plotted in the diagnostic plots (Expanded Durov and STIFF diagram) also show different types of waters: a sodium-chloride water type for the deep aquifer and a sodium-bicarbonate water for the shallow aquifer. The results show that the shallow aquifer and the deep aquifer are not hydraulically connected and therefore it is unlikely that groundwater from the gasification zone would contaminate the shallow aquifer. There were a number of distinct clusters in the anionic section of the Piper diagram which shows that the cavity water is depleted in Cl but enriched in alkalinity. The background borehole was slightly enriched in Cl (40 – 80 %) while two monitoring boreholes (G2WMD2 and G2WMD3) were highly enriched in Cl given the marine depositional environment of the deep aquifer waters.

There was stratification in all the boreholes (monitoring and verification) assessed in terms of EC and temperature. The stratification in EC shows that the quality of water that is sitting on top of the well is better than that in the bottom. This trend suggest that in the event of fractures forming due to roof collapse or any other event that could possibly create a flow path between the cavity water and the shallower strata, the water quality will not be uniform throughout the hydraulic connection. Better water quality will preferentially be at the shallow levels with low quality water concentrated at the bottom. This may be due to chemical processes such as diffusion and needs further investigations. Johnstone et al (2013) found similar trends in groundwater from a underground cavity induced by coal mining. There is a general increase in temperature in the verification borehole. This is a known factor and is expected at UCG sites and it is as a result of heat still contained in the UCG cavity even after gasifier was shut down for a period of two years. The EC profile shows better quality water in the verification borehole as compared to the monitoring boreholes. This could be a dilution effect caused by surface water introduced during quenching. The EC profile results were not related to groundwater transmissive zones in the monitoring boreholes G2WMD1 and G2WMD2. This is due to borehole construction which includes casing for the entire length of the boreholes until the coal seam depth. The variation in salinity is possibly due to diffusion as more saline water was encountered at the coal seam depth and less saline water was situated at the top of the well, away from the coal seam.

The time series data shows no evidence of inorganic contamination from UCG activities. In most cases the water from the verification boreholes were better quality than the background and monitoring boreholes. This is due to surface water that was introduced to the UCG cavity during quenching. The groundwater chemistry in the geo-reactor is reverting to background levels as seen with chloride. The

system in the cavity may have not reached full equilibrium as the data presented only shows three years on monitoring data after the gasifier shutdown. But the chemistry trend shows major elements to be reverting back to background values.

A UCG operation utilizes a lot of boreholes and this information was used to generate a geological model of the site. The geological model contributes to the knowledge gaps regarding one of South African most unexplored coalfield. The geological model shows that this coalfield has vast amounts of coal that can be explored vial UCG or by other methods. The hydrogeological conceptual model of the site correlated to the 3D geological model generated in this chapter.

The next chapter is the synthesis of the thesis and will provide conclusions made from this study. Recommendations will also be presented.

8 Conclusions and recommendations

8.1 Introduction

The aim of the study was to investigate the geochemistry of the likely sources of groundwater contamination from a spent UCG chamber and to examine their potential chemical evolution. The thesis synthesis and conclusions are included to incorporate key findings. The synthesis in this thesis involves uniting all the summaries emanating from different chapters and presenting them into a coherent whole.

8.2 Synthesis

8.2.1 Characterization of the geochemistry of potential sources of groundwater contamination from a spent UCG chamber

The first aim was achieved by undertaking geochemical and mineralogical characterization of UCG residue products (ash, char and heat affected host rock). These products represents source-terms of groundwater contamination from the gasification zone. Residue products were retrieved by two verification boreholes that intercepted the spent geo-reactor. The overburden sections were visibly heat affected with an ash layer, buchite and paralava sections with vast amount of visible vesicles. The underburden did not have any visible pyrometamorphic signs. The majority of the pyrometamorphic features were limited to within 2 m of the overburden-char contact. The QEMSCAN and XRD results showed that most of the primary mineral phases were transformed into high temperature phases including preservation of amorphous material. The following were some of the most prominent transformations:

- Pyrite transformed to pyrrhotite. This alteration was seen by an inverse relationship in the profiles of pyrite and pyrrhotite. As pyrite level reduced the pyrrhotite levels increased beyond background. High temperature crystallization of iron sulphide in the form of pyrrhotite showed crystallization from immiscible segregation of a sulphide melt from a silicate melt as pyrrhotite preferentially formed individual droplets around silica rich glass. This mode of occurrence can increase interaction with groundwater as the segregated sulphide will interact easily with groundwater relative to the original pyrite that was held interstitially between mineral grains.
- High temperature mineralization of cordierite, tridymite and cristobalite was detected in the overburden, which was higher than the background values.
- Elevated levels of mullite were detected in the overburden, which were three orders of magnitude higher than background values. The same trend was observed for sillimanite and anorthite.
- High levels of amorphous material (glass) was detected in the overburden which points to fast cooling (quenched melt) during devitrification.

The mineralogical analysis show that a spent UCG geo-reactor is composed of complex mineral phases and the incoming groundwater post gasification will interact with ash, char, glass and pyrometamorphosed rocks. All of these materials are potential sources of groundwater pollution.

While all mineral phases have the potential to become environmentally harmful, iron sulphides were identified as the phase with the highest potential to adversely affect groundwater due to association with acid generation. This makes all sections of the spent geo-reactor potential sources of groundwater contamination; ash, char, floor and roof sections. These results show that when assessing groundwater risk from any UCG operation, the leaching dynamics of all segments of the geo-reactor should be profiled using appropriate leaching tests.

Ash retrieved from the spent geo-reactor was high in metakaolinite and quartz. This makes it less of an environmental risk to groundwater contamination. Char on the other hand contained sulphide mineralization in the form of pyrrhotite. Pyrite was negligible which suggest that thermal transformations altered iron sulphides to a more stable pyrrhotite. In general, the results confirmed that char and rocks near the gasification zone contain relatively lower pyrite as compared to the pristine lithology. Char showed relatively lower levels of total sulphur as compared to natural coal. This renders char in the geo-reactor more environmentally sustainable, as lower total sulphur content means less risk of acid rock drainage. Cracks within the char were filled with molten material, which was subsequently preserved as glass. The elementary composition was determined by X-ray fluorescence (XRF) and inductively coupled plasma mass spectrometry (ICP-MS). The elementary composition varied across the different UCG residue products and this was attributed to the heterogeneous nature of trace elements in coal, which then means that products of thermal processing will also have a diversified trace element content. Rebounding groundwater in the spent geo-reactor is then expected to leach, dissolve, precipitate and adsorb a wide range of elements which all can lead to groundwater contamination. The second aim of the study was to deal with the water-rock interactions.

8.2.2 Assessment of the chemical evolution of potential groundwater contaminants from the UCG process.

The second aim of the study had three integrated tasks:

- Task 1: The assessment of the water-rock geochemistry through leaching tests under different chemical environments. This task was achieved by subjecting different sections of the geo-reactor to leaching by the following mediums: deionized water, hydrogen peroxide and sulphuric acid. The mine water elution tests were included to provide field representative investigations at temperatures recorded in the spent UCG geo-reactor. The following were the main observations and conclusions:

  - Elements showed a pH-dependent solubility as seen by the general negative correlation factor for each element. The water elution tests (no pH buffer), released the lowest concentrations of ionic species into solution and had an alkaline final pH in most cases. The water elution results were in the main, one or several orders of magnitude lower than the other elution tests results. Although deionized water is not representative of the site groundwater chemistry, it provides a good base for understanding the leaching dynamics in a spent UCG geo-reactor as it does not impose pH conditions on the samples.
  - The peroxide leaching results recorded lower final pH levels as compared to the water elution results and consequently the solubility of elements increased. Peroxide elution induces full solution oxidation and this is the basis for acid rock drainage associated with

coal mining. The decrease in pH is attributed to the oxidation of sulphide minerals which acidify the solution thereby increasing the solubility of metals and non-metals.

- Acid elution was incorporated to assess the leaching dynamics in the spent UCG geo-reactor if ARD conditions developed. The average pH recorded was 1.79 and the highest mobilization of elements was recorded under this leaching medium which represents the "worst case scenario" that the geo-reactor can encounter. Chemical dissociation of carbonates and silicates phases failed to buffer or counter the acidity by consuming the hydrogen that is responsible for the low pH. It is therefore recommended that any spent UCG geo-reactor must be periodically monitored to ensure that the pH does not drop below 4.
- The mine water elution was incorporated to assess leaching dynamics under field conditions as water-rock interactions were subjected to experimental temperatures of 25 and 70 °C, respectively. The following elements showed general decrease in concentration with increase in temperature Mn, Fe, Ni, Sr, Ca, Mg, V and SO_4. Dissolved concentrations of the major elements in silicate rocks are usually restricted in groundwater by the formation of secondary minerals of low solubility. The following elements showed general increase in concentration with increase in temperature: B, K, Cu, and SO_4.
- Contaminant migration due to dissociation of elements between groundwater and the surface of solids in an aquifer was demonstrated by the distribution coefficient. The heat-affected roof released the most metals into solution at 25 °C while the highest number of metals mobilized into solution at 70 °C were both from the roof and char samples. Aluminium and Fe were the main non-mobile elements across all sections of the geo-reactor and their relative mobility was not affected by change in experimental temperature. The semi mobile metals were Ba, Ni, Cu, Mn, V while metals with a great affinity to leach into the water phase were Sr, V, Co, Mn, Cu, Ba, Pb. The high elution of Pb from char samples at higher temperatures is an environmental concern, as generally this element was not mobilized from other sections of the geo-reactor from both deionized water and mine water eluates, which indicates that temperature plays a role in dissolving Pb from the organic surfaces.

- Task 2: Assessment of potential acid rock drainage from gasification products.

  - Acid base accounting was used as a predictive tool to assess the acid producing capacity of the spent geo-reactor. The NNP (net neutralising potential) was calculated in terms of the difference between acid producing (AP) and neutralising potential (NP). The analysis utilized both the acid base accounting (ABA) and net acid generation (NAG) methods of acid generation prediction. Utilizing both NNP and NAG tests for assessment of acid generation from earth material provides a more reliable evaluation technique than either test used alone. NNP characterized around 13% of samples as acid generating with only 7.5% as non-acid generating. NAG classified 26 samples (49%) as high acid generating while only 13 (24.5%) was characterized as non-acid generating. The low risk acid generation constituted 26.9% of samples. About 20% of samples had enough oxidisable Sulphide-S to maintain acidic conditions. In general, acid generation is possible in a spent geo-reactors, however, UCG operations are usually at great depths (>200 mbgl) where there might not be sufficient sources of oxygen for effective oxidation of sulphide minerals. Furthermore, the high temperature in the chamber is likely to eliminate any

bacterial that also forms part of the acid rock drainage development. However, oxygenated water can be introduced into the chamber during quenching or through drainage of shallow aquifers via hydraulic connections with the spent geo-reactor. It is therefore recommended that dissolved oxygen (DO) and pH be monitored in groundwater monitoring boreholes around a spent geo-reactor.

- Task 3: Field assessments relating to groundwater chemistry and evolution cycles.

  - The risk to groundwater contamination from UCG activities was assessed in terms of the source-pathway-receptor model. The spent geo-reactor was identified as the source, as it houses the residue material that contain toxic species as determined by the mineralogical assessment and leaching tests. The pathway was divided into two; (1) a borehole intercepting the spent geo-reactor which provided a vertical pathway from the coal seam aquifer to the overlying aquifers. (2) the in-seam groundwater pathway (lateral extent) that was assessed by monthly groundwater data from the coal seam aquifer taken from monitoring boreholes and compared with background.
  - The stable isotope and hydrochemistry results showed that the shallow aquifer and the deep aquifer were not hydraulically connected and therefore it is unlikely that groundwater from the gasification zone would contaminate the shallow aquifer. The deep aquifer had a distinct isotopic signature from the shallow aquifer, which confirms that there was no groundwater mixing between these aquifers.
  - There was stratification in all the boreholes (monitoring and verification) as determined by EC and temperature profiling. The EC profile showed that the quality of water sitting on top of the well was better than that in the bottom. This trend suggest that in the event of fractures forming due to roof collapse or any other event that could possibly create a flow path between the cavity water and the shallow strata, the water quality will not be uniform throughout the hydraulic connection. Better water quality will preferentially be at the shallow levels with low quality water concentrated at the bottom.
  - The time series data displayed the chemical evolution of the coal seam aquifer. The results showed no evidence of inorganic contamination from UCG activities. In most cases, the water from the verification boreholes was of better quality than background and monitoring boreholes. This is due to surface water that was injected into the UCG cavity during quenching. The groundwater chemistry in the geo-reactor showed a trend of reverting to background levels.

This study has contributed to advancing the geochemical understanding of the spent UCG geo-reactor. This study has successfully reconstructed the temperature profile during gasification using both mineralogical assessment of rocks and petrography of char. This study has also contributed to the understanding of rock-water interactions that a spent UCG chamber undergoes taking into account field conditions. The study has also addressed the question around the potential of acid rock drainage emanating from UCG activities. This study has also uncovered the chemical evolution of UCG geo-reactors and their ability to revert back to background groundwater chemistry with time. All of these observations provide a comprehensive assessment of the risk to groundwater emanating from UCG activities. This comprehensive assessment is presented below in an integrated risk profile that can be utilized for any UCG operation in the world.

8.3 Integrated groundwater risk assessment model for UCG sites

The knowledge attained through this work has provided for a simple but comprehensive groundwater risk assessment for a spent UCG chamber via an integrated model. The model follows the source-pathway-receptor arrangement where groundwater contamination sources are identified as ash, char, roof and floor (Figure 8-1). The risk to groundwater pollution is then assessed by subjecting these sources to the following tests; mineralogical and elemental analysis, petrography and chemical assessment, leaching tests and acid generation assessments. Post gasification groundwater enters the spent geo-reactor and is able to transport contaminants to secondary locations. The pathways that pollution from the UCG geo-reactor can be transmitted through were identified as; natural faults, heat induced fractures, boreholes, local aquifers. All these pathways will have to be assessed for hydraulic connections with the spent geo-reactor via stable isotopes, hydrochemistry and stratification analysis. Finally, the receptor aquifers (e.g. shallow aquifer) will have to be monitored periodically to determine if contamination has occurred. This is summarized by a simple flow diagram showing the integrated groundwater risk assessment model, that can be followed for any UCG site (Figure 8-2).

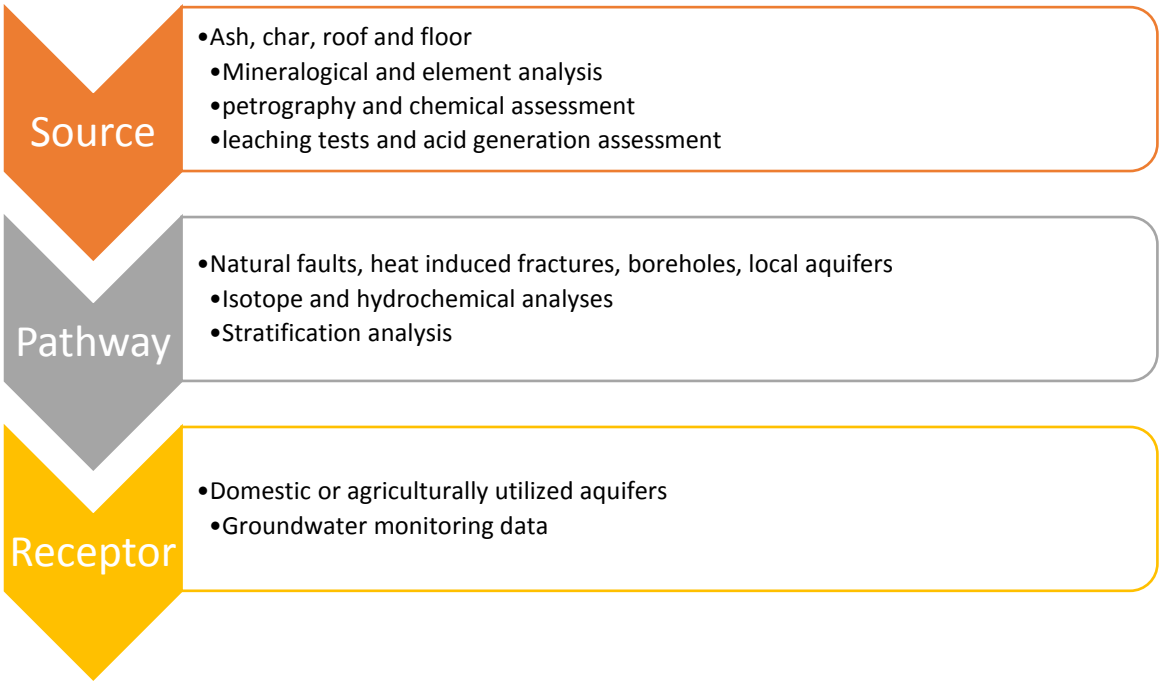

Figure 8-1 integrated groundwater risk assessment model for UCG sites

The flow diagram can be expanded to bring the analyses to a risk test (Figure 8-2). After identifying sources of groundwater contamination at UCG sites and performing the analytical tests, the model can then subject the process to a risk assessment. If for example, the analytical leaching results show unacceptably high levels of toxic cation release, then those sources will be profiled to pose a "groundwater risk". However if negligible mobilization is recorded, then the risk test will report "no groundwater risk" and hence no further investigation is needed. Where sources of groundwater contamination have been verified, then existence of pathways to receptors will have to be established. If no pathway exit, then the risk test will report "no groundwater risk" and hence no further investigation is necessary. However is pathways do exist then those channels will have to be examined using appropriate methods including but not limited to stable isotopes, hydrochemistry and

stratification analysis in order to establish the groundwater risk. If the connection do not pose any risk, then no further investigation is necessary.

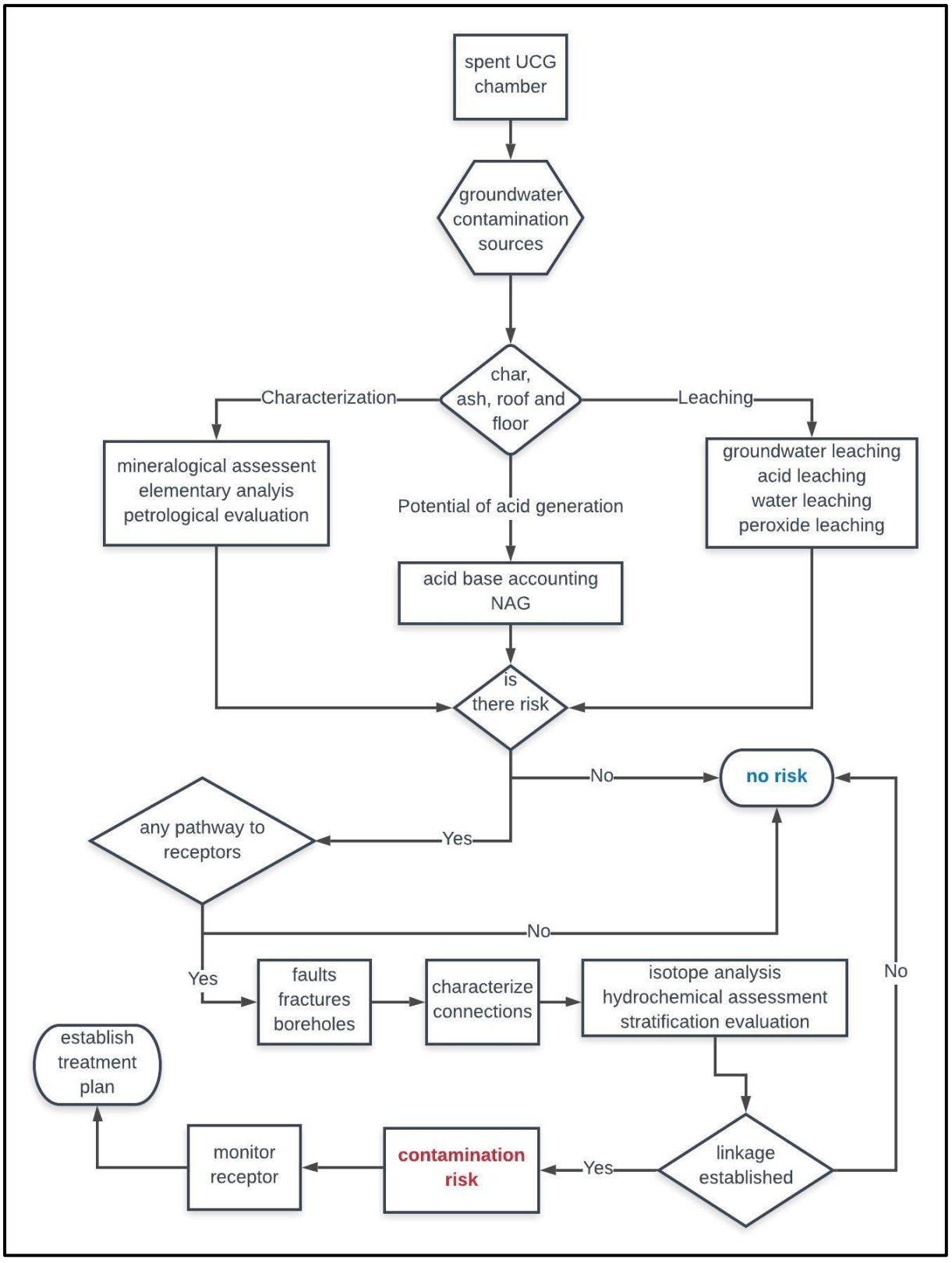

Figure 8-2 Expanded integrated groundwater risk assessment model for UCG sites

However if the connection prove that elements are indeed transmittable between the source and the receptor then the model will report that contamination is a real possibility and periodic monitoring of the receptor should be implemented, taking into account the risk profile of the source. A treatment plan for the spent UCG geo-reactor should then be established and implemented to avoid contamination of the receptor.

This research has laid a firm foundation in understanding groundwater contamination from UCG operations. The study however had limitations that can be explored by further research, especially for new UCG operations where background geochemistry can be comprehensively conducted before the gasification stage. Hopefully this research can go some way in helping UCG operators and regulators in conducting their work effectively and to provide confidence in decision making especially regarding groundwater matters.

Three papers have been published from this study and are presented in Appendix 8-A.

8.4 Recommendations and further research

With the knowledge that has been gathered from this work, the following recommendations for further studies are proposed:

- This research was commissioned by Eskom UCG team to assess the geochemistry of the spent geo-reactor. This study only was limited to the inorganic constituents of the spent geo-reactor and another Ph D study focused on the organic portion. It is recommended that both studies be integrated into a summary report highlighting the most important findings and presented in a journal article or conference proceedings.
- This study was not able to conduct kinetic tests for acid generation. This was due to having retrieved only small portions of UCG residue material from core drills. Kinetic tests require bigger samples (i.e. > 1 kg) and longer testing periods (>6 months) in order to successfully complete the assessment. Information from kinetic tests provide important input data for geochemical modelling. It is therefore recommended that the next core drills be dedicated solely for kinetic tests in order to comprehensive understanding of leaching dynamics with time factor added.
- Geochemical modelling of the geo-reactor should be undertaken as soon as kinetic information is available as this will provide a tool to predict the geochemical evolution in UCG post gasification.
- The geological model shows that the area has huge coal reserves. The decision to halt conventional mining in the study area during the 1980's whereby exploration boreholes were spaced far apart and decisions on the geology may have been erroneously made. With this new knowledge, it is recommended that the area be reassessed for possible coal exploration by conventional mining and UCG.

References

Ahern, J. J. and Frazier, J. A. (1982) *Water quality changes at underground coal gasification sites – A literature review*, Laramie, Wyoming: Water Resources Research Institute University of Wyoming.

Antonijević, M. M., Dimitrijević, M. and Janković, Z. (1997) 'Leaching of pyrite with hydrogen peroxide in sulphuric acid', *Hydrometallurgy,* 46(1), pp. 71-83.

Ayadi, Y., Mokadem, N., Besser, H., Khelifi, F., Harabi, S., Hamad, A., Boyce, A., Laouar, R. and Hamed, Y. (2018) 'Hydrochemistry and stable isotopes (δ18O and δ2H) tools applied to the study of karst aquifers in southern mediterranean basin (Teboursouk area, NW Tunisia)', *Journal of African Earth Sciences,* 137, pp. 208-217.

Ballhaus, C., Gee, C. T., Bockrath, C., Greef, K., Mansfeldt, T. and Rhede, D. (2012) 'The silicification of trees in volcanic ash - An experimental study', *Geochimica et Cosmochimica Acta,* 84, pp. 62-74.

Bhutto, A. W., Bazmi, A. A. and Zahedi, G. (2013) 'Underground coal gasification: From fundamentals to applications', *Progress in Energy and Combustion Science,* 39(1), pp. 189-214.

Blatt, H., Tracy, R. J. and Owens, B. E. (1996) *Petrology: igneous, sedimentary and metamorphic. Second edition.* New York: W.H. Freeman.

Blinderman, M. S., Blinderman, A. and Taskaev, A. (2018) '12 - What makes a UCG technology ready for commercial application?', in Blinderman, M.S. & Klimenko, A.Y. (eds.) *Underground Coal Gasification and Combustion*: Woodhead Publishing, pp. 403-434.

Blinderman, M. S. and Klimenko, A. Y. (2018) '1 - Introduction to underground coal gasification and combustion', in Blinderman, M.S. & Klimenko, A.Y. (eds.) *Underground Coal Gasification and Combustion*: Woodhead Publishing, pp. 1-8.

Bockhorn, H. (2018) '7 - Gasification kinetics', in Blinderman, M.S. & Klimenko, A.Y. (eds.) *Underground Coal Gasification and Combustion*: Woodhead Publishing, pp. 213-252.

Bouzahzah, H., Benzaazoua, M., Plante, B. and Bussiere, B. (2015) 'A quantitative approach for the estimation of the “fizz rating” parameter in the acid-base accounting tests: A new adaptations of the Sobek test', *Journal of Geochemical Exploration,* 153, pp. 53-65.

Brunauer, G., Frey, F., Boysen, H. and Schneider, H. (2001) 'High temperature thermal expansion of mullite: an in situ neutron diffraction study up to 1600°C', *Journal of the European Ceramic Society,* 21(14), pp. 2563-2567.

Budkewitsch, P. and Robin, P.-Y. (1994) 'Modelling the evolution of columnar joints', *Journal of Volcanology and Geothermal Research,* 59(3), pp. 219-239.

Bunt, J. R., Wagner, N. J. and Waanders, F. B. (2009) 'Carbon particle type characterization of the carbon behaviour impacting on a commercial-scale Sasol-Lurgi FBDB gasifier', *Fuel,* 88(5), pp. 771-779.

Busse, J., de Dreuzy, J. R., Galindo Torres, S., Bringemeier, D. and Scheuermann, A. (2017) 'Image processing based characterisation of coal cleat networks', *International Journal of Coal Geology,* 169, pp. 1-21.

Cadle, A. B., Cairncross, B., Christie, A. D. M. and Roberts, D. L. (1993) 'The Karoo Basin of South Africa: type basin for the coal-bearing deposits of southern Africa', *International Journal of Coal Geology,* 23(1), pp. 117-157.

Cairncross, B. (2001) 'An overview of the Permian (Karoo) coal deposits of southern Africa', *Journal of African Earth Sciences,* 33(3), pp. 529-562.

Camp, D. W. (2018) '4 - Underground coal gasification research and development in the United States, in Blinderman, M.S. & Klimenko, A.Y. (eds.) *Underground Coal Gasification and Combustion*: Woodhead Publishing, pp. 59-127.

Catuneanu, O., Wopfner, H., Eriksson, P. G., Cairncross, B., Rubidge, B. S., Smith, R. M. H. and Hancox, P. J. (2005) 'The Karoo basins of south-central Africa', *Journal of African Earth Sciences,* 43(1), pp. 211-253.

Chapman, G. and Cairncross, B. (1992) 'The sedimentology of the Majuba Coalfield, Permian Vryheid Formation, southeastern Transvaal, South Africa', *Geocongress 92. Geol. Soc. S.A. Biennial Congress,* Bloemfontein, Extended Abstract, pp. 71-74.

Chirita, P. (2009) 'Hydrogen Peroxide Decomposition by Pyrite in the Presence of Fe(III)-ligands', *Chemical and Biochemical Engineering,* Quarterly 23(3), pp. 259-265.

Ciesielczuk, J., Kruszewski, Ł. and Majka, J. (2015) 'Comparative mineralogical study of thermally-altered coal-dump waste, natural rocks and the products of laboratory heating experiments', *International Journal of Coal Geology,* 139, pp. 114-141.

Clark, I. and Fritz, P. (1997) *Environmental Isotopes in Hydrogeology,* Raton, CRC press.

Craig, H. and Gordon, L.I. 1965. Deuterium and oxygen 18 variations in the ocean and the marine atmosphere. Proceedings of Stable Isotopes in Oceanographic Studies and Paleotemperatures, Laboratorio di Geologia Nucleate, Spoleto, Italy. Tongiogi, E. (ed.). V. Lishi e F., Pisa. pp. 9–130.

de Oliveira, D. P. S. and Cawthorn, R. G. (1999) 'Dolerite intrusion morphology at Majuba Colliery, northeast Karoo Basin, Republic of South Africa', *International Journal of Coal Geology,* 41(4), pp. 333-349.

de Souza, Z. S., Wang, C., Jin, Z.-M., Li, J.-W., Yang, J., Botelho, N. F., Viana, R. R., dos Santos, L., Liu, P.-L. and Li, W. (2019) 'Pyrometamorphic aureoles of Cretaceous sandstones and shales by Cenozoic basic intrusions, NE Brazil: Petrograhic, textural, chemical and experimental approaches', *Lithos,* 326-327, pp. 90-109.

Deutsch, W. J. (1997) *Groundwater geochemistry: fundamentals and applications to contamination.* Boca Raton: Lewis Publishers Inc.

Dold, B. (2017) 'Acid rock drainage prediction: A critical review', *Journal of Geochemical Exploration,* 172, pp. 120-132.

Dvornikova, E. V. (2018) '8 - The role of groundwater as an important component in underground coal gasification', in Blinderman, M.S. & Klimenko, A.Y. (eds.) *Underground Coal Gasification and Combustion*: Woodhead Publishing, pp. 253-281.

Elghali, A., Benzaazoua, M., Bouzahzah, H., Bussière, B. and Villarraga-Gómez, H. (2018) 'Determination of the available acid-generating potential of waste rock, part I: Mineralogical approach', *Applied Geochemistry,* 99, pp. 31-41.

Fan, Q., Feng, X., Weng, W., Fan, Y. and Jiang, Q. (2017) 'Unloading performances and stabilizing practices for columnar jointed basalt: A case study of Baihetan hydropower station', *Journal of Rock Mechanics and Geotechnical Engineering,* 9(6), pp. 1041-1053.

Finkelman, R. B., Palmer, C. A. and Wang, P. (2018) 'Quantification of the modes of occurrence of 42 elements in coal', *International Journal of Coal Geology,* 185, pp. 138-160.

Flint, S. S., Hodgson, D. M., Sprague, A. R., Brunt, R. L., Van der Merwe, W. C., Figueiredo, J., Prélat, A., Box, D., Di Celma, C. and Kavanagh, J. P. (2011) 'Depositional architecture and sequence stratigraphy of the Karoo basin floor to shelf edge succession, Laingsburg depocentre, South Africa', *Marine and Petroleum Geology,* 28(3), pp. 658-674.

Frost, B. R. and Frost, C. D. (2014) *Essentials of igneous and metamorphic petrology.* New York: Cambridge University Press.

Ghasemi, E., Ataei, M., Shahriar, K., Sereshki, F., Jalali, S. E. and Ramazanzadeh, A. (2012) 'Assessment of roof fall risk during retreat mining in room and pillar coal mines', *International Journal of Rock Mechanics and Mining Sciences,* 54, pp. 80-89.

Goodall, W. R., Scales, P. J. and Butcher, A. R. (2005) 'The use of QEMSCAN and diagnostic leaching in the characterisation of visible gold in complex ores', *Minerals Engineering,* 18(8), pp. 877-886.

Gordon, J.J., Edward, T.W.D., Bursey, G.G., and Prowse, T.D. 1993. Estimating evaporation using stable isotopes: Quantitative results and sensitivity analysis for two catchments in northern Canada. Nordic Hydrology, vol. 24. pp. 79–94.

Govere, J.M., Durrheima, D.N., Coetzee, M., and HUNT, R.H. 2001. Malaria in Mpumalanga Province, South Africa, with special reference to the period 1987–1999. South African Journal of Science, vol. 97, no. 1–2. pp. 55–58.

Grapes, R. (2011) *Pyrometamorphism.* Second edn. Berlin Heidelberg: Spriner-Verlag.

Grapes, R., Zhang, K. and Peng, Z.-l. (2009) 'Paralava and clinker products of coal combustion, Yellow River, Shanxi Province, China', *Lithos,* 113(3), pp. 831-843.

Gupta, N., Gedam, V. V., Moghe, C. and Labhasetwar, P. (2017) 'Investigation of characteristics and leaching behavior of coal fly ash, coal fly ash bricks and clay bricks', *Environmental Technology & Innovation,* 7, pp. 152-159.

Hageman, P. L., Seal, R. R., Diehl, S. F., Piatak, N. M. and Lowers, H. A. (2015) 'Evaluation of selected static methods used to estimate element mobility, acid-generating and acid-neutralizing potentials associated with geologically diverse mining wastes', *Applied Geochemistry,* 57, pp. 125-139.

Hancox, P. J. and Götz, A. E. (2014) 'South Africa's coalfields — A 2014 perspective', *International Journal of Coal Geology,* 132, pp. 170-254.

Hatherly, P. (2013) 'Overview on the application of geophysics in coal mining', *International Journal of Coal Geology,* 114, pp. 74-84.

Hochella, M. F., Moore, J. N., Golla, U. and Putnis, A. (1999) 'A TEM study of samples from acid mine drainage systems: metal-mineral association with implications for transport', *Geochimica et Cosmochimica Acta,* 63(19), pp. 3395-3406.

Holness, M. B. and Watt, G. R. (2001) 'Quartz recrystallization and fluid flow during contact metamorphism: a cathodoluminescence study', *Geofluids,* 1(3), pp. 215-228.

Humenick, M. J. and Mattox, C. F. (1978) 'Groundwater pollutants from underground coal gasification', *Water Research,* 12(7), pp. 463-469.

Imran, M., Kumar, D., Kumar, N., Qayyum, A., Saeed, A. and Bhatti, M. S. (2014) 'Environmental concerns of underground coal gasification', *Renewable and Sustainable Energy Reviews,* 31, pp. 600-610.

Izquierdo, M. and Querol, X. (2012) 'Leaching behaviour of elements from coal combustion fly ash: An overview', *International Journal of Coal Geology,* 94, pp. 54-66.

Jeffrey, L. S. (2005) 'Characterization of the coal resources of South Africa', *Journal of The South African Institute of Mining and Metallurgy,* 105(2), pp. 95-102.

Jiang, L., Chen, Z. and Farouq Ali, S. M. (2018) 'General hydro-geological impact of cleats on underground coal gasification', *Fuel,* 224, pp. 128-137.

Jiskani, I. M., Siddiqui, F. I. and Pathan, A. G. (2018) 'Integrated 3D geological modeling of Sonda-Jherruck coal field, Pakistan', *Journal of Sustainable Mining,* 17(3), pp. 111-119.

Johnson, M. R., Anhaeusser, C. R., Thomas, R. J., Geological Society of South, A. and Council for, G. (2006) *The geology of South Africa.* Pretoria; Johannesburg: Council for Geoscience ; Geological Society of South Africa and Council for Geoscience, p. 461-499.

Johnson, M. R., Vuuren, C. J. V., Visser, J. N. J., Cole, D. I., Wickens, H. D. V., Christie, A. D. M. and Roberts, D. L. (1997) 'Chapter 12 The foreland karoo basin, south africa', in Selley, R.C. (ed.) *Sedimentary Basins of the World*: Elsevier, pp. 269-317.

Johnstone, A., Dennis, I. and McGeorge, N. (2013) 'Groundwater Stratification and Impact on Coal Mine Closure', *13th Biennial Groundwater Division Conference*, Durban.

Jones, K. B., Ruppert, L. F. and Swanson, S. M. (2012) 'Leaching of elements from bottom ash, economizer fly ash, and fly ash from two coal-fired power plants', *International Journal of Coal Geology,* 94, pp. 337-348.

Kapusta, K. and Stańczyk, K. (2011) 'Pollution of water during underground coal gasification of hard coal and lignite', *Fuel,* 90(5), pp. 1927-1934.

Kapusta, K. and Stańczyk, K. (2015) 'Chemical and toxicological evaluation of underground coal gasification (UCG) effluents. The coal rank effect', *Ecotoxicology and Environmental Safety,* 112, pp. 105-113.

Kapusta, K., Stańczyk, K., Wiatowski, M. and Chećko, J. (2013) 'Environmental aspects of a field-scale underground coal gasification trial in a shallow coal seam at the Experimental Mine Barbara in Poland', *Fuel,* 113, pp. 196-208.

Kristensen, T. J., Andrews, T. D., MacKay, G., Gotthardt, R., Lynch, S. C., Duke, M. J. M., Locock, A. J. and Ives, J. W. (2019) 'Identifying and sourcing pyrometamorphic artifacts: Clinker in subarctic North America and the hunter-gatherer response to a Late Holocene volcanic eruption', *Journal of Archaeological Science: Reports,* 23, pp. 773-790.

Kühnel, R. A., Schmit, C. R., Eylands, K. E. and McCarthy, G. J. (1993) 'Comparison of the pyrometamorphism of clayey rocks during underground coal gasification and firing of structural ceramics', *Applied Clay Science,* 8(2), pp. 129-146.

Liu, G., Peng, Z., Yang, P. and Wang, G. (2001) 'Sulfur in coal and its environmental impact from Yanzhou mining district, China', *Chinese Journal of Geochemistry,* 20(3), pp. 273.

Liu, S.-q., Li, J.-g., Mei, M. and Dong, D.-l. (2007) 'Groundwater Pollution from Underground Coal Gasification', *Journal of China University of Mining and Technology,* 17(4), pp. 467-472.

Llorens, J. F., Fernández-Turiel, J. L. and Querol, X. (2001) 'The fate of trace elements in a large coal-fired power plant', *Environmental Geology,* 40(4), pp. 409-416.

Love, D., Beeslar, M. J., Blinderman, M. S., Pershad, S. and Van der Riet, M. (2014) 'Ground water monitoring and management in Underground Coal Gasification'. *Unconventional gas – just the facts, Groundwater Division of the Geological Society of South Africa & Mine Water Division of the Water Institute of South Africa*, Pretoria, South Africa.

Lurie, J. (2008) *South African Geology for Mining, Metallurgical, Hydrological and Civil Engineering.* Lupon Pub.

Malumbazo, N., Wagner, N. J. and Bunt, J. R. (2012) 'The petrographic determination of reactivity differences of two South African inertinite-rich lump coals', *Journal of Analytical and Applied Pyrolysis,* 93, pp. 139-146.

Malumbazo, N., Wagner, N. J. and Bunt, J. R. (2013) 'The impact of particle size and maceral segregation on char formation in a packed bed combustion unit', *Fuel,* 111, pp. 350-356.

Meij, R. (1994) 'Trace element behavior in coal-fired power plants', *Fuel Processing Technology,* 39(1), pp. 199-217.

Menezes, C. P., Bezerra, F. H. R., Balsamo, F., Mozafari, M., Vieira, M. M., Srivastava, N. K. and de Castro, D. L. (2019) 'Hydrothermal silicification along faults affecting carbonate-sandstone units and its impact on reservoir quality, Potiguar Basin, Brazil', *Marine and Petroleum Geology*.

Mishra, V., Bhowmick, T., Chakravarty, S., Varma, A. K. and Sharma, M. (2016) 'Influence of coal quality on combustion behaviour and mineral phases transformations', *Fuel,* 186, pp. 443-455.

Mocek, P., Pieszczek, M., Świądrowski, J., Kapusta, K., Wiatowski, M. and Stańczyk, K. (2016) 'Pilot-scale underground coal gasification (UCG) experiment in an operating Mine "Wieczorek" in Poland', *Energy,* 111, pp. 313-321.

Mokhahlane, L. S., Gomo, M. and Vermeulen, D. (2018) 'Acid-base accounting of unburned coal from underground coal gasification at Majuba pilot plant', *Journal of the Southern African Institute of Mining and Metallurgy,* 118(10), pp. 1041-1046.

Nazari, A. M., Ghahreman, A. and Bell, S. (2017) 'A comparative study of gold refractoriness by the application of QEMSCAN and diagnostic leach process', *International Journal of Mineral Processing,* 169, pp. 35-46.

Nesse, W. D. (2000) *Introduction to Mineralogy.* Oxford University Press.

O'Connor, A. E., Luek, J. L., McIntosh, H. and Beck, A. J. (2015) 'Geochemistry of redox-sensitive trace elements in a shallow subterranean estuary', *Marine Chemistry,* 172, pp. 70-81.

Parbhakar-Fox, A. and Lottermoser, B. G. (2015) 'A critical review of acid rock drainage prediction methods and practices', *Minerals Engineering,* 82, pp. 107-124.

Perkins, G. (2018a) 'Underground coal gasification – Part I: Field demonstrations and process performance', *Progress in Energy and Combustion Science,* 67, pp. 158-187.
Perkins, G. (2018b) 'Underground coal gasification – Part II: Fundamental phenomena and modeling', *Progress in Energy and Combustion Science,* 67, pp. 234-274.
Pershad, S., Pistorius, J. and van der Riet, M. (2018a) '14 - Majuba underground coal gasification project', in Blinderman, M.S. & Klimenko, A.Y. (eds.) *Underground Coal Gasification and Combustion*: Woodhead Publishing, pp. 469-502.
Pershad, S., van der Riet, M., Brand, J., van Dyk, J., Love, D., Feris, J., Strydom, C. A. and Kauchali, S. (2018b) 'SAUCGA: The potential, role, and development of underground coal gasification in South Africa', *Journal of the Southern African Institute of Mining and Metallurgy,* 118, pp. 1009-1019.
Philpotts, A. and Ague, J. (2009) *Principles of Igneous and Metamorphic Petrology.* 2 edn. Cambridge: Cambridge University Press.
Quintero, J. A., Candela, S. A., Ríos, C. A., Montes, C. and Uribe, C. (2009) 'Spontaneous combustion of the Upper Paleocene Cerrejón Formation coal and generation of clinker in La Guajira Peninsula (Caribbean Region of Colombia)', *International Journal of Coal Geology,* 80(3), pp. 196-210.
Qureshi, A., Maurice, C. and Öhlander, B. (2016) 'Potential of coal mine waste rock for generating acid mine drainage', *Journal of Geochemical Exploration,* 160, pp. 44-54.
Roddy, D. J. and Younger, P. L. (2010) 'Underground coal gasification with CCS: a pathway to decarbonising industry', *Energy & Environmental Science,* 3(4), pp. 400-407.
Róg, L. (2018) 'Vitrinite reflectance as a measure of the range of influence of the temperature of a georeactor on rock mass during underground coal gasification', *Fuel,* 224, pp. 94-100.
Ryuh, Y.-G., Do, H.-K., Kim, K.-H. and Yun, S.-T. (2017) 'Vertical Hydrochemical Stratification of Groundwater in a Monitoring Well: Implications for Groundwater Monitoring on CO2 Leakage in Geologic Storage Sites', *Energy Procedia,* 114, pp. 3863-3869.
Simate, G. S. and Ndlovu, S. (2014) 'Acid mine drainage: Challenges and opportunities', *Journal of Environmental Chemical Engineering,* 2(3), pp. 1785-1803.
Snyman, C. P. (1998) 'Coal in the mineral resources of South Africa', *Handbook, council for geoscience,* 16, pp. 136-205.
Soukup, K., Hejtmánek, V., Čapek, P., Stanczyk, K. and Šolcová, O. (2015) 'Modeling of contaminant migration through porous media after underground coal gasification in shallow coal seam', *Fuel Processing Technology,* 140, pp. 188-197.
Stewart, W. A., Miller, S. D. and Smart, R. 'Advances in acid mine drainage (ARD) characterisation of mine wastes', *7th International Conference on Acid Rock Drainage (ICARD)*, St. Louis, MO: American Society of Mining and Reclamation (ASMR).
Strugała-Wilczek, A. and Stańczyk, K. (2015) 'Comparison of metal elution from cavern residue after underground coal gasification and from ash obtained during coal combustion', *Fuel,* 158, pp. 733-743.
Strugała-Wilczek, A. and Stańczyk, K. (2016) 'Leaching behaviour of metals from post-underground coal gasification cavity residues in water differing in mineralization', *Fuel,* 173, pp. 106-114.
Usher, B. H., Cruywagen, L. M., Necker, E. d. and Hodgson, F. D. I. (2003) *On Site and Laboratory Investigations of Spoil in Opencast Collieries and the Development of Acid Base Accounting*, Bloemfontein: Institute for groundwater studiesWRC 1055/1/03).
van Dyk, J. C., Brand, J., Strydom, C. A. and Waanders, F. B. (2018) 'Groundwater monitoring during underground coal gasification', *Journal of the Southern African Institute of Mining and Metallurgy,* 118, pp. 1021-1028.
Verma, R. P., Mandal, R., Chaulya, S., Singh, P. K., Singh, A. and Prasad, G. M. (2014) 'Contamination of groundwater due to underground coal gasification', *International Journal of Water Resource and Environmental Engineering,* 6, pp. 303-311.

Wagner, N., Malumbazo, N. and Falcon, R. (2018) *Southern African coals and carbons.* Cape Town: Struik Nature.

Wang, C., Liu, H., Zhang, Y., Zou, C. and Anthony, E. J. (2018) 'Review of arsenic behavior during coal combustion: Volatilization, transformation, emission and removal technologies', *Progress in Energy and Combustion Science,* 68, pp. 1-28.

Ward, C. R. and French, D. (2006) 'Determination of glass content and estimation of glass composition in fly ash using quantitative X-ray diffractometry', *Fuel,* 85(16), pp. 2268-2277.

White, W.W., Lapakko, K.A., Cox, R.L., 1999. The Environmental Geology of Mineral Deposits. In: G.S. Plumlee and M.J. Logsdon (Eds.), Static test methods commonly used to predict Acid-mine drainage: Practical guidelines for use and interpretation., Part A: Processes, Techniques and Health Issues, Reviews in Economic Geology Vol. 6A, Society of Economic Geologists, Inc., 325-338.

Wiatowski, M., Kapusta, K. and Muzyka, R. (2018) 'Study of properties of tar obtained from underground coal gasification trials', *Fuel,* 228, pp. 206-214.

Wolf, K.-H. and Bruining, H. (2007) 'Modelling the interaction between underground coal fires and their roof rocks', *Fuel,* 86(17), pp. 2761-2777.

Xu, B., Chen, L., Xing, B., Li, L., Zhang, L., Wang, X., Chen, H., Yi, G. and Huang, G. (2016) 'The environmental effect of underground coal gasification semi-coke on confined groundwater', *Environmental Progress & Sustainable Energy,* 35(6), pp. 1584-1589.

Yang, D., Koukouzas, N., Green, M. and Sheng, Y. (2016) 'Recent development on underground coal gasification and subsequent CO2 storage', *Journal of the Energy Institute,* 89(4), pp. 469-484.

Yurtsever, Y. and Payne, B.R. 1978. Application of environmental isotopes to groundwater investigation in Qatar. Proceeding of the International Symposium on Isotope Hydrology, Neuherberg, Germany, 19–23 June 1978, vol. 2. International Atomic Energy Agency, Vienna. pp. 465–490.

Zhang, P., Huang, W., Ji, Z., Zhou, C. and Yuan, S. (2018) 'Mechanisms of hydroxyl radicals production from pyrite oxidation by hydrogen peroxide: Surface versus aqueous reactions', *Geochimica et Cosmochimica Acta,* 238, pp. 394-410.

Zhang, Q. and Zhu, H. (2018) 'Collaborative 3D geological modeling analysis based on multi-source data standard', *Engineering Geology,* 246, pp. 233-244.

Zhao, S., Duan, Y., Lu, J., Gupta, R., Pudasainee, D., Liu, S., Liu, M. and Lu, J. (2018) 'Chemical speciation and leaching characteristics of hazardous trace elements in coal and fly ash from coal-fired power plants', *Fuel,* 232, pp. 463-469.

Appendix

Appendices are included on a separate document included as a supplementary electronic disk.

An online link to the appendices is also included below:

https://drive.google.com/drive/folders/1Yl6IGwB1yyEKN7p_MaCcrS-njSPJjsgR?usp=sharing